INDOOR LOCALIZATION UTILIZING EXISTING INFRASTRUCTURE IN SMART HOMES

A THESIS BY PUBLICATIONS PRESENTED IN PARTIAL FULFILMENT OF THE REQUIREMENTS FOR THE DEGREE OF

DOCTOR OF PHILOSOPHY

IN

COMPUTER AND ELECTRONICS ENGINEERING

MASSEY UNIVERSITY, ALBANY, NEW ZEALAND

Daniel Konings

July 2019

Abstract

Indoor positioning system (IPS) have received significant interest from the research community over the past decade. However, this has not eventuated into widespread adoption of IPS and few commercial solutions exist. Integration into Smart Homes could allow for secondary services including location-based services, targeted user experiences and intrusion detection, to be enabled using the existing underlying infrastructure. Since New Zealand has an aging population, we must ensure that the elderly are well looked after. An IPS solution could detect whether a person has been immobile for an extended period and alert medical personnel. A major shortcoming of existing IPS is their reliance on end-users to undertake a significant infrastructure investment to facilitate the localization tasks. An IPS that does not require extensive installation and calibration procedures, could potentially see significant uptake from end users. In order to expedite the widespread adoption of IPS technology, this thesis focuses on four major areas of improvement, namely: infrastructure reuse, reduced node density, algorithm improvement and reduced end user calibration requirements. The work presented demonstrates the feasibility of utilizing existing wireless and lighting infrastructure for positioning and implements novel spring-relaxation and potential fields-based localization approaches that allow for robust target tracking, with minimal calibration requirements. The developed novel localization algorithms are benchmarked against the existing state of the art and show superior performance.

Authors Declaration

This thesis was produced according to Massey University's "PhD thesis by publication" guidelines. This thesis is based on research that has either been published, or is currently under review in an IEEE journal. In accordance with IEEE's copyright policy, this thesis contains the accepted version of each published manuscript, rather than the IEEE final version. Consequently, while the content is identical to the published versions, there may be stylistic differences between the enclosed work, and the published versions. Furthermore, the work contained within this thesis was published in several different journals. Consequently, some of the submitted chapters are relatively succinct, there is some repetition (particularly in the literature review of some chapters), and there are small stylistic differences between the chapters themselves.

Acknowledgements

I would like to express my deep gratitude to my supervisors, Dr Fakhrul Alam, Dr Frazer Noble and Professor Edmund Lai: their encouragement, guidance and support over these last few years have helped me grow as an independent researcher. Furthermore, I wish to thank Fakhrul for his considerable support in providing teaching opportunities, administrative development, and co-funding activities that have helped me grow the auxiliary skills required for an academic career. I would like to extend my thanks to Massey University for supporting my studies with a Doctoral Scholarship and to the Department of Mechanical and Electrical Engineering for providing additional support. Special thanks is offered to Dr Mathew Legg and Ruth Brooks for their personal guidance and friendly demeanour that helped me keep my sanity during these past few stressful years. I would also like to acknowledge the assistance that I received from fellow research students, Baden Parr, Nathaniel Faulkner, Caleb Waddell, Tapiwanashe Wenge, and Gene Hopkins for their help in developing, deploying and testing the visible light and wireless indoor positioning testbeds, and with data collection.

On a personal note, I would like to acknowledge the support of my wife, Erin Konings; parents, Peter and Lynn Konings; brothers and sister, Joshua and Yeonie Jeong, and Aaron Konings. I would also like to thank the friends that supported and motivated me during my studies.

Finally, I give thanks to God, through whom all things are possible.

Funding

I gratefully acknowledge:

- Massey University for providing me with a Massey University Doctoral Scholarship
- Massey University's Graduate Research School for its Massey University Conference Presentation Grant in 2017
- Massey University for providing funding support through the Massey University Research Fund (MURF)

Table of Contents

List of Tables

LIST OF FIGURES

Abbreviations and Terms

AOA	Angle of Arrival
CDF	Cumulative Distribution Function
CFL	Compact Fluorescent Lamp
COTS	Commercial-off-the-shelf
CNN	Convolutional Neural Network
CRF	Conditional Random Field
CSI	Channel State information
DFL	Device-free Localization
EWMA	Exponentially Weighted Moving Average
FOV	Field of View
FMCW	Frequency Modulated Carrier Wave
FVLP	Force-based Visible Light Positioning
HD	Histogram Distance
IoT	Internet of Things
IM/DD	Intensity Modulation / Direct Detection
IMU	Inertial Measurement Unit
IPS	Indoor Positioning System
KNN	k-Nearest Neighbour
LED	Light-emitting diode
LOS	Line-of-Sight
LTH	Long-term Histogram
ML	Machine Learning
MLE	Maximum Likelihood Estimation
OLR	Outlier Link Reduction
OOK	On Off Keying
PD	Photodiode
PRR	Packet Reception Ratio
RF	Radio Frequency

RMSE	Root-Mean-Square-Error
RSS	Received Signal Strength
RSSI	Received Signal Strength Indicator
RTI	Radio Tomographic Imaging
RX	Receiving Node
SDR	Software Defined Radio
SLAM	Simultaneous Localization and Mapping
SMP	Smallest M-vertex Polygon
STH	Short-term Histogram
SVM	Support Vector Machines
TDOA	Time Difference of Arrival
TOA	Time of Arrival
TX	Transmitting Node
VL	Visible Light
VLC	Visible Light Communication
VLP	Visible Light Positioning
WKNN	Weighted k-Nearest Neighbour
WSN	Wireless Sensor Network

Introduction

Indoor positioning system (IPS) have received significant interest from the research community over the past decade because established outdoor approaches like the *global positioning system* (GPS) cannot be used for reliable indoor localization. GPS has obtained ubiquitous use globally, which we believe is largely due to its low implementation cost. End users are not required to deploy any infrastructure to utilize GPS localization services, the service is free for end users, and the radio modules required to use the service are affordable. Unfortunately, due to signal degradation, GPS cannot provide reliable sub-meter level localization accuracy, within indoor environments.

Even though IPS are an established research field, these substantial research activities have not eventuated into widespread adoption of IPS within Smart Homes, and few commercial solutions exist. We believe that this is because they have high implementation costs and require end users to perform extensive calibration procedures, unlike GPS. If an affordable IPS was developed that did not require extensive installation and calibration procedures, we believe there would be a significant uptake from the end users. We believe that this can be accomplished by creating a system that is designed to utilize the existing infrastructure, which will vastly reduce implementation costs. Furthermore, novel algorithms could be developed to increase the overall indoor localization accuracy, while also reducing the calibration burden.

As an aging population, with more people deciding to spend retirement within their own home, we must ensure the elderly are well looked after. An IPS solution could detect whether a person has been immobile for an extended period and alert family members or medical personnel. Integration into Smart Homes could also allow for secondary services including; location-based services, targeted user experiences and intrusion detection, to be enabled using the existing underlying infrastructure as shown in Fig. 1.

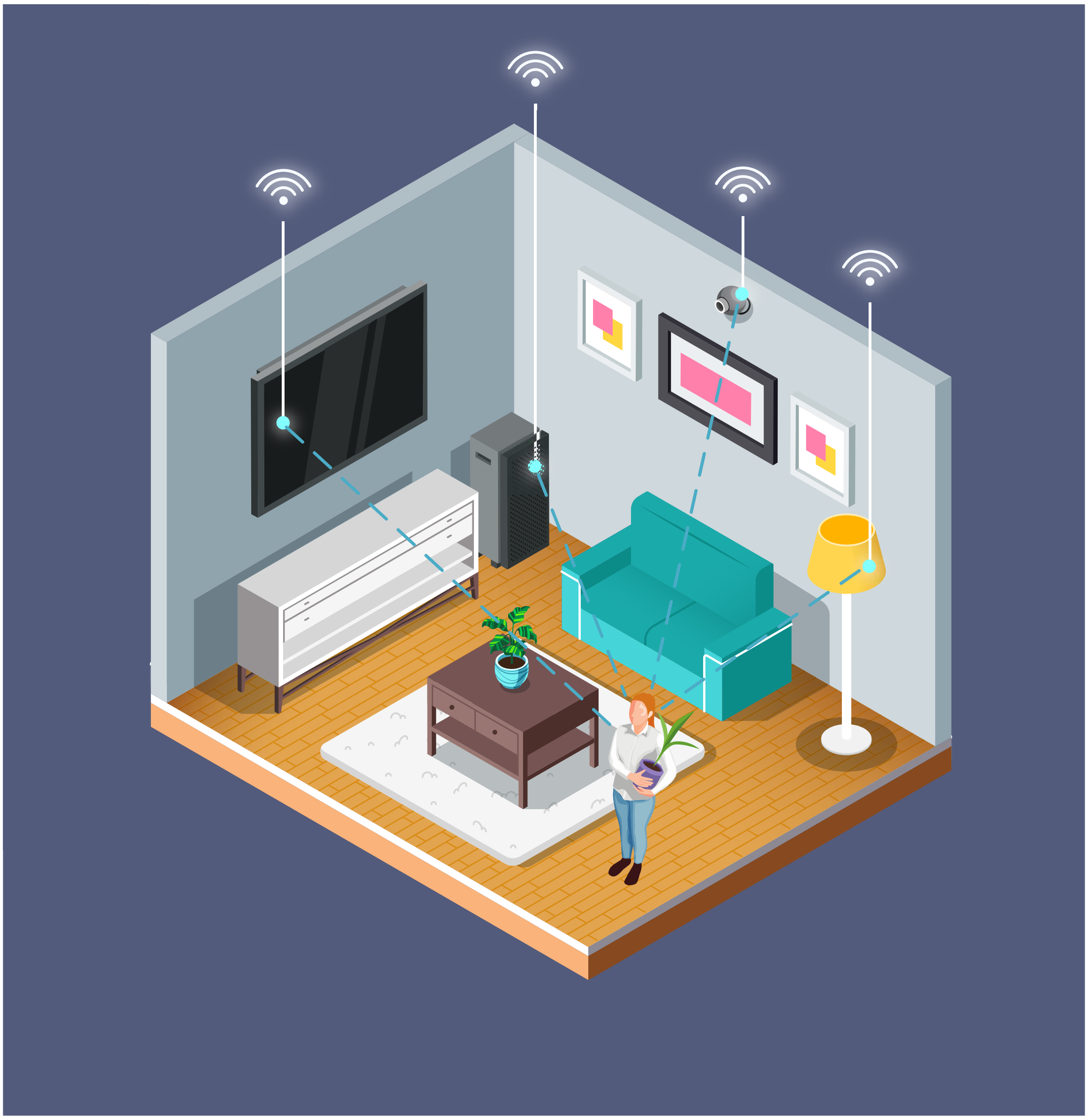

Figure. 1 – A Typical Smart Home with multiple wireless enabled smart sensors*

Localization Approaches

IPS can be divided into two broad categories. *Active* approaches use a network of stationary nodes to localize a roaming transceiver. An example would be tracking cell phones, as a way of offering personalized services within an airport or shopping mall environment. The second form of Indoor positioning is known as *device-free localization* (DFL) or *passive* localization. DFL systems do not required the tracked entity to carry a transceiver and infer a target's

* Some of the assets used in Fig. 1 were designed by macrovector / Freepik.

location by analysing their effect on the propagation of signal (e.g. wireless signal from a Wi-Fi network).

Traditional Indoor localization approaches have been implemented using a wide variety of technologies, e.g. wireless approaches (i.e. Wi-Fi, RFID, ZigBee, Cellular, and *ultra-wideband* (UWB)), *light detection and ranging* (LIDAR), Ultrasonic ranging, *inertial measurement units* (IMU), infrared sensors, optical approaches, or computer/machine vision. One of the main shortcomings of existing IPS literature is that is places an onus on the end-user to deploy custom infrastructure to enable localization. For IPS to be readily adopted within Smart Homes and residential settings, it would be highly desirable to see the implementation costs reduced. This could be facilitated by reusing the existing Smart Home infrastructure for the localization effort.

Within a modern Smart Home, several technologies are readily available that could potentially be used to construct an IPS. These include passive infrared alarm systems, camera enabled interfaces, the existing wireless network, or the lighting infrastructure.

A major shortcoming of the existing literature is that it focuses on attaining accurate positioning, but often does not prioritize usability and commercial viability for regular end users. Most existing solutions in literature either use bespoke hardware, or require a substantial offline training effort to get the system working, neither of which are tenable to a typical end user. This gap in literature is also reflected within the currently available commercial IPS offerings. Though DFL solutions have recently become available for Smart Homes, there has not been a significant adoption of the technology. We believe that this is because existing solutions require a significant additional infrastructure investment, which limits viability for normal consumers. Research involving Active localization is more mature than DFL efforts. However, a similar drawback exists for the readily available Active tracking solutions that also require a significant infrastructure investment. This has led to most IPS based businesses targeting large custom deployments within commercial warehouses, airports and supermarkets. However, few affordable active IPS exist for Smart Home deployments.

In contrast, GPS has attained widespread use when it comes to outdoor localization solutions. This is partly because the infrastructure is free to use, and it does not require the end user to transmit any data, which keeps the entry cost low. Following this premise, we believe that for IPS to attain widespread adoption in Smart Homes, the implementation needs to be achieved through infrastructure reuse, which would allow an end user to add localization services to Smart Home as a secondary service, using already existing technology within the built environment. In modern Smart Home environments, viable implementation candidates for an IPS include utilizing either the existing wireless network, or the lighting infrastructure. Other options like passive infrared alarm sensors only offer coarse room level localization, and always-on camera-based approaches create a privacy concern within indoor environments. Most current Smart Home devices communicate over a Wi-Fi, ZigBee or *bluetooth low energ*y (BLE) network. This means that Smart Homes already contain an extensive wireless network with sufficient node density for localization purposes. In recent years, *light-emitting diode* (LED)-based lighting has become popular because they are more energy and cost efficient than traditional Incandescent/*compact fluorescent lamp* (CFL) luminaires over their lifespan. They also do not release mercury when the bulbs break, removing a known health concern of CFL luminaires. As such, it is likely that LED luminaires will become the common lighting solution for residential living within the near future. In 2011, standard IEEE 802.15.7 was released which defines the PHY and MAC layers for *visible light communication* (VLC). This helped standardize the development of a new generation of communication devices (e.g. Li-Fi) which use the visible light spectrum for transmission. Since Li-Fi devices are expected to become ubiquitous within Smart Homes in the near future, they present another possible technology that can be leveraged to provide localization services, in the form of *visible light positioning* (VLP). Therefore, both VLC and VLP have become popular research topics in recent years.

Thesis Overview

Since the current state of literature shows a significant gap in knowledge relating to the practical challenges of Smart Home based IPS, this thesis aims to solve some of these issues through the concept of infrastructure reuse. It explores the extent to which we can leverage existing wireless technologies, while also providing potential secondary use cases for *visible light* (VL)-based technologies. In this work, we developed and deployed multiple full-scale experimental testbeds and show that a functional IPS can be deployed using either wireless or lighting infrastructure. Our research contains some of the first reported implementations that consider real world environment, which is a significant gap in literature. We deployed the first reported full-scale active IPS that fused both VL *received signal strength* (RSS) and wireless (ZigBee) *received signal strength indicator* (RSSI). We also developed the first passive VL-based IPS that used wall mounted sensors and removed the requirement for labelled offline training data. We also improve on existing state-of-the-art wireless-based IPS approaches, by proposing several new algorithms that require fewer static nodes and lower calibration effort.

This thesis aims to show that it is feasible to implement a cost effective IPS within residential environment, with a focus on

- infrastructure reuse,
- realistic node densities,
- reasonable end user calibration requirements.

Chapter 1 demonstrates how visible light and wireless technologies can be used together to develop an innovative indoor active IPS that is more robust. We explore the existing wireless state-of-the-art DFL through extensive experiments in Chapter 2. Chapter 3 introduces a novel wireless-based DFL system that provides increased localization accuracy, while also decreasing the end user calibration requirements. Chapter 4 shows how further improvements can be made to our and other state-of-the-art wireless DFL approaches. Chapter 5 exhibits the potential of VL-based DFL through the development of a novel technique. The suitability of the wireless infrastructure for an IPS is shown in Appendix 1. Appendix 2 reports the initial investigation of fusing wireless and visible light techniques for indoor localization. Each chapter and appendix are peer reviewed research publication and has self-contained literature review that establishes the state-of-the-art and identifies gaps in the literature. Therefore, there is no traditional literature review chapter in this thesis.

The localization performance of all the algorithms are experimentally tested with the help of custom-made real-world testbeds. The wireless testbed consisted of twenty portable ZigBee CC2530 nodes which were deployed in various environments as required. The visible light test bed consisted of up to 14 custom designed light sensors to measure the RSS of ambient light, and a wireless module to report all data back to a processing computer. When the VLP system was used for Active tracking, it also utilized modified luminaire driver boards to allow for a *commercial-off-the-shelf* (COTS) luminaire to transmit modulated signals. The details of these systems can be found in the relevant chapters within the thesis.

Metric Validation

The RSSI metric was chosen for the wireless solutions as it can easily be utilized by any existing ZigBee, Bluetooth or Wi-Fi hardware. Competing metrics like *angle of arrival* (AOA) require the network receivers to contain multiple antennas and *time of flight* (TOF) requires receivers to contain accurate, synchronized clocks. Both aspects increase the device cost and are not available in many existing Smart Home devices. Since RSSI capable devices are ubiquitous, a solution using this metric is well suited for IPS. In recent years, highly accurate approaches using software defined radio or Wi-Fi *channel state information* (CSI) have been proposed as an improvement over RSSI. The drawback of software defined radio solutions is that they cannot be implemented using COTS equipment, and typically require very large bandwidth. Wi-Fi CSI solutions offer a higher resolution than RSSI, as they can estimate the magnitude and phase across multiple subcarriers, reducing the detrimental effects of multipath propagation. The shortcoming of CSI-based approaches is that they are only available using modified drivers for legacy Wi-Fi equipment. Intel, the manufacturer of the chipsets used in this equipment, has also publicly stated that they do not plan to expose this metric to end users on modern Wi-Fi equipment. Since CSI has never been available for ZigBee or Bluetooth, and is not available on current Wi-Fi hardware, it is not suitable for use in a system that is expected to utilize existing infrastructure.

Visible Light RSS was used as the metric of choice for our VLP approach. We chose to use RSS for our *active* testbed as it does not require the receiver to contain multiple photodiodes (required for AOA) or for synchronization between the luminaires and receiver boards (required for TOF). RSS was also used for our *passive* testbed as it allows the system to utilize ambient light for localization purposes.

This research first validated the RSSI metric for localization use, before developing and testing solutions that could be feasibly applied to existing smart homes. We investigated whether a collocated Wi-Fi network or Microwave oven, two most common source of interference in a residential setting, would detrimentally interfere with the RSSI values of a ZigBee network. Our experimental results showed that a Microwave Oven has minimal effects on a ZigBee network. Our results also showed that while a collocated Wi-Fi network will affect the throughput of a ZigBee network, it would not affect the RSSI values of correctly received packets. This is important as it means that although interference may cause latency in a RSSI-based IPS, it will not have a detrimental effect on the accuracy. This work was published as a peer reviewed conference articled and constitutes appendix 1.

Chapter Overview

Chapter 1 of this thesis reports the development of an Active IPS solution termed Falcon (Fused Application of Light-based positioning Coupled with Onboard Network localization) that fused ZigBee RSSI values with visible light RSS. Falcon was highly innovative as this is first IPS reported in literature to combine wireless and visible light RSS technologies and make the localization more fault tolerant and robust. It offers superior accuracy over existing wireless approaches, while also working in realistic environments that feature occluded luminaires. Our Falcon approach also offered the best accuracy of any single photodiode-based IPS solution, deployed in a realistic full-scale environment, at the time of the publication. Preliminary tests were performed on a prototype analog VLP system coupled with a ZigBee radio. The initial results were published as a peer reviewed conference article and are included in appendix 2. Following on from the successful initial trials, the VLP receiver was redeveloped using a digital design instead of the initial analog prototype, which eventually became the basis of our Falcon implementation. The work was published in IEEE Access.

After implementing an *active* tracking solution using both visible light and ZigBee RSSI, we worked on developing DFL approaches that improved upon the state-of-art of localizing untagged targets.

The work undertaken in Chapter 2 compares three common and highly cited RSSI-based DFL solution and demonstrates how a target's walking trajectory can have a significant effect on the localization accuracy. This work provided the first reported apple-to-apple comparison of DFL solutions across the three major localization approaches within multiple common environments while considering realistic human movement behaviour. We also demonstrated the limitations of the existing RSSI-based DFL techniques in handling both varying target trajectories, and low node density deployments. We also highlight the lack of standardized metrics for comparing DFL solutions and propose using cumulative distribution function (CDF) plots instead of using the recommendations from the Active Localization standard (ISO/IEC 18305), as CDF plots provide a fair comparison across all error quartiles. This work was published in IEEE Sensors Journal.

In Chapter 3, we report the development of a novel RSSI-based DFL approach termed SpringLoc. Existing wireless RSSI approaches cannot provide robust localization services in sparse node deployments without requiring extensive offline wireless fingerprinting. SpringLoc addresses these deficiencies. It does not require fingerprinting, maintains its performance under multiple walking trajectories, and surpass the accuracy of existing approaches in low node deployments. This significantly reduces both the calibration effort and online computational requirements, as compared to existing state-of-the-art. SpringLoc treats DFL as an energy minimization problem and is the first reported work to model DFL as a network of connected artificial springs, to solve the localization problem. The work was published in IEEE Access.

In Chapter 4, we investigated whether DFL solutions that use RSSI histogram as a feature could be improved through a judicial selection of the histogram distance metrics. It was discovered that the Kernel-distance metric used in the state-of-the-art approaches is not optimal for RSSI histogram-based DFL. We demonstrate through experimental results that Bhattacharya distance and several other distance metrics are better suited for RSSI histogram-based DFL approaches. This is the first reported work in the literature where an extensive range of histogram distance metrics were benchmarked for DFL purposes. The work also demonstrated how one of the state-of-the-art DFL approaches could be further improved by removing noisy outlier values when estimating the position of a target. The work was published in IEEE Sensors Journal.

In Chapter 5, we demonstrated the feasibility of a DFL solution based on visible light. Existing approaches require extensive infrastructure modifications, or significant offline training. The developed solution, termed FieldLight, removes these limitations, while still providing good localization accuracy. FieldLight localizes and track targets using a set of artificial potential fields attached to triggered photodiodes embedded within walls. This is the first reported work that applies the artificial potential fields approach to VL-based DFL. The localization accuracy of FieldLight is evaluated by implementing it in multiple full-scale environments. Its accuracy is also experimentally compared with an existing wireless-based DFL algorithm in the same environment. This is the first reported performance comparison between wireless-based and VL-based DFL techniques. The work was published in IEEE Sensors Journal.

Chapter 1

This chapter contains content from the following article, republished with permission. In accordance with IEEE's republishing policy, any full text that has been included is the unmodified accepted article. This means that while the content is identical to the published article, there may be stylistic differences.

Falcon: Fused Application of Light based positioning Coupled with Onboard Network localization

Daniel Konings[1], Student Member, IEEE, Baden Parr[1], Fakhrul Alam[1], Member, IEEE, Edmund M-K Lai[2], Senior Member, IEEE

[1] School of Engineering and Advanced Technology, Massey University, Auckland, New Zealand
[2] Department of Information Technology and Software Engineering, Auckland University of Technology, Auckland, New Zealand

Corresponding author: Daniel Konings (e-mail: d.konings@massey.ac.nz).

This work was supported in part by the Massey University Research Fund (MURF) and Rexel Lighting.

Indoor localization based on visible light and Visible Light Communication (VLC) has become a viable alternative to radio frequency wireless based techniques. Modern Visible Light Position (VLP) systems have been able to attain sub-decimeter level accuracy within standard room environments. However a major limitation is their reliance on Line-Of-Sight (LOS) visibility between the tracked object and the lighting infrastructure. This paper introduces Falcon (Fused Application of Light based positioning Coupled with Onboard Network localization), a VLP system which incorporates Convolutional Neural Network (CNN) based wireless localization to remove this limitation. This system has been tested in real life scenarios that cause traditional VLP systems to lose accuracy. In a hallway with luminaires along one axis, Falcon managed to attain position estimates with a mean error of 0.09m. In a large room where only a few luminaires were visible or the receiver was completely occluded, the mean error was 0.12m. With the luminaires switched off, Falcon managed to correctly classify the target 99.59% of the time to within a 0.9m^2 cell and with 100% accuracy within a1.6m^2 cell in the room and hallway respectively.

INDEX TERMS Indoor Positioning Systems (IPS), Indoor Localization, Visible Light Communication (VLC), Visible Light Positioning (VLP), Zigbee Localization, Convolutional Neural Network (CNN).

I. INTRODUCTION

Indoor localization techniques could be classified into two categories: Device-Free Passive (DFP) and Active Tracking [1]. In DFP systems, the tracked target does not actively contribute to the localization effort. This allows these systems to provide generic services like intruder detection or automated lighting schemes based on human presence. Active Tracking systems are ones that require the tracked entity contributes to the localization effort. These systems benefit from knowing the identity of each tracked entity, enabling them to provide targeted services like individualized advertising, patient monitoring and asset tracking.

Most indoor localization implementations require sensors to be embedded within the target environment at regular intervals to ensure the localization error is minimized across the whole area of interest. For this reason, initial implementation costs for existing buildings can be high. In this paper a system that utilizes the existing infrastructure to provide indoor localization as a secondary service is proposed. It is based on an Active Tracking approach and incorporates fusion between visible light positioning (VLP) and radio frequency (RF) wireless localization.

In a preexisting built environment, the position of light sources or luminaires is dictated by the need for adequate illumination as per indoor lighting standards, e.g. AS/NZS-1680 [2]. The position of the luminaires may not be optimum from the perspective of localization. For smart lights, there is often a Wi-Fi/Zigbee radio incorporated as part of the light to allow for the light to be controlled through a network. We overcome the inaccuracies resulting from non-ideal placement of smart lights by combining location information from both luminaire and wireless sources. Visible Light Positioning (VLP) systems rely on the target to maintain Line-Of-Sight (LOS) with the luminaires mounted within the environment.

This means that VLP approaches suffer from blind spots when the target does not maintain LOS with an adequate number of luminaires, e.g. when the target passes under a table. Another problem arises in hallways which are typically illuminated by a single row of lighting sources. This causes issues with traditional VLP trilateration techniques as the system only has access to position information along a single axis. Since wireless signal experiences complex multipath propagation, wireless transceivers can contribute to horizontal awareness even when arranged in a single row. VLP systems also require the luminaires to be switched on which limits their use in many situations. This can be rectified by wireless augmentation. The fusion of two techniques for localization also makes the system robust, provides redundancy and fault tolerance.

The proposed solution uses slightly modified commercial luminaires and a collocated ZigBee radio to represent commercial smart lights, a photo diode coupled with a ZigBee radio as a target entity and a computer to collect all information and infer a targets location.

We propose a VLP implementation using carrier frequency allocation by inserting small amplitude sinewaves [3] biased close to the nominal voltage of the luminaire driver to provide unique ID for each luminaire. The implementation is similar to Intensity Modulation / Direct Detection (IM/DD) [4] with the difference being there is no data on the carrier. Since the lights are primarily utilized for illumination, On Off Keying (OOK) with 100% modulation depth [5] is not suitable for a VLP system using an existing lighting infrastructure since it causes a significant reduction in transmitted power resulting in lower brightness. Another major concern is that OOK creates harmonics which require more complicated multiplexing and reduce its scalability.

II. RELATED WORKS

In recent years indoor localization has been a popular research topic, partially due to the accuracy limitation of GPS signals within indoor environments. If accurate indoor localization schemes could be developed there would be many potential uses including smart robotics, elderly healthcare, targeted marketing, search and rescue etc. Wireless methods include RFID [6], ZigBee [7-9], Wi-Fi [10, 11] and Bluetooth [12, 13]. A common problem with traditional wireless approaches is that they suffer from multipath degradation [14, 15], interference [16] and struggle to attain a sub meter resolution. Some recent approaches have used visible light communication (VLC) for visible light positioning (VLP). Current methods either use a camera to take decodable images of the luminaires [17], or utilize a photodiode ranging methodology [18].

A. RF LOCALIZATION

Range-based localization methods attempt to create a functional model that accurately describes the relationship between received signal strength and distance, i.e. the path-loss regression model. After this model has been established, there are several methods for locating a remote Radio Frequency (RF) entity.

Lateration approaches require the tracked RF entity to be in contact with at least 3 known anchor nodes. Once this requirement is met, they use a least squares method to derive the entity’s location [19]. These types of method can work well in open spaces, but often struggle to attain acceptable accuracy in indoor environments as they do not properly account for multipath propagation. Attempts have been made to enhance the accuracy of RF based lateration approaches by dynamically changing the propagation model in real time [20], but the systems are still unable to attain sub meter level accuracy.

The Maximum Likelihood Estimation (MLE) approach to localization works by treating the distance between known nodes and unknown nodes as an unknown random variable with Gaussian distribution [21]. The algorithm then finds the location of maximum probability, by minimizing the variance of estimated error. This approach is more accurate than traditional ranged approaches, but its performance is determined by the number of static nodes, and the assumption that the channel model for each TX-RX pair is independent.

RSSI Map approaches, also known as RSSI fingerprinting, [10, 22, 23] are implemented in a two-stage approach, offline training and online estimation. During the offline training stage, RSSI signatures are collected with the tracked entity present in multiple known locations within the deployment region. These signatures are then stored in a database for later use. In the online estimation stage, the system tries to match current RSSI readings with a known location in the stored database. The closest match to the live values is used to infer the entity’s current location.

In an Active tracking approach, where the target caries a radio [10, 22, 23], the RSSI signature is made up of a vector of RSSI values measured between known nodes and an RF emitter the tracked entity carries. Liu, Darabi et al classify RSSI Map based algorithms into five further categories: k-nearest neighbour (KNN) [9, 24], probabilistic methods [25], neural networks [26, 27], support vector machines (SVM) [28]and smallest M-vertex polygon (SMP) [29].

This paper implements a neural network approach for the RF section as it requires minimal pre-knowledge of the expected distribution and characteristics of the measured RSSI data.

One of the major applications of the developed system could be asset tracking within built environment (e.g. tracking beds and medical equipment in a hospital). Therefore it is very important that the roaming target nodes are low cost, have long battery life, and do not interfere with existing infrastructure. Zigbee was chosen as the wireless resource as it is more energy efficient than Wi-Fi [30]. Zigbee networks also have been shown to have little impact on the throughput of neighboring Wi-Fi networks [31, 32], which means our implementation would not adversely affect existing wireless infrastructure. Finally, though Wi-Fi networks can impact the throughput of Zigbee networks, they do not affect the RSSI values of correctly received packets which are required for localization [16].

Channel State Information (CSI) has been shown to be a better metric for implementing indoor localization systems than RSSI as it can mitigate the effects of multipath propagation [33, 34] resulting in higher accuracy. However, the CSI metric is not commonly accessible in Off-The-Shelf wireless equipment, and current localization implementations are based around custom drivers for a very limited set of Intel [35] or Atheros [36] hardware. CSI has not been utilized in Falcon for this reason. However, it is advised that future implementations should use CSI over RSSI if the metric receives widespread commercial adoption.

Even though RSSI localization is limited due to multipath-channel effects and RF interference, it can still provide coarse indoor localization estimates [7, 12, 37]. The role of RF localization in Falcons sensor fusion is to help mitigate the limitations of the more accurate VLP implementation.

B. VISIBLE LIGHT POSITIONING

Visible Light Positioning systems benefit from very dominant line-of-sight (LOS) components which help mitigate the effect of multipath which allows implementations to attain a higher accuracy than traditional RF based systems [38, 39]. Recent research into VLP largely falls into two approaches; photodiode-based localization or image-sensor based localization. Photodiode approaches typically aim to triangulate/trilaterate a receiver node with reference to multiple stationary luminaires. This is accomplished by transforming chosen metric readings into an angle/distance from a specific luminaire. Some common metrics available to photodiode based VLP systems include received signal strength (RSS) [5, 40], time of arrival (TOA) [41], time difference of arrival (TDOA) [42, 43] or angle of arrival (AOA) [44, 45]. When multiple luminaires are concurrently visible, a multiplexing scheme [3, 46] needs to be employed to ensure the receiver can decode and isolate the metric for each luminaire. For VLP approaches using phosphor-coated white LEDs, the accuracy is limited by the signal bandwidth since the response speed of the phosphor coating is slow. However, the bounds on position estimation accuracy are typically within the order of centimeters which is suitable for most indoor localization systems [41, 47].

Image-sensor based VLP uses a camera to capture an image of the visible luminaires. This approach benefits from less multi-luminaire interference than photodiode approaches as the image contains physically separated luminaires. A downside of this approach is that the off-the-shelf camera sensors may be required to exploit the rolling shutter effect to attain decodable images [38]. Since physical characteristics vary between camera sensors, image-sensor based VLP results may not translate between camera platforms. Another limitation is that the separation between the transmitter and receiver must be small to ensure each luminaire contains enough pixels within the image to localize [17]. Simulations involving typical indoor scenes, where the Cramer-Rao Lower Bound (CRLB) was derived show that the positioning accuracy of an Image-sensor approach is in the order of centimeters, with an azimuth angle error of less than 1 degree [47].

Recent VLP implementations include a novel Gaussian Process approach tracking a Tablet [48], with an average accuracy of 0.56m. However this work does not consider occlusion, as the receiver always maintain LOS with the luminaires. A hybrid solution was presented in [44] using simulated Wi-Fi and VLP with a reported accuracy of 0.1395m. However they did not implement a working system, and simulation also assumes ideal luminaires with no furniture within the room. Many implementations rely on a trilateration based approach [49] and recent implementations have been able to attain sub decimetre level accuracy within standard indoor environments [5], which is significantly better than the performance of most RF based RSSI implementations.

One of the major limitations of the reported physical implementations of VLP is that they do not properly account for the intermittent light occlusion that VLP receivers suffer from in common indoor, furniture rich environments. Our proposed system seeks to rectify the problem with occlusion by implementing a practical implementation featuring a fusion of a VLP receiver and zigbee radio. The fusion will also allow for localization in areas like hallways with row aligned VLP sensors that cannot normally converge and will allow for a coarse position estimate even when the luminaires are turned off. This will also provide localization results from multiple physical environments which is lacking in existing literature.

C. SENSOR FUSION

Multiple sensor approaches have been proposed for indoor localization in existing literature. Mobile phones are commonly used as localization targets which has allowed for the fusion of Inertial Measurement Unit (IMU), Wi-Fi and Bluetooth metrics for localization efforts [50-52]. Simultaneous Localization And Mapping (SLAM) was developed to help robots define their current location whilst also creating a map of the environment. SLAM implementations fuse information from multiple sensors to improve the accuracy of localization/mapping. Traditionally these systems have had a high implementation cost. However, recent research has looked into solving SLAM using low-cost sensors which typically fuse a camera with odometers and ultrasonic rangefinder sensors[53-55]. A comparison of the proposed Falcon and existing Sensor Fusion approaches is given in Table 1. As we can observe, the Falcon is very low cost, flexible and robust compared to the other existing systems.

D. CONTRIBUTION

As far as the authors are aware, this is the first reported work to physically implement a hybrid VLP/RF solution. The work also contains the following novel components:

1) The hybrid Falcon system (incorporating both VLP and RF) solves the problem of visible light occlusion within existing VLP approaches. This allows Falcon to work in realistic environments when the lights are

not always turned on. Falcon also offers superior accuracy over existing wireless approaches, when a lighting resource is available.

2) The proposed Falcon system presents a new hybrid Potential Fields and Neural Net based approach that has not previously been implemented for VLP or RF Indoor Localization.
3) Falcon is designed to work in hallways that feature row aligned luminaires, a scenario in which traditional VLP approaches are unable to converge.

III. SYSTEM OVERVIEW

The Falcon system tracks a target node based on its relative position to known ceiling mounted anchor nodes. The target node features a tag equipped with both a zigbee radio and a photodiode, whilst each anchor features a collocated VLP transmitter and zigbee module. VLP is the primary localization system in Falcon as it provides a higher accuracy than the wireless based localization. Wireless localization using zigbee is incorporated to overcome several key issues with the VLP localization approach. Firstly, it enables the system to remain operational when the lights are off. Secondly, it allows for localization even if the luminaires are mounted in a straight line or some of the luminaires are occluded. Finally, it prevents the VLP approach to converge to incorrect local minima.

The Falcon system works in two stages, as outlined in Fig. 1. During the Offline phase, the system collects both optical and RF samples. The RF samples are used to train a convolution neural net [56] that infers which region of interest (cell) a target is likely residing within. The optical samples are used to create two models. The first model maps the relationship between the received lights power intensity and the distance between the receiver and anchor nodes. The second model applies weights to the distance model based on how reliable the model is at varying distances from an anchor node.

The Online phase can be broken down into a further two stages. In the first stage, the RF neural net classifies a region of interest based on the trained model and the current RF samples. The system also uses the current optical samples to calculate a weighted distance between the tag and each anchor node. More details can be found in the Algorithm 1 pseudo-code. In the second stage, the iterative Force based Visible Light Positioning (FVLP) converges on a position estimate by using the RF region of interest as a starting point, and the VLP distances to refine a final estimate.

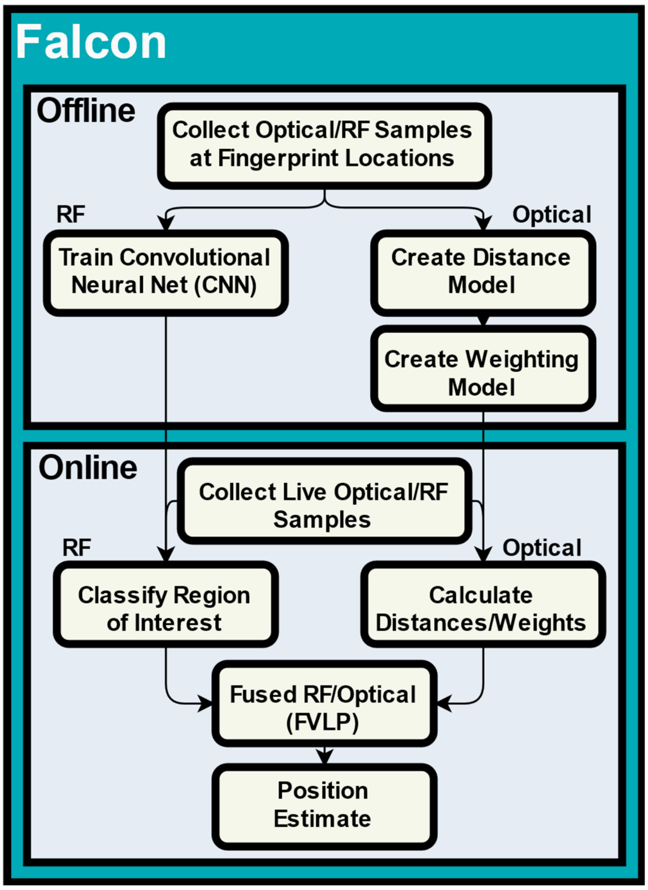

FIGURE 1. Falcon Algorithm Overview

TABLE I
SENSOR FUSION IMPLEMENTATIONS

Name	Technology	Average Accuracy	Tag Cost	Works in the dark	Resistant to Transient Interference	Works with Row Aligned Luminaires
Falcon	Photodiode RSS, Zigbee RSSI	0.12m	Low	Yes	Yes	Yes
KAILOS [57]	Wi-Fi RSSI, magnetometer, accelerometer, gyroscope, compass, barometer	1m	High	Yes	Unknown	N/A
LiFS [58]	Wi-Fi RSSI, accelerometer	5m	High	Yes	No	N/A
KILA [59]	Wi-Fi RSSI, RFID	>1m	Low	Yes	Yes	N/A
SVD-SF [60]	Image Sensor, accelerometer, gyroscope	0.05m	High	No	No	Unknown
LIPS [61]	Multiple Photodiode RSS, magnetometers, accelerometers	<1m	Medium	No	No	Unknown
Yasir et al [62]	Photodiode RSS, accelerometer	0.14m	Low	No	No	No
Yang et al [63]	Multiple Photodiode RSS, Multiple Photodiode AOA	0.06m	Low	No	No	Unknown

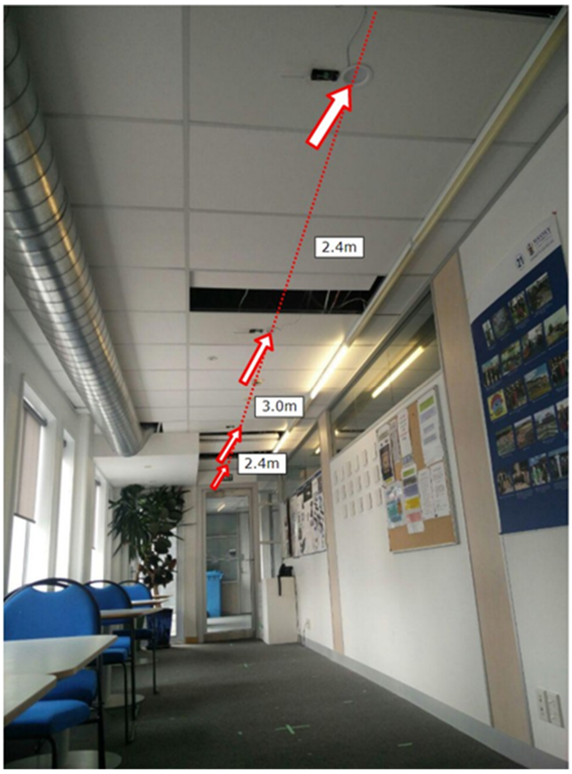

FIGURE 2. **Anchor Nodes Installed in Hall**

A. Falcon HARDWARE

The Falcon hardware was designed to use a remote tag node to receive optical and RF signals from ceiling mounted anchor nodes. The roaming target node periodically broadcasts a communications request. Each ceiling node in range of this broadcast replies to the roaming node. The target records the RF RSSI value, ID and VLP power of each reply it receives and passes these to the processing computer for training during the offline period, or classification during the online phase. The Visible Light Positioning system consists of a photo diode acting as a receiver to measure the intensity of the received light at different frequencies. This approach was chosen over an image-sensor based approach as it allows for lower cost receivers (photodiode tags). One of the objectives of the developed VLP is to employ it for asset tracking by leveraging existing lighting infrastructure. Therefore a photodiode approach has deliberately been chosen as it makes the deployment of a large number of tags economically feasible. We also recognize the fact that phosphor-coated white LED luminaires are limited by their response time. However, off the shelf luminaires have been chosen to represent the realistic lighting infrastructure of a built environment. The developed VLP is not a VLC based data communication system. Rather than transmitting data, each luminaire is transmitting an unmodulated sinewave of a unique frequency so that the signal strength from each visible luminaire can be estimated. Therefore, the bandwidth constraint of the LEDs is not a major concern for our VLP approach. The bandwidth is large enough to accommodate a sufficient number of unique sinewave frequencies to be chosen to provide ID for each luminaire.

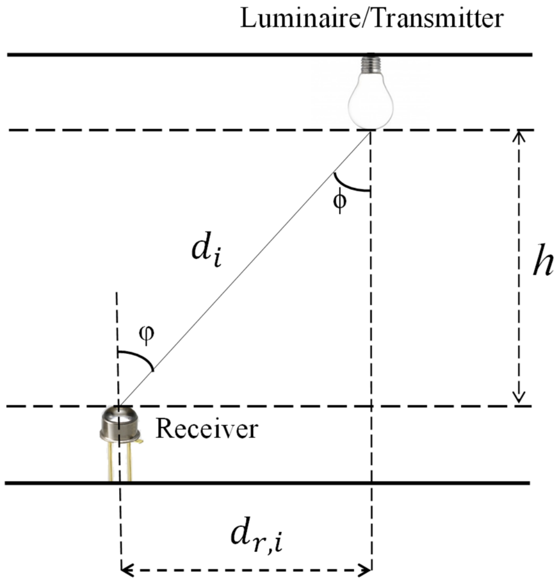

Figure 3. **Side View of VLP System**

The photodiode intensity information is passed through an inverse Lambertian propagation model [64] to determine the distance between the receiver and each transmitter. A custom potential fields approach, FVLP, is then used to localize the target receiver.

Since this paper is focusing on systems that are affordable and could be implemented into preexisting built environments, a driver board was developed that can be retrofitted into existing LED luminaires by sitting between their driver and the luminaire itself.

The modulation/demodulation circuitry is based on IM/DD. The modulator was designed to work on frequencies between 2kHz and 4kHz. This allows the use of cheaper components as lower frequencies could be more easily generated and literature shows that any flicker generated above 1.25kHz can be considered low risk for humans [65]. The five frequencies chosen for modulation were 2.6kHz, 2.8kHz, 3kHz, 3.2kHz and 3.4kHz. A proportional integral system fine-tunes the oscillators. This results in a generated frequency error of less than 5Hz even with cheap capacitors and potentiometers.

The custom modulation boards were installed as part of the Anchor Nodes in two environments, a small Laboratory (1.8m x 2.7m) and an adjacent hallway shown in Fig. 2. A summary of the hardware used can be seen in Table 2.

TABLE II
FALCON HARDWARE

Module	Name	Features
RF/VLP	Anchor Nodes	9 Ceiling Mounted CC2530 with ESP8266 and IM/DD modulator
RF/VLP	Tag Node	1 Mobile tag featuring a CC2530, ESP8266 equipped with a photo-diode
RF/VLP	PC	Win10 I7 Laptop with NVIDIA 960M Graphics Card and connected CC2530
VLP	Laboratory Luminaires	9 Ceiling Mounted REX13CDL

IV. Algorithm

As discussed before, Falcon requires an offline phase followed by an online one. During the Offline phase, Falcon is given a list of cell locations. Each cell represents an area of ground defined by user in advance. Further information about the cell layout used is given in Section V. Falcon takes the raw RSSI fingerprint values collected during the offline phase and allocates them to their appropriate known cell. These raw RSSI values, and their associated cell form the input data for training the CNN. During the Online phase, the trained CNN will then output (classify) a cell of interest, for any given raw RSSI input vector.

Falcon also creates a distance model between the tag and each of the anchor nodes using the VLP resources.

It should be noted that a CNN was chosen as it offers a simple implementation for classification based on raw RSSI values that have not been pre-processed, and where the absolute position of the anchor nodes may be unknown. Other approaches such as SVM, Particles Filters or Euclidean distance are also viable for providing a coarse RF based position estimate [66].

At the beginning of the Online phase, Falcon collects live RF and VLP samples. The RF section uses the live samples to infer a region of interest (cell) from the pre-trained CNN. The VLP section calculates the distances and weights from the live samples, based on the pre-calibrated models. The Potential Fields based VLP algorithm (FVLP) then uses the RF CNN cell of interest, VLP distances and VLP weights to iteratively converge on a final position estimate.

A. OFFLINE PHASE

During an initial calibration stage the target node collected optical samples in 13 locations in the Laboratory and Hallway respectively. RF samples were taken at 26 locations in the Laboratory and 18 locations in the Hallway. A raw RSSI sample is 1 byte long and represents a estimation of the received signal strength of a zigbee packet. The raw sample is converted to dBm by subtracting a vendor specific offset. A raw VLP sample is an estimation of the received power from the receiving photodiode. The output of the photodiode at location (*x* ,*y*) is given by:

$$r(t) = \sum_{i=1}^{L} C_i B \sin(2\pi f_i t + \theta_i) \quad (1)$$

where L is the number of visible luminaires at location (*x*,*y*), i is the amplitude of the sinewave, f_i is the frequency of the sinewave ID of the i^{th} luminaire, θ_i is the phase of the sinewave ID of the i^{th} luminaire at location (*x*,*y*) and i_i depends on the response of the photodiode at the frequency f_i and the optical channel between the i^{th} luminaire and location (*x*,*y*). This is essentially a function of the distance, d_i between the photodiode at location (*x*,*y*) and the i^{th} luminaire.

By assuming that the receiver and transmitter planes are in parallel, we can simplify the well-known Lambertian propagation model [64] for the received power to:

$$P_{r,i} = \frac{P_t}{d_i^2} \left(\frac{m+1}{2\pi}\right) cos^m(\emptyset) A cos(\varphi) \quad (2)$$

where d_i is distance between the transmitter / receiver, m is the Lambertian order, $\emptyset$ is the irradiation angle, A is the area of the VLP detector, φ is the incidence angle, P_t is the power of the sinewave carrier and is given by $(B/\sqrt{2})^2$. This value is constant for all luminaires, at all receiver locations. $P_{r,i}$ is the received power of the i^{th} luminaires carrier.

Since the VLP transmitter and receiver planes are in parallel, we have $cos(\emptyset) = cos(\varphi) = h/d$. This allows for (2) to be further simplified to:

$$P_{r,i} = \frac{GP_t}{d_i^{(m+2+k)}} \quad (3)$$

where G is a constant gain of $A\left(\frac{m+1}{2\pi}\right) h^{(m+k)}$, and k is a constant added to adjust the fall off characteristics, which are affected by unique hardware differences in the transceiver pair.

Using the Pythagoras theorem, the radial distance is given by $d_{r,i} = \sqrt{d_i^2 - h^2}$. Combining this with (3) and rearranging, we have

$$d_{r,i} = \sqrt{\left(\frac{GP_t}{P_{r,i}}\right)^{\frac{2}{(m+2+k)}} - h^2} \quad (4)$$

The relationship between the transmitting luminaire, the receiving photo-diode and the radial distance from (4) can be seen in Fig. 3. Since the environment contains multiple luminaires, we can estimate, $P_{r,i}$, the power for each luminaire by using periodogram analysis.

Assuming that $r(t)$ is windowed by a length-N window $w(n), 0 \le n \le N-1$, where $x(n) = r(t) \cdot w(n)$. The discrete-time Fourier transform (DTFT) of $x(n)$ is given by:

$$X(e^{j\omega}) = \sum_{n=0}^{N-1} x(n) e^{-j\omega n} \quad (5)$$

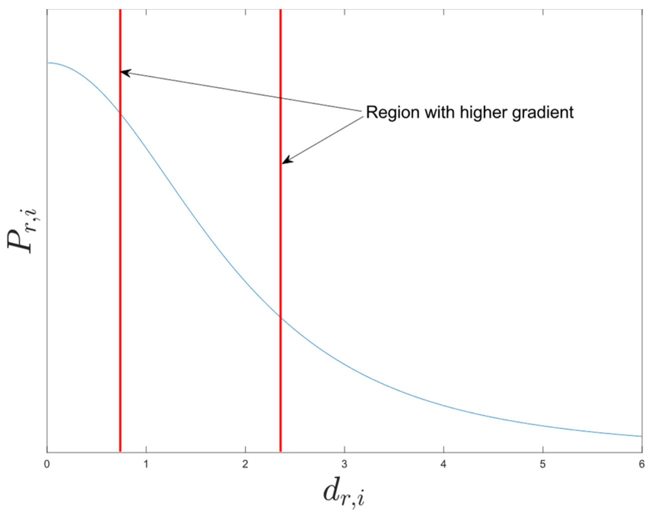

Figure 4. Model relating received power (Pr) and radial distance (dr).

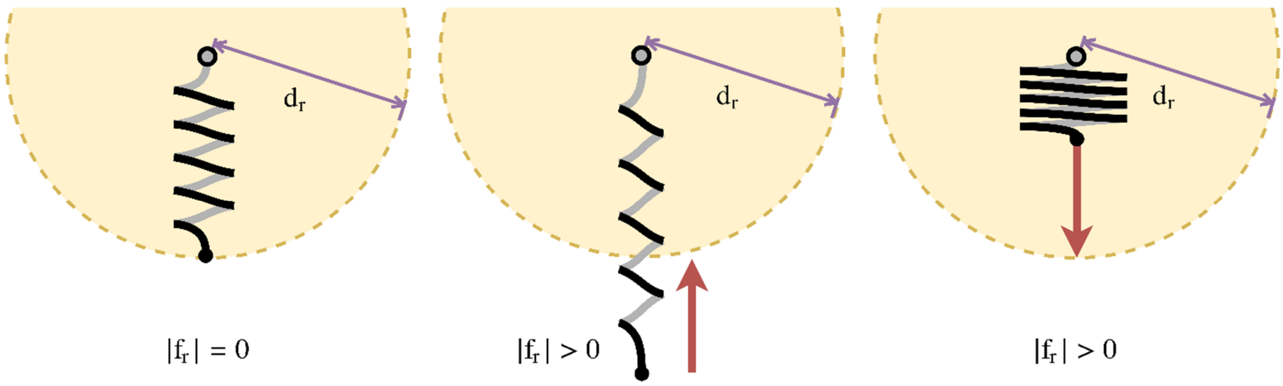

FIGURE 5. (a) FVLP Force = 0 . (b) Attractive Force. (c) Repulsive Force.

This can be used to estimate the power spectrum as:

$$\hat{P}_{xx}(w) = \frac{1}{\beta N}\left|X(e^{j\omega})\right|^2 \quad (6)$$

where β is a constant normalization factor. We can ignore β as it will act as a constant scaling factor that would remain the same at all locations. We can use (6) and the known modulation frequencies to estimate the $P_{r,i}$ for each luminaire.

During the Offline phase, we collect $P_{r,i}$ estimates for each luminaire, at multiple locations (18 for the Hallway, 26 for the Laboratory) with known radial distances. We can then minimize the error between the estimated radial distances ($d_{r,i}$) and the actual radial distances ($d_{a,i}$) to attain the best values for G and k in (4). This can be defined as using minimization to solve :

$$\arg\min_{G,k}\left\|\boldsymbol{d}_{r,i} - \boldsymbol{d}_{a,i}\right\| \quad (7)$$

where $\boldsymbol{d}_{r,i}$ is a vector of the estimated radial distances from the i^{th} luminaires at the offline calibration locations (18 for the Hallway), and $\boldsymbol{d}_{a,i}$is a vector of the actual corresponding radial distances.

Once optimal values are calculated for G and k, (4) can be used as a model to map a radial distance to any given luminaires P_r in the Online phase.

A typical model showing the relationship between $P_{r,i}$ and $d_{r,i}$ is shown in Fig. 4. The Lambertian model has regions with steep gradients, as shown in Fig. 4. Measurements from this region are preferable as $d_{r,i}$ has a higher resolution when predicted using equation (4). This can be exploited by weighting each luminaire with an absolute of the derivative of (8). This results in the region indicated in Fig. 4 receiving higher weights. The weighting index model ($W_{1:i}$) is created to act as an index lookup table which contains a weight model (W_i) for each luminaire within the system. When the system receives a new $P_{r,i}$ estimate, it is passed to the weighting index model which returns an individual weight. The process for creating each weight model (W_i) inside the weighting index model ($W_{1:i}$) is as follows. We rearrange (3) and (4) to obtain

$$P_{r,i} = \frac{GP_t}{(d_{r,i}{}^2+h^2)^{\frac{m+2+k}{2}}} \quad (8)$$

Let

$$\acute{P_{r,i}} = \left|\frac{d}{dd_{r,i}}P_{r,i}\right| \quad (9)$$

Then it can be normalized by

$$q_i = \left(\frac{\acute{P_{r,i}} - \min(\acute{P_{r,i}})}{\max(\acute{P_{r,i}}) - \min(\acute{P_{r,i}})}\right) \quad (10)$$

so that $0 \leq q_i \leq 1$. The i^{th} luminaires weighting model is then obtained by subtracting an LED's offset to shorten the tails, giving us

$$W_i = H(q_i - g_i) \quad (11)$$

where H is the Heaviside step function, used to set any tail with a negative weighting to 0, and g_i is the i^{th} luminaires tail offset.

Once the VLP distance model (4) and weight model (11) have been calculated, the system begins calibrating the wireless model. The wireless system uses the RSSI samples to create a convolutional neural network that divides the physical environment into predetermined grid sizes. The structure of the CNN used in Falcon is kept constant, but a separate CNN is trained for each partitioned location present. This has been done as it offers several benefits. Firstly, by having a smaller CNN that only incorporates the RF resources visible on a per location basis, CNN training is simplified. This means that on average it takes less than 2 minutes to train a room using the processing pc. RF localization systems based on RSSI are highly susceptible to multipath, which means their dynamics can significantly change due to environmental changes such as moved furniture. By segmenting the system per location, we can retrain the CNN on a per location basis. This ensures that the system is scalable and doesn't need complete retraining when environmental changes occur, but rather localized retraining should be sufficient.

A CNN was chosen as a fully connected architecture was deemed to be unnecessary for RSSI based localization as long as local features can be identified. Since RSSI data arrives at regular intervals at a higher frequency than expected movement, the data should exhibit strong autocorrelation over small intervals. Since convolutional networks assume locality, they should perform well with raw time series RSSI data.

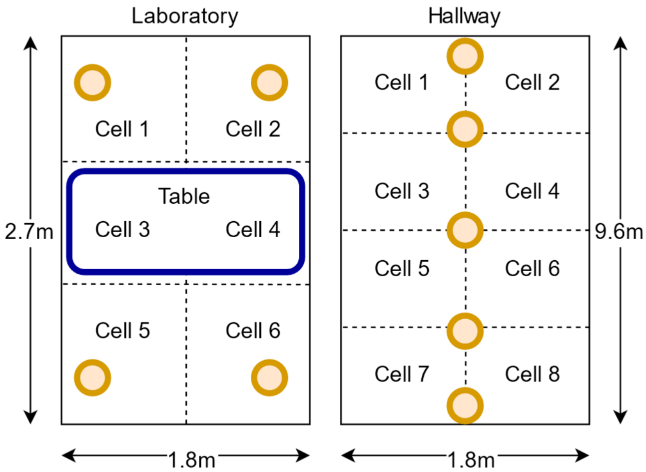

FIGURE 6. **Laboratory and Hallway Cell layouts**

When collecting offline samples, 800 samples were taken from each ceiling mounted radio within range, at each test point. In the hallway 5 radios were detected and measurements were taken at 18 test locations which resulted in a [5 x 800 x 18] output RSSI array. To turn the RSSI samples into RSSI 'images' ready for CNN training, we create square matrices, grouping RSSI samples based on how many radios were detected. For the hallway scenario, this meant splitting each of the 18 test locations into 160 [5 x 5] matrices where each column represents RSSI from each radio and each row represents multiple samples from a single radio. These images are then randomly split in a 3 to 1 ratio of training images and validation images and passed to the CNN. The structure of the CNN used is outlined in Table 3.

The training was controlled by an output function which would stop the CNN training period if over any 6 consecutive validations, there had been no accuracy improvement seen in any of the validations. At this stage, the Falcon system transitions from the Offline training phase to the Online localization phase. A summary of the Offline phase is provided as Algorithm 1.

Algorithm 1 Offline Phase

```
procedure CALIBRATION(trainingLocations, LEDs)
    Cells = number of cells
    K[1 : count(LEDs)] = a constant per light derivative offset factor
    for each location in trainingLocations do
        VLPfft = fft(location.signal)
        VLP_Intensity = isolate_per_freq(VLP_fft, LEDs)
        if location is inside a new predefined cell then
            Cell_id = Cell_id + 1
        end if
        RF_data = [location.RF_RSSI, Cell_id]
    end for
    Distance_vector = 0.01 : 0.01 : 8          ▷ artificial distance index from 0.01 - 8m
    for i = 1 : count(LEDs) do      ▷ Calculate distance and weighting models for each LED
        VLP[i].model = lambertian(VLP_Intensity[i, :], LEDs[i])
        Power_vector = inverse(VLP[i].model).predict(Distance_vector)
        tempw = normalize(−1 ∗ derivative(Power_vector)) − K[i]
        VLP[i].weights = U(tempw) ∗ tempw          ▷ Where U(x) is the Unit Step Function
    end for
    [RF_t, RF_v] = random(RF_data)          ▷ Randomly split into training/validation sets
    RF_CNN = train(RF_t, RF_v)                                   ▷ Train the Neural Net
    Return [VLP, RF_CNN]
end procedure
```

TABLE III

CONVOLUTION NEURAL NETWORK PARAMETERS

Layer	Name	Features
1	Image Input Layer	Hallway – 18 training points - 160 [5 x 5] samples Laboratory – 26 training points – 200 [4 x 4] samples
2	Convolutional Layer	16 3x3 filters, padding of 1
3	Batch Normalization Layer	
4	Activation Function Layer	ReLU
5	Convolutional Layer	32 3x3 filters, padding of 1
6	Batch Normalization Layer	
7	Activation Function Layer	ReLU
8	Fully Connected Layer	
9	Softmax Layer	
10	Classification Layer	

B. ONLINE PHASE – STAGE 1

The first stage of the Online phase involves preparing the inputs for the final iterative FVLP approach, as can be seen in Fig. 1. During each update, the RF section uses the live RSSI samples to classify a region of interest (cell) based on the pre-trained CNN from the offline phase. The VLP system estimates the received power from each luminaire and uses Equation (4) to map each received power measurement to a radial distance between the tag and its respective luminaire. Each luminaires distance is then assigned a weight by passing the distance through the weighting lookup table created during the Offline phase. Finally, the VLP Distances, VLP Weights and the CNN region of interest are passed onto the FVLP algorithm for final position estimation. Online Phase – Stage 1 is given by Algorithm 2.

Algorithm 2 Online Phase

```
procedure LOCALIZATION(VLP, RF_CNN, RF_RSSI, LEDs)
    for each timestep do
        VLP_fft = fft(VLP.signal)
        VLP_Intensity = isolate_per_freq(VLP_fft)
        Cell = classify(RF_CNN, RF_RSSI) ▷ Retrieve the predicted cell from trained CNN
        for i = 1 : count(LEDs) do ▷ Calculate radial distance and weight for each visible LED
            VLP_Distances[i] = VLP[i].model(VLP_Intensity[i, :])
            weights[i] = VLP[i].weights(floor(VLP_Distances[i]) + 1)
        end for
        Position = FVLP(LEDs, VLP_Distances, weights, Cell)
    end for
    Return Position
end procedure
```

C. ONLINE PHASE – STAGE 2

The FVLP system initializes its initial position state reported from the CNN as the center of the cell of interest. The FVLP localization system is an iterative approach that is based on the pathing method using Virtual Potential Fields [67, 68]. FVLP is passed a $d_{r,i}$ for each visible luminaire. This is equivalent to creating a circle around each luminaire with radius d_r as shown in Fig. 5. We define the distance between the previous position state and the current position state as:

$$\overrightarrow{d_{\Delta,\imath}} = P - L_i \qquad (12)$$

where $\overrightarrow{d_{\Delta,\imath}}$ is the (x, y) distance vector between the previous position estimate and the ith Luminaire, P is the (x, y)

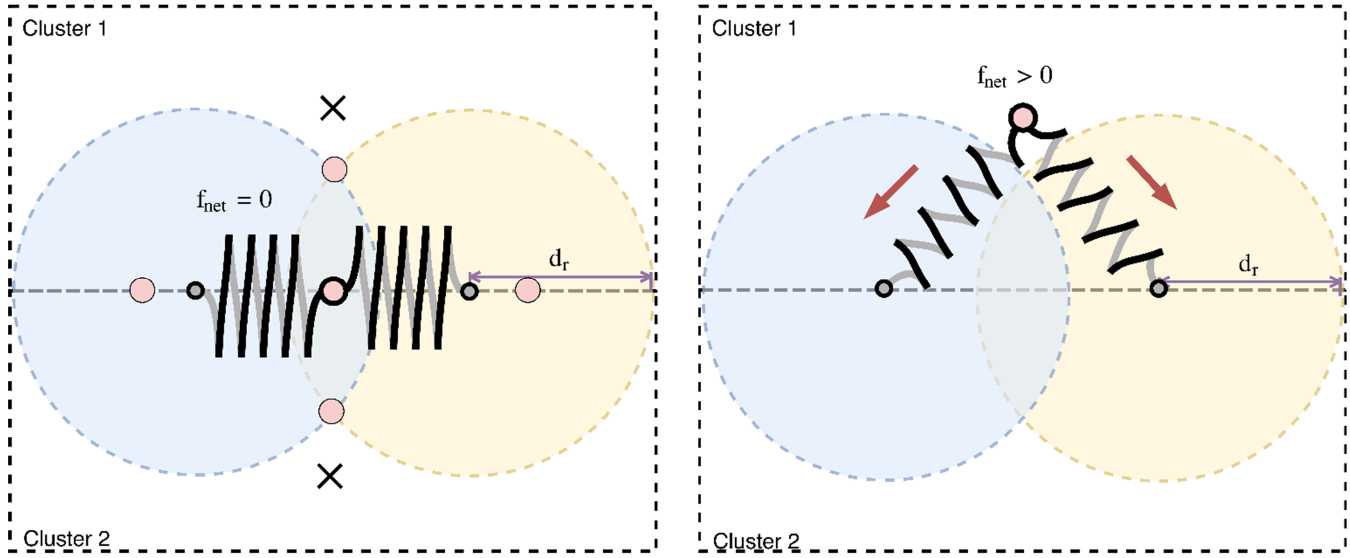

FIGURE 7. **(a) FVLP Convergence issues. (b) FVLP forces direction.**

coordinate of the previous position state estimate, and L_i is the (*x*, *y*) coordinate of the ith Luminaire.

If the previous position state lies outside the luminaire's circle, an attractive force is applied from the previous position state towards the luminaire's location. If the previous position state lies within the circle, a repulsive force is applied from the luminaires location towards the circles circumference. This is detailed in Fig. 9. The force applied to P, with respect to L_i can be defined as:

$$\vec{F_i} = -\left(\frac{\vec{d_{\Delta,1}}}{|\vec{d_{\Delta,1}}|}\right) F_{\mathrm{i}} \tag{13}$$

where F_{i} is defined as:

$$F_{\mathrm{i}} = S\left(|\vec{d_{\Delta,1}}| - d_{r,i}\right)W_i \tag{14}$$

where S is a force scaling factor used to limit the maximum movement per iteration, $d_{r,i}$ is the radial distance of L_i, as defined in (4), and W_i is a weight for L_i, as defined in (11).

The total force applied at an iteration can be given by:

$$F_T = \sum_{i=1}^{L} \vec{F_i} \tag{15}$$

At the end of each iteration F_T is applied to P to attain a new position state estimate.

$$P_{new} = P + F_T \tag{16}$$

If F_T is very small or FVLP reaches its maximum allowable iterations, P_{new} is returned as the final position estimate. Otherwise P_{new} is used as P in the next iteration . The pseudo code for this process can be found in Algorithm 3.

V. EXPERIMENT AND RESULTS

The testing was undertaken in two locations (Laboratory room and Hallway) with two states (Smart Lights switched on / off).

Algorithm 3 Visible Light Positioning - Force based Localization

```
procedure FVLP(LEDs, VLP_Distances, weights, RF_Cell)
    max_iterations = 100
    Position = center(RF_Cell)
    forceVector = [0, 0]
    stepSize = 0.1
    anchors.LEDs = LEDs
    anchors.weights = weights

    for i =1:max_iterations do
        netForce = [0, 0]
        for j=1:count(anchors) do
            deltaPos = Position − anchors(j).LEDs
            force = (mag(deltaPos) − VLP_Distances(j)) ∗ anchors(j).weights
            netForce = netForce − 1 ∗ (deltaPos/mag(deltaPos)) ∗ force
        end for
        Position = Position + netForce ∗ stepSize
        if mag(NetForce) < 0.01 then          ▷ If convergence reached then return early
            break
        end if
    end for
    Return Position
end procedure
```

It is assumed that when a Smart Light is switched off, the luminaire is switched off but the radio resource remains available.

The laboratory area was split into 6 contiguous cells of 0.9m x 0.9m to define the test area. The Hallway was split into 8 contiguous cells with an average cell size of 0.9m x 2.4m. The test layouts can be seen in Fig. 6.

A summary of the Experimental Results can be found in Table 4.

A. EXPERIMENT 1 – LABORATORY – LIGHTS ON

In an ideal environment where the luminaries have good spatial separation across 2 axes, VLP localization can provide much higher accuracy than RF based active tracking. The Falcon system uses the RF resource to define a region of interest. The region of interest is passed to the FVLP section which uses the VLP information to converge towards a refined position estimate.

The target traversed from one side of the room to another, passing under a table (where LOS to the luminaires was lost) in the process. The system was 100% accurate at detecting whether the target was underneath the table (and thus using RF tracking) or within an unobstructed area (using VLP). This translated to a real world error of less than 0.4m (cell level) when the lighting was completely occluded by the table. The system attained an average error of 0.12m for the rest of the room. It should be noted that the system was able to achieve a similar level of accuracy when partially occluded (only two luminaires visible when the tag is partially under the table) and when all luminaires were visible.

B. EXPERIMENT 2 – LABORATORY – LIGHTS OFF

When the lights are off the localization is estimated solely by the RF section. The CNN had a cell level accuracy of 99.92% during training. During the live period, the CNN was asked to classify live data based on the trained network. The target was positioned in 26 test locations within the laboratory, with 800 samples taken per location. The live samples were turned into RSSI 'images' in the same way as the training samples. The system could correctly classify which 0.9m^2 cell the target was in during the live phase with 99.59% accuracy.

C. EXPERIMENT 3 –HALLWAY – LIGHTS ON

In the hallway the luminaires are aligned in a single row. Traditional VLP will not function as trilateration schemes will not resolve due to the system only having information from one axis. It should be noted that VLP fingerprinting methods could also resolve this, but would require significant offline training to attain decimeter level accuracy.

To rectify this convergence issue, we first used the RF localization to determine a cell of interest. The center point of the chosen cell is then used as the initial position state estimate for the FVLP algorithm. As shown by Table 3, we were able to attain an average error of 0.09m, and a maximum error of 0.16m, as the system can correctly converge when initialized with a course localization estimate.

D. EXPERIMENT 4 –HALLWAY – LIGHTS OFF

During the live phase the target was randomly positioned 10 times with 800 samples taken per position. It was also ensured that at least one position was taken within each of the 8 cells. Both the trained CNN and live CNN classification had 100% accuracy. We attribute this localization improvement to the fact that the average cell size (2.16m^2) was larger than the laboratory (0.9m^2) and that the hallway was much less cluttered than the laboratory, reducing the effects of multipath.

TABLE IV

EXPERIMENTAL RESULTS

Experiment	Accuracy	Max Error
Experiment 1	0.12 average error	0.4m when completely obscured by table
Experiment 2	99.59% cell classification	NA
Experiment 3	0.09 average error	0.16m
Experiment 4	100% cell classification	NA

E. CONVERGENCE

Typical trilateration schemes fail when the anchors are row aligned as there are multiple solutions. In Fig. 8a this can be represented by the two red circles closest to the cluster centers which represent the two possible (mirrored) solutions.

The FVLP Potential Fields localization method has five possible locations of convergence as shown by all five red circles in Fig. 7a. FVLP has more regions of convergence than traditional trilateration because the dynamic weighting method used allows for the springs to have a net force of zero even if the current position estimate is not along the radial distances. The complete Falcon solution solves this by passing a cell center reference from the CNN implementation. The center of each cell (cluster) is represented by an 'X' in Fig. 7a. By passing the correct cluster center as an initial starting condition, the FVLP approach will converge towards the closest convergence candidate, which will always be the correct solution. This allows for the Falcon approach to correctly converge even if only two VLP anchors are visible. It also works when only one anchor is visible as the visible anchor will pull the coarse RF estimate towards a region of interest which will always offer higher accuracy than solely using the RF cell of interest.

Sensor fusion has been extensively studied in the literature and several common pitfalls have been identified [69]. In particular, the issue of poor performance due to incorrect sensor information is a valid concern. In Falcon we can identify 3 areas where performance may suffer; line of sight obstructions between the VLP receiver and ceiling mounted luminaries, multipath obstructions within the RF environment, and total loss of VLP information (e.g. the lights are switched off). Falcon has been implemented in a way that though these situations will cause performance degradation, the chance of critical failure is minimized.

The proposed FVLP approach has several features that facilitate its robustness. Namely, it runs in real time continuously during the online phase. It can identify sudden unexpected changes in VLP signal quality and react appropriately. In the case of complete VLP signal loss it can fall back to an RF based coarse position estimate.

If line of sight is lost between the VLP receiver and corresponding luminaire, sudden unexpected change in received power will result in a reduction of the weight/trust assigned to that link distance estimate. If two luminaries remain within sight of the receiver, the position estimate should not be affected. The trust/weight will be restored to the lost link when it reports a reasonable distance correlating with the remaining links. This means that performance is only reduced when only one luminaire is visible. The system's accuracy will still be higher than what can be achieved through the sole utilization of the RF section.

In case of an RF failure due to a miss classification from the neural-net, the final position estimate will be largely unaffected. This is due to the fact that Falcon is primarily reliant on VLP for localization. For example, consider a situation where the location reported by the FVLP system indicates that it is heading towards a region of uncertainty within the environment (row aligned lights in a hallway). At such a time, the system will start to add more weight to the RF measurement to ensure it correctly tracks through the region. The boundaries of the RF cells can be used as the regions of uncertainty. This means that once the system has a lock on where the target is, transient interference, even if it causes significant misclassification of cell position, does not significantly degrade the overall performance of the system.

In the extreme case where no luminaires are visible or the lights are turned off completely, the system can fall back to an RF based approach. This has no impact on the accuracy of the RF section.

In the worst case scenario where the lights are turned off and there is significant interference affecting wireless propagation, Falcon will fail to function. However, it should be noted that in these situations, standalone VLP or RF Localization systems would also fail.

V. CONCLUSION & FUTURE WORKS

Falcon has shown that fusing a RF RSSI localization system with VLP can increase the robustness and performance in real life scenarios. In the hallway, a traditional trilateration based localization approach was impossible as the lights only provided information along one axis. By using the collocated RF resource to infer a region of interest, a horizontal displacement offset could be achieved. The VLP system used the displacement offset information provided as a secondary axis to attain sub decimeter level accuracy in that scenario. The wireless localization capability also keeps the system functional when the lights are off or there is occlusion.

The CNN for the RF data only focused on a stationary target at given locations. RSSI data for moving targets could be recorded and incorporated as a second channel to the CNN input image. The Falcon RF Classification stage uses the unique cell ID as the output. Sub cell RF localization could potentially be obtained by using the probabilities for each cell rather than the final cell id. By using the probabilities as weights, trilateration could be performed between the high probability cells to attain sub-cell resolution. Another option would be to explore different wireless localization approaches such as using SVM, particle filters or the Bayesian methodology.

A dynamic calibration scheme could be developed to check the accuracy of the RF classification vs the VLP, and to periodically retrain the CNN to ensure the accuracy remained acceptable.

The Falcon transmitter and receiver were kept in parallel. Receiver rotation due to the movement of the target would introduce error to the Lambertian model. Further development is required to measure the device rotation as it is being tracked and calibrate the model accordingly.

The experiments were conducted in the evening to avoid people walking through the target area. Therefore, the receiver did not need to mitigate the effect of ambient light as it was not strong enough to saturate the receiver. Further work will explore using variable gain amplifiers to allow the system to work under all lighting conditions.

REFERENCES

[1] M. Seifeldin, A. Saeed, A. E. Kosba, A. El-Keyi, and M. Youssef, "Nuzzer: A Large-Scale Device-Free Passive Localization System for Wireless Environments," (in English), *Ieee Transactions on Mobile Computing,* vol. 12, no. 7, pp. 1321-1334, Jul 2013.

[2] *AS/NZS 1680.2.1:2008*. Available: https://shop.standards.govt.nz/catalog/1680.2.1%3A2008%28AS%7CNZS%29/view

[3] X. Guo, S. Shao, N. Ansari, and A. Khreishah, "Indoor Localization Using Visible Light Via Fusion of Multiple Classifiers," *IEEE Photonics Journal,* vol. 9, no. 6, pp. 1-16, 2017.

[4] P. H. Pathak, X. T. Feng, P. F. Hu, and P. Mohapatra, "Visible Light Communication, Networking, and Sensing: A Survey, Potential and Challenges," (in English), *Ieee Communications Surveys and Tutorials,* vol. 17, no. 4, pp. 2047-2077, 2015.

[5] D. Konings, B. Parr, C. Waddell, F. Alam, K. M. Arif, and E. M-K Lai, "HVLP: Hybrid Visible Light Positioning of a Mobile Robot," in *Mechatronics and Machine Vision in Practice (M2VIP), 2017 24th International Conference*, 2017: IEEE.

[6] J. Guang-yao, L. Xiao-yi, and P. Myong-Soon, "An indoor localization mechanism using active RFID tag," in *IEEE International Conference on Sensor Networks, Ubiquitous, and Trustworthy Computing (SUTC'06)*, 2006, vol. 1, p. 4 pp.

[7] D. Konings, A. Budel, F. Alam, and F. Noble, "Entity tracking within a Zigbee based smart home," in *Mechatronics and Machine Vision in Practice (M2VIP), 2016 23rd International Conference on*, 2016, pp. 1-6: IEEE.

[8] M. Sugano, T. Kawazoe, Y. Ohta, and M. Murata, *Indoor localization system using RSSI measurement of wireless sensor network based on ZigBee standard*. 2006, pp. 1-6.

[9] C.-N. Huang and C.-T. Chan, "ZigBee-based indoor location system by k-nearest neighbor algorithm with weighted RSSI," *Procedia Computer Science,* vol. 5, pp. 58-65, 2011/01/01 2011.

[10] A. S. Paul and E. A. Wan, "RSSI-Based Indoor Localization and Tracking Using Sigma-Point Kalman Smoothers," (in English), *Ieee Journal of Selected Topics in Signal Processing,* vol. 3, no. 5, pp. 860-873, Oct 2009.

[11] L. Zhao, H. Wang, P. Li, and J. Liu, "An improved WiFi indoor localization method combining channel state information and received signal strength," in *2017 36th Chinese Control Conference (CCC)*, 2017, pp. 8964-8969.

[12] M. Altini, D. Brunelli, E. Farella, and L. Benini, "Bluetooth indoor localization with multiple neural networks," in *IEEE 5th International Symposium on Wireless Pervasive Computing 2010*, 2010, pp. 295-300.

[13] Y. Wang, Q. Ye, J. Cheng, and L. Wang, "RSSI-Based Bluetooth Indoor Localization," in *2015 11th International Conference on Mobile Ad-hoc and Sensor Networks (MSN)*, 2015, pp. 165-171.

[14] D. Konings, N. Faulkner, F. Alam, F. Noble, and E. M-K Lai, "Do RSSI values reliably map to RSS in a localization system?," in *Recent Trends in Telecommunications Research (RTTR), Workshop on*, 2017, pp. 1-5: IEEE.

[15] S. Adler, S. Schmitt, and M. Kyas, "Path loss and multipath effects in a real world indoor localization scenario," in *2014 11th Workshop on Positioning, Navigation and Communication (WPNC)*, 2014, pp. 1-7.

[16] D. Konings, N. Faulkner, F. Alam, F. Noble, and E. M-K Lai, "Does Interference Affect The RSSI Values of a ZigBee Based Indoor Localization System?," in *Mechatronics and Machine Vision in Practice (M2VIP), 2017 24th International Conference*, 2017: IEEE.

[17] Y.-S. Kuo, P. Pannuto, K.-J. Hsiao, and P. Dutta, "Luxapose," presented at the Proceedings of the 20th annual international conference on Mobile computing and networking - MobiCom '14, Maui, Hawaii, USA, 2014.

[18] L. Li, P. Hu, C. Peng, G. Shen, and F. Zhao, "Epsilon: A Visible Light Based Positioning System," in *NSDI*, 2014, pp. 331-343.

[19] J. Yang and Y. Chen, "Indoor Localization Using Improved RSS-Based Lateration Methods," in *GLOBECOM 2009 - 2009 IEEE Global Telecommunications Conference*, 2009, pp. 1-6.

[20] S. Mazuelas *et al.*, *Robust Indoor Positioning Provided by Real-Time RSSI Values in Unmodified WLAN Networks*. 2009, pp. 821-831.

[21] J. Xu, J. S. He, Y. Q. Zhang, F. Xu, and F. B. Cai, "A Distance-Based Maximum Likelihood Estimation Method for Sensor Localization in Wireless Sensor Networks," (in English), *International Journal of Distributed Sensor Networks,* vol. 12, no. 4, p. 2080536, 2016/04/19 2016.

[22] J. So, J.-Y. Lee, C.-H. Yoon, and H. Park, "An improved location estimation method for Wifi fingerprint-based indoor localization," *International Journal of Software Engineering and Its Applications,* vol. 7, no. 3, pp. 77-86, 2013.

[23] V. Honkavirta, T. Perala, S. Ali-Loytty, and R. Piche, "A comparative survey of WLAN location fingerprinting methods," in *2009 6th Workshop on Positioning, Navigation and Communication*, 2009, pp. 243-251.

[24] N. Pirzada, M. Y. Nayan, F. Subhan, M. F. Hassan, and M. A. Khan, "Comparative Analysis of Active and Passive Indoor Localization Systems," (in English), *2013 Aasri Conference on Parallel and Distributed Computing and Systems,* vol. 5, pp. 92-97, 2013/01/01 2013.

[25] W. Ruan, Q. Z. Sheng, L. Yao, T. Gu, M. Ruta, and L. Shangguan, "Device-free indoor localization and tracking through Human-Object Interactions," in *2016 IEEE 17th International Symposium on A World of Wireless, Mobile and Multimedia Networks (WoWMoM)*, 2016, pp. 1-9.

[26] G. Deak, J. Condell, D. Deak, and K. Curran, "Detection of multi-occupancy using device-free passive localisation," *IET Wireless Sensor Systems,* vol. 4, no. 3, pp. 130-137, 2014.

[27] S. H. Fang and T. N. Lin, "Indoor location system based on discriminant-adaptive neural network in IEEE 802.11 environments," *IEEE Trans Neural Netw,* vol. 19, no. 11, pp. 1973-8, Nov 2008.

[28] P. Cassarà, F. Potortì, P. Barsocchi, and M. Girolami, "Choosing an RSS device-free localization algorithm for Ambient Assisted Living," in *2015 International Conference on Indoor Positioning and Indoor Navigation (IPIN)*, 2015, pp. 1-8.

[29] H. Liu, H. Darabi, P. Banerjee, and J. Liu, "Survey of wireless indoor positioning techniques and systems," (in English), *Ieee Transactions on Systems Man and Cybernetics Part C-Applications and Reviews,* vol. 37, no. 6, pp. 1067-1080, Nov 2007.

[30] J. Drake, D. Najewicz, and W. Watts, "Energy Efficiency Comparisons of Wireless Communication Technology Options for Smart Grid Enabled Devices," General Electric Company2010, Available: https://energypriorities.com/library/ge_zigbee_vs_wifi_101209.pdf.

[31] R. Challoo, A. Oladeinde, N. Yilmazer, S. Ozcelik, and L. Challoo, "An Overview and Assessment of Wireless Technologies and Co- existence of ZigBee, Bluetooth and Wi-Fi Devices," *Procedia Computer Science,* vol. 12, pp. 386-391, 2012/01/01/ 2012.

[32] K. Shuaib, M. Boulmalf, F. Sallabi, and A. Lakas, "Co-existence of Zigbee and WLAN, A Performance Study," in *2006 Wireless Telecommunications Symposium*, 2006, pp. 1-6.

[33] Z. Yang, Z. Zhou, and Y. Liu, "From RSSI to CSI: Indoor localization via channel response," *ACM Comput. Surv.,* vol. 46, no. 2, pp. 1-32, 2013.

[34] K. Wu, J. Xiao, Y. Yi, D. Chen, X. Luo, and L. M. Ni, "CSI-Based Indoor Localization," *IEEE Transactions on Parallel and Distributed Systems,* vol. 24, no. 7, pp. 1300-1309, 2013.

[35] D. Halperin, W. Hu, A. Sheth, and D. Wetherall, "Tool release: gathering 802.11n traces with channel state information," *SIGCOMM Comput. Commun. Rev.,* vol. 41, no. 1, pp. 53-53, 2011.

[36] Y. Xie, Z. Li, and M. Li, "Precise Power Delay Profiling with Commodity WiFi," presented at the Proceedings of the 21st Annual International Conference on Mobile Computing and Networking, Paris, France, 2015.

[37] S. M. Yiu, M. Dashti, H. Claussen, and F. Perez-Cruz, "Wireless RSSI fingerprinting localization," (in English), *Signal Processing,* vol. 131, pp. 235-244, Feb 2017.

[38] Z. P. Li, M. Jiang, X. N. Zhang, X. Y. Chen, and W. K. Hou, "Space-Time-Multiplexed Multi-Image Visible Light Positioning System Exploiting Pseudo-Miller-Coding for Smart Phones," (in English), *Ieee Transactions on Wireless Communications,* vol. 16, no. 12, pp. 8261-8274, Dec 2017.

[39] L. B. Zeng *et al.*, "High Data Rate Multiple Input Multiple Output (MIMO) Optical Wireless Communications Using White LED Lighting," (in English), *Ieee Journal on Selected Areas in Communications,* vol. 27, no. 9, pp. 1654-1662, Dec 2009.

[40] Y. Cai, W. P. Guan, Y. X. Wu, C. Y. Xie, Y. R. Chen, and L. T. Fang, "Indoor High Precision Three-Dimensional Positioning System Based on Visible Light Communication Using Particle Swarm Optimization," (in English), *Ieee Photonics Journal,* vol. 9, no. 6, pp. 1-20, Dec 2017.

[41] T. Q. Wang, Y. A. Sekercioglu, A. Neild, and J. Armstrong, "Position Accuracy of Time-of-Arrival Based Ranging Using Visible Light With Application in Indoor Localization Systems," (in English), *Journal of Lightwave Technology,* vol. 31, no. 20, pp. 3302-3308, Oct 15 2013.

[42] T. H. Do and M. Yoo, "TDOA-based indoor positioning using visible light," (in English), *Photonic Network Communications,* vol. 27, no. 2, pp. 80-88, Apr 2014.

[43] S. Y. Jung, S. Hann, and C. S. Park, "TDOA-Based Optical Wireless Indoor Localization Using LED Ceiling Lamps," (in English), *Ieee Transactions on Consumer Electronics,* vol. 57, no. 4, pp. 1592-1597, Nov 2011.

[44] G. B. Prince and T. D. C. Little, "A two phase hybrid RSS/AoA algorithm for indoor device localization using visible light," in *2012 IEEE Global Communications Conference (GLOBECOM)*, 2012, pp. 3347-3352.

[45] Y. S. Eroglu, I. Guvenc, N. Pala, and M. Yuksel, "AOA-based localization and tracking in multi-element VLC systems," in *2015 IEEE 16th Annual Wireless and Microwave Technology Conference (WAMICON)*, 2015, pp. 1-5.

[46] Z. Tian, K. Wright, and X. Zhou, "The darklight rises: visible light communication in the dark," presented at the Proceedings of the 22nd Annual International Conference on Mobile Computing and Networking - MobiCom '16, New York City, New York, 2016.

[47] X. Zhao and J. Lin, "Theoretical Limits Analysis of Indoor Positioning System Using Visible Light and Image Sensor," *ETRI Journal,* vol. 38, no. 3, pp. 560-567, 2016.

[48] K. Qiu, F. Zhang, and M. Liu, "Visible Light Communication-based indoor localization using Gaussian Process," in *2015 IEEE/RSJ International Conference on Intelligent Robots and Systems (IROS)*, 2015, pp. 3125-3130.

[49] K. Moriya, M. Fujimoto, Y. Arakawa, and K. Yasumoto, "Indoor localization based on distance-illuminance model and active control of lighting devices," in *2016 International Conference on Indoor Positioning and Indoor Navigation (IPIN)*, 2016, pp. 1-6.

[50] H. Zou, Z. Chen, H. Jiang, L. Xie, and C. Spanos, "Accurate indoor localization and tracking using mobile phone inertial sensors, WiFi and iBeacon," in *2017 IEEE International Symposium on Inertial Sensors and Systems (INERTIAL)*, 2017, pp. 1-4.

[51] Y. Li, J. Chen, Y. Shi, Y. Cheng, and L. Wang, "WiFi-assisted multi-floor indoor localization with inertial sensors," in *2016 8th International Conference on Wireless Communications & Signal Processing (WCSP)*, 2016, pp. 1-5.

[52] J. L. Carrera, Z. Zhao, T. Braun, and Z. Li, "A real-time indoor tracking system by fusing inertial sensor, radio signal and floor plan," in *2016 International Conference on Indoor Positioning and Indoor Navigation (IPIN)*, 2016, pp. 1-8.

[53] L. Buonocore, S. R. B. d. Santos, A. A. Neto, and C. L. Nascimento, "FastSLAM filter implementation for indoor autonomous robot," in *2016 IEEE Intelligent Vehicles Symposium (IV)*, 2016, pp. 484-489.

[54] B. Vincke, A. Elouardi, and A. Lambert, "Real time simultaneous localization and mapping: towards low-cost multiprocessor embedded systems," *EURASIP Journal on Embedded Systems,* journal article vol. 2012, no. 1, p. 5, July 18 2012.

[55] J. Vazquez and C. Malcolm, *Fusion of triangulated sonar plus infrared sensing for localization and mapping*. 2005, pp. 1097-1102 Vol. 2.

[56] J. Schmidhuber, "Deep learning in neural networks: an overview," *Neural Netw,* vol. 61, no. Supplement C, pp. 85-117, Jan 2015.

[57] D. Han, S.-h. Jung, and S. Lee, "A sensor fusion method for Wi-Fi-based indoor positioning," *ICT Express,* vol. 2, no. 2, pp. 71-74, 2016/06/01/ 2016.

[58] Z. Yang, C. Wu, and Y. Liu, "Locating in fingerprint space: wireless indoor localization with little human intervention," presented at the Proceedings of the 18th annual international conference on Mobile computing and networking, Istanbul, Turkey, 2012.

[59] Y. Wang and X. Xu, "Indoor Localization Service Based on the Data Fusion of Wi-Fi and RFID," in *2016 IEEE International Conference on Web Services (ICWS)*, 2016, pp. 180-187.

[60] R. Zhang, W. D. Zhong, D. Wu, and K. Qian, "A Novel Sensor Fusion Based Indoor Visible Light Positioning System," in *2016 IEEE Globecom Workshops (GC Wkshps)*, 2016, pp. 1-6.

[61] B. Xie *et al.*, "LIPS: A Light Intensity--Based Positioning System for Indoor Environments," *ACM Trans. Sen. Netw.,* vol. 12, no. 4, pp. 1-27, 2016.

[62] M. Yasir, S. W. Ho, and B. N. Vellambi, "Indoor Positioning System Using Visible Light and Accelerometer," (in English), *Journal of Lightwave Technology,* vol. 32, no. 19, pp. 3306-3316, Oct 1 2014.

[63] S. H. Yang, H. S. Kim, Y. H. Son, and S. K. Han, "Three-Dimensional Visible Light Indoor Localization Using AOA and RSS With Multiple Optical Receivers," *Journal of Lightwave Technology,* vol. 32, no. 14, pp. 2480-2485, 2014.

[64] J. M. Kahn and J. R. Barry, "Wireless infrared communications," *Proceedings of the IEEE,* vol. 85, no. 2, pp. 265-298, 1997.

[65] B. Lehman and A. J. Wilkins, "Designing to Mitigate Effects of Flicker in LED Lighting: Reducing risks to health and safety," *IEEE Power Electronics Magazine,* vol. 1, no. 3, pp. 18-26, 2014.

[66] S. N. He and S. H. G. Chan, "Wi-Fi Fingerprint-Based Indoor Positioning: Recent Advances and Comparisons," (in English), *Ieee Communications Surveys and Tutorials,* vol. 18, no. 1, pp. 466-490, 2016.

[67] J. Borenstein and Y. Koren, "Real-Time Obstacle Avoidance for Fast Mobile Robots," (in English), *Ieee Transactions on Systems Man and Cybernetics,* vol. 19, no. 5, pp. 1179-1187, Sep-Oct 1989.

[68] J. Barraquand, B. Langlois, and J. C. Latombe, "Numerical Potential-Field Techniques for Robot Path Planning," (in English), *Ieee Transactions on Systems Man and Cybernetics,* vol. 22, no. 2, pp. 224-241, Mar-Apr 1992.

[69] D. Hall and A. Steinberg, *Dirty Secrets in Multisensor Data Fusion*. 2001.

Chapter 2

This chapter contains content from the following article, republished with permission. In accordance with IEEE's republishing policy, any full text that has been included is the unmodified accepted article. This means that while the content is identical to the published article, there may be stylistic differences.

Device-free Localization Systems Utilizing Wireless RSSI: A Comparative Practical Investigation

Daniel Konings, *Student Member, IEEE,* Fakhrul Alam, *Member, IEEE,* Frazer Noble, and Edmund M-K Lai, *Senior Member, IEEE*

***Abstract*—Device-free localization (DFL) systems that rely on the wireless received signal strength indicator (RSSI) metric to localize targets with no device attached to them have been reported in the literature for almost a decade. Approaches using RSSI can be split into three main categories. Link-based approaches utilize weighted summation or probabilistic methods to infer location. Location-based approaches create a fingerprint map of an area. Radio Tomographic Imaging treat DFL as an imaging problem solved with a linear inverse. In this article, we implement and investigate the performance of all three major RSSI approaches in two test environments. We demonstrate how different environments and walking trajectories can have significant effects on the localization accuracy. The experimental results lead us to the conclusion that without implementing and testing within the same environment for the same target trajectories, the performance of various classes of DFL systems cannot be reliably evaluated. Relying on the stated accuracy from the literature for comparison is a flawed premise.**

***Index Terms*—Device-free Localization (DFL), Indoor Positioning Systems (IPS).**

I. Introduction

THE widespread adoption of wireless technology and growing popularity of the Internet of Things (IoT) have led to increased interest in indoor localization technologies. Indoor Positioning Systems (IPS) have potential application in a diverse range of fields, including assisted living [1], office monitoring [3], multi-subject counting/tracking [5], [6], hostage negotiation [7], human-robot interaction [8] and smart homes [9]. Indoor localization implementations can either be Device-based or Device-free. Device-based systems work by localizing a tag that is attached to the tracked entity. Device-free localization (DFL) does not require the tracked entity to carry any form of tag. Wireless DFL systems work by measuring the changes a tracked entity causes on wireless links within an environment, and use those to infer the location of the target. While DFL systems can be implemented using Radio Frequency (RF) [1]–[7], [9]–[12], or other approaches, such as visible light [13], in this paper we only focus on RF based implementations using the Received Signal Strength Indicator (RSSI).

This work was supported in part by the Massey University Research Fund (MURF) and the Massey University Doctoral Scholarships.

D. Konings, F. Alam and F. Noble are with the School of Engineering and Advanced Technology, Massey University, Auckland, NZ, corresponding e-mail: d.konings@massey.ac.nz.

E. M-K. Lai is with the School of Engineering, Computer and Mathematical Sciences, Auckland University of Technology, Auckland, NZ.

Manuscript received April XX, 2018; revised August XX, 2018.

RSSI is the most popular metric for localization as it is implemented in many mainstream wireless technologies (Wi-Fi, Zigbee, Bluetooth) and is commonly available in commercial-off-the-shelf (COTS) equipment. This is very important as implementations within a standard built environment would likely require multiple devices, which makes cost and the ability to integrate with and/or utilize existing infrastructure extremely important. The RSSI metric is also immune to the effects of interference, though the networks packet reception ratio (PRR) may be affected [14]. Since the PRR would only effect system latency and not overall system accuracy, Wi-Fi interference is not a major concern in this paper. However, a major limitation of RSSI is its vulnerability to multipath. Since the RSSI is a non-coherent metric with no phase information, it is unable to resolve multipath components. This limits its suitability for indoor ranging approaches as multiple locations may share the same RSSI value over a LOS link path [15]. Other limitations include large variance between successive RSSI values and varying receiver sensitivity [16]. Variations between different chipsets have also been observed [17]. Channel State Information (CSI) values have a significantly higher resolution than RSSI values and are more immune to the adverse effects of multipath [15], [18], [19]. However among COTS devices, CSI is only available on a few Atheros [20] and Intel [21] devices using modified drivers. Another problem with wireless based localization is the issue of secure localization. Both RSSI and CSI approaches assume that the senders MAC address reported by a packet is authentic. This makes it possible for a malicious entity to cause the system to report incorrect position estimates. This can also be exploited to attain location-based information from users. Recent literature suggests these may be mitigated through utilizing new network architectures [22], or utilizing cloaking areas [23]. However, wireless technologies are inherently vulnerable due to the broadcast nature of propagation and thus localization systems based on them are vulnerable to privacy exploitation. Recently, anonymous authentication protocols have been developed to resolve this problem for RFID systems [24], which may lead to breakthroughs for COTS equipment.

Device-free wireless positioning systems utilizing RSSI can be implemented on any platform that uses that (RSSI) metric. We chose to use Zigbee radios as they are prevalent within smart home applications and hence justify device-free localization as a secondary service. Wi-Fi nodes could also be utilized provided there was sufficient node density. In order to be commercially attractive, device-free localization should be a secondary service, where the primary service of the network

TABLE I
RTI IMPLEMENTATIONS

Features	Through-wall	Online Calibration	Stationary Target	Channel Diversity	Antenna Selection	Major Contribution
RTI	No	No	Yes	No	No	Formulated DFL as a regularized linear equation, with the output as an image [12].
VRTI	Yes	No	No	No	No	Enabled better tracking of moving targets and through wall imaging [36].
SubVRT	Yes	No	No	No	No	Reduce localization errors occurring due to intrinsic motion which cannot be removed from the environment [37].
CDRTI	Yes	No	Yes	Yes	Yes	Accuracy of through wall attenuation based DFL improved by switching the channel of measurement based on either the packet reception ratio (PRR) or the channels fade level [38].
dRTI	Yes	Optional	Yes	No	Yes	Directional antennas provide better localization accuracy in both attenuation based and variance based RTI schemes [39].
ARTI	Yes	Yes	Yes	Optional	No	Presented a spatial model that can retrain itself using live unlabeled data [40].
KRTI	Yes	Yes	Yes	Optional	No	Can localize moving and stationary targets, works through walls and requires less nodes than previous RTI efforts [7], [41].

would be to provide data communication, sensing etc. While other technologies can potentially provide a higher level of accuracy, they are often prohibitively expensive for consumer smart homes.

DFL implementations using RSSI can be divided into three categories: region-based approaches, link-based approaches and Radio Tomographic Imaging (RTI). In region-based approaches, RSSI information is collected from multiple links and associated with a specific location within the target area. These algorithms are often defined as fingerprinting approaches as they collect offline data before localization begins, and attempt to compare it with live data during the localization process [2], [6], [25], [26]. In link-based approaches, the system attempts to either model a tracked entity's effect on specific links which can be used to infer location [9], or use a probabilistic method to maximize the expected region of interest, for a given entity [3], [27]. RTI [12] approaches assume that the magnitude of change caused by a person near a link can be modelled by an ellipsoid formed along the line-of-sight (LOS) link path, and that location can be estimated by solving the inverse of a linear equation.

A. Contribution

The literature lacks an apple-to-apple comparison of DFL schemes across the three major techniques. Most works test their algorithm within their own test environment, benchmarking it against previous works of a similar type. For example, a reported work on RTI compares the developed system against an RTI based system. It also holds true for a fingerprint-based work. As far as the authors are aware of, no work compares the performances of DFL systems across all three major approaches based on a common physical implementation with multiple trajectories. Cassara et al performed a good comparison in [1]. However, out of the three algorithms tested, two were from RTI and they did not provide a comparison between all three major approaches. They also did not consider varying human trajectories, which we show have a significant impact on tracking accuracy.

Survey papers have compared the *stated* accuracy of DFL techniques [10], [28]–[30]. They try to compare tests by stating the size of the test area, protocol and number of nodes used. However, they incorrectly assume that algorithms from different works are environment agnostic, and do not implement the DFL systems themselves. Thus, they are unable to provide a true comparison of existing work. We demonstrate that the environment has significant impact on the performance of the localization algorithms by providing experimental results from multiple algorithms in contrasting indoor environments which show significant inconsistencies in localization and tracking accuracy.

Another area that has been overlooked is the potential for real-world implementation. If DFL technology is to become a standard part of a built environment installation, it must be incorporated into and operate alongside existing smart devices, in real-time and with a low node density. Commercial DFL solutions are not readily available at present. A standard 2 story home with a ground floor area of approximately 140m2 would require more than 30 nodes for reasonable performance using the commercial solution from [31]. This also assumes that the home has that many available power sockets with spatial separation around the home, which is unrealistic for many smart homes. Fair algorithm comparisons have also been hindered by the lack of a standardized performance metric. The EvAAL framework has been proposed to ensure fair comparison of multiple algorithms within a physical test environment [32]. However, the EvAAL framework was primarily designed for use in active tracking solutions. EvAAL uses the 75^{th} percentile Euclidean error as their accuracy score. This does not provide enough information about the difference between the average errors and maximum errors to choose an appropriate implementation candidate. The first known formal attempt to standardize IPS systems is the ISO/IEC 18305:2016 International Standard [33], which defines a framework for testing and evaluating IPS systems. It proposes several accuracy score metrics based on the Root-Mean-Square-Error (RMSE), median 2D error (termed as Circular Error Probable),

TABLE II
FINGERPRINT IMPLEMENTATIONS

Features	Through-wall	Stationary Target	Multiple Targets	Calibration Required	Cycle Duration	Major Contribution
Nuzzer	Yes	Yes	Yes	High	Low	Defines the DFL problem in terms of a discrete space estimator followed by a continuous space estimator [4].
SCPL	Yes	Yes	Yes	Medium	High	Adopts a novel sequential counting strategy followed by classification (LDA), a conditional random field (CRF) as a geometric filter and Viterbi tracking for probabilistic pathing [6].
ACE	Yes	Yes	Yes	High	Low	Incorporates a novel fingerprinting approach which is followed by an energy minimization framework for localization, and a second order Hidden Markov Model to track multiple targets [5].
GL-FDFL	Yes	Yes	No	Medium	Unknown	Uses a probabilistic localization approach coupled with an improvement strategy which limits the number of cell estimates based on the significance and location of shadowed links [2]

and the 95^{th} percentile 2D error (termed as Circular Error 95%). There are two fundamental issues with the ISO/IEC 18305 standard when applying it to DFL. Firstly, it provides no explicit provisions for DFL techniques. Secondly, Circular Error Probable (CEP) and Circular Error 95% (CE95) are insufficient in describing the whole behavior of each individual approach.

The best-known localization comparison testing is provided by the annual Microsoft Indoor Localization Competition [34], or the Indoor Positioning and Indoor Navigation (IPIN) competition [32]. However they are not ISO/IEC 18305 compliant [35], and are primarily focused on active tracking, and therefore are not useful for benchmarking DFL efforts, or addressing problems that arise in DFL approaches. In commenting on the deficiencies of ISO/IEC 18305, Potortì et al proposes the use of the 50^{th} (CEP), 75^{th}, 90^{th}, and 95^{th} (CE95) percentile errors to allow for easier comparison of two approaches [35]. We believe that this should be extended further and that using empirical Cumulative Distribution Function (CDF) error plots should be standardized, as it allows for algorithm comparison at any percentile level. ISO/IEC 18305 also does not include any accuracy metrics related to the overall trajectory traveled. This is flawed as the subject's trajectory can have a significant impact on the localization error.

This paper seeks to address these gaps by implementing algorithms from multiple DFL approaches and comparing them within a common environment. One representative algorithm from each of the three major approaches were selected based on their accuracy, and likelihood of implementation into existing built environments. This enables us to make credible and fair performance comparisons, appropriately comment on their strengths and limitations, and demonstrate the deficiencies of current evaluation regime and findings of the literature. By testing the implemented DFL's in two indoor environments, this paper contributes the following novel aspects:

1) A true comparison of leading Device free localization schemes from the three major localization approaches.
2) A comparison of multiple walking trajectories within each indoor environment to compare the accuracies and limitations of tracking. This also shows the impact of walking trajectory on the performance of DFL algorithms which has not been considered by others.
3) Propose empirical CDF error plots to be used as an information rich accuracy score in place single statistic like median or percentile errors and support this through experimental findings.
4) A critical analysis on the limitations of current DFL schemes and their suitability for real world implementation.

II. Device-free Localization

A. Fingerprinting

Fingerprinting schemes assume that the influence of an entity on the RSSI values remains relatively constant and time invariant. The system localizes the target based on the best match with the live RSSI values and the ones previously stored. They have the advantage of not requiring knowledge of where the nodes are located. However, they require significant calibration since RSSI values from every possible location of interest must be obtained in advance. Also, the assumption of RSSI remaining time invariant is flawed in practical environments. Any substantial changes to the physical environment, such as moved furniture, significantly changes the global RSSI values, and therefore degrades the systems accuracy.

Fingerprinting approaches typically take two sets of measurements during an offline phase, which are then compared to live values in the online phase for localization purposes. The first offline measurement set typically consists of RSSI values from all links when the environment is empty of entities. The second set typically consists of K batches of N RSSI values from L links; where K is the number of possible locations (cells) an entity can be present within; N is the number of samples per location, and L is the number of recorded TX-RX link pairs. Fingerprinting approaches have the benefit of allowing for fewer nodes, at the cost of a significant calibration effort , as it needs to be recalibrated regularly. As such, they are not applicable to emergency situations, where a system cannot be calibrated beforehand and their usefulness in Smart Homes may be limited as the calibration effort required exceeds the ability of typical consumers. These systems may be ideal for factory installations with fixed physical layouts where the calibration effort can be justified. A summary of the comparable features of fingerprinting based DFL systems can be seen in Table II.

We have chosen to implement SCPL for our fingerprinting localization benchmark. SCPL is well documented and easy to implement while also attaining a very similar CDF error plot when compared to multi-entity ACE [5]. GL-FDFL was not implemented as it did not include a tracking approach.

B. Link-based

Link-based schemes work by using models to analyse link behaviour and trigger the detection of anomalous activity based on predefined thresholds. To simplify localization and tracking, particle filters (also termed as Sequential Monte Carlo) are commonly used as they allow for location estimate to be defined as the centroid of multiple weighted particles within a region of multiple triggered links. A summary of the comparable features of link-based DFL systems can be seen in Table III.

All three link-based methods presented share similarities. Guo et al uses an Exponential-Rayleigh model for a link model [3], in contrast to an exponential model used by Zheng and Men [27]. All three methods implement particle filters, with Ichnaea defining a movement vector for state updates while Zheng and Men model movement as a zero-mean gaussian white noise. We chose to implement Ichnaea's method as it contains a novel way of updating its state orientation motion vector, by referencing the midpoints of changing dominant links, and we wish to investigate its tracking consistency in different environments [9].

C. Radio Tomographic Imaging

Radio Tomographic Imaging (RTI) creates an image of the attenuation caused by physical objects within wireless networks. While RTI analyses the behavior an entity causes on overlapping links, RTI divides up the environment into an image of fixed pixel locations. By solving the inverse of a linear equation, location of the entity can be estimated as the brightest pixel of the output image. RTI has the benefit of not requiring extensive calibration efforts, however it does require knowledge of where the nodes have been positioned. Patwari and Wilson first implemented RTI using the RSSI attenuation as the contributing feature [12]. This worked in wide open spaces, but performs significantly worse in typical indoor environments due to the undue influence of multipath components. RTI has gained wide acceptance in the literature and there have been subsequent improvements. A summary of the features provided by various RTI implementations and the improvement provided can be seen in Table I.

RTI systems can track moving or stationary targets and require minimum offline calibration to operate which makes them ideal for deploying in unknown environments in emergency situations. A major drawback to RTI approaches is that they typically require a large amount of nodes to operate, for relatively small deployment areas, which makes them hard to justify for incorporating into Smart Home equipment. For this paper we chose to implement Kernel RTI (KRTI). RTI does not work well in through wall environments and in complex environments with many multipath components; whereas, KRTI has also been shown to have higher performance than

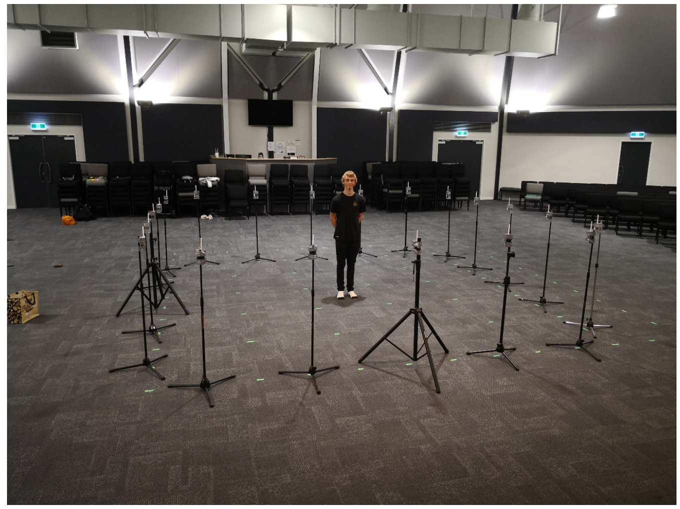

Fig. 1. Auditorium Test Environment.

Varience RTI (VRTI) and Subspace RTI (SubVRT). Channel Diversity RTI (CDRTI) requires more bandwidth than normal RTI as it searches for channels not under deep fade. With the ubiquitous use of wireless technology, and the density of network deployment in urban areas, it is unreasonable to expect that multiple bands can be dedicated to an IPS, especially within commonly used ISM bands. The use of direction antennas makes directional RTI (dRTI) unrealistic for utilization in Smart Homes as it would complicate its incorporation into existing Smart Home devices, and would require a dedicated calibration / placement procedure that may be difficult to follow for an end user. Adaptive RTI (ARTI), which seems very promising, has not been implemented in this paper for several reasons. ARTI's online calibration approach assumes that most affected links will exhibit an attenuation effect from a targets presence. This is problematic as even though most links typically do exhibit an attenuating effect, this cannot be guaranteed in a complex indoor environment.

III. Implementation

The network used for testing was implemented using Texas Instruments CC2530 Zigbee radios on channel 26. A token ring protocol was used where each node would broadcast a packet while all other nodes recorded the RSSI value from it. The broadcast packet from each node contained a list of the last received RSSI value from every other node. This allowed for a Master node to listen in on all network traffic, and to send the RSSI values from all links to a processing computer. The system was set up to run at 5Hz, allowing for 5 RSSI values from all links to be recorded each second. For both experiments, Wi-Fi was disabled to avoid interference [14]. Tests were performed in two contrasting indoor environments. The first environment was an open auditorium where there were no walls or structural pillars within 5m of the test setup as seen in Fig. 1. The second environment consisted of a cluttered university laboratory where there were many objects (e.g. walls, computer monitors, desks and chairs) that could contribute to multipath. A Rohde & Schwarz Spectrum Rider

TABLE III
LINK-BASED IMPLEMENTATIONS

Features	Through-wall	Stationary Target	Multiple Targets	Computational Complexity	Major Contribution
Ichnaea	Yes	Yes	No	High	Monitors a global link score to detect movement within the environment, updates the offline silence profile with online links that do not show considerable variation, then uses a particle filter to track an entity where the motion vector is defined by the current/previously most affected links [9].
Zheng and Men	Yes	Yes	No	High	Models the link behaviour as a Gaussian mixture, use a particle filter to track an entity and update the parameters of the Gaussian mixture model online to ensure the algorithm is robust to environmental changes [27].
Guo et al	Yes	Yes	Yes	High	Introduces an Exponential-Rayleigh model for classifying the effect entities have on TX-RX RSSI links to achieve superior accuracy to traditional magnitude or exponential models. Localization is done through Bayesian inference, with a particle filter used for tracking purposes [3].

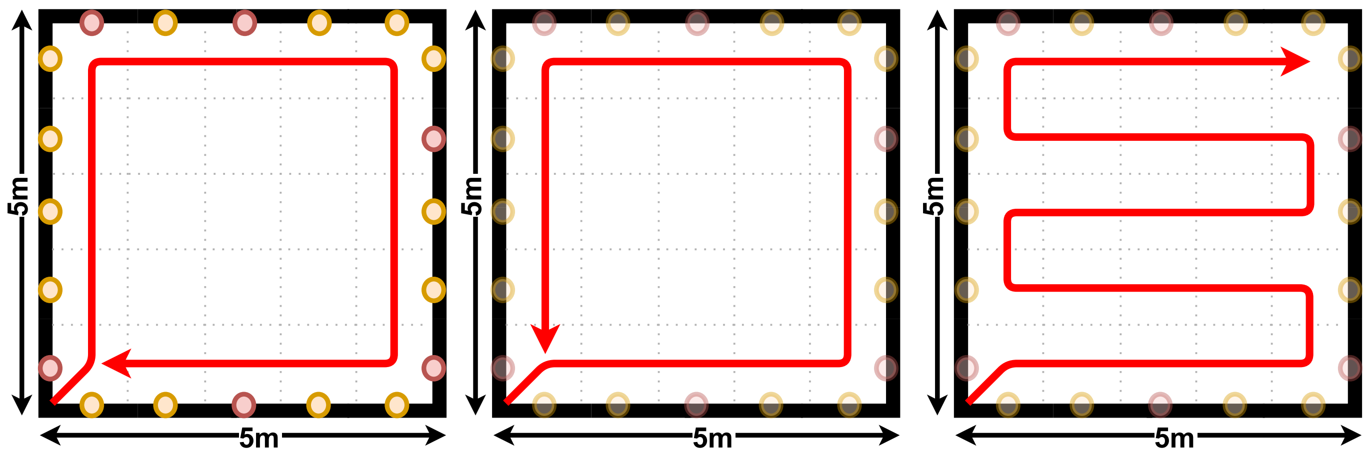

(a) (b) (c)

Fig. 2. Auditorium Walking Trajectories - (a) Clockwise, (b) Anticlockwise; and (c) Zigzag.

FPH spectrum analyser was used in both environments when the experiments were undertaken to ensure that no measurable 2.4GHz interference was present.The nodes were mounted at 1.2m above the ground on stands in the auditorium, and were wall mounted at 1.4m above the ground in the laboratory. The minimum Euclidean distance between deployed nodes was 0.7m in the auditorium and 1.0m in the laboratory. The maximum Euclidean distances were 6.4m and 10.1m respectively. In both environments the subject's were asked to walk following a clockwise, anticlockwise or zigzag trajectory as outlined in Fig. 2 and Fig. 3. Subjects walked in a heel-toe fashion while using a metronome. This ensured that all step sizes remained consistent between tests with the same subject, the walking speed remained constant, and a ground truth could be captured over the course of the trajectory, at any given time. Since homes are not likely to have 20 devices available to cover a small area, for the second sets of tests we reduced the number of nodes to the lowest number of nodes (6) that resulted in consistent performance with the algorithms. The node placement are represented by the small circles in Fig. 2 and Fig. 3. The node placement used for the 6 node tests is marked with red circles. Each set of experiments was repeated three times with at least 30 minutes between each test.

IV. ALGORITHMS

In this section, implementations of KRTI, SCPL and Ichnaea are described [6], [7], [9]. Each algorithms parameters were fine-tuned empirically. For a more in-depth explanation of the algorithms used the reader is urged to read the respective original works.

A. KRTI

A histogram based RTI implementations calculates the difference between histograms calculated for each link to determine whether a specific link is currently affected by the presence of an entity. Assuming RSSI values have the range $1-N$, each histogram is constructed with N bins, where the *N-th* bin value increases as the frequency of recorded RSSI value N increases. A scheme based on an exponentially weighted moving average (EWMA) calculates the histograms as:

$$h^{l,t} = (1-\beta)h^{l,t-1} + \beta\zeta(R^{l,t}) \quad (1)$$

where $h^{l,t}$ is the histogram of length N for link l at time t where each value is between $0-1$; $\beta$is the forgetting factor between $0-1$, which determines the weight put on recent measurements; ζ is an indication vector; and $R^{l,t}$ is the RSSI

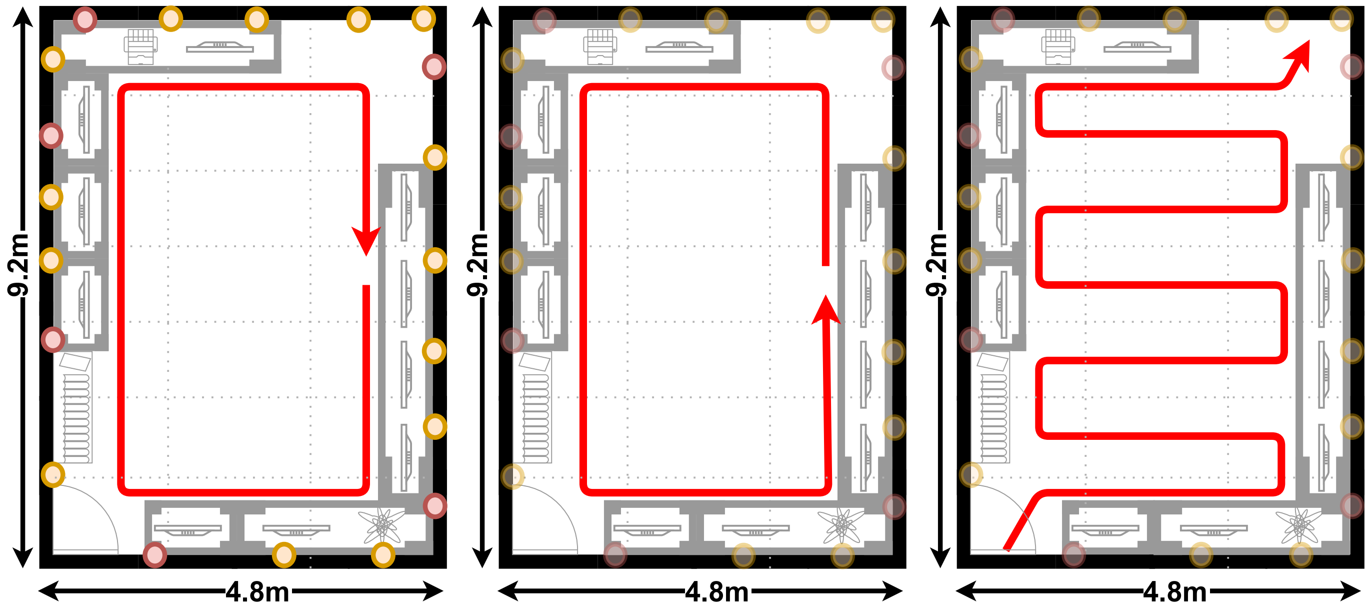

(a) (b) (c)

Fig. 3. Laboratory Walking Trajectories - (a) Clockwise, (b) Anticlockwise; and (c) Zigzag.

of link l at time t. ζ is a vector of length N where the index given by $R^{l,t}$ is 1 and every other position is 0.

If we define the long term histogram as L and the short term histogram as S, where $\beta_L < \beta_S$, then the kernel distance between them can be defined by:

$$D(S, L) = S^T KS + L^T KL - 2S^T KL \tag{2}$$

where K in a N by N kernel matrix and T represents a transpose operation. The Epanechnikov kernel was utilised for this paper [42]. KRTI assumes that the location of a person can be given by the maximum value of the image x, where x can be defined by the vector $x = [x_0, , x_{P-1}]$ and P is the number of pixels. KRTI also assumes that d, the set histograms differences for each link, can be expressed as a linear combination of x:

$$d = Wx + n \tag{3}$$

where n is a noise vector; and W is a weighting model, where $W_{l,p}$ for pixel P is zero unless it is located within an 2D ellipse defined with foci at link l's transmitter and receiver nodes. Since RTI is by nature an ill-posed inverse problem, regularization is used. By utilizing a least squares formulation the image x can be defined by:

$$x = (W^T W + \sigma_n^2 C_x^{-1})^{-1} W^T d \tag{4}$$

where σ_n^2 is the noise variance and C_x is the covariance matrix of x. For tracking, KRTI uses a Kalman filter where the state transition model includes the persons location and velocity, and the observation inputs are provided by the location estimate from x. All the parameter values used for implementing KRTI in both environments are contained in Table IV.

TABLE IV
KRTI PARAMETERS

Parameter	Value	Description
β_S	0.9	Forgetting factor S
β_L	0.05	Forgetting factor L
σ_E^2	30	Epanechnikov kernel width*
σ^2	0.01	Regularization parameter*
δ	1.3	Space parameter*

*Following the process outlined in [7], K in (2) is formulated using σ_E^2, while C_x^{-1} in (4) is formulated using σ^2 and δ.

B. SCPL

Since this paper only focusses on single target tracking, SCPL can be simplified to a classification problem using Linear Discriminant Analysis (LDA), a conditional random field (CRF) and Viterbi tracking [6]. SCPL splits the environment into cells and uses offline RSSI measurement vectors from all links while a person is standing within a cell as a class. By assuming the density of each class c is a multivariate Guassian with mean μ_c and a shared covariance matrix Σ, given an RSSI vector R:

$$f_c(R) = \frac{1}{(2\pi)^{0.5L}|\Sigma|^{0.5}} e^{(-0.5(R-\mu_c)^T \Sigma^{-1}(R-\mu_c)} \tag{5}$$

By applying Bayes rule, the objective function is defined as:

$$y = \underset{c}{\text{argmax}}\, f_c(R)\pi_c \tag{6}$$

The discriminant function in log scale is defined as:

$$\delta_c(R) = R^T \Sigma^{-1} \mu_c - \frac{1}{2}\mu_c^T \Sigma^{-1} \mu_c + \log \pi_c \tag{7}$$

where T represents a transpose operation; and the final cell estimate model is:

$$\begin{aligned} V_c(1) &= \delta_c(R^{t=1}) \\ V_c(t) &= \underset{c}{\operatorname{argmax}}\, V_c(t-1)\delta_c(R^t)M_{c_0,c} \end{aligned} \tag{8}$$

where R^t is a RSSI vector of all links at time t, M is a transition model based on a a 1^{st} order trajectory ring and $M_{c_0,c}$ defines the probability of a transition from state c_0 at $t-1$ to state c at time t. For SCPL the auditorium was split into 25 cells (states), and the laboratory into 21 cells as shown in Fig. 2 and Fig. 3. SCPL was set up to use a 1st order trajectory ring.

C. Ichnaea

Ichnaea works in two phases. The offline phase creates a normal profile for each stream, followed by the monitoring phase where each link is iteratively checked for anomalous behaviour. Links flagged as anomalous are passed to a particle filter which tracks the subject and defines the location estimate as the centroid of the weighted particles.

Ichnaea represents each stream as a density function where:

$$f_j(x) = \frac{1}{h_j}\sum_{i=1}^{n} w_i V\left(\frac{x - x_{j,i}}{h_j}\right) \tag{9}$$

where j, represents a link, n is a set of sliding windows each of length l samples, $x_{j,i}$ is the variance of the RSSI values within a window of length $n+l-1$, h_j is the bandwidth, w is a weight, and V is the kernel function. The motion tracking module is activated if sufficient global activity is detected over a threshold, defined by:

$$G_t = (1-\beta)G_{t-1} + \beta\alpha_t \tag{10}$$

where β is a smoothing coefficient and α_t is a global anomaly score defined by $\alpha_t = \Sigma\alpha_{j,t}$, where:

$$\alpha_{j,t} = \frac{x_{j,t}}{F_j^{-1}(\gamma)} \tag{11}$$

where: $F_j^{-1}(\gamma)$ is the γth percentile of the CDF, of the distribution shown in Equation [9]. The final location of the entity is tracked using a particle filter and can be defined as the centroid of the particles by:

$$p_t = \sum_{i=1}^{N}\left[p_{i,t}\max_j\left(a_{j,t}\frac{d_j}{dAP_{j,i} + dMP_{j,i}}\right)\right] \tag{12}$$

where N is the total number of particles; d_j is the length of stream j; $dAP_{j,i}$ is the length between the particle and the AP, and $dMP_{j,i}$ the length between the particle and the MP. The parameter values for the smoothing coefficient and particle filter implementation were kept the same as in [9].

V. Results

The results were averaged over three iterations of each route taken.

A. Auditorium

This was an ideal open indoor environment, with minimal objects that could cause multipath within the immediate vicinity. However, there were still small dead spots within the test area where all DFL solutions struggled to localize a person correctly. This was surprising, as this experiment had a high node density (one node per 1.25m^2) and there was no interference. The experiments were repeated with the same subjects three times, with a time separation to minimize the risk of radio links remaining in a deep fade for the entire duration of the experiment. If the algorithms cannot correctly track through the dead spots, it takes a while for the tracking to catch up once the subject can be localized correctly again. This behaviour results in strong transient errors getting extended over a longer period than which they occurred within, leading to further degradation to the overall accuracy. The most interesting effect this has on the DFL solutions presented, is that the accuracy of walking clockwise around the environment is not always the same as walking anticlockwise.

Fig. 4 and Fig. 5 show the CDF error plots from the clockwise and anticlockwise routes. KRTI significantly outperforms the other two algorithms when walking clockwise, while Ichnaea performed better on the anticlockwise route. KRTI outperformed both Ichnaea and SCPL in the zigzag route which was the longest and covered the entire test area. Though some of the maximum errors experienced by KRTI exceeded those of Ichnaea.

Reducing the nodes from 20 to 6 in the second set of tests resulted in a significant decrease in performance with the worst median error of 2.49m, in contrast to a worst median error of 1.7m for 20 nodes. Whilst KRTI still functioned and had the most consistent performance across all routes with 6 nodes, the lack of node density resulted in a significant increase in error with the mean error almost doubling. Ichnaea's unique tracking strategy has a significant effect on the results achieved in the 6 Node tests. Since Ichnaea creates a motion vector from the midpoint of the last dominant link to the midpoint of the current one, it performs well in some situations even with sparse links. If the subject crossed links that were approximately parallel, Ichnaea's tracking would perform well. For the anticlockwise route, these characteristics helped Ichnaea perform as expected. The contrast was seen in the clockwise test when the successive dominant triggered links were near perpendicular in several cases. This resulted in a motion vector being used that did not accurately follow the motion of the subject and resulted in large errors.

B. Cluttered Laboratory

In the cluttered laboratory environment with 20 nodes both KRTI and SCPL had consistent performance across all 3 routes and attained overall median errors of under 1m as shown in Table V. Both KRTI and SCPL suffered significant performance degradation when only 6 nodes were used. KRTI maintained a more consistent performance across multiple routes while SCPL's performance was largely route dependant as the algorithm failed to reliably track through dead spots when approached from certain directions. Ichnaea performed

TABLE V
OVERALL LOCALIZATION ERRORS (M) FOR COMBINED TRAJECTORIES IN EACH ENVIRONMENT

Auditorium 20 Nodes	**Mean**	**Median**	**RMSE**	**90^{th} per-centile**	**Max**
Ichnaea	1.21	1.14	1.34	2.01	**2.65**
KRTI	**1.09**	**0.97**	**1.29**	**1.99**	3.48
SCPL	1.33	1.24	1.55	2.23	4.68
Auditorium 6 Nodes					
Ichnaea	**1.37**	**1.25**	**1.52**	**2.29**	**3.03**
KRTI	2.08	2.06	2.18	3.02	4.02
SCPL	1.82	1.55	2.20	3.81	4.90
Laboratory 20 Nodes					
Ichnaea	1.72	1.70	1.88	2.62	4.37
KRTI	**0.99**	**0.75**	**1.23**	**2.06**	3.79
SCPL	1.05	0.94	1.27	2.13	**3.46**
Laboratory 6 Nodes					
Ichnaea	2.15	2.06	2.35	**3.40**	**4.74**
KRTI	**2.00**	**1.85**	**2.33**	3.80	6.70
SCPL	2.45	2.49	2.70	3.65	5.37

considerably worse in the 20 node route tests, though the results were more consistent with the other approaches when only 6 nodes were utilized.

C. Overall Comparison

Table V was created by combining the route data, to give overall errors for each environment and associated node deployment density. KRTI outperformed Ichnaea and SCPL in both environments when 20 nodes were present, and in the cluttered laboratory when only 6 nodes were available. SCPL performed poorly in comparison to the other approaches in all trials except for the cluttered laboratory, utilizing 20 nodes. This is understandable as when 6 nodes were used, the system struggled to clearly classify neighbouring cells. The effect of this was exacerbated as both the auditorium and cluttered laboratory were open environments with minimal movement constraints which can improve SCPL's accuracy. Since the cluttered laboratory had better spatial separation across the whole room, SCPL performed better than in the auditorium when 20 nodes were present. It should be worth noting that we attempted to use both zero order trajectory rings and second order trajectory rings, but they resulted in degraded performance. A problem with the utilized first order ring was that occasionally SCPL would report a constant unchanging location when the subject walked through a blind spot. Even with correct cell responses after leaving the blind spot, the trajectory ring would not allow for the tracking system to catch up, resulting in large errors. This was partially improved by allowing for diagonal cell transitions in the movement model in the first order ring, but the problem still occurred occasionally. Ichnaea performed adequately in the auditorium, and poorly within the cluttered laboratory. It was discovered that the accuracy of Ichnaea, both in localization and tracking, is strongly dependant on node positioning. As previously mentioned, Ichnaea works well when a subject traversing an environment passes through links that are approximately parallel to each other. It also performs better when crossing shorter links than longer ones as the estimated motion vector is more likely to be accurate.

The ambiguity resulting from using a single valued statistic, (CEP and CE95 accuracy scores), can be clearly observed in Fig. 5 and Fig. 7. Figure 5 (b) and (c) show that while SCPL has a better median (CEP) error, KRTI has better CE95 performance. Depending on which of the two metrics is used, either of these algorithms can be presented as the more accurate one. The 75^{th} percentile accuracy score used by EvAAL also suffers from the same issue. Figure 7 (a) and (b) show similar ambiguity where the CEP and CE95 errors do not adequately identify the best localization candidate.

Experimental results show that existing RSSI approaches have an acceptable accuracy, with KRTI attaining sub-meter median error across both environments. However all have constraints that limit real world implementation. RTI approaches require the least calibration effort, but require a high

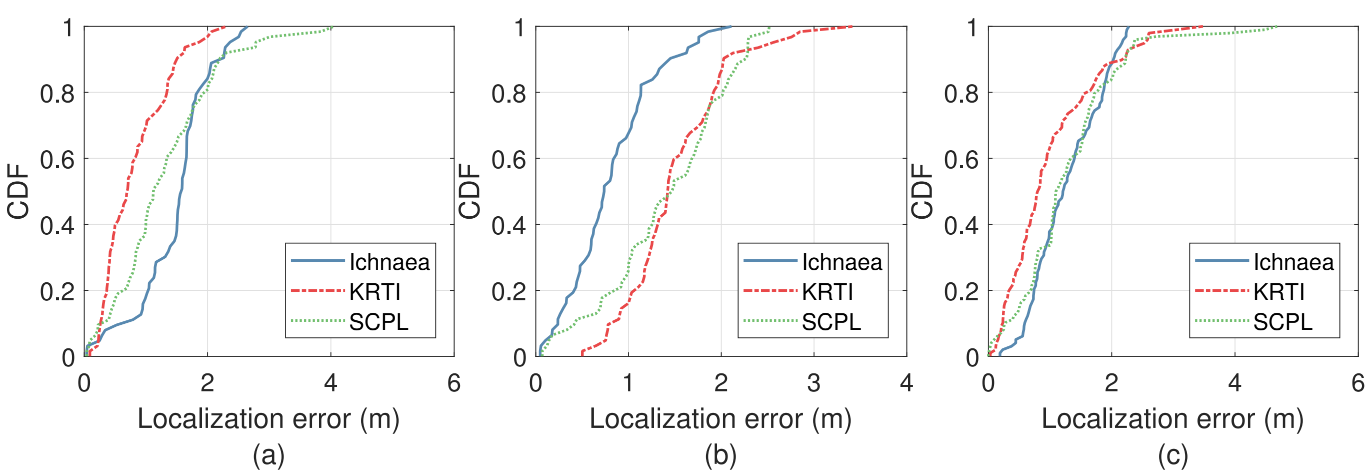

Fig. 4. Auditorium 20 Node CDF - (a) Clockwise, (b) Anticlockwise, (c) Zigzag.

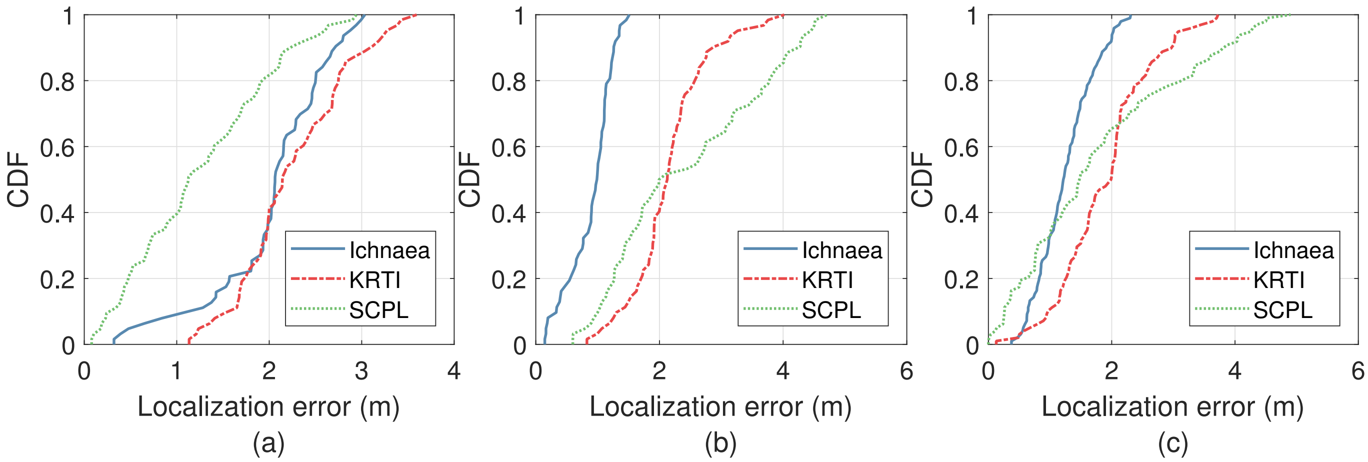

Fig. 5. Auditorium 6 Node CDF - (a) Clockwise, (b) Anticlockwise, (c) Zigzag.

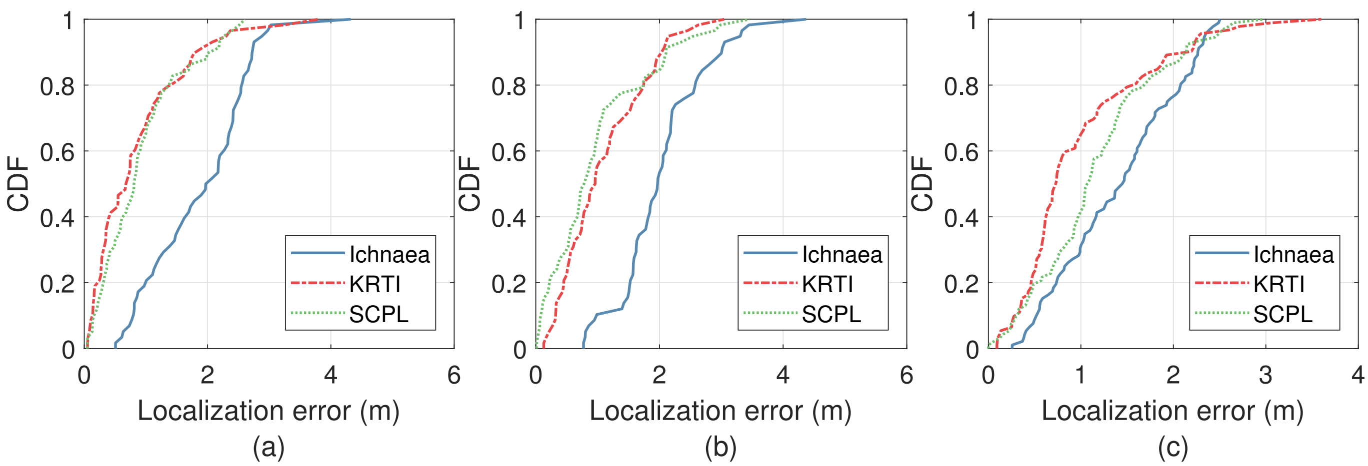

Fig. 6. Laboratory 20 Node CDF - (a) Clockwise, (b) Anticlockwise, (c) Zigzag.

deployment density. Probabilistic link-based approaches, like Ichnaea, offer benefits over RTI and Fingerprinting approaches in that they require less nodes than RTI and do not require a site survey. However existing probabilistic approaches often require a floorplan of the environment with nodes placed in strategic positions to attain an acceptable accuracy. This is demonstrated in the 6 Node tests where Ichnaea had a significantly better accuracy in the auditorium than the laboratory. Even though SCPL performed poorly, this was partially due to both environments being open with few movement restrictions, which increases error in classification approaches. Since SCPL can track multiple targets with less complexity than a particle filter, it could be considered when constraints can be placed on valid movement, such as within small corridors and cubicle environments. Existing approaches are also presented in literature with simplistic human mobility expectations, which do not hold up well with realistic human movement. Overall for real world viability and widespread adoption to be achieved, a system needs to be developed that requires few nodes and minimalistic human involvement during the initial calibration process. Such a system must also maintain long term accuracy and not assume excessive mobility constraints for tracked targets.

VI. Conclusion and Future Works

Experimental results suggest that although significant work has been reported in the literature on indoor localization, the DFL problem has not yet been solved for realistic environments. Existing wireless DFL implementations in literature typically only use a single route for their measurement. We have shown that despite the infrastructure remaining constant, wireless DFL solutions cannot guarantee a consistent tracking accuracy across the whole environment. Experimental investigation is the only way to fairly compare differing DFL approaches. Review or survey papers are not able to do a true, apple-to-apple comparison of the different approaches. Results obtained using different platforms and hardware and conducted in different conditions can not be used for benchmarking and comparisons.

Our experimental results clearly show that walking trajectory has a significant impact on the precision of all algorithms. Therefore, even at identical test locations, the localization accuracy of an algorithm can be significantly different depending on the trajectory taken or the path navigated. This also suggests that localization error is not uniform across a test environment. Furthermore, since the shapes of the CDF

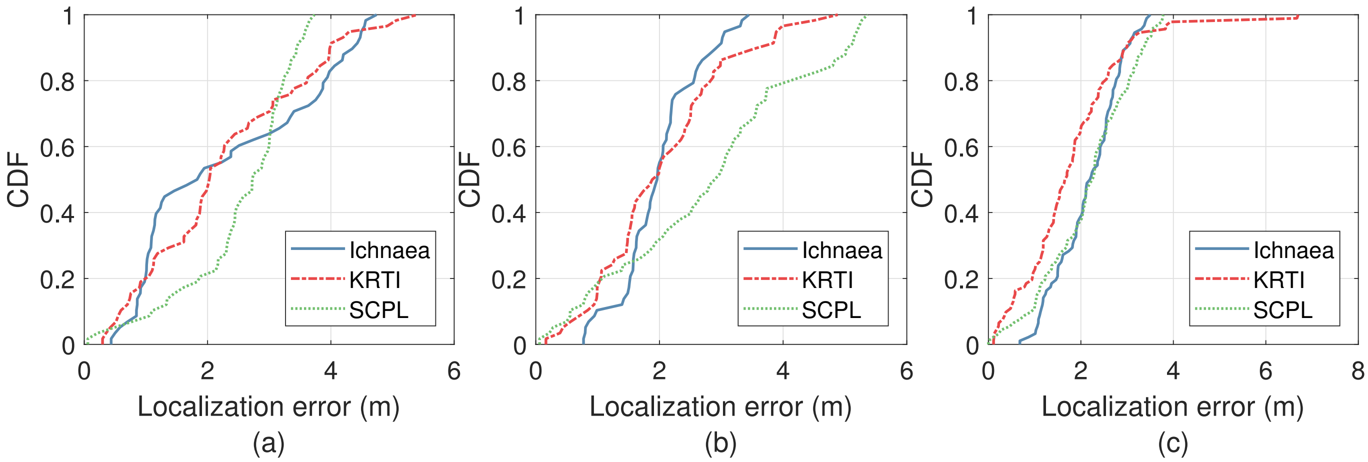

Fig. 7. Laboratory 6 Node CDF - (a) Clockwise, (b) Anticlockwise, (c) Zigzag.

curves are different across algorithms, spatial error variations affect each algorithm differently. As far as the authors are aware of, the significant impact of trajectories and the spatial error variation have not been shown in any published literature and are not appropriately addressed by the ISO/IEC 18305 standard. Further testing strategies need to be developed which appropriately include multiple trajectories within each test.

Both EvAAL and ISO/IEC 18305's accuracy score metrics are inferior to an empirical CDF plot which provides full percentile comparison. We believe that using graphical CDF error plots as an accuracy score should be standardized as it is more information rich than any singular percentile error.

While KRTI showed the best overall performance in both environments with a sub-meter median error when 20 nodes were used, it also had the worst overall median error in the 6 node auditorium test. Ichnaea showed the most consistent performance in the 6 node tests, but experienced severe accuracy issues caused by the orientation of sequential triggered links. This could potentially be fixed by modifying the motion model and how the direction of motion is determined. Overall the results show that no singular algorithm could surpass all others across all tests.

We noticed that several links did not show significant change even in the presence of movement, and others that triggered when no user was present. To be effective, localization schemes should aim to identify links that are either currently experiencing a deep fade, or spurious behaviour and reduce their weighting, for the duration of the measured abnormal behaviour. Existing approaches have used channel diversity to help partially mitigate this effect [38]. However, relying on multiple frequency channels being available may not be possible in urban environments. The system that achieved the best median error with a low node density (Ichnaea) was largely affected by node placement. Node placement was not a focus of this paper, but future works should explore how an installation methodology can be developed to optimize placement for unknown environments. All algorithms suffered from several incorrect position estimates, which occasionally caused KRTI and Ichnaea to head in the wrong direction, and SCPL to stop moving in any direction. Work needs to be done to predict human trajectories more accurately and enable reliable tracking on an entity through blind spots. While there are some reported works in this area using particle filters, more work needs to be done to ensure the tracking solution can function in real time on low cost COTS hardware. Also, significant work needs to be undertaken to allow for consistent performance in environments with sparse node deployment.

REFERENCES

[1] P. Cassar, F. Potort, P. Barsocchi, and M. Girolami, "Choosing an rss device-free localization algorithm for ambient assisted living," in *2015 International Conference on Indoor Positioning and Indoor Navigation (IPIN)*, 2015, Conference Proceedings.

[2] B. Han, Z. Wang, H. Liu, S. Xu, X. Bu, and J. An, "Shadow fading assisted device-free localization for indoor environments," in *2016 8th International Conference on Wireless Communications & Signal Processing (WCSP)*, 2016, Conference Proceedings, pp. 1–5.

[3] Y. Guo, K. Huang, N. Jiang, X. Guo, Y. Li, and G. Wang, "An exponential-rayleigh model for rss-based device-free localization and tracking," *IEEE Transactions on Mobile Computing*, vol. 14, no. 3, pp. 484–494, 2015.

[4] M. Seifeldin, A. Saeed, A. E. Kosba, A. El-Keyi, and M. Youssef, "Nuzzer: A large-scale device-free passive localization system for wireless environments," *IEEE Transactions on Mobile Computing*, vol. 12, no. 7, pp. 1321–1334, 2013.

[5] I. Sabek, M. Youssef, and A. V. Vasilakos, "Ace: An accurate and efficient multi-entity device-free wlan localization system," *IEEE Transactions on Mobile Computing*, vol. 14, no. 2, pp. 261–273, 2015.

[6] C. Xu, B. Firner, R. S. Moore, Y. Zhang, W. Trappe, R. Howard, F. Zhang, and N. An, "Scpl: Indoor device-free multi-subject counting and localization using radio signal strength," in *2013 ACM/IEEE International Conference on Information Processing in Sensor Networks (IPSN)*, 2013, Conference Proceedings, pp. 79–90.

[7] Y. Zhao, N. Patwari, J. M. Phillips, and S. Venkatasubramanian, "Radio tomographic imaging and tracking of stationary and moving people via kernel distance," *Proceedings of the 12th international conference on Information processing in sensor networks - IPSN '13*, pp. 229–240, 2013.

[8] S. Savazzi, V. Rampa, F. Vicentini, and M. Giussani, "Device-free human sensing and localization in collaborative humanrobot workspaces: A case study," *IEEE Sensors Journal*, vol. 16, no. 5, pp. 1253–1264, March 2016.

[9] A. Saeed, A. E. Kosba, and M. Youssef, "Ichnaea: A low-overhead robust wlan device-free passive localization system," *IEEE Journal of Selected Topics in Signal Processing*, vol. 8, no. 1, pp. 5–15, 2014.

[10] S. Shukri and L. M. Kamarudin, "Device free localization technology for human detection and counting with rf sensor networks: A review," *Journal of Network and Computer Applications*, vol. 97, pp. 157–174, 2017.

[11] S. Savazzi, M. Nicoli, F. Carminati, and M. Riva, "A bayesian approach to device-free localization: Modeling and experimental assessment," *IEEE Journal of Selected Topics in Signal Processing*, vol. 8, no. 1, pp. 16–29, 2014.
[12] J. Wilson and N. Patwari, "Radio tomographic imaging with wireless networks," *IEEE Transactions on Mobile Computing*, vol. 9, no. 5, pp. 621–632, 2010.
[13] S. Zhang, K. Liu, Y. Ma, X. Huang, X. Gong, and Y. Zhang, "An accurate geometrical multi-target device-free localization method using light sensors," *IEEE Sensors Journal*, vol. 18, no. 18, pp. 7619–7632, Sept 2018.
[14] D. Konings, N. Faulkner, F. Alam, F. Noble, and E. M. K. Lai, "The effects of interference on the rssi values of a zigbee based indoor localization system," in *2017 24th International Conference on Mechatronics and Machine Vision in Practice (M2VIP)*, 2017, Conference Proceedings, pp. 1–5.
[15] D. Konings, N. Faulkner, F. Alam, F. Noble, and E. M-K Lai, "Do rssi values reliably map to rss in a localization system?" in *Workshop on Recent Trends in Telecommunications Research (RTTR)*. IEEE, 2017, Conference Proceedings, pp. 1–5.
[16] T. Heurtefeux and F. Valois, "Is RSSI a Good Choice for Localization in Wireless Sensor Network?," *2012 IEEE 26th International Conference on Advanced Information Networking and Applications*, 2012, Conference Proceedings, pp. 732–739.
[17] G. Lu, T. Gallagher, B. Li, A. G. Dempster and C. Rizos, "Differences in RSSI readings made by different Wi-Fi chipsets: A limitation of WLAN localization," *2011 International Conference on Localization and GNSS (ICL-GNSS)*, 2011, Conference Proceedings, pp. 53–547.
[18] Z. Yang, Z. Zhou, and Y. Liu, "From rssi to csi," *ACM Computing Surveys*, vol. 46, no. 2, pp. 1–32, 2013.
[19] R. Zhou, X. Lu, P. Zhao, and J. Chen, "Device-free presence detection and localization with svm and csi fingerprinting," *IEEE Sensors Journal*, vol. 17, no. 23, pp. 7990–7999, Dec 2017.
[20] Y. Xie, Z. Li, and M. Li, "Precise power delay profiling with commodity wifi," *Proceedings of the 21st Annual International Conference on Mobile Computing and Networking - MobiCom '15*, pp. 53–64, 2015.
[21] D. Halperin, W. Hu, A. Sheth, and D. Wetherall, "Tool release: Gathering 802.11n traces with channel state information," *ACM SIGCOMM Computer Communication Review*, vol. 41, no. 1, pp. 53–53, 2011.
[22] G. Sun, Y. Xie, D. Liao, H. Yu and V. Chang, "User-defined privacy location-sharing system in mobile online social networks," *Journal of Network and Computer Applications*, 2007, vol. 86, pp. 34–45.
[23] T. Xu and Y. Cai, "Location anonymity in continuous location-based services," *Proceedings of the 15th annual ACM international symposium on Advances in geographic information systems*, 2007, Conference Proceedings, pp. 39–46.
[24] P. Gope, R. Amin, S.K.H. Islam, N. Kumar and V.K. Bhalla, "Lightweight and privacy-preserving RFID authentication scheme for distributed IoT infrastructure with secure localization services for smart city environment," *Future Generation Computer Systems*, 2018, pp. 629–637.
[25] B. Mager, P. Lundrigan, and N. Patwari, "Fingerprint-based device-free localization performance in changing environments," *IEEE Journal on Selected Areas in Communications*, vol. 33, no. 11, pp. 2429–2438, 2015.
[26] X. Li, S. Ding, Z. Li, and B. Tan, "Device-free localization via dictionary learning with difference of convex programming," *IEEE Sensors Journal*, vol. 17, no. 17, pp. 5599–5608, Sept 2017.
[27] Y. Zheng and A. Men, "Through-wall tracking with radio tomography networks using foreground detection," in *2012 IEEE Wireless Communications and Networking Conference (WCNC)*, 2012, Conference Proceedings, pp. 3278–3283.
[28] S. Palipana, B. Pietropaoli, and D. Pesch, "Recent advances in rf-based passive device-free localisation for indoor applications," *Ad Hoc Networks*, vol. 64, pp. 80–98, 2017.
[29] J. Xiao, Z. Zhou, Y. Yi, and L. M. Ni, "A survey on wireless indoor localization from the device perspective," *ACM Computing Surveys*, vol. 49, no. 2, pp. 1–31, 2016.
[30] N. Pirzada, M. Y. Nayan, F. S. M. F. Hassan, and M. A. Khan, "Device-free localization technique for indoor detection and tracking of human body: A survey," *Procedia - Social and Behavioral Sciences*, vol. 129, pp. 422–429, 2014.
[31] XANDEM, "Secure, monitor, and control your space," 2018. [Online]. Available: http://xandem.com/
[32] F. Potort, S. Park, A. R. Jimnez Ruiz, P. Barsocchi, M. Girolami, A. Crivello, S. Y. Lee, J. H. Lim, J. Torres-Sospedra, F. Seco, R. Montoliu, G. M. Mendoza-Silva, M. D. C. Prez Rubio, C. Losada-Gutirrez, F. Espinosa, and J. Macias-Guarasa, "Comparing the performance of indoor localization systems through the evaal framework," *Sensors (Basel, Switzerland)*, vol. 17, no. 10, p. 2327, 2017.
[33] I. 18305:2016, *Information technology – Real time locating systems – Test and evaluation of localization and tracking systems*, ser. Standard ISO/IEC 18305:2016. ISO/IEC JT, 2016. [Online]. Available: https://www.iso.org/standard/62090.html
[34] D. Lymberopoulos and J. Liu, "The microsoft indoor localization competition: Experiences and lessons learned," *IEEE Signal Processing Magazine*, vol. 34, no. 5, pp. 125–140, 2017.
[35] F. Potort, A. Crivello, P. Barsocchi, and F. Palumbo, "Evaluation of indoor localisation systems: Comments on the iso/iec 18305 standard," in *2018 International Conference on Indoor Positioning and Indoor Navigation (IPIN)*, Sept 2018, pp. 1–7.
[36] J. Wilson and N. Patwari, "See-through walls: Motion tracking using variance-based radio tomography networks," *IEEE Transactions on Mobile Computing*, vol. 10, no. 5, pp. 612–621, 2011.
[37] Y. Zhao and N. Patwari, "Robust estimators for variance-based device-free localization and tracking," *IEEE Transactions on Mobile Computing*, vol. 14, no. 10, pp. 2116–2129, 2015.
[38] O. Kaltiokallio, M. Bocca, and N. Patwari, "Enhancing the accuracy of radio tomographic imaging using channel diversity," in *2012 IEEE 9th International Conference on Mobile Ad-Hoc and Sensor Systems (MASS 2012)*, 2012, Conference Proceedings, pp. 254–262.
[39] B. Wei, A. Varshney, N. Patwari, W. Hu, T. Voigt, and C. T. Chou, "drti: Directional radio tomographic imaging," *Proceedings of the 14th International Conference on Information Processing in Sensor Networks - IPSN '15*, pp. 166–177, 2015.
[40] O. Kaltiokallio, R. Jantti, and N. Patwari, "Arti: An adaptive radio tomographic imaging system," *IEEE Transactions on Vehicular Technology*, vol. 66, no. 8, pp. 7302–7316, 2017.
[41] Y. Zhao and N. Patwari, "Demo abstract: Histogram distance-based radio tomographic localization," in *2012 ACM/IEEE 11th International Conference on Information Processing in Sensor Networks (IPSN)*, 2012, Conference Proceedings, pp. 129–130.
[42] D. Comaniciu and P. Meer, "Mean shift: a robust approach toward feature space analysis," *IEEE Transactions on Pattern Analysis and Machine Intelligence*, vol. 24, no. 5, pp. 603–619, 2002.

Daniel Konings Daniel Konings received his BE(Hons) from Massey University, Auckland, New Zealand in Computer Systems and Electronics Engineering in 2014, where he is currently pursuing the Ph.D. degree with the School of Engineering and Advanced Technology (SEAT). His research interests include indoor localization, digital signal processing, machine learning, IoT & wireless sensor networks. Daniel is a Student Member of the Institute of Electrical and Electronics Engineers (IEEE).

Fakhrul Alam Fakhrul Alam received his BSc (Hons) in Electrical & Electronic Engineering from BUET, Bangladesh and MS and Ph.D. in Electrical Engineering from Virginia Tech, USA. He is currently a senior lecturer at the School of Engineering and Advanced Technology, Massey University, New Zealand. His research interests include indoor localization, 5G & visible light communication, disaster management with 5G, IoT & wireless sensor networks. He is a member of Institute of Electrical and Electronics Engineers (IEEE) and Institution of Engineering and Technology (IET).

Frazer Noble Frazer K. Noble received his BE (Hons) in Mechatronics, ME (Hons) in Engineering, and PhD in Engineering from Massey University, New Zealand. He is currently a lecturer at the School of Engineering and Advanced Technology, Massey University, New Zealand. His research interests include mechatronics, robotics and automation, machine vision, and machine learning.

Edmund M-K Lai Edmund Lai received his BE(Hons) and PhD from The University of Western Australia, both in Electrical Engineering, in 1982 and 1991 respectively. He is currently a Professor of Information Engineering at Auckland University of Technology, New Zealand. He has previously held faculty positions at universities in Australia, Hong Kong, and Singapore. His research interests include digital signal processing, digital communications and networks, computational and swarm intelligence, and artificial neural networks. Dr Lai is a fellow of the Institution of Engineering and Technology (IET) and a senior member of the Institute of Electrical and Electronics Engineers (IEEE).

Chapter 3

This chapter contains content from the following article, republished with permission. In accordance with IEEE's republishing policy, any full text that has been included is the unmodified accepted article. This means that while the content is identical to the published article, there may be stylistic differences.

SpringLoc: A Device-free Localization Technique for Indoor Positioning and Tracking using Adaptive RSSI Spring Relaxation

DANIEL KONINGS[1], (Student Member, IEEE), FAKHRUL ALAM[1], (Senior Member, IEEE), FRAZER NOBLE[1], AND EDMUND M-K LAI[2], (Senior Member, IEEE)

[1]School of Food and Advanced Technology, Massey University, Auckland 0632, New Zealand
[2]School of Engineering, Computer and Mathematical Sciences, Auckland University of Technology 1010, Auckland, New Zealand

Corresponding author: Daniel Konings (e-mail: d.konings@massey.ac.nz).

This work was supported in part by the Massey University Doctoral Scholarships and the Massey University Research Fund (MURF).

ABSTRACT Device-free Localization (DFL) algorithms using the Received Signal Strength Indicator (RSSI) metric, have become a popular research focus in recent years as they allow for location-based service using Commercial-off-the-shelf (COTS) wireless equipment. However, most existing DFL approaches have limited applicability in realistic smart home environments as they typically require extensive offline calibration, large node densities or use technology that is not readily available in commercial smart homes. In this paper, we introduce SpringLoc, a DFL algorithm that relies on simple parameter tuning and does not require offline measurements. It localizes and tracks an entity using an adaptive spring relaxation approach. The anchor points of the artificial springs are placed in regions containing the links that are affected by the entity. The affected links are determined by comparing the kernel-based histogram distance of successive RSSI values. SpringLoc is benchmarked against existing algorithms in two diverse and realistic environments, showing significant improvement over the state-of-the-art, especially in situations with low node deployment density.

INDEX TERMS Device-free Localization (DFL), Histogram distance, Indoor Positioning Systems (IPS), Smart Homes, Spring-relaxation

I. INTRODUCTION

Device-free Localization (DFL) systems that utilize the Received Signal Strength Indicator (RSSI) metric can track untagged subjects, unlike traditional Device-based/Active Tracking approaches. They can facilitate location-based services such as lighting/music control and intruder detection, based on human presence alone. However, since the tracked entity is untagged, it can be hard to uniquely identify each entity when multiple targets are present. Improved localization accuracy can potentially lead to more accurate entity identification. The purpose of this paper is to provide an improved algorithm for DFL that can be implemented in practical scenarios e.g. smart homes without requiring the deployment of significant additional infrastructure.

Existing indoor DFL systems have three main shortcomings with respect to practical implementation. The first one is that they require many sensors within the target environment. This can lead to high implementation cost due to the large number of sensors required, and the requirement of easily accessible power across the whole environment [1-4]. The second shortcoming is that DFL implementations also require a large number of offline measurements to calibrate the system to the target environment [5-10]. This restricts their usability, as standard end users cannot be expected to install new power sockets and undertake excessive calibration procedures to facilitate localization within their home. The third shortcoming is that recent attempts at DFL solutions use hardware that is inaccessible to standard end users. For example, Channel State Information (CSI) based DFL has been shown to be quite accurate. However, CSI is not available on the majority of wireless platforms e.g. Zigbee or Bluetooth. Moreover, even with Wi-Fi, CSI is only available on two outdated modules with bespoke modified drivers [11, 12]. Other leading approaches makes use of Frequency Modulated Carrier Wave (FMCW) signals using a software defined radio platform [13, 14]. This limits usability as rather than using pre-existing wireless infrastructure or widely

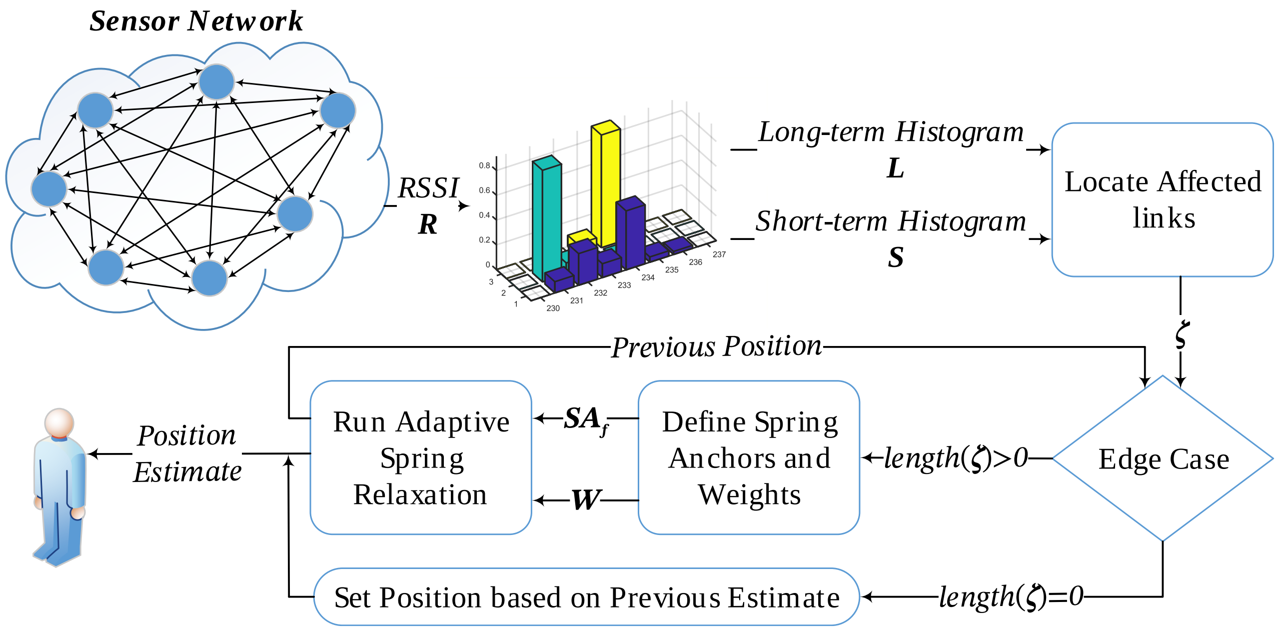

FIGURE 1. SpringLoc Algorithm Overview

available Commercial Off-The-Shelf (COTS) equipment, these solutions require the deployment of custom designed additional wireless infrastructure for the sole purpose of localization. Camera based pose estimation techniques can also be used for multi-target localization [15, 16], however they have privacy concerns and would likely not be able to access existing infrastructure. To solve these problems, we propose SpringLoc, a new DFL algorithm based off RSSI histogram difference and Spring-relaxation, as shown in Fig. 1. It requires fewer sensor nodes while maintaining an acceptable localization accuracy. Thus, one is able to utilize existing smart home infrastructure, e.g. existing Wi-Fi, Zigbee or Bluetooth smart sensors, to provide indoor localization as a secondary service. SpringLoc also does not require any offline calibration measurements.

SpringLoc records the RSSI values between all transmitting (TX) and receiving (RX) nodes and forms two RSSI histograms for each link. The first histogram is formed by taking a weighted average of recent RSSI values. The second histogram is formed using a long-term weighted average of the RSSI values. At each timestep, the difference between these two histograms is calculated for each link. Links whose histogram difference exceed a predefined threshold are deemed to be ‘affected links’. These are the links whose RSSI values have been impacted by the presence of the entity, with the short-term histogram exhibiting significant variation from the long-term one. An artificial spring anchor is defined at the intersection point of the affected links after removing outliers. Each spring acts as an attractive force on the tracked entity, pulling it towards its own anchor, as shown by the springs in Fig. 2. The spring-relaxation algorithm then iteratively localizes the target by equalizing the forces between the set of springs. Each spring has a weight based on the distance between the contributing affected links. The force associated with each spring is defined by this weight and the distance from the previous position estimate. If the intersection between two links does not fall within the localization environment, the closest point from each link is taken as the location of the anchor.

This is how the rest of the paper is organized. Section II covers related DFL techniques, why RSSI has been utilized over CSI and an overview of previous Spring Relaxation approaches. Section III describes the proposed SpringLoc algorithm. Section IV outlines the experimental setup and results. Section V provides a discussion on the experimental results and Section VI concludes the manuscript.

II. RELATED WORKS

DFL has become a popular research topic, as it allows for untagged entities to be tracked, enabling a wide range of usage scenarios. DFL techniques that are based on technologies readily available in a smart home, e.g. Bluetooth, ZigBee or Wi-Fi, can be categorized into three major approaches: 1) Fingerprinting, 2) Link-based or 3) Radio Tomographic Imaging.

A. FINGERPRINTING

Fingerprinting schemes consist of two phases. In the offline phase, the environment is divided into a grid. An initial measurement is taken when the environment is empty, and successive RSSI measurements are taken with an entity in each known grid location. This measurement set forms the fingerprint database. During the online phase, live RSSI

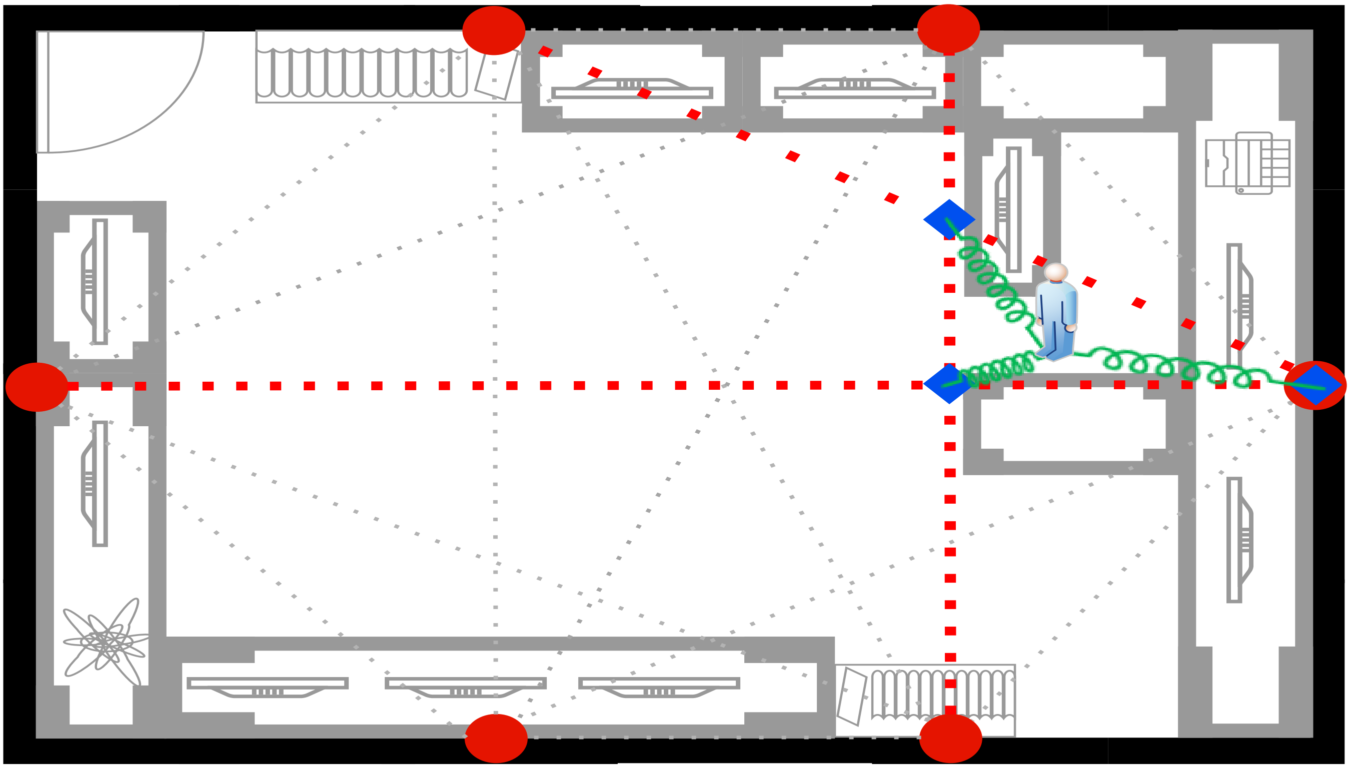

FIGURE 2. SpringLoc with Three Affected Links

measurements are compared with the fingerprint database, with location estimation performed via classification.

The 'Sequential Counting, Parallel Localization' (SCPL) algorithm first counts the number of subjects in an environment by using successive cancellation to remove the influence of the subjects with the strongest influence each round. Once the number of subjects is known, SCPL incorporates human movement constraints and environmental geometric constraints to track each subject using a conditional random field (CRF) [17]. The 'ACcurate and Efficient' (ACE) localization algorithm incorporates an energy-minimization framework followed by a Markov-based CRF and clustering to smooth transitions between neighboring locations [18]. The 'geometrical localization, fingerprinting device free localization' (GL-FDFL) algorithm improved traditional fingerprinting by reducing the search area of possible fingerprint locations by geometrically restricting it based on the area bounded by shadowed links [19]. The 'Energy-Efficient High-Precision Multi-Target-Adaptive' (E-HIPA) algorithm used compressive sensing and an adaptive orthogonal matching pursuit algorithm to track multiple targets, using a sparse link network [20]. Chiang et al [21] integrated fuzzy logic into a support vector machine (SVM) based DFL approach to improve the classification accuracy of a pure SVM DFL approach by 7.8%. Mager et al [22] sought to improve the accuracy of fingerprint-based approaches as the database degrades due to environmental changes. Experimental results show that Random Forest based classification is more robust to environmental changes than traditional K-Nearest Neighbour (KNN), Linear Discriminant Analysis (LDA) or SVM approaches.

Wang et al [8] proposed a novel deep learning approach to reduce the offline training effort by automatically learning features using a sparse autoencoder network. A SoftMax regression-based classifier is then used to predict a user's location, activity and gesture. The WiDet approach [23] augments the offline training data by resampling some windowed sample sub-sets to simulate different walking speeds. Localization is performed using a Convolutional Neural Network (CNN), which is shown to outperform a traditional approach based on RSSI wavelet features and Bayes classification. Huang et al [5] model DFL as a spare representation problem which they solve using a variant of the iterative shrinkage-thresholding algorithm. Zhang et al [24] implemented a parametrized extreme learning machine (ELM) approach to DFL which was shown to outperform existing WKNN, SVM and RTI techniques.

Though E-HIPA was able to reduce the number of nodes required, and Mager et al reduced the retraining effort, all fingerprinting approaches require extensive offline calibration, and suffer degradation due to any significant environmental changes. This limits their usability in smart homes, where it would be difficult to create a generalized calibration approach that could be followed by a regular end-user. Another difficulty is that calibration must be redone any time the environment changes significantly, which may be untenable in diverse, realistic environments.

B. LINK-BASED

Link-based or model-based schemes work by creating models to analyze the effect a subject has on a TX-RX link. A

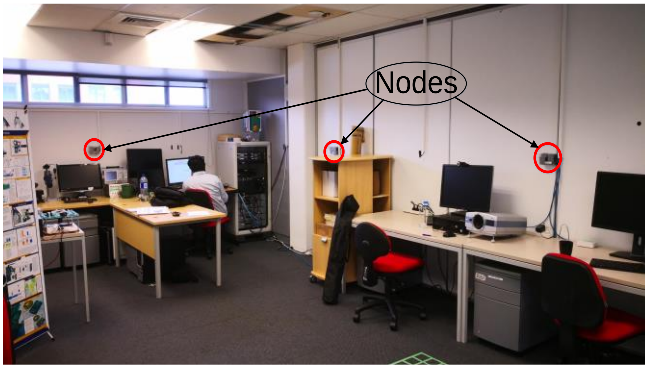

FIGURE 3. Cluttered Office space Environment

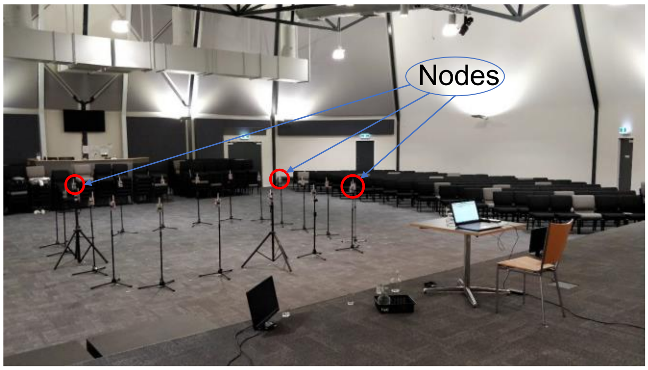

FIGURE 4. Church Hall Environment

target is considered present along a link when the model deviates away from its steady-state by a predefined threshold. Particle filters are often used for positioning as they allow for a subject to be localized as the centroid of multiple affected links [2, 25-27].

Guo et al [25] developed an Exponential-Rayleigh model for received signal strength (RSS), coupled with a particle filter for multi-target localization and tracking. Zheng and Men [26] represent the RSS model as a Gaussian mixture, with online re-parameterization to ensure correct detection, and a particle filter for localization and tracking. Ichnaea [27] estimates a density function for each link based on a sliding window of RSSI variance. The system detects links as anomalous if they exceed a predetermined critical bound of the density function. The anomalous links are passed to a particle filter which performs localization and tracking [27].

Link-based schemes' accuracy is based on the reliability of their link model. If the model is not updated regularly, environmental change can degrade the system. Moreover, if noisy live measurements are used to update the link models, they may diverge over time. Secondly, most link-based models use a particle filter to solve the localization problem. Particle filters are very computationally expensive and unlikely to be feasibly run on commercial-off-the-shelf (COTS) embedded devices. Furthermore, since parallel particle filters would likely be required for multi-target tracking to ensure convergence in noisy environments, these algorithms do not scale well for realistic environments.

C. RADIO TOMOGRAPHIC IMAGING

Radio Tomographic Imaging (RTI) solves an ill posed linear inverse problem to generate an output image. The brightest pixel within the output image defines a subject's location estimate. RTI approaches are typically coupled with a Kalman filter on the output images to provide subject tracking. The original RTI implementation used RSSI attenuation as a feature [28]. More recent approaches have improved RTI by using variance as a feature and performing subspace decomposition [4], using multiple channels [29], using directional antenna arrays [30], or using a histogram difference feature [3]. Recently, a multi-frequency approach using both 433MHz and 868MHz radios managed to attain sub-meter accuracy in a complex indoor environment of approximately 115m2, using 39 nodes [31].

Modern RTI approaches require minimal calibration and are less computationally complex (in the online phase) than link-based approaches, while still being able to track multiple targets. However, they require a significant node density to attain their accuracy, making them unsuitable for smart home use, where significant infrastructure modification cannot be justified.

D. CHANNEL STATE INFORMATION

The Channel State Information (CSI) metric has become a popular localization metric over RSSI as it is more immune to the adverse effects of multipath propagation [32] and outperforms RSSI based methods [33]. Since CSI offers more fine-grained information than RSSI, it has been extensively utilized in machine learning based DFL approaches including shapelet learning [34], SVM [9, 35], Random Forest [36], HMM [37], and Deep Learning [38]. A shortcoming of CSI is that it is currently only accessible using modified drivers in legacy Intel 5300 [11, 39], Atheros ath9k [12] based devices, or by using Software Defined Radio (SDR) platforms like USRP [40] or WARP [41]. Even though there has been significant research interest in using the modified drivers since they were released in 2011 and 2015 respectively [42], no vendor has provided access to the CSI metric to end users in any subsequent hardware releases. This means that a CSI based DFL solution cannot be recommended for smart homes, as the metric is not readily available in COTS hardware. Furthermore, smart home networks are commonly implemented using Zigbee, Bluetooth Low Energy (BLE) or Wi-Fi equipment. While the RSSI metric supports Zigbee, BLE and Wi-Fi equipment, the CSI metric only supports the aforementioned legacy Wi-Fi devices. Therefore, it is not suitable for integration into existing smart homes.

E. SPRING-RELAXATION

Spring-relaxation aims to reach equilibrium among a set of artificial springs. It has been used for sensor localization in Wireless Sensor Networks (WSNs) [43-45]. A similar energy minimization technique called 'potential fields' has found extensive use in obstacle avoidance and navigation of autonomous robots [46-49]. As far as the authors are aware, the concept of spring-relaxation has not been applied to DFL.

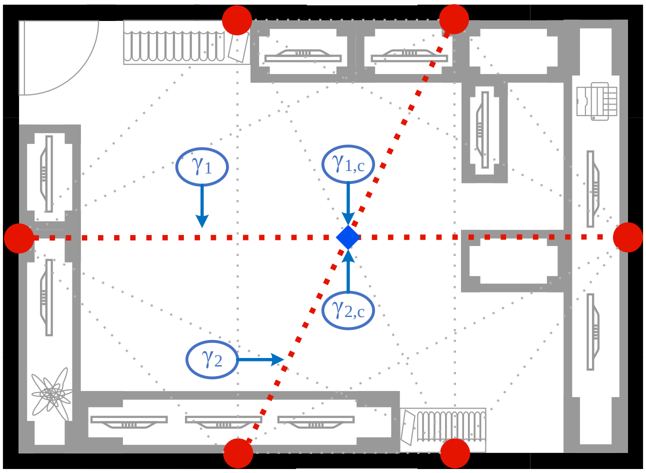

FIGURE 5. Affected Link pair with intersection point

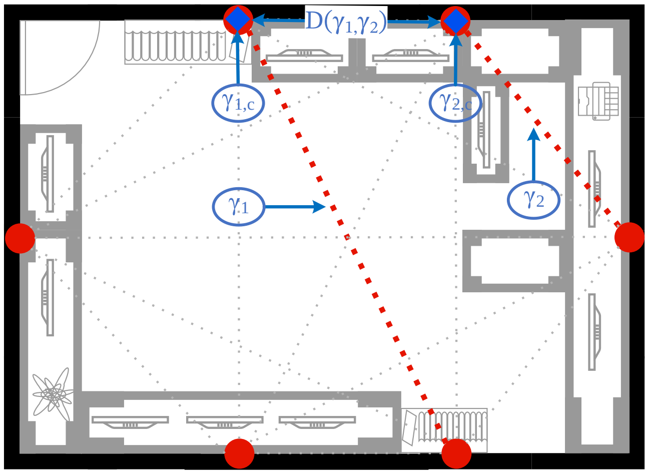

FIGURE 6. Affected Link pair with no intersection point

Spring-relaxation has the benefit of only requiring a few anchors per target, as opposed to potentially thousands of particles used per target in a traditional particle filter. Spring-relaxation techniques require spring anchors, which are not readily apparent in the concept of DFL. Therefore they must first be defined in our calibration-free algorithm, as described in Section III. Spring-relaxation also has the benefit of allowing for adaptively weighted springs, which, with respect to DFL, can ensure high accuracy across a range of different target speeds.

F. CONTRIBUTIONS

As far as the authors are aware, the concept of spring-relaxation has never been practically implemented with respect to wireless DFL. This leads to the following novel contributions:

1) Apply the concept of spring-relaxation to wireless DFL as a form of localization and tracking
2) Provide a calibration-free way of providing the DFL spring-relaxation algorithm with artificial anchor points, during live operations
3) Provide experimental results across two diverse and realistic environments which show that spring-relaxation can outperform existing state-of-the-art RSSI-based DFL approaches, under both high and low node densities, for varying walking trajectories

III. ALGORITHM

DFL systems that use RSSI values must choose a feature to determine whether an entity is influencing the propagation of any specific link. A commonly utilized feature has been either RSSI difference or absolute difference (also termed as RSSI attenuation) where the current RSSI value is subtracted from one taken during offline measurements when no one is present. Unfortunately, this metric does not work well in through-wall environments and requires offline measurements. RSSI variance is another commonly utilized feature that works better in through-wall environments. However, it cannot track stationary targets.

RSSI histogram difference, as featured in [3] has the benefit of incorporating both mean and variance RSSI features, with neither of their limitations. This is beneficial as it allows for a feature detector that does not require an offline calibration phase. Another benefit of this feature is that it looks for change in the RSSI values caused by movement, irrespective of whether the change increases or decreases the RSSI values. This allows for the metric to work in multipath rich environments, where the magnitude RSSI change cannot be predicted in advance. This allows the metric to work with both stationary and moving targets, and in both open and through-wall environments.

The SpringLoc approach is broken into five modules which are described below and shown in Fig. 1. The first module forms the long-term and short-term histograms of each link, required for calculating the RSSI histogram difference feature. Module two extracts the most prominently affected links. Module three handles cases when too few affected links were detected. Module four defines the spring anchor points and their weights and module five performs an iterative adaptive spring relaxation approach that localizes and tracks a subject.

A. HISTOGRAM FORMATION

The RSSI difference feature is formulated by arranging incoming RSSI values into histograms averaged over either a short or a long period of time. The histogram difference for each link can then be found by computing an empirical histogram distance between the long-term histogram (L) and short-term histogram (S) for each link. Using an exponentially weighted moving average (EWMA) weighting scheme, the histograms can be defined as:

$$h_l^t = (1-\alpha)h_l^{t-1} + \alpha f_R(R_l^t) \qquad (1)$$

where h_l^t is the histogram of link l at time t and R_l^t is the RSSI value of link l at time t. α, the forgetting factor, has a value between 0 and 1 and governs how much recent RSSI values contribute to the histogram. Hence a large value will help formulate the S while a low value will formulate the L. Assuming RSSI values are quantized with a step-size of one, and have a range between 1 and N, f_R is a function that given an RSSI value will return a vector of length N, with a value of 1 at the index of the RSSI value, and 0 elsewhere.

The difference, $KD(S,L)$, between the two histograms S and L, are computed using the Epanechnikov kernel distance in accordance with the literature [3], and can be defined as:

$$KD(S,L) = S^T KS + L^T KL - 2S^T KL \qquad (2)$$

where T represents a transpose operation and K is an $N\ x\ N$ matrix defined by:

$$K(i,j) = \begin{cases} \frac{3}{4}\left(1 - \frac{|i-j|^2}{\varpi}\right), |i-j| \leq \varpi \\ 0,\ \ otherwise \end{cases} \qquad (3)$$

where ϖ is a kernel smoothing parameter.

B. LOCATE AFFECTED LINKS

After computing the histogram difference for each link, the system must determine which links have been triggered by a target's presence. Since the presence of a target will cause an increased difference between the short-term (S) and long-term (L) histograms, a link threshold is defined as:

$$\zeta^t = f(KD(S,L)_{1:l}^t) \qquad (4)$$

$$f(x) = \begin{cases} x,\ x > \beta \\ nothing,\ x \leq \beta \end{cases} \qquad (5)$$

where function f iterates through each link l in KD, adding them to an array, ζ, if they exceed predefined link threshold constant, β.

After locating the affected links, SpringLoc defines appropriate spring anchors, and their weights. This requires the successful detection of at least two affected links. If less than two affected links are detected, the algorithm utilizes the approach outlined in Section E.

C. DEFINE SPRING ANCHORS / WEIGHTS

Once all the affected links have been located, the system needs to translate this into the target's location. Intuitively, the subject is more likely to be in a region where there is a higher density of affected links. To help define this region, we locate a set of points that reside within the unknown region. For each link l in ζ, we define the coordinate of the transmitting node as TX_l, the coordinate of the receiving node as RX_l, and the line segment formed between TX_l and RX_l as γ_l. Sunday's geometric method [50] was used to either: find the intersection point of each pair of line segments, or the minimum distance between them within the environment. This can be clearly observed in Fig. 5 and Fig. 6. Fig. 5 shows two intersecting affected links γ_1 and γ_2. By defining the closest point in line segment one as $\gamma_{1,c}$ and the closest point in line segment two as $\gamma_{2,c}$, we know that $\gamma_{1,c} = \gamma_{2,c}$ as the links intersect. These points are represented by the blue diamond in Fig. 5. This also means that the minimum distance between the two links, $D(\gamma_1, \gamma_2) = 0$. In Fig. 6, the affected link pair does not intersect within the test environment. This means that the $\gamma_{1,c}$ and $\gamma_{2,c}$ points are defined by the node locations as shown in Fig. 6. In this case since $\gamma_{1,c} \neq \gamma_{2,c}$, $D(\gamma_1, \gamma_2) > 0$.

Once all intersection points have been calculated, the system needs to define each spring anchor, and its associated weight. The spring anchor points set (SA), are defined as:

$$SA = g(\gamma_{1:end}) \qquad (6)$$

$$g(x_i, x_j) = \begin{cases} [\gamma_{i,c}\ \gamma_{j,c}],\ D(x_i, x_j) < \eta \\ nothing,\ D(x_i, x_j) \geq \eta \end{cases} \qquad (7)$$

where g is a function that iterates through each pair of intersection points, adding them to the array of spring anchor points, SA, if the distance between them, $D(\gamma_i, \gamma_j)$, as shown in Fig. 6, is less than the distance constant, η. This is done to exclude link pairs that do not share close proximity.

After selecting the initial anchor points, a filter is applied to only keep points surrounding the median coordinate values in both x and y directions. The final set of spring anchor points (SA_f) is defined as:

$$SA_f = m(SA_{1:end}) = \begin{cases} SA_i, \begin{matrix} (\tilde{x} - \rho\sigma_x) \leq SA_{i,x} \leq (\tilde{x} + \rho\sigma_x) \\ (\tilde{y} - \rho\sigma_y) \leq SA_{i,y} \leq (\tilde{y} + \rho\sigma_y) \end{matrix} \\ nothing, otherwise \end{cases} \qquad (8)$$

where m is a function that iterates through each spring anchor, only returning ones that are close to the median x and y value. $SA_{i,x}$ and $SA_{i,y}$ represent the x and y coordinate of spring anchor i respectively, $\tilde{x}$ is the median x coordinate from the SA point set, ρ is a SA selection constant, σ_x is the standard deviation of the x values from the SA point set, $SA_{i,x}$ is the x coordinate for point i in SA, $\tilde{y}$ is the median y coordinate value in SA, $SA_{i,y}$ is the y coordinate for point i in SA, and σ_y is the standard deviation of the y values from the s the x coordinate for point i in SA point set.

Once the final spring anchor points have been defined at timestep t, SA_f^t, they need to be weighted. Each spring in SA_f^t receives a weight defined by:

$$W_k^t = KD_i^t * KD_j^t \qquad (9)$$

where indexes i and j were used by (7) for defining a SA point, now stored in $SA_{f,k}^t$. The weights are then normalized between 0 and 1 using:

$$W^t = \frac{(W^t - min(W^t))}{(max(W^t) - min(W^t))} \qquad (10)$$

D. ADAPTIVE SPRING RELAXATION

The iterative spring-relaxation approach takes the final anchor points set, spring weights, and the previous position estimate as arguments. It is defined by parameters including a max number of iterations (ψ), a step size (τ), and breakout parameter (δ) which stops the algorithm early if convergence is reached. In a single iteration, the distance vector between the previous location estimate, $prevPos$, and each spring anchor is calculated as:

Algorithm 1: SpringLoc Algorithm

for $t = 1{:}t\_end$	*At time instant t*
for $i = 1{:}l$	*Iterate through each link*
$S_i^t = (1-\alpha_s)S_i^{t-1} + \alpha_s f_R(R_i^t)$	*Compute the short-term histogram (S) using (1)*
$L_i^t = (1-\alpha_L)L_i^{t-1} + \alpha_L f_R(R_i^t)$	*Compute the long-term histogram (L) using (1)*
$KD_i^t = {S_i^t}^T K S_i^t + {L_i^t}^T K L_i^t - 2{S_i^t}^T K L_i^t$	*Compute the kernel-distance between S and L using (2)*
if $KD_i^t > \beta$	*Check if link is affected by subject's presence*
$\zeta^t = [\zeta^t\ KD_i^t]$	*Add affected links to the end of the link set using (4)*
end	
end	
if $(length(\zeta^t) == 0)\&\&(length(\zeta^{t-1}) > 0)$	*Check for edge cases*
$\mathbf{posEstimate} = \mathbf{prevPos} + \overrightarrow{\mathbf{project}}$	*Accounting for an edge case, as in (15)*
elseif $(length(\zeta^t) == 0)\&\&(length(\zeta^{t-1}) == 0)$	
$\mathbf{posEstimate} = \mathbf{prevPos}$	
else	
if $length(\zeta^t) == 1$	*Fix edge case if only one affected link present using (17)*
$TX_{injected} = \mathbf{prevPos}$	
$RX_{injected} = \mathbf{prevPos} + \overrightarrow{\mathbf{project}}$	
$\zeta^t = [\zeta^t\ (TX_{injected}, RX_{injected})]$	
end	
for $j = 1{:}length(\zeta^t)$-1	*Iterate through each pair of affected links*
for $k = 2{:}length(\zeta^t)$	
$[\gamma_{j,c}, \gamma_{k,c}] = ClsPoints(TX_j, RX_j, TX_k, RX_k)$	*Calculate the closest point pairs using Sunday's method [50]*
$D(\gamma_{j,c}, \gamma_{k,c}) = DisBetSeg(TX_j, RX_j, TX_k, RX_k)$	*Calculate the distance between each affected pair using Sunday's method [50]*
if $D(\gamma_{j,c}, \gamma_{k,c}) < \eta$	*If affected link pairs points are within close proximity, add to spring anchor set using (7)*
$SA = [SA\ \gamma_{j,c}\ \gamma_{k,c}]$	
$W_{tmp} = [W_{tmp}\ (KD_j^t * KD_k^t)\ (KD_j^t * KD_k^t)]$	*Calculate weights with same indexing as SA*
end	
end	
end	
for $i = 1{:}length(SA)$	
if $((\tilde{x} - \rho\sigma_x) \le SA_{i,x} \le (\tilde{x} + \rho\sigma_x))$ && $((\tilde{y} + \rho\sigma_y) \le SA_{i,y} \le (\tilde{y} + \rho\sigma_y))$	*If both x and y coordinates of SA fall within bounds set around the medians, include SA in the final SA_f using (8)*
$SA_f^t = [SA_f^t\ SA_i]$	
$W^t = [W^t\ W_{tmp_i}]$	*Create final weight set as in (9)*
end	
end	
for $i = 1{:}length(W^t)$	*Iterate through each final weight*
$W_i^t = \frac{W_i^t - min(W^t)}{max(W^t) - min(W^t)}$	*Normalize final weight set to between 0-1, as in (10)*
end	
$posEstimate = ASR(SA_f^t, W^t, prevPos)$	*Apply adaptive spring-relaxation, for t=1, set the previous position estimate as the environments entrance coordinate*
end	
$\overrightarrow{project} = posEstimate - prevPos$	*Create projection vector for edge cases, as in (16)*
$prevPos = posEstimate$	*Update previous position estimate*
end	

Algorithm 2: $[posEstimate] = ASR(SA_f^t, W^t, prevPos)$	
for $\boldsymbol{i = 1{:}\psi}$	*Iterate until hitting the max number of iterations*
for $\boldsymbol{j = 1{:}n}$	*Iterate through each spring anchor* ($n = length(SA_f^t)$)
$\boldsymbol{\overrightarrow{dis} = prevPos - SA_{f,j}}$	*Create a distance vector between the previous location estimate and current spring anchor using (11)*
$\boldsymbol{f = \overrightarrow{dis} * W_j^t}$	*Define the force for spring anchor j as in (12)*
$\boldsymbol{netf = netf - f}$	*The net force is defined equivalent to (13)*
end	
$\boldsymbol{posEstimate = prevPos + \tau * \frac{netf}{n}}$	*Define the current iterations position estimate, as in (14)*
$\boldsymbol{prevPos = posEstimate}$	*Update the previous position estimate*
if $\boldsymbol{\frac{mag(netf)*\tau}{n} < \delta}$	*Return early if position estimate has reached predicted location*
break	
end	
end	

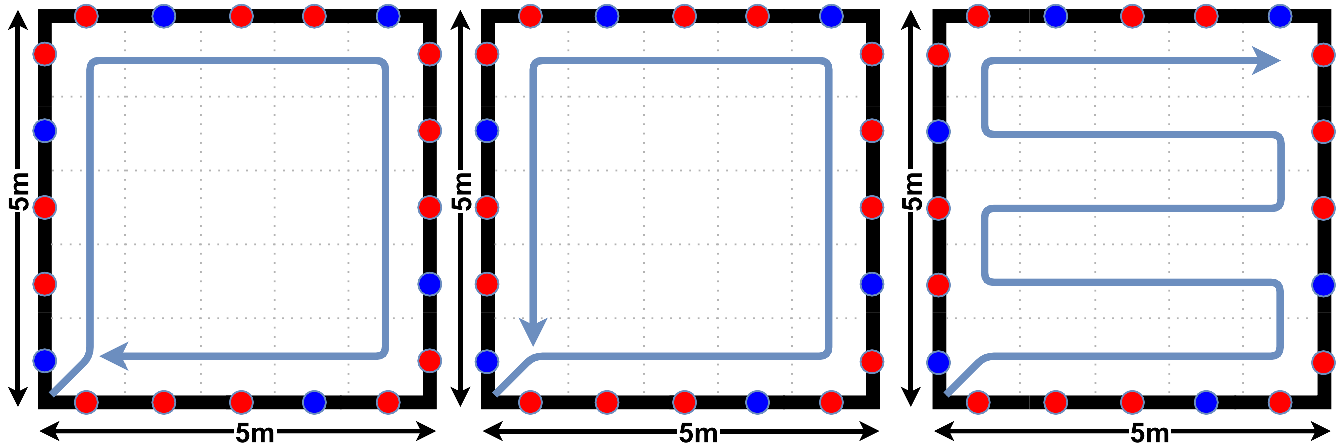

FIGURE 7. Church Hall Test Environment – Node Placement and Walking Trajectories

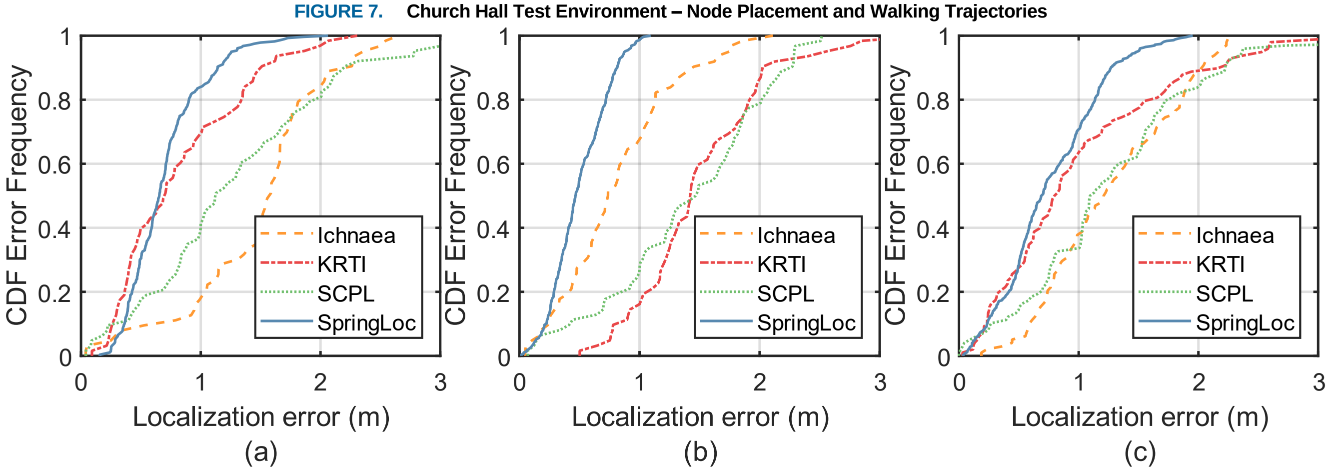

FIGURE 8. Church Hall 20 Node Results – (a) Clockwise trajectory, (b) Anticlockwise trajectory, (c) Zigzag trajectory

$$\overrightarrow{\mathrm{dis}_k} = \mathrm{prevPos} - \mathrm{SA}_{\mathrm{f,k}} \quad (11)$$

with the force defined as:

$$f_k = \overrightarrow{dis_k} * W_k \quad (12)$$

Assuming there are n springs, the net force over all springs is defined as:

$$\textstyle\sum_{k=1}^{n}(netf = netf - f_k) \quad (13)$$

with the position estimate defined as:

$$Pos = prevPos + \tau * \frac{netf}{n} \quad (14)$$

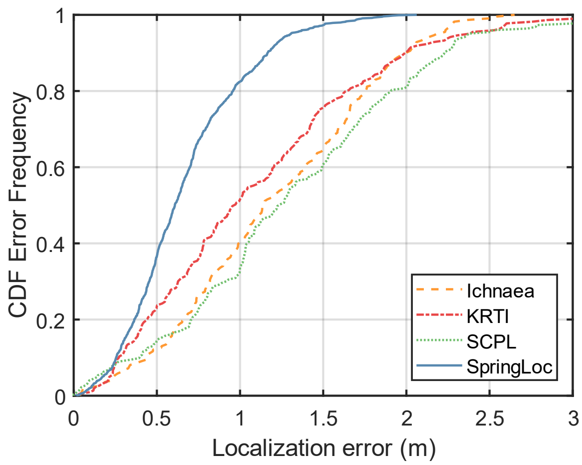

FIGURE 9. **Church Hall 20 Node Results – Combined Trajectories**

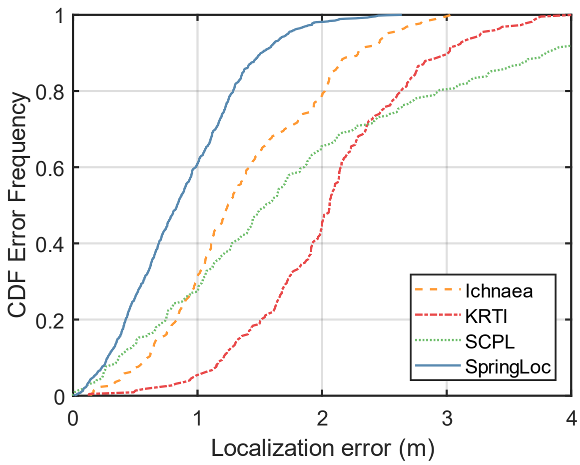

FIGURE 10. **Church Hall 6 Node Results – Combined Trajectories**

A full pseudocode breakdown of the SpringLoc algorithm is included in Algorithm 1 and Algorithm 2 and all parameter values used are given in Table 1.

E. ALGORITHM EDGE CASES

These are the scenarios that may cause the algorithm to either not converge correctly or perform suboptimally. The first case arises when no affected links, ζ^t, are triggered in module two. This can occur if the target is walking through a temporary blind-spot or has stood relatively motionless for a considerable duration of time. To resolve this, we implement two cases.

If there are no affected links across multiple timesteps, ($length(\zeta^t) = 0$) and ($length(\zeta^{t-1}) = 0$), we assume the subject is currently stationary and set the current position estimate to the previous prediction estimate ($posEstimate = prevPos$). This ensures the subject stays located at the last known spring convergence target. However, if the previous timestep had affected links, $length(\zeta^{t-1}) > 0$, we assume that the subject is moving through a momentary blind-spot. Since no location information is available in the current timestep, the subject is assumed to be maintaining the same velocity and heading as their previous timestep. Their position estimate is given as:

$$posEstimate = prevPos + \overrightarrow{project} \tag{15}$$

where $\overrightarrow{project}$ is a vector defined by the previous trajectory:

$$\overrightarrow{project}_t = posEstimate_{t-1} - prevPos_{t-1} \tag{16}$$

The other edge case occurs when only one affected link is detected, $length(\zeta^t) = 1$. Since module four requires at least two affected links to calculate spring anchors, an artificial link is inserted into the affected links array. The artificial 'injected' link is defined by:

$$\begin{aligned} &\boldsymbol{TX}_{\boldsymbol{injected}} = prevPos \\ &\boldsymbol{RX}_{\boldsymbol{injected}} = prevPos + \overrightarrow{project} \\ &\zeta^t_{injected} = [\boldsymbol{TX}_{injected}, \boldsymbol{RX}_{injected}] \end{aligned} \tag{17}$$

IV. EXPERIMENT AND RESULTS

SpringLoc infers a subject's location by analyzing the changes in RSSI values across a network of wireless links. The network consisted of 20 Texas Instruments CC2530 Zigbee radios for the first experiment, and six radios for the

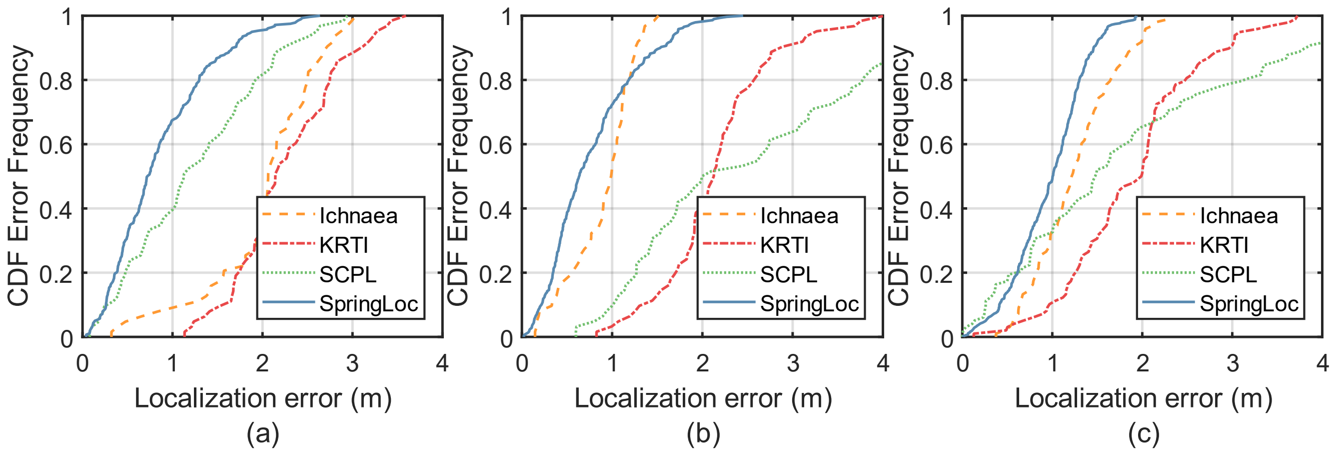

FIGURE 11. **Church Hall 6 Node Results – (a) Clockwise trajectory, (b) Anticlockwise trajectory, (c) Zigzag trajectory.**

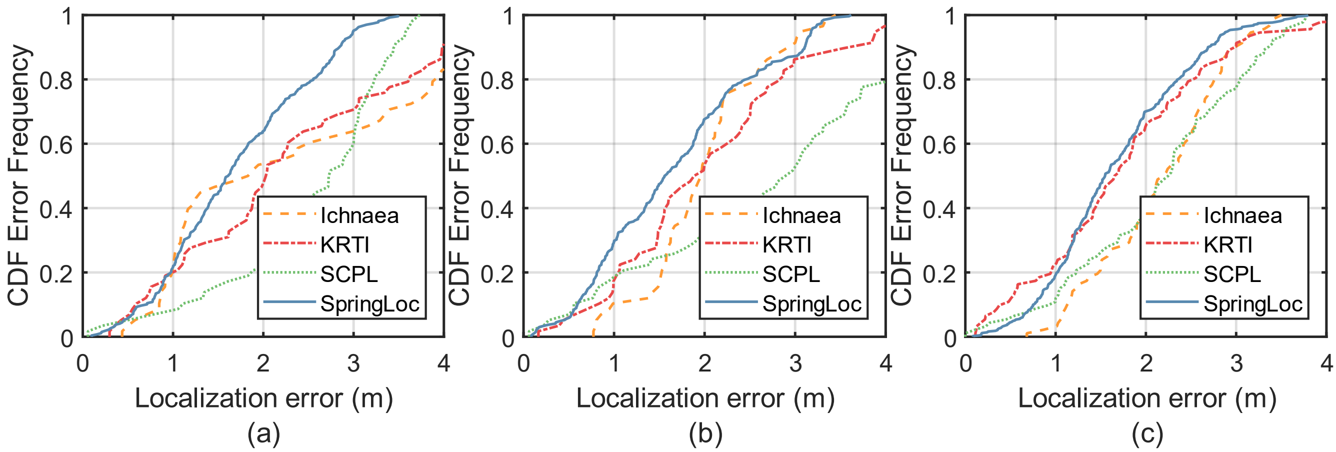

FIGURE 12. **Office Space Results – (a) Clockwise trajectory, (b) Anticlockwise trajectory, (c) Zigzag trajectory.**

second and third experiments. The radios operated at maximum power and were set to channel 26. The network was set up with a token ring protocol, where each node takes turns sending a broadcast packet. The broadcast packet's are received by every other node within range, which would record the ID of the transmitting (TX) node and the packets RSSI value. Each transmitted broadcast packet would contain its own ID, followed by a list of the last round's received RSSI values. A master node listens to all network traffic and sends all link RSSI values back to a PC for live processing. The network was set up to run at 5Hz (i.e. 5 RSSI values for every network link, every second). If the master node detects that a node has missed incoming packets
(as its broadcast RSSI list only contained a few values), it would fill in the missing RSSI values with known dummy values to keep the data structure sizes consistent. This also allows for the PC to know which packets were dropped for each node, for each time frame.

Experiments were conducted in two diverse environments. The first environment consisted of a church hall, which had

TABLE I
SPRINGLOC PARAMETERS

Symbol	Description	Value
α_S	short-term histogram forgetting factor	0.9
α_L	long-term histogram forgetting factor	0.05
ϖ	kernel smoothing parameter	30
β_{20}	affected link threshold (20 nodes)	1.4
β_6	affected link threshold (6 nodes)	0.63
η	affected link proximity constant	0.5
ρ	spring anchor selection constant	2
ψ	maximum spring iterations per timestep	8
τ	spring step size scaling parameter	0.05
δ	Spring early breakout parameter	0.015

the chairs removed from the center of the room, giving approximately 120m^2 of open space. The sensors were mounted on stands 1.2m above the ground and placed in a square encompassing 25m^2 in the center of the open space.

FIGURE 13. Office Space Results – Combined Trajectories

The second environment consisted of a cluttered office space of approximately 44m^2, where computers and laboratory equipment were set up around the perimeter of the room. The nodes were wall-mounted around the perimeter of the room at 1.4m above the ground. In both environments, the Wi-Fi was turned off and a Rohde & Schwarz Spectrum Rider FPH spectrum analyzer was used to ensure that there was no significant 2.4GHz interference present. Multiple walking trajectories were used per subject in both environments to ensure that we measured the algorithm's performance across the entire test space. For the test involving 20 nodes, the red and blue nodes were used, as shown in Fig. 7. For tests involving only 6 nodes, only the blue nodes were used.
We compared SpringLoc with three well cited DFL approaches from literature: Fingerprinting-based SCPL, link-based Ichnaea and RTI-based KRTI. For SCPL's fingerprinting, the office space was divided into 21 cells, and the church hall was divided into 25 cells. Though SpringLoc can run in real time, for these experiments, all RSSI values received by the processing pc were stored to a file. This allows for SpringLoc to be fairly compared with existing approaches across both environments, using the exact same readings.

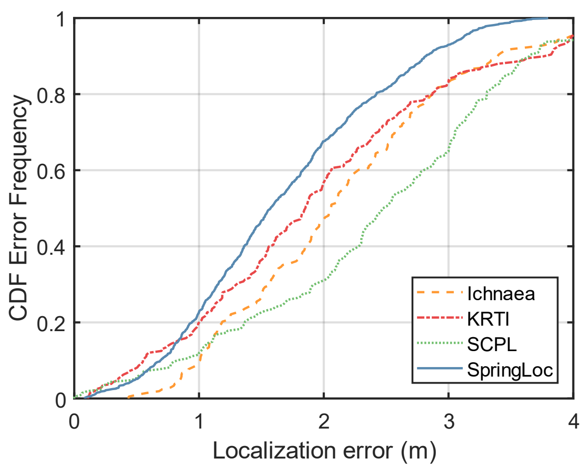

FIGURE 13. **Office Space Results – Combined Trajectories**

During testing, SpringLoc took an average of 8 milliseconds to process each timesteps RSSI values. Since this is significantly faster than the network rate of 5Hz, it confirms real-time viability. For each test, two sets of data were recorded. The first set of data included three fingerprint subsets. The first subset recorded RSSI readings when no subject was present in the test environment. The second subset consisted of labelled RSSI readings when a single roaming target was standing stationary at the center of each known cell. The third subset included labelled RSSI readings from when a single subject was moving randomly within the confines of a single known cell. This dataset was used by any algorithm that required them for offline calibration. The second dataset consisted of the RSSI values recorded at 5Hz intervals when a subject was walking at a known constant speed, through a known trajectory. Care was taken to ensure that the walking speed remained constant for each subject. For each of the two environments, three walking trajectories were explored. The subject would either walk near the perimeter in a clockwise or anticlockwise route, or the subject would follow a zig-zag trajectory covering the whole test environment. The trajectories traversed are outlined in Fig. 7 and were the same in both the church hall and cluttered office space environments. This allowed us to compare whether the trajectory had any influence on a DFL systems accuracy, and whether the effect of walking along different trajectories affected DFL algorithms differently.

For the first experiment, we utilized 20 nodes positioned in a square, in the church hall, as shown in Fig. 7. The church hall has no walls, support pillars or furniture within the immediate vicinity of the test environment. This minimizes the likelihood of dominant multipath propagation components, providing an opportunity to compare SpringLoc with other approaches under reasonably ideal conditions.

The second experiment, undertaken in the church hall, and third experiment, undertaken in the office, utilized only six nodes each. This was done to benchmark SpringLoc against other RSSI based DFL approaches with a node density that would be realistically found within a Smart Home deployment. We have represented the results with two Cumulative Distribution Function (CDF) plots for each experiment, (Fig. 8/Fig. 9 for experiment 1, Fig. 10/Fig. 11 for experiment 2 and Fig. 12/Fig. 13 for experiment 3). The first plot shows the accuracy of each separate walking trajectory (clockwise/anticlockwise/zig-zag) within an experiment. The second CDF plot combines the data from each trajectory into one dataset and shows the overall performance for a given experiment.

A. EXPERIMENT 1

Figure 8 clearly shows that a subject's trajectory can greatly influence the tracking ability of the traditional approaches. This is not an issue with SpringLoc as shown by the consistent shape of the empirical CDF error curve. SpringLoc also outperformed all other benchmarked approaches, achieving better median and 90th percentile errors across every trajectory. When the data across trajectories is combined, as seen in Fig. 9, the effect of this becomes more pronounced, with SpringLoc outperforming existing approaches by a significant margin. This suggests that SpringLoc is more robust to spurious large errors than other approaches. This can also be clearly seen by the maximum error in Fig. 9, where SpringLoc's maximum error is more than 1m lower than any other approach.

B. EXPERIMENT 2

When the number of deployed nodes was reduced to six, the performance of all algorithms degraded as expected. However, unlike the other approaches, SpringLoc managed to maintain a sub-meter overall median error, as shown in Fig. 10, proving its viability even under a low node density. It was also relatively unaffected by the subject's trajectory as shown in Fig. 11. This shows that SpringLoc is resilient to varying walking trajectories and is also able to maintain a superior accuracy to existing approaches, even when the number of deployed nodes is reduced from 20 to 6.

C. EXPERIMENT 3

Experiment 3 utilized 6 nodes in a cluttered office environment with potential for significant multipath components, as shown in Fig. 3. SpringLoc outperformed all other benchmarked algorithms and maintained consistent performance across all trajectories as shown in Fig. 12. This suggests that SpringLoc's superior accuracy is less susceptible to environmental variations, as it maintained the best localization error across multiple indoor test locations. It was also the only approach that did not suffer from errors exceeding 4m, as shown in Fig. 13.

V. DISCUSSION

The CDF plots have been provided for SpringLoc as they allow for algorithms performance to be compared over the whole quartile range, rather than using a singular numerical metric. To provide consistency with existing literature, numerical results are also provided in Table II. Since literature does not have an agreed numerical standard for benchmarking DFL algorithms, we use metrics standardised by indoor active tracking. The EvAAL framework recommends using the 'third quartile of point Euclidiean error', equivalent to the 75th percentile error [51]. The formal standard ISO/IEC 18305 has been recently introduced to standardize indoor localization scoring, however it does not provide explicit guidelines for DFL [52]. ISO/IEC 18305 mentions three scoring metrics that can be utilized by a DFL approach. It recommends using the Root-Mean-Square-Error (RMSE), Circular Error Probable (CEP), and Circular Error 95% (CE95). CEP is equivalent to the 2d 50th percentile Euclidean error, and CE95 is equivalent to the 2d 95th percentile Euclidean error. We have incorporated these, alongside the 90th percentile error in Table II. As can be observed, SpringLoc significantly outperforms the other algorithms in every scenario. As expected, when the node density decreased to 6 nodes in experiment 2, from 20 in experiment 1, localization performance decreased with every algorithm. With the lower node density, SpringLoc was the only algorithm that managed to maintain a sub-meter median error. SpringLoc also outperformed other approaches in experiment 3 which featured both a low node density, and complex multipath propagation paths caused by the environment itself. It was the only approach that managed to maintain an RMSE below 2m, and a 90th percentile error below 3m.

Though SpringLoc outperformed all other approaches, it did experience a significant increase in median error from 0.83m in the open church hall, to 1.57m in the cluttered office space. SpringLoc utilizes EWMA weighted histograms, which actively dampen the effect of any spurious outlier values. However, it still suffers increased error if the multipath propagation introduces significant non-transient fading. This shows that while SpringLoc does not presume the noise will follow a zero mean gaussian distribution, it is still detrimentally affected if the complex propagation environment interferes with the average variance that a person introduces to the environment. If an accurate noise model could be attained for complex indoor environments, the accuracy of SpringLoc could improve by better understanding how the attenuation introduced by a target fluctuates due to noise.

Since SpringLoc can form its long-term histogram during live operation, it does not require offline measurements. Therefore, its parameters can be optimized in advance and deployed at an unknown environment without a significant setup cost. Parameters were tuned empirically within a test room, before being deployed in both the Church Hall and Office Space shown. Only the affected link threshold parameter (β) optimized for Church Hall and Office Space respectively. With the other parameters being kept unchanged from their initial test room tuning, SpringLoc still managed to outperform all existing approaches. This shows that the parameters are largely transferable between varying environments, while maintaining an acceptable localization accuracy. Since the affected link threshold is largely coupled with the number of nodes deployed, this could be further generalized based on a given number of nodes and deployment area. An end user only needs to know the number of deployed nodes, and approximate localization area to set up a SpringLoc based system. For example, based on our empirical testing, the maximum β value can be heuristically estimated as: $2 \times \left(\sqrt{\text{Nodes}}/\sqrt{\text{Area (m}^2)}\right)$. Thus, a 140m^2 house utilizing 8 nodes would have an estimated maximum β value of 0.53. When a large number of links are available, a large value can be set for β, which causes the system to only react to strongly affected links, resulting in increased accuracy. For low node deployments, there may be multiple areas with very sparse link density. Since this reduces the likelihood that moving subjects will trigger strong link interactions, the threshold is reduced. This acts to reduce the number of potential blind spots within an environment.

TABLE II

Numerical Results

Experiment	Algorithm	RMSE	50% Error	75% Error	90% Error	95% Error
Experiment 1 Church Hall 20 Nodes	Ichnaea	1.34	1.138	1.66	2.01	2.20
	KRTI	1.29	0.97	1.48	1.99	2.39
	SCPL	1.54	1.23	1.78	2.23	2.42
	SpringLoc	**0.75**	**0.60**	**0.86**	**1.16**	**1.30**
Experiment 2 Church Hall 6 Nodes	Ichnaea	1.51	1.24	1.92	2.29	2.53
	KRTI	2.18	2.06	2.48	3.01	3.27
	SCPL	2.19	1.55	2.60	3.80	4.27
	SpringLoc	**1.00**	**0.83**	**1.21**	**1.51**	**1.72**
Experiment 3 Office Space 6 Nodes	Ichnaea	2.34	2.05	2.71	3.39	3.98
	KRTI	2.32	1.85	2.60	3.80	3.98
	SCPL	2.70	2.48	3.18	3.65	4.58
	SpringLoc	**1.85**	**1.57**	**2.22**	**2.82**	**3.12**

VI. CONCLUSIONS AND FUTURE WORKS

SpringLoc has shown that careful 'affected link' selection based on histogram difference, coupled with spring-relaxation can increase the performance of an RSSI based DFL approach in real life scenarios. In the initial 20 node benchmark, SpringLoc surpassed all other algorithms, achieving median and 90th percentile errors of 0.60m and 1.16m respectively. SpringLoc achieved a median localization accuracy of 0.83m in the church hall and 1.57m in the office space, surpassing existing approaches median error by up to 59%, when the node density was reduced.

Though SpringLoc does not require any offline measurements, it does need to know the location of the transceiver nodes. Future work could include performing self-localization [53-55] on the nodes themselves, while following a deployment strategy that could be realistically followed by end users. This paper only investigated single entity localization; multi-entities is left for future work. This could be accomplished by using a separate set of springs for each detected entity, after accurately counting the number of subject's present, and the affected links for each. Furthermore, RSSI is a coarse metric when compared to Wi-Fi CSI. If CSI ever became readily accessible in COTS equipment, SpringLoc could be implemented using CSI to further improve the performance.

ACKNOWLEDGMENT

The authors thank Baden Parr for his suggestions on how to formulate DFL as a spring-relaxation problem and Nathaniel Faulkner and Gene Hopkins for their help with data collection. The authors would also like to thank the anonymous reviewers for their insightful comments that helped improve the quality of this paper.

REFERENCES AND FOOTNOTES

[1] Q. Lei, H. Zhang, H. Sun, and L. Tang, "Fingerprint-Based Device-Free Localization in Changing Environments Using Enhanced Channel Selection and Logistic Regression," *Ieee Access*, vol. 6, pp. 2569-2577, 2018.

[2] Z. Wang, H. Liu, S. Xu, X. Bu, and J. An, "Bayesian Device-Free Localization and Tracking in a Binary RF Sensor Network," *Sensors (Basel)*, vol. 17, no. 5, p. 969, Apr 27 2017.

[3] Y. Zhao, N. Patwari, J. M. Phillips, and S. Venkatasubramanian, "Radio tomographic imaging and tracking of stationary and moving people via kernel distance," in *Proceedings of the 12th international conference on Information processing in sensor networks - IPSN '13*, Philadelphia, Pennsylvania, USA, 2013, 2461410: ACM, pp. 229-240.

[4] Y. Zhao and N. Patwari, "Robust Estimators for Variance-Based Device-Free Localization and Tracking," *IEEE Transactions on Mobile Computing*, vol. 14, no. 10, pp. 2116-2129, 2015.

[5] H. Huang, H. Zhao, X. Li, S. Ding, L. Zhao, and Z. Li, "An Accurate and Efficient Device-Free Localization Approach Based on Sparse Coding in Subspace," *Ieee Access*, vol. 6, pp. 61782-61799, 2018.

[6] D. Yu, Y. Guo, N. Li, and D. Fang, "Dictionary Refinement for Compressive Sensing Based Device-Free Localization via the Variational EM Algorithm," (in English), *Ieee Access*, vol. 4, pp. 9743-9757, 2016.

[7] R. Zhou, M. Hao, X. Lu, M. Tang, and Y. Fu, "Device-Free Localization Based on CSI Fingerprints and Deep Neural Networks," in *2018 15th Annual IEEE International Conference on Sensing, Communication, and Networking (SECON)*, 2018, pp. 1-9.

[8] J. Wang, X. Zhang, Q. Gao, H. Yue, and H. Wang, "Device-Free Wireless Localization and Activity Recognition: A Deep Learning Approach," *IEEE Transactions on Vehicular Technology*, vol. 66, no. 7, pp. 6258-6267, 2017.

[9] R. Zhou, X. Lu, P. Zhao, and J. Chen, "Device-Free Presence Detection and Localization With SVM and CSI Fingerprinting," *Ieee Sens J*, vol. 17, no. 23, pp. 7990-7999, 2017.

[10] X. Chen, C. Ma, M. Allegue, and X. Liu, "Taming the inconsistency of Wi-Fi fingerprints for device-free passive indoor localization," in *IEEE INFOCOM 2017 - IEEE Conference on Computer Communications*, 2017, pp. 1-9.

[11] D. Halperin, W. Hu, A. Sheth, and D. Wetherall, "Tool release," *ACM SIGCOMM Computer Communication Review*, vol. 41, no. 1, pp. 53-53, 2011.

[12] Y. Xie, Z. Li, and M. Li, "Precise Power Delay Profiling with Commodity WiFi," in *Proceedings of the 21st Annual International Conference on Mobile Computing and Networking - MobiCom '15*, Paris, France, 2015, 2790124: ACM, pp. 53-64.

[13] M. Zhao *et al.*, "Through-Wall Human Pose Estimation Using Radio Signals," in *2018 IEEE/CVF Conference on Computer Vision and Pattern Recognition*, 2018, pp. 7356-7365.

[14] M. Zhao *et al.*, "RF-based 3D skeletons," presented at the Proceedings of the 2018 Conference of the ACM Special Interest Group on Data Communication - SIGCOMM '18, Budapest, Hungary, 2018.

[15] G. Papandreou *et al.*, "Towards accurate multi-person pose estimation in the wild," in *CVPR*, 2017, vol. 3, no. 4, p. 6.

[16] R. Girdhar, G. Gkioxari, L. Torresani, M. Paluri, and D. Tran, "Detect-and-Track: Efficient Pose Estimation in Videos," in *Proceedings of the IEEE Conference on Computer Vision and Pattern Recognition*, 2018, pp. 350-359.

[17] C. Xu *et al.*, "SCPL: Indoor device-free multi-subject counting and localization using radio signal strength," in *2013 ACM/IEEE International Conference on Information Processing in Sensor Networks (IPSN)*, 2013, pp. 79-90.

[18] I. Sabek, M. Youssef, and A. V. Vasilakos, "ACE: An Accurate and Efficient Multi-Entity Device-Free WLAN Localization System," *IEEE Transactions on Mobile Computing*, vol. 14, no. 2, pp. 261-273, 2015.

[19] B. Han, Z. Wang, H. Liu, S. Xu, X. Bu, and J. An, "Shadow fading assisted device-free localization for indoor environments," in *2016 8th International Conference on Wireless Communications & Signal Processing (WCSP)*, 2016, pp. 1-5.

[20] J. Wang *et al.*, "E-HIPA: An Energy-Efficient Framework for High-Precision Multi-Target-Adaptive Device-Free Localization," (in English), *IEEE Transactions on Mobile Computing*, vol. 16, no. 3, pp. 716-729, Mar 2017.

[21] Y. Chiang, W. Hsu, S. Yeh, Y. Li, and J. Wu, "Fuzzy support vector machines for device-free localization," in *2012 IEEE International Instrumentation and Measurement Technology Conference Proceedings*, 2012, pp. 2169-2172.

[22] B. Mager, P. Lundrigan, and N. Patwari, "Fingerprint-Based Device-Free Localization Performance in Changing Environments," (in English), *Ieee J Sel Area Comm*, vol. 33, no. 11, pp. 2429-2438, Nov 2015.

[23] H. Huang and S. Lin, "WiDet," presented at the Proceedings of the 21st ACM International Conference on Modeling, Analysis and Simulation of Wireless and Mobile Systems - MSWIM '18, Montreal, QC, Canada, 2018.

[24] J. Zhang, W. Xiao, S. Zhang, and S. Huang, "Device-Free Localization via an Extreme Learning Machine with Parameterized Geometrical Feature Extraction," *Sensors (Basel)*, vol. 17, no. 4, p. 879, Apr 17 2017.

[25] Y. Guo, K. Huang, N. Jiang, X. Guo, Y. Li, and G. Wang, "An Exponential-Rayleigh Model for RSS-Based Device-Free Localization and Tracking," (in English), *IEEE Transactions on Mobile Computing*, vol. 14, no. 3, pp. 484-494, Mar 2015.

[26] Y. Zheng and A. Men, "Through-wall tracking with radio tomography networks using foreground detection," in *2012 IEEE Wireless Communications and Networking Conference (WCNC)*, 2012, pp. 3278-3283.

[27] A. Saeed, A. E. Kosba, and M. Youssef, "Ichnaea: A Low-Overhead Robust WLAN Device-Free Passive Localization System," (in English), *Ieee J-Stsp*, vol. 8, no. 1, pp. 5-15, Feb 2014.

[28] J. Wilson and N. Patwari, "Radio Tomographic Imaging with Wireless Networks," (in English), *IEEE Transactions on Mobile Computing*, vol. 9, no. 5, pp. 621-632, May 2010.

[29] O. Kaltiokallio, M. Bocca, and N. Patwari, "Enhancing the accuracy of radio tomographic imaging using channel diversity," in *2012 IEEE 9th International Conference on Mobile Ad-Hoc and Sensor Systems (MASS 2012)*, 2012, pp. 254-262.

[30] B. Wei, A. Varshney, N. Patwari, W. Hu, T. Voigt, and C. T. Chou, "dRTI," presented at the Proceedings of the 14th International Conference on Information Processing in Sensor Networks - IPSN '15, Seattle, Washington, 2015.

[31] S. Denis, R. Berkvens, G. Ergeerts, and M. Weyn, "Multi-frequency sub-1 GHz radio tomographic imaging in a complex indoor environment," in *2017 International Conference on Indoor Positioning and Indoor Navigation (IPIN)*, 2017, pp. 1-8.

[32] Z. Yang, Z. Zhou, and Y. Liu, "From RSSI to CSI," *ACM Computing Surveys*, vol. 46, no. 2, pp. 1-32, 2013.

[33] J. Xiao, K. Wu, Y. Yi, L. Wang, and L. M. Ni, "Pilot: Passive Device-Free Indoor Localization Using Channel State Information," in *Distributed Computing Systems (ICDCS), 2013 IEEE 33rd International Conference on*, 2013, pp. 236-245.
[34] Z. Han, Z. Yuxun, Y. Jianfei, G. Weixi, X. Lihua, and J. S. Costas, "WiFi-Based Human Identification via Convex Tensor Shapelet Learning," *AAAI Conference on Artificial Intelligence; Thirty-Second AAAI Conference on Artificial Intelligence*, 2018.
[35] X. Dang, Y. Huang, Z. Hao, and X. Si, "PCA-Kalman: device-free indoor human behavior detection with commodity Wi-Fi," *Eurasip J Wirel Comm*, vol. 2018, no. 1, p. 214, 2018.
[36] H. Zou, Y. Zhou, J. Yang, W. Gu, L. Xie, and C. Spanos, "FreeDetector: Device-Free Occupancy Detection with Commodity WiFi," in *2017 IEEE International Conference on Sensing, Communication and Networking (SECON Workshops)*, 2017, pp. 1-5.
[37] H. Zhang *et al.*, "Wireless non-invasive motion tracking of functional behavior," *Pervasive Mob Comput*, vol. 54, pp. 29-44, 2019/03/01/ 2019.
[38] X. Wang, L. Gao, S. Mao, and S. Pandey, "CSI-based Fingerprinting for Indoor Localization: A Deep Learning Approach," *IEEE Transactions on Vehicular Technology*, vol. 66, no. 1, pp. 1-1, 2016.
[39] S. Kumar, D. Cifuentes, S. Gollakota, and D. Katabi, "Bringing cross-layer MIMO to today's wireless LANs," *ACM SIGCOMM Computer Communication Review*, vol. 43, no. 4, pp. 387-398, 2013.
[40] (2019). *USRP Software Defined Radio Device* [Online]. Available: https://www.ettus.com.
[41] (2019). *WARP Project* [Online]. Available: http://warpproject.org.
[42] Y. Ma, G. Zhou, and S. Wang, "WiFi Sensing with Channel State Information: A Survey," *ACM Computing Surveys*, vol. 52, no. 3, p. 35, 2019.
[43] W.-T. Yu, J.-W. Choi, Y. Kim, W.-H. Lee, and S.-C. Kim, "Self-organizing Localization with Adaptive Weights for Wireless Sensor Networks," *Ieee Sens J*, vol. 18, no. 20, pp. 1-1, 2018.
[44] B.-C. Seet, Q. Zhang, C. H. Foh, and A. C. M. Fong, "Hybrid RF Mapping and Kalman Filtered Spring Relaxation for Sensor Network Localization," *Ieee Sens J*, vol. 12, no. 5, pp. 1427-1435, 2012.
[45] J. Eckert, F. Villanueva, R. German, and F. Dressler, "Distributed Mass-Spring-Relaxation for Anchor-Free Self-Localization in Sensor and Actor Networks," in *2011 Proceedings of 20th International Conference on Computer Communications and Networks (ICCCN)*, 2011, pp. 1-8.
[46] J. Stipes, R. Hawthorne, D. Scheidt, and D. Pacifico, "Cooperative Localization and Mapping," in *2006 IEEE International Conference on Networking, Sensing and Control*, 2006, pp. 596-601.
[47] A. S. Paul and E. A. Wan, "RSSI-Based Indoor Localization and Tracking Using Sigma-Point Kalman Smoothers," (in English), *Ieee J-Stsp*, vol. 3, no. 5, pp. 860-873, Oct 2009.
[48] B. Li, H. Du, and W. Li, "A Potential Field Approach-Based Trajectory Control for Autonomous Electric Vehicles With In-Wheel Motors," *IEEE Transactions on Intelligent Transportation Systems*, vol. 18, no. 8, pp. 2044-2055, 2017.
[49] W. Li, C. Yang, Y. Jiang, X. Liu, and C.-Y. Su, "Motion Planning for Omnidirectional Wheeled Mobile Robot by Potential Field Method," *Journal of Advanced Transportation*, vol. 2017, pp. 1-11, 2017, Art no. 4961383.
[50] D. Sunday, "Distance between lines and segments with their closest point of approach," *Softsurfer. com Algorithm*, vol. 7, 2004.
[51] F. Potorti *et al.*, "Comparing the Performance of Indoor Localization Systems through the EvAAL Framework," *Sensors (Basel)*, vol. 17, no. 10, p. 2327, Oct 13 2017.
[52] "ISO/IEC 18305:2016," ISO/IEC JT, Information technology -- Real time locating systems --Test and evaluation of localization and tracking systems. 2016, [Online]. Available: https://www.iso.org/standard/62090.html.
[53] M. Al-Hattab, M. Takruri, H. Attia, and H. Al-Omari, "Decentralized localization in wireless sensor networks," in *Electrical and Computing Technologies and Applications (ICECTA), 2017 International Conference on*, 2017: IEEE, pp. 1-5.
[54] C. Alippi and G. Vanini, "A RSSI-based and calibrated centralized localization technique for Wireless Sensor Networks," in *Pervasive computing and communications workshops, 2006. PerCom workshops 2006. Fourth annual IEEE international conference on*, 2006: IEEE, pp. 5 pp.-305.
[55] A. T. Ihler, J. W. Fisher, R. L. Moses, and A. S. Willsky, "Nonparametric belief propagation for self-localization of sensor networks," *Ieee J Sel Area Comm*, vol. 23, no. 4, pp. 809-819, 2005.

Daniel Konings (M'17) received his BE(Hons) from Massey University, Auckland, New Zealand in Computer Systems and Electronics Engineering in 2014, where he is currently pursuing the Ph.D. degree with the School of Food and Advanced Technology (SF&AT). His current research interests include indoor localization, digital signal processing, machine learning, IoT & wireless sensor networks. Daniel is a Student Member of the Institute of Electrical and Electronics Engineers (IEEE).

Fakhrul Alam (M'17-SM'19) received his BSc (Hons) in Electrical & Electronic Engineering from BUET, Bangladesh and MS and Ph.D. in Electrical Engineering from Virginia Tech, USA. He is currently a senior lecturer at the School of Food and Advanced Technology, Massey University, New Zealand. His research interests include indoor localization, 5G & visible light communication, disaster management with 5G, IoT & wireless sensor networks. He is a senior member of Institute of Electrical and Electronics Engineers (IEEE) and a member of the Institute of Engineering and Technology (IET).

Frazer Noble received his BE (Hons) in Mechatronics, ME (Hons) in Engineering, and PhD in Engineering from Massey University, New Zealand. He is currently a lecturer at the School of Food and Advanced Technology, Massey University, New Zealand. His research interests include mechatronics, robotics and automation, machine vision, and machine learning.

Edmund M-K Lai (M'82-SM'95) received his BE(Hons) and PhD from The University of Western Australia, both in Electrical Engineering, in 1982 and 1991 respectively. He is currently a Professor of Information Engineering at Auckland University of Technology, New Zealand. He has previously held faculty positions at universities in Australia, Hong Kong, and Singapore. His research interests include digital signal processing, digital communications and networks, computational and swarm intelligence, and artificial neural networks. Prof. Lai is a fellow of the Institution of Engineering and Technology (IET) and a senior member of the Institute of Electrical and Electronics Engineers (IEEE).

Chapter 4

This chapter contains content from the following article, republished with permission. In accordance with IEEE's republishing policy, any full text that has been included is the unmodified accepted article. This means that while the content is identical to the published article, there may be stylistic differences.

doi: 10.1109/JSEN.2019.2922772

Improved Distance Metrics for Histogram based Device-free Localization

Daniel Konings, *Student Member, IEEE*, Fakhrul Alam, *Senior Member, IEEE*, Frazer Noble and Edmund M-K Lai, *Senior Member, IEEE*

***Abstract*— Device-free localization (DFL) systems that that rely on the wireless received signal strength indicator (RSSI) metric have been reported in literature for almost a decade. Histogram Distance based DFL (HD-DFL) techniques that operate by constructing RSSI histograms are highly effective as they can localize stationary and moving people in both outdoor and complex indoor environments. A key step in the histogram approaches is the estimation of the difference between the "long-term" and "short-term" histograms. Existing HD-DFL methods use either Kullback-Leibler or the subsequent improvement, Kernel distance, to measure this difference. This paper is the first known work to compare an extensive range of histogram distance metrics within a DFL context and demonstrate how a judicious selection of a distance metric can significantly increase the performance of an HD-DFL system. Results from practical implementation in two different environments show that some distance metrics perform considerably better than Kernel distance when used for existing DFL techniques like Radio Tomographic Imaging (RTI) and SpringLoc, with the overall median tracking error reducing by up to 25%.**

***Index Terms*— Device-free Localization, Radio Tomographic Imaging, Indoor Positioning Systems, Spring relaxation, Histogram Distance**

I. INTRODUCTION

THE spatial features of wireless signals can be used to infer the location of an entity which has led to significant interest in Indoor Positioning Systems (IPS). Potential applications can include healthcare and assisted living [1, 2], search and rescue [3], multi-subject counting/tracking[4, 5], offices [6], human-robot workspaces [7] or smart homes [8].

Device-free Localization (DFL) is a form of IPS that does not require the tracked entity to carry a device (e.g. a wireless transceiver). This allows all subjects within an environment to be tracked using the system and can facilitate location-based services. Recent literature has largely focused on maximizing the accuracy of DFL approaches using Wi-Fi Channel State Information (CSI) [1, 6, 9], software defined radio (SDR) [10], fingerprint refinement [11], classification improvement [12-15], or environmental robustness [16]. Since CSI offers finer-grained features than the competing Received Signal Strength Indicator (RSSI) metric, recent machine learning approaches have largely focused on CSI-based DFL using: shapelet learning [17], Support-vector machines (SVM) [6, 18], Random Forest [19], Hidden Markov Models (HMM) [20], and Deep Learning [21]. Though CSI is routinely used in recent literature, it can only currently be implemented using SDR or legacy Wi-Fi radios with modified drivers [22-25]. This means that CSI methods cannot currently utilize modern commercial-off-the-shelf (COTS) equipment and are therefore unsuitable for a Smart Home deployment. CSI methods also do not support Bluetooth or Zigbee hardware which are commonly utilized COTS radios alongside Wi-Fi. Another issue is that recent software defined radio approaches typically makes use of Frequency Modulated Carrier Waves (FMCW) for localization, however these techniques require significant bandwidth and custom radio frontends. This limits usability as neither CSI or FMCW approaches would be able to utilize existing wireless infrastructure.

The RSSI metric is useful for implementing an IPS as it is commonly available in COTS equipment, across multiple popular wireless platforms including Bluetooth, Wi-Fi and Zigbee. This allows for IPS systems to be designed with the intention of integrating them within a standard built environment, using existing infrastructure, with a minimal cost associated with installation. Since existing mains powered Smart Home devices are often required to have their wireless modules on at all times to listen for commands, the added requirement of regular wireless transmissions will not significantly increase the system's power consumption. The RSSI metric is also stable under interference, as RSSI values of correctly received packets, remain unchanged [26].

Recent literature pertaining to RSSI based approaches predominately focus on improving classification approaches by using robust channel selection [27], fusing RSSI/CSI features [28], or improving classification accuracy through using novel machine learning (ML) techniques. Recently employed ML techniques include: extreme learning[15], Convolutional Neural Networks (CNN) [13], logistic regression [27], sparse coding [14]. The problem with ML approaches is that they

This work was supported in part by the Massey University Doctoral Scholarships.

Daniel Konings is with the Department of Mechanical & Electrical Engineering, Massey University, Auckland 0632, New Zealand (email: d.konings@massey.ac.nz).

Fakhrul Alam is with the Department of Mechanical & Electrical Engineering, Massey University, Auckland 0632, New Zealand.

Frazer Noble is with the Department of Mechanical & Electrical Engineering, Massey University, Auckland 0632, New Zealand.

Edmund M-K is with the School of Engineering, Computer and Mathematical Sciences, Auckland University of Technology, Auckland 1010, New Zealand.

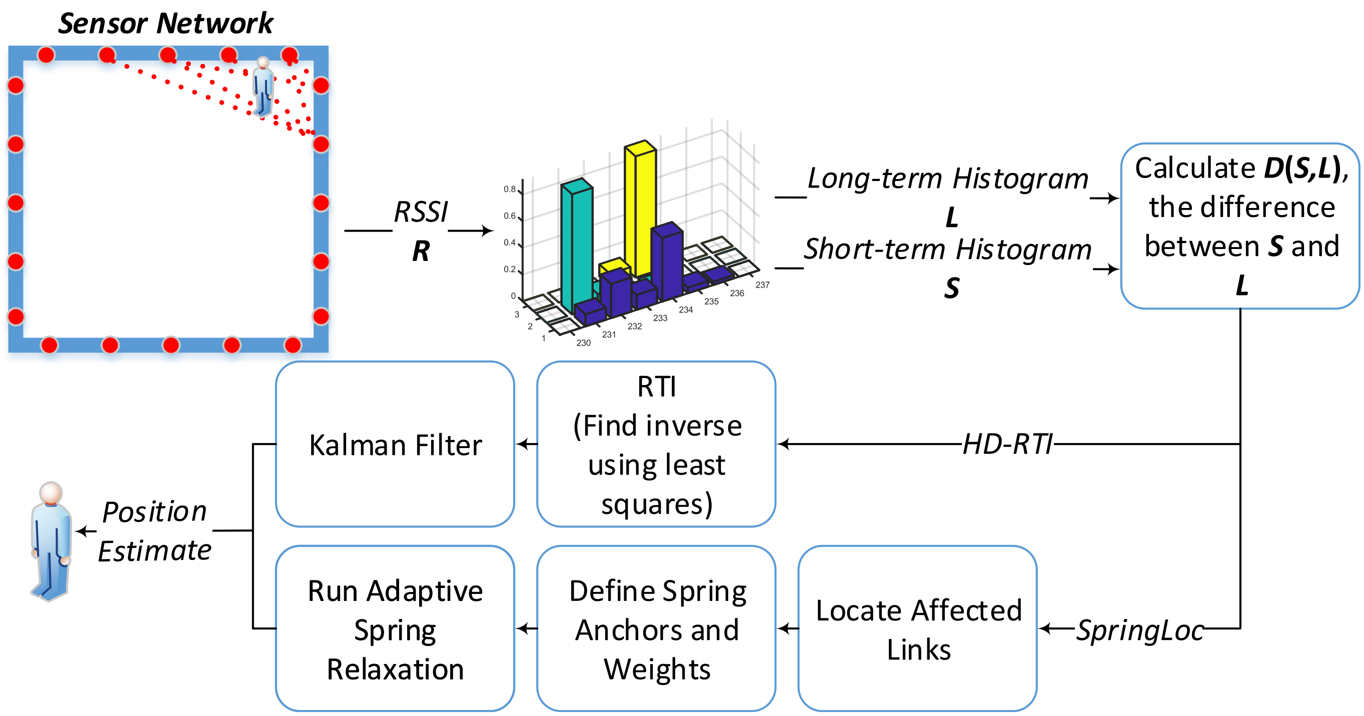

Fig. 1. Overview of HD-RTI and SpringLoc Algorithms

require extensive offline data collection to train the classifier. To enable DFL IPS systems to be easily utilized by general consumers, they must be simple to use with minimal setup requirements. Since an offline site survey cannot be easily performed by end users, ML classification approaches and fingerprint refinement techniques have limited use in practical implementations, where offline data collection cannot be guaranteed. The Radio Tomographic Imaging (RTI) approaches to DFL have an advantage over ML techniques, as they do not require a substantial set of labelled offline training data and have low run-time complexity. The downside to existing RTI approaches is that they require a significant number of nodes (transceivers) to provide robust localization estimates. Existing literature has shown that the nodes can perform self-localization which reduces the human involvement in setup, at the cost of a reduction in accuracy [29, 30].

RTI was first proposed as an IPS implementation by Wilson and Patwari in [31]. They used RSSI attenuation as their feature and looked at the effect a person would have on blocking the Line-Of-Sight (LOS) link path. The problem with RSSI attenuation is that it does not work well in through-wall scenario. In addition, multipath components can often significantly contribute to the change of RSSI values, which can make modelling the LOS change difficult. Recently there have been many attempts to improve on the original RTI approach [32-38] and these have been summarized in Table 1.

Histogram Distance-based RTI (HD-RTI) was first proposed by Zhao and Patwari in [38] and subsequently improved by using Kernel Distance as the histogram difference metric in [32].

SpringLoc is another Histogram Distance-based DFL (HD-DFL) method that has been recently proposed that offers

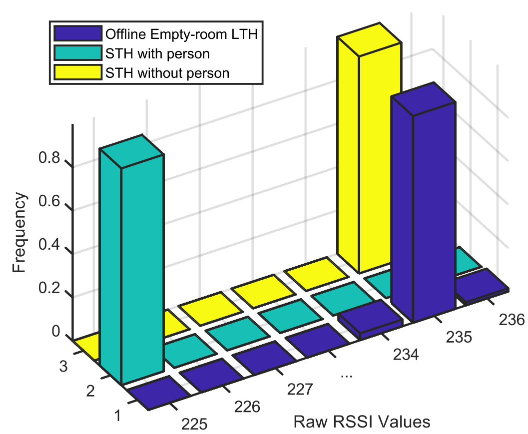

Fig. 2. The effect of a Stationary person's presence on the Short-term histogram (STH), compared to the Long-term histogram (LTH).

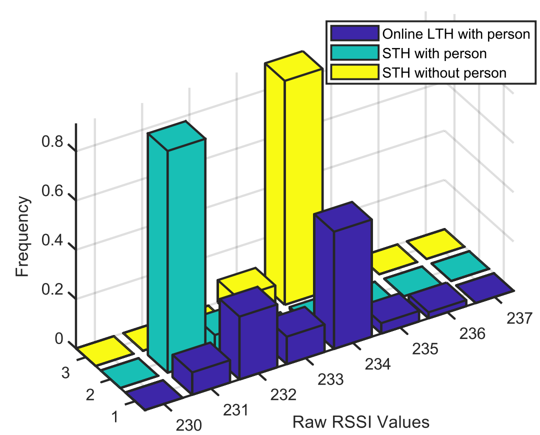

Fig. 3. The effect of a Moving persons presence on both the Short-term (STH) and Long-term histograms (LTH).

TABLE I

Radio Tomographic Imaging Approach Comparisons

Approaches	Localize Stationary Targets	Works Through-walls	Main Limitation
RTI [31]	Yes	No	Original RTI implementation. Using RSSI attenuation as a feature results in poor performance in through-wall/multipath rich environments.
VRTI [33]	No	Yes	Using RSSI variance as the feature prevents the detection of stationary targets.
LSVRT / SubVRT [34]	No	Yes	Using RSSI variance as the feature prevents the detection of stationary targets.
cdRTI [35]	Yes	Yes	Requires large available bandwidth.
dRTI [36]	Yes	Yes	Requires a custom antenna frontend not found in common COTS radios.
ARTI [37]	Yes	Yes	Requires large available bandwidth. It may incorrectly calibrate if links are sparse or there is significant multipath.
HD-RTI [32, 38]	Yes	Yes	Accuracy can be hampered if a non-ideal histogram difference metric is used.

superior accuracy than RTI, especially for low node densities [39]. SpringLoc uses histograms of RSSI values as its feature like HD-RTI. However rather than solving a linear inverse, it treats localization as an energy minimization problem. This is implemented in the form of an adaptive spring relaxation-based tracking algorithm.

In both SpringLoc and HD-RTI, RSSI values are collected for each pairwise link within a network of nodes, as shown in Fig. 1. When an entity traverses through the environment, they inevitably walk close to a LOS link path between a set of nodes. This causes fluctuations in the RSSI values seen by the receiving node. Successive RSSI samples can then be used to form a long-term and short-term RSSI histogram for each link pair, based on a predefined weighting scheme. Histogram based DFL assumes that an entity traversing through an environment will cause a links short-term histogram (STH) to deviate away from the long-term histogram (LTH). By examining which histogram pairs exhibit large differences, the location of an entity can be inferred. The Long-term histogram (LTH) represents a measure of the background while the Short-term histogram (STH) represents the current state. The difference between the LTH and STH represents both the presence of a target, and it’s proximity to the link’s line-of-sight (LOS) path. Both the LTH and STH can be formulated during live operation (as detailed in Section II) which removes the need for offline calibration. The histogram also inherently combines features from both RSSI attenuation and RSSI variance, allowing the system to work well in both open spaces and through-wall environments, and with both moving and stationary people. HD-DFL schemes also do not need recalibration due to environmental change as the histogram feature adapts over time automatically.

A. *Contribution*

This paper makes three main contributions to improve HD-DFL:

- Multiple distance metrics for computing the histogram difference are demonstrated to outperform the current state-of-the-art Kernel Distance by up to 25%
- The concept of Outlier Link Reduction is introduced to HD-RTI, to reduce the effect of erroneous link values. Experimental results show that it reduces the 90% percentile error by up to 8%
- Experimental results in two different environments, a multipath rich laboratory, and an open auditorium verify the proposed implementation for improving both HD-RTI and SpringLoc approaches

The rest of this paper is organized as follows. Section II outlines the software algorithm, Section III discusses the importance of exploring different distance metrics, and their effect on overall accuracy, Section IV covers the physical system implementation, Section V discusses the results and Section VI concludes the paper.

II. Algorithms

For brevity, this paper only provides a concise description of the HD-RTI and SpringLoc approaches to HD-DFL and for a more in-depth understanding, readers are referred to [32] and [39] respectively. Both algorithms compute the difference between RSSI histograms for each link to determine whether a specific link is currently affected by the presence of an entity (using (1) and (2)). Assuming RSSI values have the range $[1, N]$, each histogram is constructed with N bins, where the Nth bin value increases as the frequency of recorded RSSI value N increases. A scheme based on an exponentially weighted moving average (EWMA) calculates the histograms as:

$$h^{l,t} = (1 - \beta)h^{l,t-1} + \beta\zeta(R^{l,t}) \qquad (1)$$

where $h^{l,t}$ is the histogram of link l, at time t , where the value in each bin is between $0 - 1$. β is the forgetting factor between 0 - 1 which determines the weight put on recent measurements, ζ is an indication vector and $R^{l,t}$ is the RSSI of link l at time t.

ζ is a vector of length N where the index given by $R^{l,t}$ is one and every other position is zero.

If we define the long term histogram as L and the short term histogram as S where the forgetting factors beta are set to low and high values respectively in (1) so that $\beta_L < \beta_S$. The kernel distance between them can then be defined by:

$$\mathrm{D(S,L)} = \mathrm{S^T KS} + \mathrm{L^T KL} - 2\mathrm{S^T KL} \qquad (2)$$

where K in a N by N kernel matrix and T represents a transpose. The Epanechnikov kernel was utilized for this paper, following the standard practices from the literature [40]. HD-RTI assumes that the location of a person can be given by the maximum value of the image x, where x can be defined by the vector $x = [x_0, \ldots, x_{P-1}]$ and P is the number of pixels. HD-RTI assumes that d, the set histograms differences for each link, can be expressed as a linear combination of x:

$$d = Wx + n \qquad (3)$$

Where n is a noise vector and W is a weighting model where $W_{l,p}$ for pixel P is zero unless it is located within an 2D ellipse defined with foci at links ls transmitter and receiver nodes.

The aim of RTI is to find the least-squares solution that minimizes the noise, while taking the inverse of (3) to find x. RTI is by nature an ill-posed inverse problem, as W is not full-rank, which means that small amounts of noise in the measurement data can be amplified significantly when (3) is inverted [31]. To minimize this, regularization is used. By utilizing a regularized least-squares formulation, the image x can be defined by:

$$x = (W^T W + \sigma_n^2 C_x^{-1})^{-1} W^T d \qquad (4)$$

where σ_n^2 is the noise variance and C_x is the covariance matrix of x.

For tracking, HD-RTI uses a Kalman filter where the state transition model includes the persons location and velocity, and the observation inputs are provided by the coordinates of the brightest pixel in x.

SpringLoc performs localization by creating an artificial set of anchor points connecting a corresponding fictitious set of springs to the target. This is done by first locating the most affected links. Affected links are found by iterating through each $\mathrm{D(S,L)}$, defined by (2), and saving them to an array if they exceed a predefined threshold. The locations of the artificial anchors are then defined as the coordinates of the intersection points, calculated for each pair of links in the affected links array. A weight is then applied to each spring anchor based on the $\mathrm{D(S,L)}$ from both contributing links. An adaptive spring-relaxation approach is then used to localize and track the target using the targets previous position, the current spring anchors, and the spring anchor weights. SpringLoc has the benefit of peforming well under both low and high node densities, while having a lower runtime complexity than competing particle filter tracking systems.

Histograms created from experimental results, on the system outlined in Section IV, can be seen in Fig. 2 and Fig. 3. Both stationary and moving people can have a significant impact on a histogram formed from the live RSSI values. When a person moves through an area, both the LTH and Short-term histogram (STH), defined by (1), are affected. However, the LTH maintains a significant portion of the RSSI information from before a person was present. In Fig. 2, both the LTH and STH maintain the same value when the environment is empty. When a person enters the environment and stands stationary at a fixed point, the STH quickly updates to a new value, indicating a change has occurred within the environment. In Fig. 3, the effect β has on the LTH and STH can be seen. Though the LTH is slowly changing when a person moves through the environment, the dominant bin maintains the same index as when no entity was present. Therefore, the LTH can be used as a background baseline value, as long as β_L remains small. In contrast with the LTH, the STH's dominant bin quickly settles to a new value. The difference in both the values and shapes of the histograms formed when comparing LTH and STH suggests that they contain information that could be used to infer

TABLE II

HD-RTI - Histogram Distance Implementation Error (m)

		Auditorium		Laboratory	
Distance Metrics	Implementation	Median	90% Error	Median	90% Error
1 - Dice	$D(S,L) = \frac{\sum_{i=1}^{d}(S_i - L_i)^2}{\sum_{i=1}^{d} {S_i}^2 + \sum_{i=1}^{d} {L_i}^2}$	0.57	1.43	1.24	2.82
Bhattacharyya	$D(S,L) = -\ln \sum_{i=1}^{d} \sqrt{S_i L_i}$	0.54	1.32	1.06	2.58
Squared-chord	$D(S,L) = \sum_{i=1}^{d} \left(\sqrt{S_i} - \sqrt{L_i}\right)^2$	0.53	1.36	1.19	2.72
Kernel	$D(S,L) = S^T KS + L^T KL - 2S^T KL$	0.71	1.50	1.38	3.07
Kullback-Leibler	$D(S,L) = \sum_{i=1}^{d} S_i \ln \frac{S_i}{L_i}$	1.27	2.80	2.06	4.05
Chi Squared	$D(S,L) = \frac{1}{2} \sum_{i=1}^{d} \frac{(S_i - L_i)^2}{S_i + L_i}$	0.54	1.34	1.26	2.86
Pearson X^2	$D(S,L) = \sum_{i=1}^{d} \frac{(S_i - L_i)^2}{L_i}$	0.60	1.41	1.12	2.65

TABLE III

SpringLoc - Histogram Distance Implementation Error (m)

	Auditorium		Laboratory	
Distance Metrics	Median	90% Error	Median	90% Error
1 - Dice	0.59	1.22	0.97	1.78
Bhattacharyya	0.57	0.98	0.97	1.59
Squared-chord	0.56	0.97	0.97	1.58
Kernel	0.58	1.17	1.07	2.11
Kullback-Leibler	2.77	3.48	1.97	3.24
Chi Squared	0.58	1.09	0.94	1.64
Pearson X^2	0.68	1.47	0.99	2.05

TABLE IV

HD-RTI (with OLR) - Histogram Distance Implementation Error (m)

	Auditorium		Laboratory	
Distance Metrics	Median	90% Error	Median	90% Error
1 - Dice	0.53	1.30	1.19	2.81
Bhattacharyya	0.52	1.30	1.04	2.56
Squared-chord	0.53	1.34	1.15	2.50
Kernel	0.70	1.51	1.36	3.05
Kullback-Leibler	1.22	2.78	2.19	4.16
Chi Squared	0.54	1.31	1.20	2.82
Pearson X^2	0.57	1.38	1.04	2.63

location. Since the relationship between the LTH, STH and human presence is unknown, metrics are explored in section III of this paper, to optimize overall localization accuracy.

III. Distance Metrics

HD-DFL approaches work by defining regions of interest based on global link behavior. RTI systems work by creating an intensity image where each pixel (region) is affected by a sum of the links that pass through its vicinity. SpringLoc defines each region of interest as an artificial spring anchor point. Since multiple links can contribute to each region, it is very important to appropriately weight each link according to its contribution. For HD-DFL this is implemented in two steps.

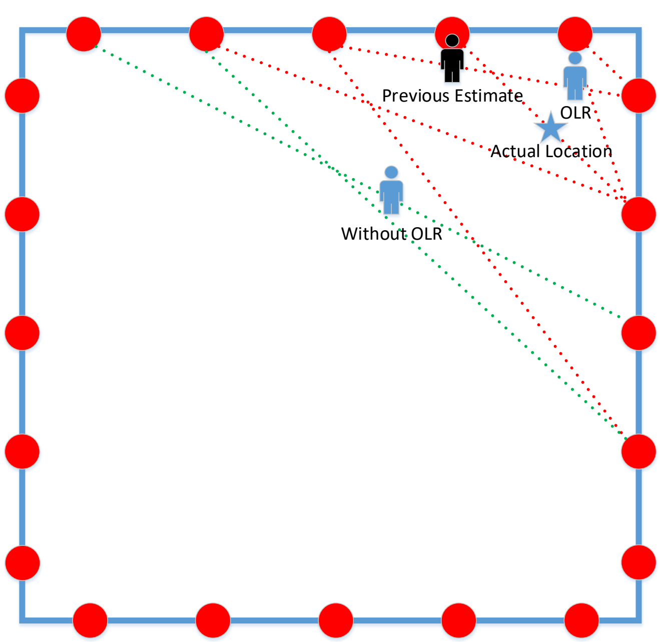

Fig. 4. HD-RTI Position Estimates With/Without Outlier Link Reduction

Firstly, a weighting model is defined which ensures only links close to each region of interest are included in the calculation of the position estimate. The second influence comes from the chosen distance metric. Since each distance metric calculates the 'histogram difference' in a different manner for the same pair of histograms, this can be leveraged to choose a metric that optimizes the relationship between a person passing through a link and standing within a corresponding region. Recent work in visible light positioning (VLP) has shown that varying distance metrics can have a significant effect on the overall localization accuracy of weighted K-nearest neighbor (WKNN) algorithm [41]. While no distance metric can strictly be better than any other in terms of generalization ability, some metrics have a higher probability of good generalization (improvement) as they are better matched to the types of data variation that will likely occur [42]. The problem with indoor radio propagation

Fig. 5. Auditorium Node Placement

is that the existence of multipath prevents the formation of a reliable indoor model [43]. Consequently, the ideal distance metric was found through empirical investigation. Introducing different histogram metrics involves replacing (2) with an alternative distance metric. We chose to focus on the distance metrics reported in [44] as they present a broad array of approaches across multiple mathematical families. Table 2 presents the metrics that performed better than the HD-RTI's Kernel and Kullback-Leibler benchmark metrics used in [32]. Table 3 presents metrics that surpassed the Kernel benchmark used by SpringLoc in [39]. Some of these metrics suffer from potential divide-by-0 or log(0) errors. Potential divide-by-0 errors were fixed by replacing the denominator ($denom$) with:

$$denom_{fixed} = \frac{max(\alpha, denom)}{\sum max(\alpha, denom)} \tag{5}$$

where α is a small constant. Similarly potential log(0) were fixed by replacing 0 with a very small constant, ε, if a log(0) scenario was encountered.

A. Outlier Link Reduction

When a person is traversing the monitored environments, they generally induce the largest histogram difference when they cross the LOS link path. However, multipath propagation and scattering can cause links far away from the traversing person to spuriously trigger strongly. SpringLoc contains filtering approaches to address this issue however HD-RTI does not. If the strength of these triggers is stronger than the current LOS links, it can cause a significantly erroneous location estimate which then pulls the tracking Kalman filter in the wrong direction. To combat the magnitude of this effect in HD-RTI we add a secondary weighting system termed Outlier Link Reduction (OLR), that favors links that are closer to the previous tracked state estimate. This is achieved by modifying (4) to :

$$x = (W^T W + \sigma_n^2 C_x^{-1})^{-1} W^T (\varphi \circ d) \tag{6}$$

where φ is a histogram difference weighting vector, $\varphi = [\varphi_0, \ldots, \varphi_{d-1}]$ of the same length as d, and $\circ$ represents the

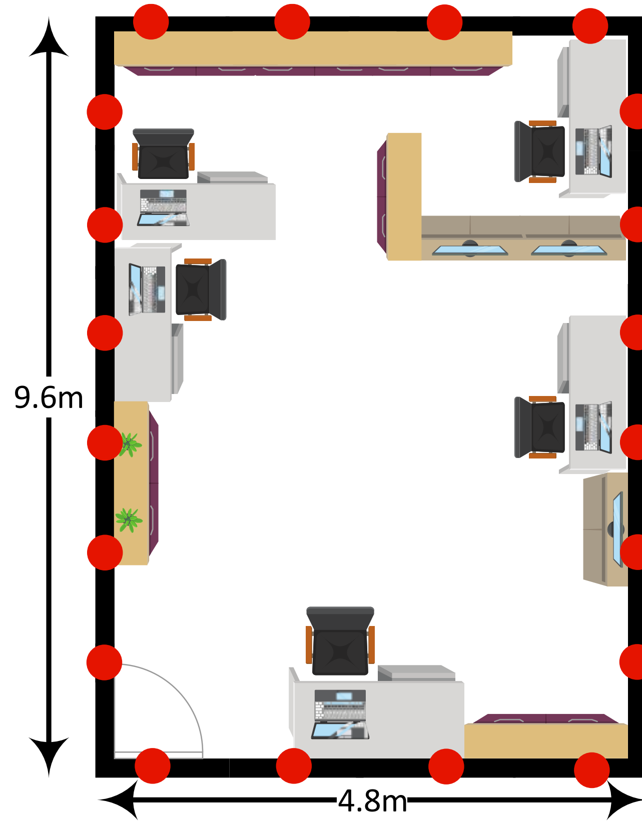

Fig. 6. Laboratory Floorplan / Node Placement

Hadamard product. Each element in φ, represents a weight for a single link defined as:

$$\varphi_l = e^{\left(-\gamma \frac{\omega_l}{\|\omega_l\|}\right)} \tag{7}$$

where γ is a weighting constant and ω_l represents the minimum distance between the previous state estimate and the line formed between the transmitter and receiver of link l. We define ω_l as:

$$\omega_l = \frac{\left(\frac{y_{RX} - y_{TX}}{x_{RX} - x_{TX}}\right)(x_S - x_{TX}) + y_{TX} - y_S}{\sqrt{\left(\frac{y_{RX} - y_{TX}}{x_{RX} - x_{TX}}\right)^2 + 1}} \tag{8}$$

where $[x_S, y_S]$ is the previous state estimate, $[x_{TX}, y_{TX}]$ is the coordinates of the transmitting node for link l, and $[x_{RX}, y_{RX}]$ is

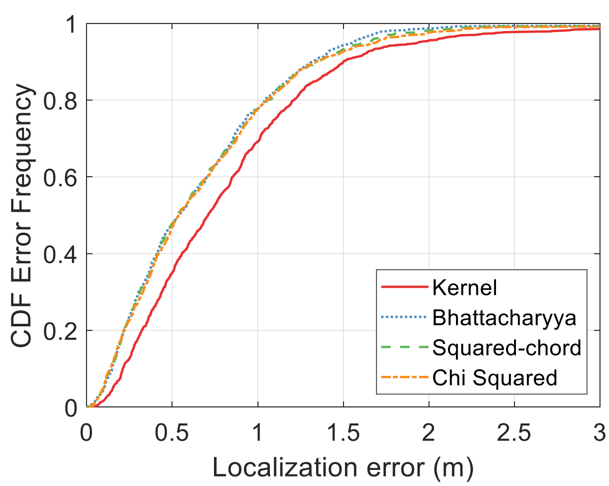

Fig. 7. Auditorium Overall RTI (OLR) CDF Error plot

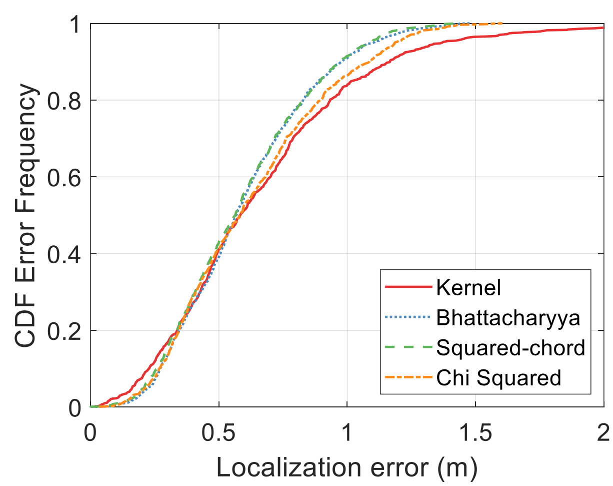

Fig. 8. Auditorium Overall SpringLoc CDF Error plot

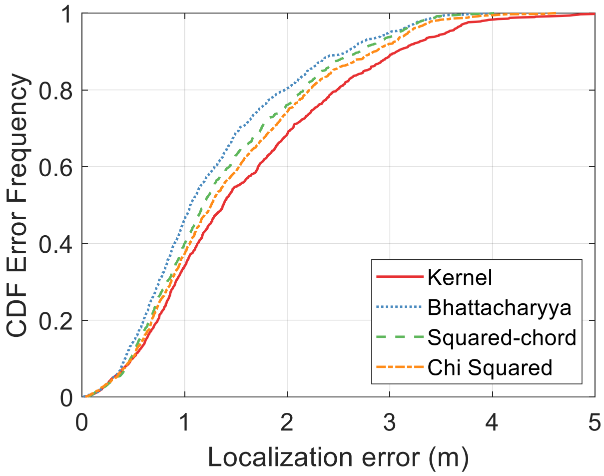

Fig. 9. Laboratory Overall RTI (OLR) CDF Error plot

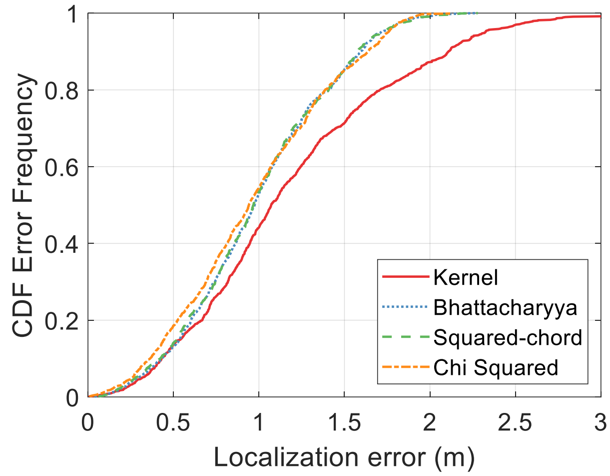

Fig. 10. Laboratory Overall SpringLoc CDF Error plot

the coordinates of the receiving node for link l. An example of OLR from experimental data, is given in Fig. 4, with the node locations marked with red circles. Triggered links between node pairs are shown by the dotted lines, with the green lines denoting dominant outlier links. Without employing OLR, the current position estimate is pulled towards the noisy outlier links resulting in significant error in the localization estimate. While employing OLR, the weight of these links is significantly reduced, and the current location estimate is much closer to the actual location.

IV. Implementation

Experiments were performed using a network of 20 Texas Instruments CC2530 Zigbee radios on channel 26, communicating using a token ring protocol. In each cycle, the network would report a set of M RSSI values, where M is the number of links within the network. The cycle duration was set to 200ms and Wi-Fi was disabled during the experiments to ensure the throughput of the Zigbee packets were not affected. This was done to eliminate Wi-Fi as a factor from the experiments. However, we note that existing research shows that Wi-Fi interference would have no impact on the RSSI values themselves [26], therefore having minimal impact on the overall accuracy. Experiments were conducted in two environments, an auditorium with ideal LOS between all nodes, as shown in Fig.4/Fig. 5, and a cluttered laboratory as shown in Fig. 6, featuring a complex, multipath rich environment. The Zigbee radios are represented by the red circles in Fig. 4 and Fig. 6. The auditorium test area was 5m x 5m, and the Laboratory test area was 9.6m x 4.8m. The auditorium featured high ceilings and had no objects or walls within 5m of the test area, in all horizontal directions. This means that the multipath is minimized (excluding ground reflection), and the test area can be considered a "best-case" indoor environment. In contrast, as shown in Fig. 6, the laboratory featured desks, bookshelves, and monitor stands which have the potential to introduce significant multipath components to the propagation environment.

Nodes were mounted on stands at 1.2m above the ground in the auditorium, and were wall mounted in the laboratory at 1.4m above the ground. This is consistent with the deployment height used by both of the original works [32, 39]. However, it should be noted that wireless DFL implementations can utilize other deployment configurations including ceiling mounted nodes,

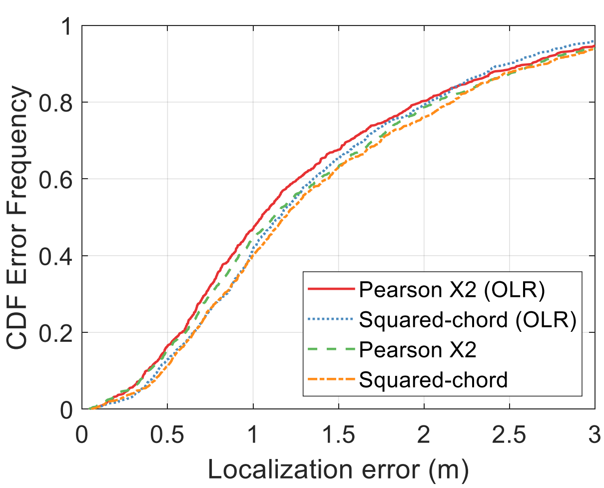

Fig. 11. Laboratory OLR vs No OLR RTI Performance

TABLE V

HD-RTI Parameter Values

Parameter	Value	Description
β_S	0.9	Forgetting Factor S
β_L	0.05	Forgetting Factor L
σ_E^2	30	Epanechnikov kernel width
σ^2	0.00064	Regularization parameter [32]
δ	1.3	Space parameter [32]
α	10^{-3}	Divide-by-0 constant
ε	10^{-100}	Log(0) constant
γ	1.5	OLR weighting constant

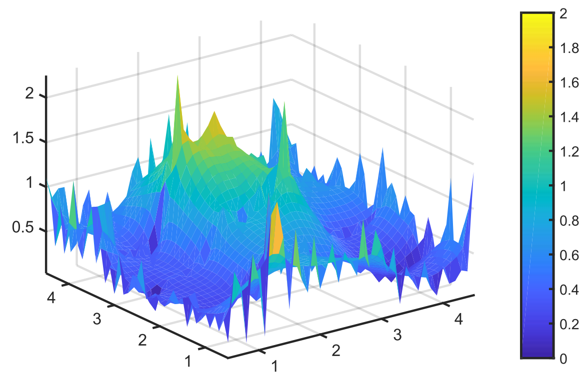

Fig. 12. Auditorium RTI – Interpolated Errors for Bhattacharyya Distance

with a similar level of accuracy [45]. Subjects were asked to walk along a marked clockwise, anticlockwise or zigzag route in each environment. The subjects walked in a heel-to-toe fashion to ensure their step size remained constant and used a metronome to ensure their speed remained constant. This enabled us to compare the localization result of specific samples, with their ground truth counterpart. The data from each trajectory was combined to produce the overall accuracy plots in Fig. 7-Fig. 10.

V. Results

Fig. 7 and Fig. 8 show the overall cumulative distribution function (CDF) of the localization error in the auditorium, with Fig. 9 and Fig. 10 showing the cluttered laboratory, for some of the best performing metrics. Table 2 and Table 3 summarize the overall performance of all tested metrics, across both environments, for both HD-RTI and SpringLoc.

Table 4 shows the improved performance of HD-RTI, when utilizing OLR. Since OLR is designed to minimize the effect of spurious erroneous outliers, its contribution is small. However, it does increase the overall performance. The effect of OLR is more pronounced in the Laboratory environment, where there is significant multipath, and larger global errors. A CDF Error plot is given in Fig. 11 to demonstrate the overall effect of OLR on the Pearson X^2 and Squared-chord metrics.

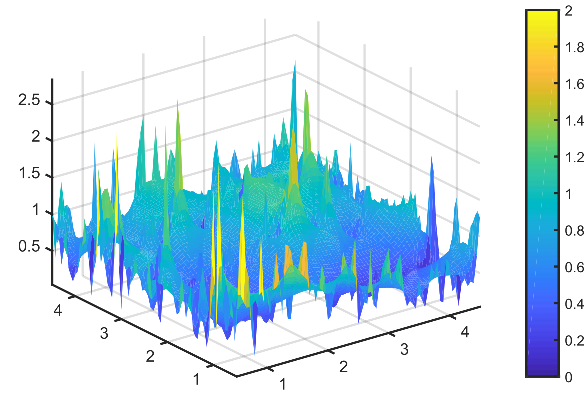

Fig. 13. Auditorium RTI – Interpolated Errors for Kernel Distance

Parameter values used for the HD-RTI experiments can be seen in Table 5. The first six parameters were initialized to the values used in [32], before all values were empirically tuned to find global, optimum values. Interestingly, though we collected RSSI samples at 5Hz rather than the 3Hz used in [32], our optimum β_S was the same as [32], however our δ is significantly larger. We believe that this is caused by our target walking considerably faster than the person used during the experiments conducted in [32]. The parameter values used for SpringLoc are the same as implemented in [39]. Overall the Bhattacharyya, Squared-chord, Chi Squared and Pearson X^2 metrics outperformed both Kernel and Kullback-Leibler metrics across both environments with Squared-chord providing a substantial 25% improvement in median error over Kernel for the auditorium environment, using HD-RTI. SpringLoc also saw significant improvement in the 90^{th} percentile and maximum errors when using Bhattacharyya or Squared-chord metrics. This shows that care should be taken when choosing a distance metric for HD-DFL as they can significantly affect the overall tracking accuracy.

The HD-RTI outlier link reduction technique also provided a modest improvement for most metrics, with significant accuracy increases of over 8% seen by 1 – Dice Auditorium 90% Percentile and Pearson X^2 Laboratory Median results. The outlier link reduction appeared to not noticeably affect the accuracy of the Kernel-distance based results. The Kullback-

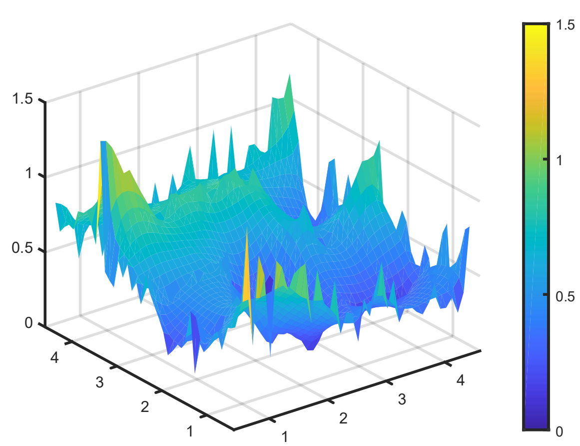

Fig. 14. Auditorium SpringLoc – Interpolated Errors for Bhattacharyya Distance

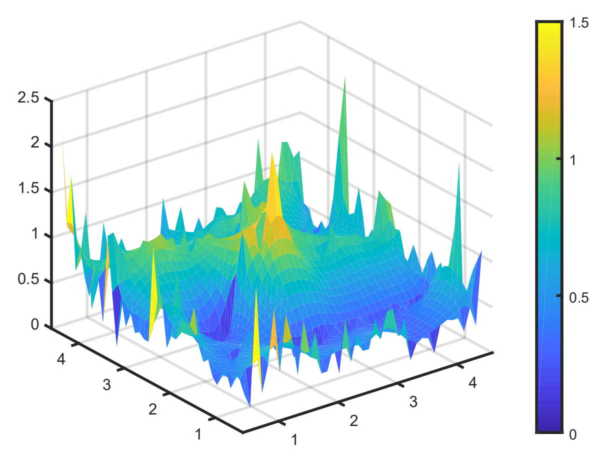

Fig. 15. Auditorium SpringLoc – Interpolated Errors for Kernel Distance

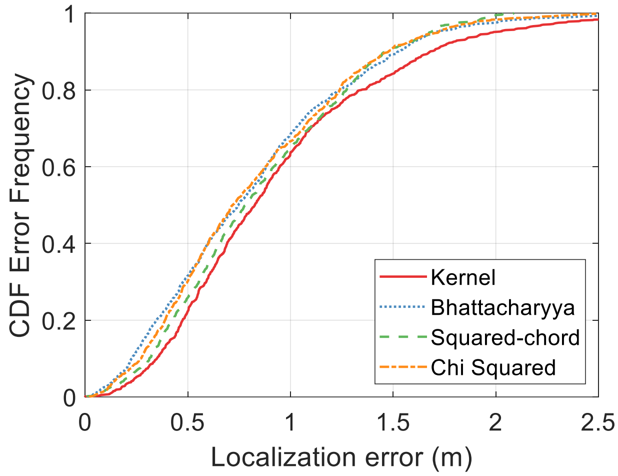

Fig. 16. Auditorium Overall SpringLoc (6 Nodes) CDF Error plot

Leibler performance was degraded by the outlier link reduction. However since this distance performed significantly worse than every other metric in every test, it suggests that this metric is not appropriate for HD-RTI localization efforts.

Interesting behavior was observed in both environments as the clockwise and anticlockwise routes in both the auditorium and laboratory environments saw many metrics surpassing Kernel distance, whereas their performance was relatively similar in the zigzag route for HD-RTI. To explore why this occurred, we plotted the interpolated errors across the whole test area for each metric. Figure 12 shows the performance of the Bhattacharyya metric in the auditorium, with Fig. 13 showing the Kernel distance performance. Figures 14 and 15 show the interpolated errors for SpringLoc in the auditorium, with the Bhattacharyya and Kernel metrics respectively. What becomes apparent is that the Bhattacharyya distance performs significantly better than Kernel distance when the person is near the nodes. This is shown by Bhattacharyya having most interpolated edge errors under 1m, while the Kernel distance has many errors over 1.4m when using either HD-RTI or SpringLoc. Since the clockwise / anticlockwise routes only cover the perimeter compared to the zigzag route which covers the whole test environment, the Kernel CDF plots are considerably worse. Another interesting observation is that there is a region at approximately [3.2, 3.2] where the Kernel metric performed poorly with both HD-RTI and SpringLoc. Using the Bhattacharyya metric removed this erroneous region for SpringLoc, but only partially mitigated it for HD-RTI. This shows that the performance of a HD-DFL implementations accuracy is not only route and algorithm dependent, but also exhibits significant spatial variation within the distance metrics themselves, even across an uncluttered environment like the auditorium. Though the magnitude of the improvement caused by metric substitution is dependent on the algorithm that follows (RTI or SpringLoc), the metrics implemented offered a considerable improvement over both the original Kernel and Kullback-Leibler metrics, for both RTI and SpringLoc. Furthermore, the metrics were tested in two environments that were setup to represent both the "best case" and "worst case" propagation environments, using realistic room layouts. This leads us to believe that the distance metrics implemented should offer a consistent improvement compared to the existing Kernel metric across varying indoor environments, with varying multipath characteristics. HD-RTI's performance severely degrades under low node density, however SpringLoc's performance remains more consistent [39]. In order to show how the metrics affect overall localization when fewer nodes are available, the laboratory localization estimates were recalculated using only six nodes for SpringLoc. As shown in Fig. 16, Bhattacharyya, Squared-chord and Chi Squared distances still outperform the Kernel distance, even under low node density, across all quartiles.

VI. Conclusion and Future Works

Existing HD-DFL implementations in literature have only explored two distance metrics for localization. This work experimentally implemented many other metrics in two different environments, with multiple walking trajectories. The results show that 5 distance metrics surpass the performance of the state-of-the-art Kernel metric, across multiple environments, by up to 25%. We also noticed that different metrics exhibit different spatial properties in HD-DFL systems with the Kernel metric experiencing error spikes when a person traverses near node locations, which was not as pronounced among the other metrics. This explains why the Kernel metrics performed considerably worse than other approaches when the walking trajectory followed the node perimeter. We have also shown that an HD-RTI algorithm can use outlier link reduction in the form of a weighting scheme, which increased overall localization accuracy in most tests.

Future work could be done to either fuse multiple distance metrics together, or use a location-based switching scheme, where a distance metric is chosen based on the current state estimate, and an assumption of the current spatial relationship to the nodes. Work can also be done to expand this implementation to cater for multiple people at once. Finally, HD-RTI's Kalman tracking filter smooths the location estimates but performs poorly at tracking through dead-spots and at times of significant system noise. A better approach to tracking would be to detect whether the RSSI set had been significantly corrupted by noise and to discard the set completely, using the previous measurement and a known movement model to infer location until the noise fades. In contrast with HD-RTI, SpringLoc already incorporates geometric filtering into its tracking approach to help discard samples that have been corrupted by noise. However, further work needs to be done to define more accurate spring weights, based on which histogram distance metric is utilized.

For the experiments reported in this paper, subjects walked at a brisk walking pace, in a heel-to-toe fashion. This means that our β_S value will work for any walking subject within an indoor environment but may not be suitable for higher mobility subjects. This can be addressed by either increasing the β_S to allow for higher mobility, or by increasing the network sampling rate, at the cost of higher energy consumption [32].

VII. Acknowledgment

The authors would like to thank Nathaniel Faulkner and Gene Hopkins for their assistance with the measurements.

VIII. References

[1] Y. Wang, K. Wu, and L. M. Ni, "WiFall: Device-Free Fall Detection by Wireless Networks," (in English), *IEEE Transactions on Mobile Computing*, vol. 16, no. 2, pp. 581-594, Feb 1 2017, doi: 10.1109/tmc.2016.2557792.

[2] X. Liu, J. Cao, S. Tang, J. Wen, and P. Guo, "Contactless Respiration Monitoring Via Off-the-Shelf WiFi Devices," *IEEE Transactions on Mobile Computing*, vol. 15, no. 10, pp. 2466-2479, 2016, doi: 10.1109/tmc.2015.2504935.

[3] H. Xiong, T. Latif, E. Lobaton, A. Bozkurt, and M. L. Sichitiu, "Characterization of RSS variability for biobot localization using 802.15.4 Radios," in *2016 IEEE Topical Conference on Wireless Sensors and Sensor Networks (WiSNet)*, 24-27 Jan. 2016 2016, pp. 1-3, doi: 10.1109/WISNET.2016.7444305.

[4] C. Xu *et al.*, "SCPL: Indoor device-free multi-subject counting and localization using radio signal strength," in *2013 ACM/IEEE International Conference on Information Processing in Sensor Networks (IPSN)*, 8-11 April 2013 2013, pp. 79-90, doi: 10.1145/2461381.2461394.

[5] J. Wang *et al.*, "E-HIPA: An Energy-Efficient Framework for High-Precision Multi-Target-Adaptive Device-Free Localization," (in English), *IEEE Transactions on Mobile Computing*, vol. 16, no. 3, pp. 716-729, Mar 2017, doi: 10.1109/tmc.2016.2567396.

[6] R. Zhou, X. Lu, P. Zhao, and J. Chen, "Device-Free Presence Detection and Localization With SVM and CSI Fingerprinting," *IEEE Sensors Journal*, vol. 17, no. 23, pp. 7990-7999, 2017, doi: 10.1109/JSEN.2017.2762428.

[7] S. Savazzi, V. Rampa, F. Vicentini, and M. Giussani, "Device-Free Human Sensing and Localization in Collaborative Human–Robot Workspaces: A Case Study," *Ieee Sens J*, vol. 16, no. 5, pp. 1253-1264, 2016, doi: 10.1109/jsen.2015.2500121.

[8] D. Konings, A. Budel, F. Alam, and F. Noble, "Entity tracking within a Zigbee based smart home," in *Mechatronics and Machine Vision in Practice (M2VIP), 2016 23rd International Conference on*, 2016: IEEE, pp. 1-6, doi: 10.1109/M2VIP.2016.7827294.

[9] K. Qian, C. Wu, Y. Zhang, G. Zhang, Z. Yang, and Y. Liu, "Widar2.0," presented at the Proceedings of the 16th Annual International Conference on Mobile Systems, Applications, and Services - MobiSys '18, Munich, Germany, 2018. [Online]. Available: https://dl.acm.org/citation.cfm?doid=3210240.3210314.

[10] M. Zhao *et al.*, "RF-based 3D skeletons," presented at the Proceedings of the 2018 Conference of the ACM Special Interest Group on Data Communication - SIGCOMM '18, Budapest, Hungary, 2018.

[11] X. Li, S. Ding, Z. Li, and B. Tan, "Device-Free Localization via Dictionary Learning with Difference of Convex Programming," *Ieee Sens J*, vol. 17, no. 17, pp. 1-1, 2017, doi: 10.1109/jsen.2017.2730226.

[12] J. Wang, X. Zhang, Q. Gao, H. Yue, and H. Wang, "Device-Free Wireless Localization and Activity Recognition: A Deep Learning Approach," *IEEE Transactions on Vehicular Technology*, vol. 66, no. 7, pp. 6258-6267, 2017, doi: 10.1109/tvt.2016.2635161.

[13] H. Huang and S. Lin, "WiDet," presented at the Proceedings of the 21st ACM International Conference on Modeling, Analysis and Simulation of Wireless and Mobile Systems - MSWIM '18, Montreal, QC, Canada, 2018.

[14] H. Huang, H. Zhao, X. Li, S. Ding, L. Zhao, and Z. Li, "An Accurate and Efficient Device-Free Localization Approach Based on Sparse Coding in Subspace," *Ieee Access*, vol. 6, pp. 61782-61799, 2018, doi: 10.1109/access.2018.2876034.

[15] J. Zhang, W. Xiao, S. Zhang, and S. Huang, "Device-Free Localization via an Extreme Learning Machine with Parameterized Geometrical Feature Extraction," *Sensors (Basel)*, vol. 17, no. 4, p. 879, Apr 17 2017, doi: 10.3390/s17040879.

[16] B. Mager, P. Lundrigan, and N. Patwari, "Fingerprint-Based Device-Free Localization Performance in Changing Environments," (in English), *Ieee J Sel Area Comm*, vol. 33, no. 11, pp. 2429-2438, Nov 2015, doi: 10.1109/jsac.2015.2430515.

[17] H. Zou, Y. Zhou, J. Yang, W. Gu, L. Xie, and C. J. Spanos, "WiFi-Based Human Identification via Convex Tensor Shapelet Learning," presented at the AAAI Conference on Artificial Intelligence, 2018, Human Identification; Shapelet Learning. [Online]. Available: https://aaai.org/ocs/index.php/AAAI/AAAI18/paper/view/16150.

[18] X. Dang, Y. Huang, Z. Hao, and X. Si, "PCA-Kalman: device-free indoor human behavior detection with commodity Wi-Fi," *Eurasip J Wirel Comm*, vol. 2018, no. 1, p. 214, 2018.

[19] H. Zou, Y. Zhou, J. Yang, W. Gu, L. Xie, and C. Spanos, "FreeDetector: Device-Free Occupancy Detection with Commodity WiFi," in *2017 IEEE International Conference on Sensing, Communication and Networking (SECON Workshops)*, 12-12 June 2017 2017, pp. 1-5, doi: 10.1109/SECONW.2017.8011040.

[20] H. Zhang *et al.*, "Wireless non-invasive motion tracking of functional behavior," *Pervasive Mob Comput*, vol. 54, pp. 29-44, 2019/03/01/ 2019, doi: 10.1016/j.pmcj.2019.01.006.

[21] X. Wang, L. Gao, S. Mao, and S. Pandey, "CSI-based Fingerprinting for Indoor Localization: A Deep Learning Approach," *IEEE Transactions on Vehicular Technology*, vol. 66, no. 1, pp. 1-1, 2016, doi: 10.1109/tvt.2016.2545523.

[22] D. Halperin, W. Hu, A. Sheth, and D. Wetherall, "Tool release," *ACM SIGCOMM Computer Communication Review*, vol. 41, no. 1, pp. 53-53, 2011, doi: 10.1145/1925861.1925870.

[23] S. Kumar, D. Cifuentes, S. Gollakota, and D. Katabi, "Bringing cross-layer MIMO to today's wireless LANs," *ACM SIGCOMM Computer Communication Review*, vol. 43, no. 4, pp. 387-398, 2013, doi: 10.1145/2534169.2486034.

[24] Y. Xie, Z. Li, and M. Li, "Precise Power Delay Profiling with Commodity WiFi," in *Proceedings of the 21st Annual International Conference on Mobile Computing and Networking - MobiCom '15*, Paris, France, 2015, 2790124: ACM, pp. 53-64, doi: 10.1145/2789168.2790124.

[25] Y. Ma, G. Zhou, and S. Wang, "WiFi Sensing with Channel State Information: A Survey," *ACM Computing Surveys*, vol. 52, no. 3, p. 35, 2019.

[26] D. Konings, N. Faulkner, F. Alam, F. Noble, and E. M. K. Lai, "The effects of interference on the RSSI values of a ZigBee based indoor localization system," in *2017 24th International Conference on Mechatronics and Machine Vision in Practice (M2VIP)*, 21-23 Nov. 2017 2017, pp. 1-5, doi: 10.1109/M2VIP.2017.8211460. [Online]. Available: https://ieeexplore.ieee.org/ielx7/8168204/8211426/08211460.pdf?tp=&arnumber=8211460&isnumber=8211426

[27] Q. Lei, H. Zhang, H. Sun, and L. Tang, "Fingerprint-Based Device-Free Localization in Changing Environments Using Enhanced Channel Selection and Logistic Regression," *Ieee Access*, vol. 6, pp. 2569-2577, 2018, doi: 10.1109/access.2017.2784387.

[28] L. Zhao, H. Wang, P. Li, and J. Liu, "An improved WiFi indoor localization method combining channel state information and received signal strength," in *2017 36th Chinese Control Conference (CCC)*, 26-28 July 2017 2017, pp. 8964-8969, doi: 10.23919/ChiCC.2017.8028783. [Online]. Available: http://ieeexplore.ieee.org/ielx7/8020036/8027314/08028783.pdf?tp=&arnumber=8028783&isnumber=8027314

[29] N. Patwari, J. N. Ash, S. Kyperountas, A. O. Hero, R. L. Moses, and N. S. Correal, "Locating the nodes: cooperative localization in wireless sensor networks," *IEEE Signal processing magazine*, vol. 22, no. 4, pp. 54-69, 2005.

[30] C. Alippi and G. Vanini, "A RSSI-based and calibrated centralized localization technique for Wireless Sensor Networks," in *Pervasive computing and communications workshops, 2006. PerCom workshops 2006. Fourth annual IEEE international conference on*, 2006: IEEE, pp. 5 pp.-305.

[31] J. Wilson and N. Patwari, "Radio Tomographic Imaging with Wireless Networks," (in English), *IEEE Transactions on Mobile Computing*, vol. 9, no. 5, pp. 621-632, May 2010, doi: 10.1109/tmc.2009.174.

[32] Y. Zhao, N. Patwari, J. M. Phillips, and S. Venkatasubramanian, "Radio tomographic imaging and tracking of stationary and moving people via kernel distance," in *Proceedings of the 12th international conference on Information processing in sensor networks - IPSN '13*, Philadelphia, Pennsylvania, USA, 2013, 2461410: ACM, pp. 229-240, doi: 10.1145/2461381.2461410.

[33] J. Wilson and N. Patwari, "See-Through Walls: Motion Tracking Using Variance-Based Radio Tomography Networks," *IEEE Transactions on Mobile Computing*, vol. 10, no. 5, pp. 612-621, 2011, doi: 10.1109/tmc.2010.175.

[34] Y. Zhao and N. Patwari, "Robust Estimators for Variance-Based Device-Free Localization and Tracking," *IEEE Transactions on*

Mobile Computing, vol. 14, no. 10, pp. 2116-2129, 2015, doi: 10.1109/tmc.2014.2385710.

[35] O. Kaltiokallio, M. Bocca, and N. Patwari, "Enhancing the accuracy of radio tomographic imaging using channel diversity," in *2012 IEEE 9th International Conference on Mobile Ad-Hoc and Sensor Systems (MASS 2012)*, 8-11 Oct. 2012 2012, pp. 254-262, doi: 10.1109/MASS.2012.6502524. [Online]. Available: https://ieeexplore.ieee.org/ielx7/6493538/6502495/06502524.pdf?tp=&arnumber=6502524&isnumber=6502495

[36] B. Wei, A. Varshney, N. Patwari, W. Hu, T. Voigt, and C. T. Chou, "dRTI," presented at the Proceedings of the 14th International Conference on Information Processing in Sensor Networks - IPSN '15, Seattle, Washington, 2015.

[37] O. Kaltiokallio, R. Jantti, and N. Patwari, "ARTI: An Adaptive Radio Tomographic Imaging System," *IEEE Transactions on Vehicular Technology,* vol. 66, no. 8, pp. 7302-7316, 2017, doi: 10.1109/tvt.2017.2664938.

[38] Y. Zhao and N. Patwari, "Demo abstract: Histogram distance-based radio tomographic localization," in *2012 ACM/IEEE 11th International Conference on Information Processing in Sensor Networks (IPSN)*, 16-20 April 2012 2012, pp. 129-130, doi: 10.1109/IPSN.2012.6920930. [Online]. Available: https://ieeexplore.ieee.org/ielx7/6909388/6920920/06920930.pdf?tp=&arnumber=6920930&isnumber=6920920

[39] D. Konings, F. Alam, F. Noble, and E. M. K. Lai, "SpringLoc: A Device-Free Localization Technique for Indoor Positioning and Tracking Using Adaptive RSSI Spring Relaxation," *Ieee Access,* vol. 7, pp. 56960-56973, 2019, doi: 10.1109/access.2019.2913910.

[40] D. Comaniciu and P. Meer, "Mean shift: a robust approach toward feature space analysis," *IEEE Transactions on Pattern Analysis and Machine Intelligence,* vol. 24, no. 5, pp. 603-619, 2002, doi: 10.1109/34.1000236.

[41] F. Alam, M. T. Chew, T. Wenge, and G. S. Gupta, "An Accurate Visible Light Positioning System Using Regenerated Fingerprint Database Based on Calibrated Propagation Model," *Ieee T Instrum Meas,* pp. 1-10, 2018, doi: 10.1109/tim.2018.2870263.

[42] D. R. Wilson and T. R. Martinez, "Improved heterogeneous distance functions," *J. Artif. Int. Res.,* vol. 6, no. 1, pp. 1-34, 1997.

[43] D. Konings, N. Faulkner, F. Alam, F. Noble, and E. Lai, "Do RSSI values reliably map to RSS in a localization system?," in *2017 2nd Workshop on Recent Trends in Telecommunications Research (RTTR)*, 10-10 Feb. 2017 2017, pp. 1-5, doi: 10.1109/RTTR.2017.7887867.

[44] S.-H. Cha, "Comprehensive survey on distance/similarity measures between probability density functions," *City,* vol. 1, no. 2, p. 1, 2007.

[45] D. Zhang, Y. Liu, and L. M. Ni, "RASS: A real-time, accurate and scalable system for tracking transceiver-free objects," in *Pervasive Computing and Communications (PerCom), 2011 IEEE International Conference on*, 21-25 March 2011 2011, pp. 197-204, doi: 10.1109/PERCOM.2011.5767585. [Online]. Available: http://ieeexplore.ieee.org/ielx5/5762825/5767569/05767585.pdf?tp=&arnumber=5767585&isnumber=5767569

Daniel Konings (M'17) received his BE(Hons) from Massey University, Auckland, New Zealand in Computer Systems and Electronics Engineering in 2014, where he is currently pursuing the Ph.D. degree with the School Food and Advanced Technology (SF&AT). His research interests include indoor localization, digital signal processing, machine learning, IoT & wireless sensor networks. Daniel is a Student Member of the Institute of Electrical and Electronics Engineers (IEEE).

Fakhrul Alam (M'17-SM'19) received his BSc (Hons) in Electrical & Electronic Engineering from BUET, Bangladesh and MS and Ph.D. in Electrical Engineering from Virginia Tech, USA. He is currently a senior lecturer at the School Food and Advanced Technology (SF&AT), Massey University, New Zealand. His research interests include indoor localization, 5G & visible light communication, disaster management with 5G, IoT & wireless sensor networks. He is a senior member of the Institute of Electrical and Electronics Engineers (IEEE) and a member of the Institution of Engineering and Technology (IET).

Frazer Noble received his BE (Hons) in Mechatronics, ME (Hons) in Engineering, and PhD in Engineering from Massey University, New Zealand. He is currently a lecturer at the School Food and Advanced Technology (SF&AT), Massey University, New Zealand. His research interests include mechatronics, robotics and automation, machine vision, and machine learning.

Edmund M-K Lai (M'82-SM'95) received his BE(Hons) and PhD from The University of Western Australia, both in Electrical Engineering, in 1982 and 1991 respectively. He is currently a Professor of Information Engineering at Auckland University of Technology, New Zealand. He has previously held faculty positions at universities in Australia, Hong Kong, and Singapore. His research interests include digital signal processing, digital communications and networks, computational and swarm intelligence, and artificial neural networks. Prof. Lai is a fellow of the Institution of Engineering and Technology (IET) and a senior member of the Institute of Electrical and Electronics Engineers (IEEE).

Chapter 5

This chapter contains content from the following article, republished with permission. In accordance with IEEE's republishing policy, any full text that has been included is the unmodified accepted article. This means that while the content is identical to the published article, there may be stylistic differences.

doi: 10.1109/JSEN.2019.2944178

FieldLight: Device-free Indoor Human Localization using Passive Visible Light Positioning and Artificial Potential Fields

Daniel Konings, *Student Member, IEEE*, Nathaniel Faulkner, Fakhrul Alam, *Senior Member, IEEE*, Edmund M-K Lai, *Senior Member, IEEE,* Serge Demidenko*, Fellow, IEEE*

***Abstract*— Device-free or passive localization techniques allow positioning of targets, without requiring them to carry any form of transceiver or tag. In this paper, a novel device-free visible light positioning technique is proposed. It exploits the variation of the ambient light levels caused by a moving entity. The target is localized by employing a system of artificial potential fields associated with a set of photodiodes embedded into an indoor environment. The system does not require the existing lighting infrastructure to be modified. It also employs a novel calibration procedure that does not require labelled training data, thus significantly reducing the calibration cost. The developed prototype system is installed in three typical indoor environments consisting of a corridor, foyer, and laboratory and was able to attain median errors of 0.68m, 1.20m and 0.84m respectively. Through experimental results, the proposed VLP technique is benchmarked against an existing wireless RSSI-based device-free localization approach, and was able to attain a median error 0.63m lower than the wireless technique.**

***Index Terms*— Indoor localization, Visible Light Positioning (VLP), Device Free Localization (DFL), Passive VLP, Artificial potential fields.**

I. Introduction

ROBUST Location based services (LBS) for Smart Homes could enable personalized control of existing infrastructure including lighting, heating, air quality, and water temperature/flow [1, 2]. This could have a tremendous impact on wellbeing and assistive living as it would allow appliances to be controlled remotely. It could also be used to detect emergencies or falls, and automatically contact appropriate response personnel. This would thus enable the elderly to maintain higher autonomy, while providing the family the peace-of-mind of knowing that their elderly family members are safe and well.

While cameras can provide a suitable solution for public environments, they may create privacy concerns in residential areas. It is desirable also that the solution would utilize readily available hardware to facilitate ubiquitous deployment.

In the recent years, numerous wireless technology-based solutions have been proposed and reported in the literature. They utilized *Radio Tomographic Imaging* (RTI) [3-6], energy minimization [7, 8], and machine learning approaches (including: *Support Vector Machines* (SVM) [9, 10], Random Forest [11], *Hidden Markov Models* (HMM) [12], and Deep Learning [13]) to mention a few. These approaches are commonly implemented using either the *received signal strength indicator* (RSSI) metric, or the Wi-Fi *channel state information* (CSI) metric. CSI approaches have been shown to offer improved accuracy over RSSI approaches [14], however the metric is not readily available in current Wi-Fi equipment and relies on legacy drivers [15, 16].

A major disadvantage of the wireless approaches is their potential vulnerability to malicious activities, which could lead to unlawful acquirement of location-based information from unsuspecting users, thus creating serious privacy concerns [17]. Other popular approaches include the use of passive infrared sensors [18, 19], load cells [20], capacitive sensing [21], electric field sensing [22-24], or microphone arrays [25]. The main concern with existing approaches is that they either require a significant deployment/calibration effort, or that they are not yet available as standard *commercial-off-the-shelf* (COTS) equipment. This makes it significantly more difficult to provide ubiquitous deployment of the wireless approaches for end users in the foreseeable future.

In recent years, *light-emitting diode* (LED) luminaires have become very popular light sources in indoor environments. In addition, they provide the opportunity to leverage the existing lighting infrastructure for a secondary purpose – indoor object localization (sensing). Visible light sensing applications can be classified into four groups: *full-active:* modified source and tagged target, *passive-src:* unmodified source and tagged target, *passive-obj:* modified source and untagged target, and *full-*

This paragraph of the first footnote will contain the date on which you submitted your paper for review. This work was supported in part by the Massey University Doctoral Scholarships.

D. Konings, N. Faulkner, F. Alam are all with the Department of Mechanical & Electrical Engineering (MEE), School of Food & Advanced Technology (SF&AT), Massey University, Auckland 0632, New Zealand (d.konings@massey.ac.nz, n.faulkner@massey.ac.nz, f.alam@ massey.ac.nz).

E. M-K. Lai is with the School of Engineering, Computer & Mathematical Sciences, Auckland University of Technology, Auckland 1142, New Zealand (edmund.lai@aut.ac.nz).

S. Demidenko is with the School of Science & Technology, Sunway University, 47500 Selangor, Malaysia and (as a co-supervisor) with the Department of MEE, SF&AT, Massey University, Auckland 0632, New Zealand (sdemidenko@sunway.edu.my, and s.demidenko@massey.ac.nz).

TABLE I
FEATURE COMPARISON OF VISIBLE LIGHT POSITIONING SYSTEMS

Algorithm	Works without LED modulation	Does not require labelled training data	Localizes and tracks passive targets	Extra infrastructure Investment	Experimental verification
FieldLight	Yes	Yes	Yes	Low	2D localization + tracking
Smart Wall	Yes	No	Yes	Low	2D localization + tracking
CeilingSee	Yes	No	No	Low	Occupancy Count
Ibrahim et al	No	Unknown	No	Low	2D region detection
LocaLight	Yes	Yes	No	Low	1D position estimates
AMTP	No	Yes	localizes	Very High	Blocking LOS attenuates PD signal
EyeLight	No	Activity recognition requires labelled data	Yes	Medium	2D localization + tracking + activity recognition
StarLight	No	PD placement requires room layout	Yes	High	2D localization + 3D skeleton reconstruction
LiSense	No	Yes	Skeleton reconstruction	Very High	3D skeleton postures

passive: unmodified source and untagged target [26].

The focus of this paper is on implementing a full-passive localization system that does not require any modification of the lighting infrastructure to emit signals, and can localize tag-free targets. This offers unique challenges as full-passive systems either assume that a roaming entity fully absorbs the visible light as it occludes an area, or that the reflectance off the target follows a deterministic model. Since the reflectance is affected by the color worn by the target, calibration requirements should be kept minimal to allow for multi-entity calibration.

The CeilingSee approach reported in [27] employs a machine learning algorithm to infer an occupancy count. It can be technically categorized as full-passive since it utilizes commodity COTS luminaires having no communication functionalities, and can localize untagged targets. However, the proposed solution requires the existing luminaire driver boards to be modified to allow for the luminaires to act as light sensors.

Another solution is reported in [28] where the luminaire drivers are modified to output an ID number. Each luminaire is co-located with a *photodiode* (PD). During every cycle, the proposed system checks whether each PD's current values exceed a predefined threshold. This is used to detect whether a person is present at one of several predefined locations, or whether a door is open.

The LocaLight [29] prototype employs 3 ceiling mounted COTS luminaires, and 5 PDs located on the floor, to detect the shadow of a passing person. However, this solution only identifies the presence of people (static or walking in a straight line) rather than offering target level localization/tracking.

The novel *device-free localization* (DFL) *adaptive multi-target positioning* (AMTP) algorithm is proposed in [30]. It identifies locations of shadowed PDs on the floor, and then clusters them into groups. The clusters are used to identify probable targets. The main problem associated with this approach is the limited real-world experimental verification. Most of the provided results are based solely on simulation. However, the simulation is performed using somewhat unrealistic assumptions and models; making the approach questionable for a real-world smart home deployment.

The EyeLight solution [31] uses modulated ON-OFF keyed luminaires, co-located with PDs to detect targets crossing virtual light barriers, while the StarLight approach [32] employs custom designed lighting panels containing multiple LEDs with

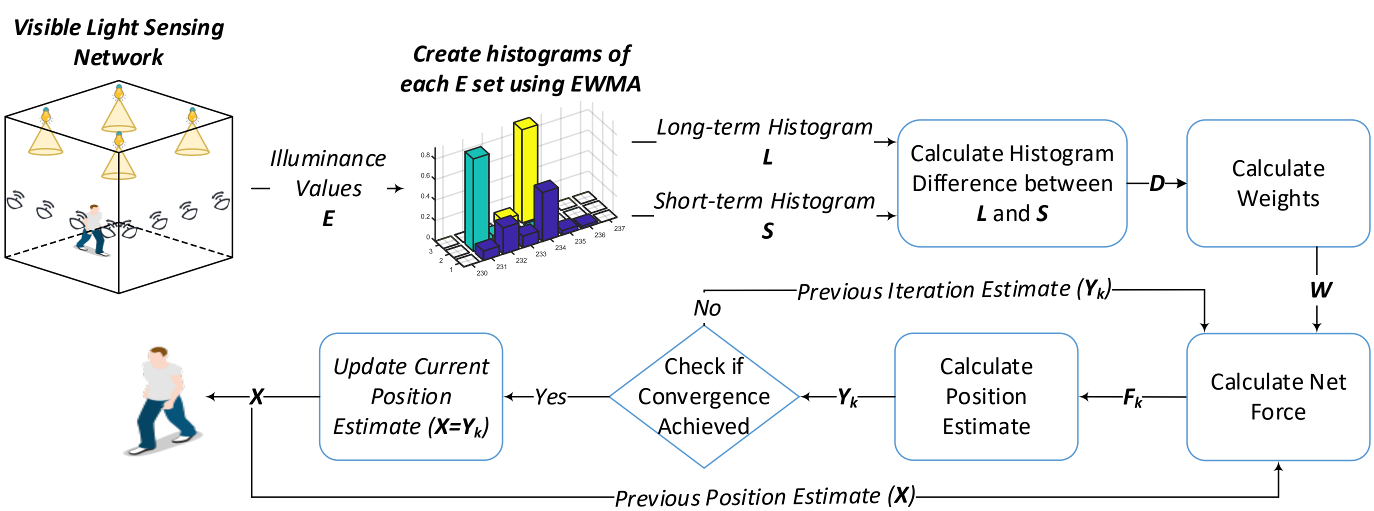

Fig. 1. FieldLight algorithm overview. **E** represents a stream of illuminance values for each wall mounted node. An exponentially weighted moving average (EWMA) scheme is used to create a long-term histogram (**L**) and a short-term histogram (**S**) for each node. The Bhattacharyya distance is taken between each nodes **L** and **S** histogram (**D**) which is used to generate a set of weights (**W**) for localization. The weights are used to calculate the net force on the system ($\mathbf{F_k}$), which continuously updates a position estimate ($\mathbf{Y_k}$) until the system either converges, or reaches its maximum iteration threshold. The final output position estimate for time t is then stored in **X**.

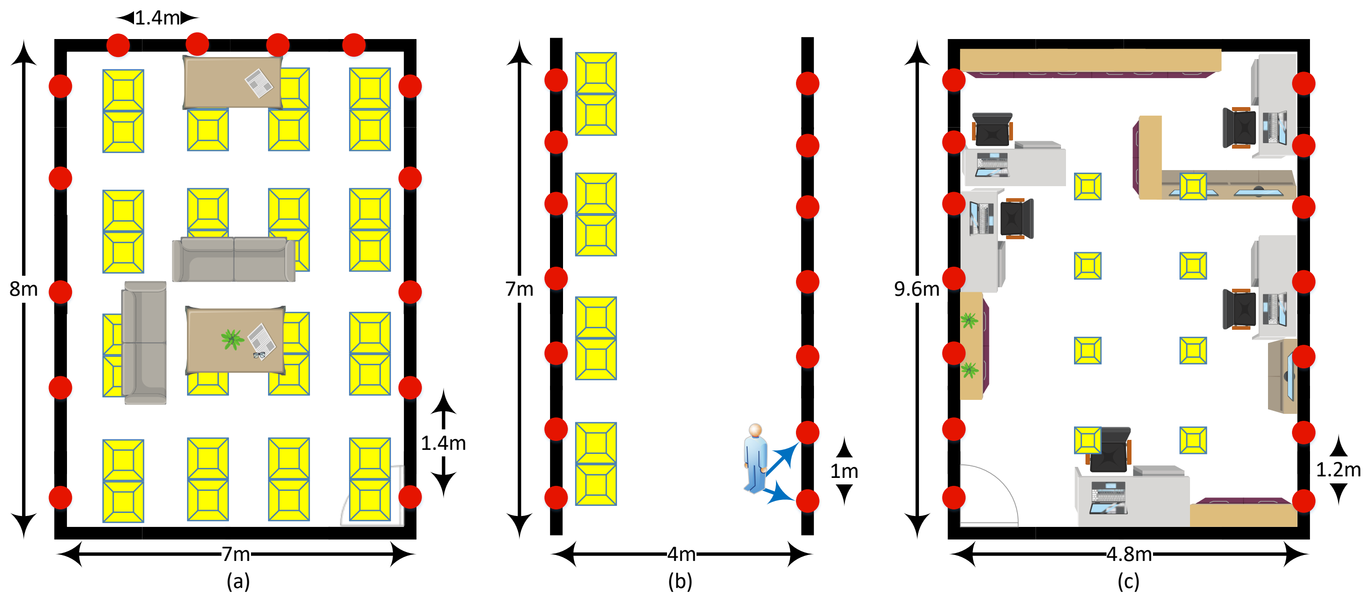

Fig. 2. FieldLight floorplan – (a) Foyer, (b) Corridor, (c) Laboratory. The yellow blocks represent the overhead luminaires used for localization. In each environment 14 nodes (red circles) were deployed which measured the changes in ambient light caused by a roaming entity and transmitted the information to a server for localization.

each LED being modulated separately. StarLight detects shadowed PDs by calculating the normalized frequency power change (for each PD-LED pair), considering them shadowed if they exceed a predefined threshold. A similar detection strategy is employed by LiSense in [33] that utilizes several ceiling-mounted modulated luminaires, and a multitude of floor-mounted PDs, to perform 3D skeleton reconstruction.

A simulation of visible light sensing is reported in [34], based on a multitude of luminaires collocated with PDs within an indoor environment. It proposes the use of either the likelihood-ratio test, or mean spectral radius, as the system variance indicators to enable indoor localization. The approach looks promising. However, no results of real-world experiments are provided in the paper. Besides, the number of luminaires assumed in the simulation is quite high (i.e., exceeding the quantity that would normally be deployed in a real-world premise).

In the Smart Wall solution [35], a target is localized by measuring the change it creates in the *received signal strength* (RSS) of the ambient light, at an array of PDs embedded in the wall. The system shows promising localization capability. However, it relies on extensive fingerprinting making it a less attractive option for real-world implementations.

Spring-relaxation is an energy minimization technique that aims to reach an equilibrium state within a system of springs [36]. It is realized by attaching a set of artificial springs to the roaming target, with the other spring ends being attached to known static locations. The system then iteratively works to find the global minima, where the net force applied by the springs to the target is minimized. Traditionally, the approach has been utilized to locate a sensor within a *wireless sensor network* (WSN) [37]. More recently, the concept was applied to the low-power and low-data-rate close proximity wireless *ad hoc* network-based DFL system described in [7]. It has also been applied to localize a PD-based tag for an active VLP system [38]. A Similar energy minimization technique (originally employed for robot path planning) is Artificial Potential Fields [39, 40]. Instead of using a spring notation, it models the localization problem as a set of attractive and repulsive forces, emitted from known locations.

Until now, the concept of potential fields have not been applied to visible light-based DFL. A particularly attractive benefit of DFL based on the potential fields approach is that potential fields are more computationally efficient than competing techniques such as particle filters [41, 42]. The approach also maintains the valuable benefit of a dynamically assigned weighting scheme, which allows for high localization accuracy across varying target speeds.

A novel device-free localization approach employing *visible light* (VL-DFL) and artificial potential fields based localization is proposed in this paper, called FieldLight. The approach provides localization and tracking of targets without the need to modify the existing lighting infrastructure, and without the utilization of extensive labelled training data. It offers an overall superiority over the previous discussed techniques as demonstrated by the feature comparison given in Table I.

The main contributions of this papers work are summarized as follows:

1) A novel VL-DFL algorithm called FieldLight is developed which can localize and track targets using a set of potential fields attached to triggered photodiodes. To the extent of the authors' knowledge, this is the first reported work that applies the artificial potential fields approach to VL-DFL
2) A calibration procedure that does not require any labelled training data is proposed for the developed VL-DFL. This makes the system less labor intensive, and easy to deploy.
3) The performance of FieldLight is evaluated by implementing it in multiple full-scale environments.

The impact of various parameters on the localization accuracy is investigated.

4) The localization accuracy of FieldLight is experimentally compared with an existing wireless DFL algorithm in the same environment. As far as the authors are aware, this is the first reported performance comparison between wireless- and visible light-based DFL techniques. FieldLight is demonstrated to be more accurate than a state of the art wireless DFL technique.

II. System Overview

Assuming an environment where the ambient light level remains constant, the change in illuminance can be calculated as:

$$\Delta E = E_{T1} - E_{T0}, \tag{1}$$

where E_{T1} and E_{T0} represent two consecutive illuminance samples in time, measured in lux. Since the PDs are mounted on the walls rather than on the floor (as in the existing approaches, e.g., [29, 33]), the shadowing influence caused by a roaming target does not completely occlude the attenuated node, as the node receives dispersed multipath light components from a number of luminaires available within the environment. It is hypothesized that even though each node receives illumination from multiple sources, the impact from the closest sources remains dominant when the *field of view* (FOV) remains unobstructed. This suggests that if the shadowing target does not fully occlude the FOV, it would still have some proportional attenuation effect on the amount of light sensed by nearby PDs. To exploit this effect, FieldLight uses an energy minimization concept in the form of artificial potential fields, weighted by the attenuation seen at each receiving node. All symbols used in this manuscript to outline the FieldLight approach are included in Table II. Since FieldLight assumes that background ambient light level remains constant, care must be taken to either ensure the illumination is predominantly made up of artificial light sources with a constant output, or the system must be calibrated to account for the changes in sunlight over the course of the day. In this paper experiments were conducted during the early evening when sunlight was minimal. Another consideration is the reflectance properties of the roaming targets attire. FieldLight was trained using a subject wearing dark attire to minimize reflectance during the offline training phase.

Let $\mathcal{N}$ light sensing nodes be deployed around the perimeter of the monitored area, within an indoor environment (Fig. 1).

Each node contains a PD, wall mounted at 1.4 m above the ground, to ensure that no furniture occludes the line-of-sight path between the luminaires and nodes. The sensing nodes measure the illuminance of the visible light and employ their onboard wireless modules to relay the information to a centralized server. The server collects the illuminance values from all PDs, detects which ones have been shadowed, and uses this information to localize a roaming target.

The FieldLight system tracks a roaming target based on its relative position to known wall mounted PDs (shown as the red circles in Fig. 2). The target does not carry any device (tag). Its presence is determined, and the target is located based on the visible light attenuation it causes to nearby nodes. A simplified side-view of the FieldLight setup is shown in Fig. 3.

TABLE II
FIELDLIGHT SYMBOLS

Parameter	Description
E	Illuminance
β	Maximum attenuation constant
$\mathbb{D}$	Illuminance dataset
$\mathbb{h}$	Illuminance histogram
α	Smoothing factor
$\mathcal{J}$	Indication vector
$\mathbb{L}$	Illuminance histogram – long-term average
$\mathbb{S}$	Illuminance histogram – short-term average
$\mathcal{D}$	Histogram distance between $\mathbb{L}$ and $\mathbb{S}$
c	ln(0) constant
d	Euclidean distance
$\mathcal{X}$	Position estimate from previous timestep
$\mathcal{n}$	Wall mounted node containing a photodiode
$\mathcal{W}$	Thresholding weight set
γ	Affected link threshold
$\mathcal{E}$	Geometric travel threshold
$\mathbb{W}$	Final weight set
$\mathcal{K}$	Maximum iteration constant
$\vec{\mathcal{F}}$	Net force
τ	Spring stepsize constant
$\mathcal{U}$	Spring energy threshold

The system implementing FieldLight operates in two stages. During the initial (offline) phase, the system collects two sets of readings. The first sample set consists of illuminance readings from all PDs when no target is present within the environment. The second sample set involves the target walking around the perimeter of the environment (as close as practically possible), ensuring that each PD is passed by. The system then calculates the maximum attenuation observed by

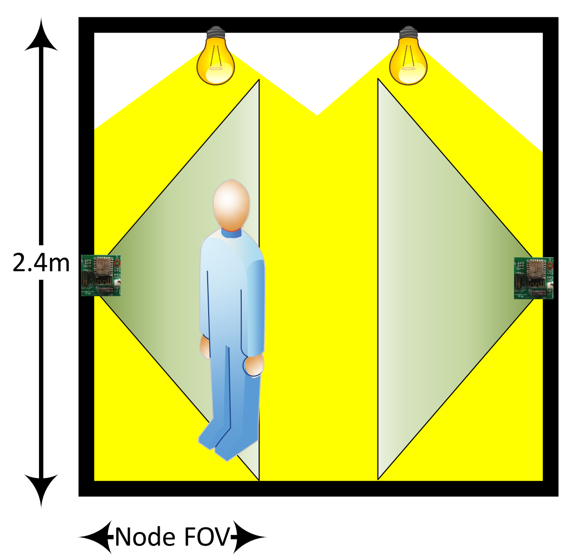

Fig. 3. Side-view of a person partially occluding the field of view of a wall mounted node.

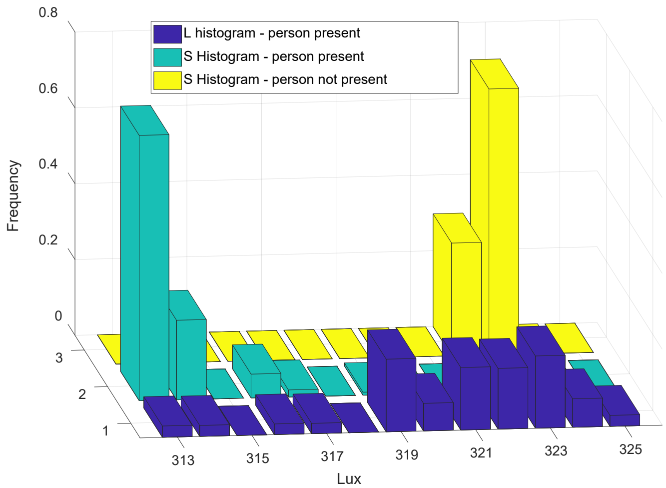

Fig. 4. The effect of a moving persons presence on both the Short-term ($\mathbb{S}$) and Long-term histograms ($\mathbb{L}$).

each PD as a difference between the readings of the two sets. This results in the maximum reference threshold for each PD.

During the second (online) phase, the system uses the current illuminance sample to check which receiving nodes experience an attenuation that exceeds the established, predefined threshold. These nodes are then assigned as virtual field anchor points and they receive a weight based on the ratio between their current attenuation values, and the maximum attenuation calculated during the initial offline phase. The reasoning for this is that if a PD shows a similar level of attenuation to the offline maximum, it is likely that the target is within close proximity to the node. The iterative potential fields approach then uses each anchor with its associated weight, alongside the previous position estimate to converge on a new predicted location. This is done by assigning an attractive force to each of the affected nodes. An example of this is illustrated in Fig. 2(b), where the blue arrows represent the attractive forces.

III. Algorithm

As outlined in Section II, FieldLight requires the offline phase to determine the maximum attenuation threshold for each PD, followed by the online phase where a static or moving target is iteratively localized.

A. *Offline Phase*

To find the maximum attenuation value for each receiving node, the difference between the illuminance of the visible light in an ambient non-blocked and blocked (shadowed) conditions is calculated as:

$$\beta_n = \max_n \mathbb{D}_0 - \min_n \mathbb{D}_1 , \qquad (2)$$

where β_n is the scalar attenuation value at the nth receiving node, $\mathbb{D}_0$ is the offline illuminance dataset with no target within the environment, and $\mathbb{D}_1$ is the offline illuminance dataset containing a target roaming around the perimeter of the indoor site. The $\mathbb{D}_1$ dataset contains illuminance values recorded at the light sensors when a target is walking along the perimeter of the environment. Its minima value is associated with the target being within close proximity to a given node. This is achieved by taking the minimum value from the set. It is the largest attenuation experienced for the route, which is assumed to correlate with an entity passing nearby the node.

B. *Online Phase*

The FieldLight approach is based on the assumption that a roaming (or static) target prevents a portion of the ambient light from reaching nearby PDs placed on the walls in some fixed locations. To be able to calculate a target position from a set of raw E values (produced by PDs), an appropriate information feature (or metric) needs to be carefully chosen. It should be resilient to both varying environmental conditions, and random effects of a roaming entity. FieldLight utilizes histogram distances as it's metric. In the FieldLight approach, a set of long-term histograms ($\mathbb{L}$), that represent the background state of E at the PDs; and a set of short-term histograms ($\mathbb{S}$), which represent the current state are defined. The difference between the $\mathbb{L}$ and $\mathbb{S}$ histograms is the feature that is used as a representation of the target's presence. The number of bins used by each histogram is equivalent to the resolution of the PD-based sensing node. Assuming that the output signal of each PD is digitized into 1000 states, to represent E between 1-1000 lux, the corresponding value range is $[1,\mathcal{Z}]$, where $\mathcal{Z} = 1000$. Each histogram is therefore constructed with $\mathcal{Z}$ bins. The value contained in each histogram bin is based on the frequency of its respective illuminance value occurring within a stream of data. For example, a node recording an illuminance value of 319 lux will increase the value of the 319th bin, representing an increased occurrence rate of the 319 lux value. These values are then normalized to a frequency between 0-1 and weighted based on their time-of-arrival. An example of the histogram is shown in Fig. 4. When a person (or some other mobile object) passes near a PD, the $\mathbb{S}$ histogram quickly diverges from its steady-state values. Since the $\mathbb{L}$ histogram diverges slower (as shown in Fig. 4) the difference between the two can be used as a feature to detect an object's presence. To facilitate the use of the histogram distance feature, two histogram sets are created using an exponentially weighted moving average (EWMA) scheme using:

$$\mathbb{h}_n^t = (1-\alpha)\mathbb{h}_n^{t-1} + \alpha \hat{\mathcal{J}}(E_n^t), \qquad (3)$$

where: $\mathbb{h}_n^t$ is a histogram (with $\mathcal{Z}$ bins) for node n at the time t, with every value of the histogram being within ($\in[0,1]$); α is a constant smoothing factor ($\in[0,1]$); $\hat{\mathcal{J}}$ is an indication vector of the length $\mathcal{Z}$ that returns 1 for the index given by illuminance value E_n^t, and 0 at every other position.

Bhattacharyya distance [43] is chosen as FieldLight's histogram distance metric as it can detect when the compared histograms have different standard deviations, even if their means are similar. This increases the sensitivity when a person (or object) is located near the edge of a PD's FOV thus causing very small changes to the node's received E values. In existing literature, Kernel and Kullback–Leibler distances have been used for histogram-based wireless localization [7, 44]. A recent study on various histogram distances showed that Bhattacharyya and Chi Squared distances perform well when used for a spring-relaxation based wireless approach [34]. Bhattacharyya distance provided the highest accuracy across all environments (e.g. 0.68m median error in the corridor environment vs 1.33m for Kernel distance and 2.69m for the

Kullback-Leibler distance). It was therefore chosen as the distance metric.

By using (3) to formulate each histogram in $\mathbb{L}$ and $\mathbb{S}$ sets, while ensuring $\alpha_{\mathcal{L}} < \alpha_{\mathcal{S}}$, the Bhattacharyya distance between $\mathbb{L}$ and $\mathbb{S}$ can be defined as:

$$\mathcal{D}_n = -\ln\left(c + \sum \sqrt{\mathbb{L}_n \cdot \mathbb{S}_n}\right), \tag{4}$$

where: $\mathbb{L}_n$ and $\mathbb{S}_n$ represent the long-term and short-term histograms for node n, created using (3), respectively; $\cdot$ is the *dot product*, the small constant term c is added to ensure that no $\ln(0)$ error occurs if no bin values overlap between the $\mathbb{L}$ and $\mathbb{S}$ histograms.

After a distance metric has been defined, thus enabling FieldLight to detect changes occurring around the nodes due to object movement, a selection criterion is established to identify and pick only the strongly impacted nodes, and to weigh them accordingly. This is achieved by using a thresholding process, utilizing: the Bhattacharyya distance for each node ($\mathcal{D}_{1:\mathcal{N}}$), and $d(\mathcal{X}, n)$, where $d(\mathcal{X}, n)$ is defined as the *Euclidean distance* between the previous position estimate $\mathcal{X}$, and the node n. When FieldLight is first turned on, $\mathcal{X}$ is initialized to the coordinate of the center of the entry doorway. Through the thresholding, FieldLight collects two weights for each receiving node.

The first weight is defined by:

$$\mathcal{W}_n^1 = \begin{cases} \mathcal{D}_n, & \mathcal{D}_n > \gamma \\ & \text{and } d(\mathcal{X}, n) < \mathcal{E}, \\ 0, & \text{otherwise} \end{cases} \tag{5}$$

where: γ and $\mathcal{E}$ are predefined thresholding constants, with γ ensuring that only strongly affected links are selected, while $\mathcal{E}$ provides a geometric restriction on the maximum level of target movement allowed between the chosen time steps.

The second weight uses the same thresholding condition. However, it stores the current attenuation as a proportion of the offline calibration value β_n:

$$\mathcal{W}_n^2 = \begin{cases} \dfrac{|mode(\mathbb{L}_n) - mode(\mathbb{S}_n)|}{\beta_n}, & \mathcal{D}_n > \gamma \\ & \text{and } d(\mathcal{X}, n) < \mathcal{E}, \\ 0, & \text{otherwise} \end{cases} \tag{6}$$

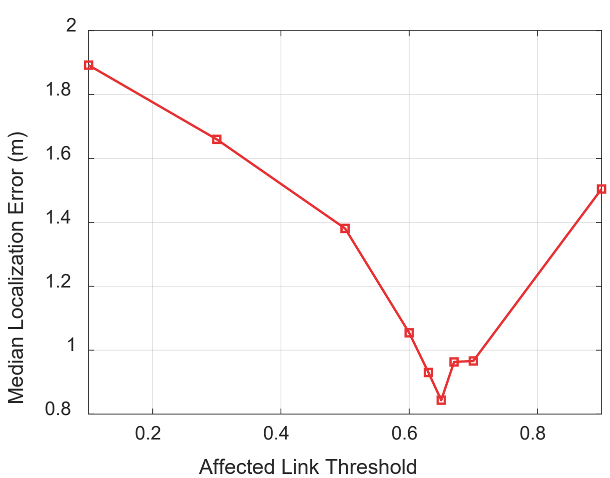

Fig. 5. Impact of affected link threshold, γ, on FieldLight's performance (shown as median localization error). Laboratory environment.

where the $mode()$ function returns the modal value (i.e. the bin index with the largest value) of a given histogram.

After the weights are calculated for all receiving nodes, the two weight sets are combined into a single set as:

$$\mathbb{W} = \frac{(\mathcal{W}^1 \circ \mathcal{W}^2) - \min(\mathcal{W}^1 \circ \mathcal{W}^2)}{\max(\mathcal{W}^1 \circ \mathcal{W}^2) - \min(\mathcal{W}^1 \circ \mathcal{W}^2)}, \tag{7}$$

where $\circ$ is the *Hadamard product*. This is performed to normalize the weight sets since $\mathcal{W}^1$ and $\mathcal{W}^2$ have different ranges, and maximum values.

After the histogram distances and weights are calculated for each receiving node, FieldLight implements an iterative potential fields procedure to both localize and track a moving target. The maximum number of iterations per the time step is defined in advance by the constant $\mathcal{K}$.

In a single iteration, the FieldLight computes an attractive force between the previous target position estimate, and each affected node. The net force within the system is calculated by summing the forces across the overlapping potential fields using:

$$\overrightarrow{\mathcal{F}_k} = \tau \sum_{n=1}^{\mathcal{N}} \vec{\mathcal{X}}_n \mathbb{W}_n, \tag{8}$$

where: k represents a single iteration (k iterates from $0{:}\mathcal{K}$); $\vec{\mathcal{X}}_n$ is a vector between the previous position estimate $\mathcal{Y}_{k-1}$ and the position of the nth receiving node; τ is a scaling constant.

In each iteration, the current position estimate is given using:

$$\mathcal{Y}_k = \begin{cases} \mathcal{X}, & k = 0 \\ \mathcal{Y}_{k-1} + \overrightarrow{\mathcal{F}_k}, & k > 0 \end{cases}, \tag{9}$$

where $\mathcal{X}$ is the position estimate from the previous time step. The final position estimate for the current time step can then be found as:

$$\mathcal{X} = \begin{cases} \mathcal{Y}_k, & |\overrightarrow{\mathcal{F}_k}| < \mathcal{U} \text{ and } k < \mathcal{K} \\ \mathcal{Y}_{\mathcal{K}}, & k = \mathcal{K} \end{cases}, \tag{10}$$

where $\mathcal{U}$ is the efficiency threshold that is used to terminate the potential fields algorithm early if the field equilibrium has already been reached (i.e., the net force on the system is small enough).

IV. Parameter Tuning

For FieldLight to perform adequately, its parameter values need to be carefully tuned to optimize the localization accuracy.

TABLE III
FIELDLIGHT PARAMETERS

Parameter	Description	Value
$\alpha_{\mathcal{L}}$	Smoothing Factor – Long-term	0.03
$\alpha_{\mathcal{S}}$	Smoothing Factor – Short-term	0.7
c	ln(0) Factor	0.00001
γ_{Foyer}	Affected Link Threshold	0.7
$\gamma_{Corridor}$	Affected Link Threshold	1.05
$\gamma_{Laboratory}$	Affected Link Threshold	0.65
$\mathcal{E}$	Geometric Travel Threshold	5
$\mathcal{K}$	Maximum Iteration Constant	6
τ	Stepsize Constant	0.06
$\mathcal{U}$	Energy Threshold	0.05

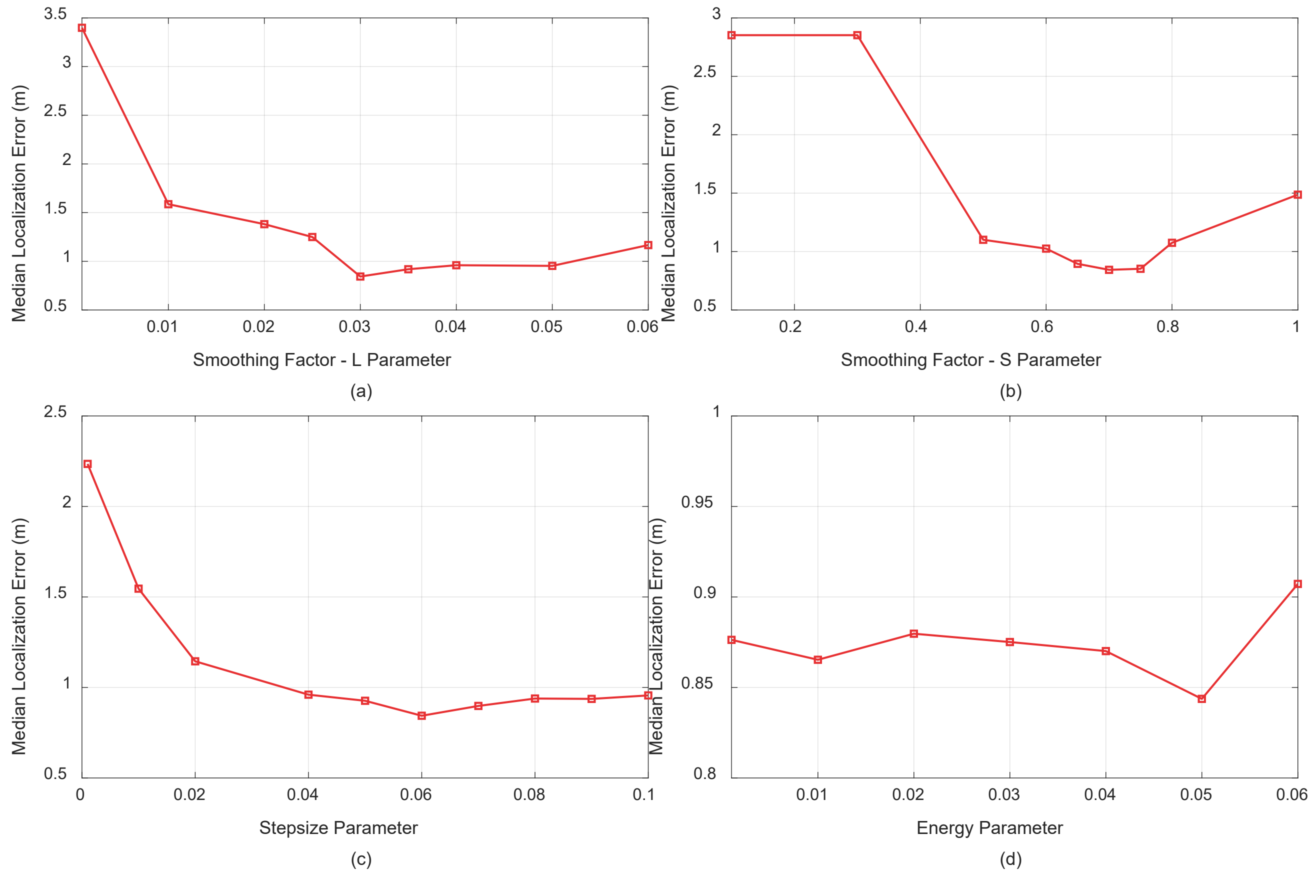

Fig. 6. The effect of varying parameter values on FieldLight's performance (shown as median localization error) for the Laboratory environment.

In this manuscript all localization errors are calculated by taking the Euclidean distance between the ground truth and estimated positions. Fig. 5 and Fig. 6 show how varying parameter values affect the overall localization accuracy within the laboratory environment (Fig. 2(c)/Fig. 7). The results for the laboratory environment comparison is given here since the LED luminaires were utilized in it for illumination – the same as in most *visible light positioning* (VLP) approaches presented in the literature.

The parameters shown in Fig. 5 and Fig. 6 were initialized to the values used for wireless histogram localization in [7, 44, 45]. Each parameter was then manually tuned while keeping all others at their initial value. A recorded illuminance dataset from each environment was used to ascertain which of the parameter changes produced the largest positive influence on the overall localization error. The parameter with the largest positive change was then re-initialized to the new tuned value. The manual tuning was then repeated for all other parameters, fixing

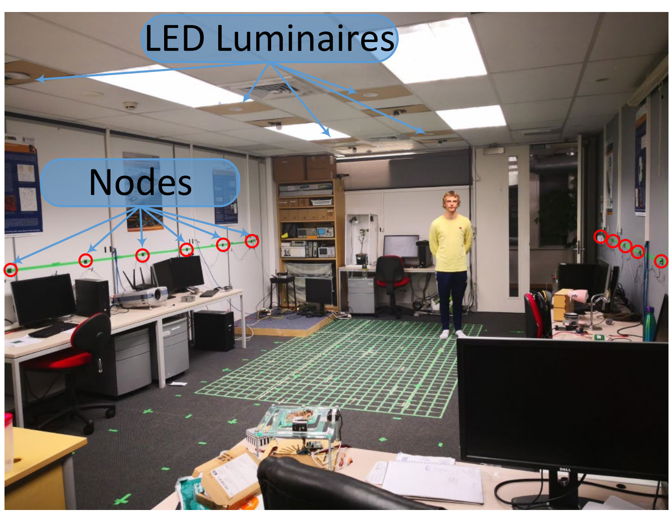

Fig. 7. FieldLight Laboratory environment. The fluorescent tubes shown were only turned on to produce a clear image. During experiments, only the LED luminaires were turned on.

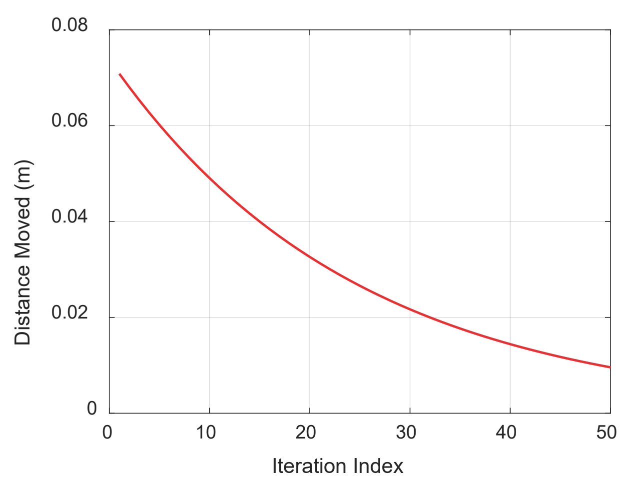

Fig. 8. An example of FieldLights iterative convergence approach, for a target that has travelled a significant distance since the previous timestep. The 'Distance Moved' represents how much the output position estimate is updated for each iteration of FieldLight.

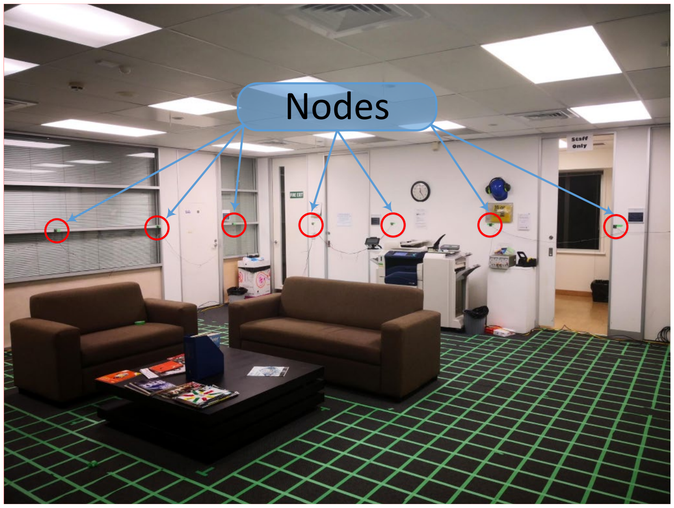

Fig. 9. FieldLight Foyer environment

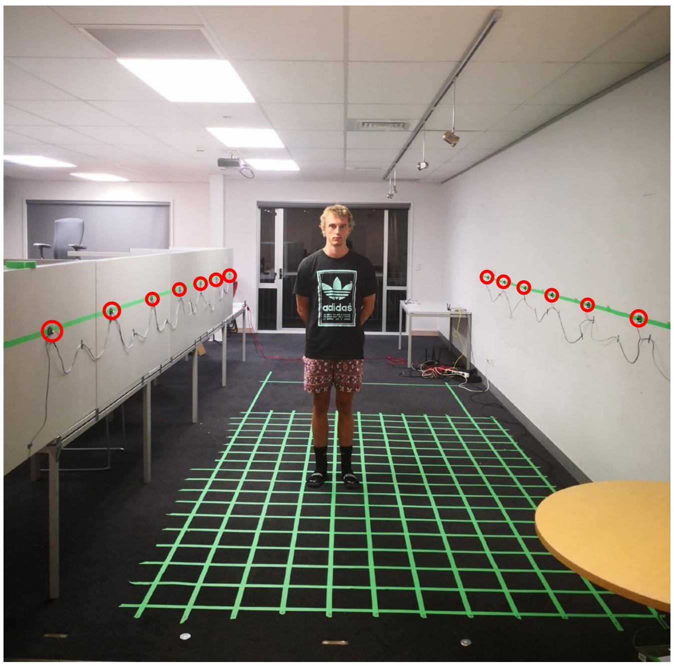

Fig. 10. FieldLight Corridor environment

one parameter to its new optimum value each round. This was repeated until all parameters had been tuned.

After empirically tuning the parameter values for each environment, it was discovered that most parameters were environmentally agnostic. This means that though the Affected link threshold (γ) was needed to be tuned for each environment, the other parameter values could be kept constant, which would minimize the required user input during the calibration process. As it could be seen in Fig. 6, there is a wide "optimum" range within which the parameters provide adequate performance. For example, $\alpha_{\mathcal{L}}$ has an acceptable range between 0.03-0.05, $\alpha_{\mathcal{S}}$ - between 0.6-0.75, τ - between 0.05-0.09, and $\mathcal{U} < 0.06$.
Fig. 8 shows an example of the distance that the target position estimate is updated by, with each iteration. For example, if FieldLight has updated its position estimate 4 times within the current timestep (*iteration index* = 4), the *distance moved* represents $\mathcal{Y}_4 - \mathcal{Y}_3$. As shown in Fig. 8, the distance moved decreases with each iteration, as FieldLight converges towards its final position estimate for the current timestep. The experiment was based on the extreme case where the previous position estimate was far away from the current location. The algorithm did not finish converging after 50 iterations. At the same time, by using 6 as a value of $\mathcal{K}$ (Table III) and 0.07m as an average iteration step, while also employing the 10Hz E sample rate, the system can accommodate a maximum target roaming speed of 4.2m/s. Since this is already significantly higher than the average adult walking speed (1.4m/s), the full convergence is not actually required. Besides, achieving the full convergence would introduce an unnecessary computational burden. This shows that careful considerations should be undertaken when deploying the FieldLight system, as the required maximum iteration number is intrinsically linked to both the desired performance level, and the overall network speed.

V. Experimental Setup and Results

The FieldLight hardware consists of 14 wall mounted custom boards that were designed to take ongoing readings of the perceived light level at a 10Hz sampling rate, and then wirelessly transmit these reading to the dedicated processing server, consisting of a laptop with an intel i7 processor, running windows 10 [35]. Preliminary tests performed with the nodes mounted within a range of heights of 0.75m-1.4m show no noticeable impact on the localization accuracy. The sensors were eventually mounted at 1.4m high to ensure that they were above the room furniture, to avoid occlusions.

Since the nodes are detecting changes in ambient light, they do not need to be placed relative to the light bulbs. However, careful placement is required to ensure coverage. In our experiments, we discovered that the sensors register a measured change in RSS level for approximately 3m-4m distance from the wall itself. This means that larger rooms will require either ceiling mounted, or floor mounted sensors (or fusion with another technology like wireless) to extend the coverage to the center of the room.

The custom boards (receiving nodes) consist of the Renesas Electronics ISL29023 Digital Ambient Light Sensor connected to an ESP 8266 microcontroller sampling the PD output, and sending the data to the processing server over Wi-Fi. The ISL29023 offers the onboard 50/60Hz flicker rejection and UV rejection. It is also very affordable, thus facilitating the potential for ubiquitous system adoption within smart home environments (the prototype cost remains below USD 5 per sensor node). It is envisioned that the sensors will be embedded within the walls, operating on mains power with the power cables running behind the wall panels like regular power conduits. Since only the photodiode will be visible on the wall, this will not be conspicuous, and will not have an unfavorable effect on an environments aesthetics. Once VLC adoption becomes widespread, many smart appliances will be equipped with VLC receivers (e.g. smart TV/fridge). Since these appliances are commonly positioned against walls and run off the mains power, they could potentially be used to provide a secondary localization benefit, without requiring the sensors to be embedded within the walls at those locations.

The custom boards, were mounted on the walls in 3 experimental environments (Fig. 2): a 7m x 8m foyer (Fig. 9)

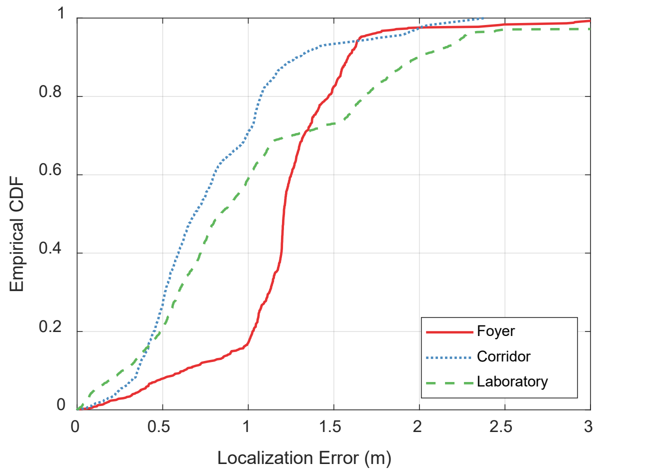

Fig. 11. FieldLight localization performance in all experimental environments

with 1.4m node spacing, a 4m x 7m corridor (Fig. 10) with 1m node spacing, and a 4.8m x 9.6m laboratory (Fig. 7) with 1.2m node spacing. All experiments were undertaken in the evening so that the overhead luminaires provided all the illumination within each test environment. The corridor and foyer employed fluorescent tubes for illumination while the laboratory utilized REX10CDLDIM LED luminaires. The LED luminaires had a rated power of 13W, beam angle of 90°, and were driven by a constant current of 350mA. The fluorescent lights seen in Fig. 7 were not turned on during the experiments at the laboratory.

To calibrate the system during the offline phase, a 1.84m tall subject moved around the perimeter of each site (as close as possible to the walls, while navigating around the furniture). The E values were collected from each receiving node at a 10Hz rate. The parameters of FieldLight were optimized using empirical tuning, and the employed final values are given in Table III.

During the online phase, the target walked along a marked path through each of the environments in a heel-toe fashion at 0.78m/s, with the steps being synchronized to a metronome. Illuminance values were recorded of the subject walking 3 times in each direction along the marked path, which was combined to form a single dataset. This ensured that both the step size and walking speed remained constant, and the ground truth location was known at each time step. One of the trials showing the ground truth path and estimated paths for each environment is shown in Fig. 12, Fig. 13 and Fig. 14. In the corridor, foyer, and laboratory environments, FieldLight achieved median errors of 0.68m, 1.20m, and 0.84m respectively. The *cumulative distribution function* (CDF) of the localization error for all the three test locations are shown in Fig. 11, and the median/95th percentile errors are shown in Table IV. Interestingly, the performance in the clear corridor was similar (within 0.2m error difference) to the cluttered laboratory for the first two error quartiles (Fig. 11). This suggests that a cluttered environment has stronger negative influence in areas where localization performance is already poor. Another key observation was that the localization ability in the foyer was significantly inferior to that in the other two environments. This was mainly caused by the larger dimension of the foyer. In both the corridor and laboratory environments, the walking subject always remains within 3m of a PD.

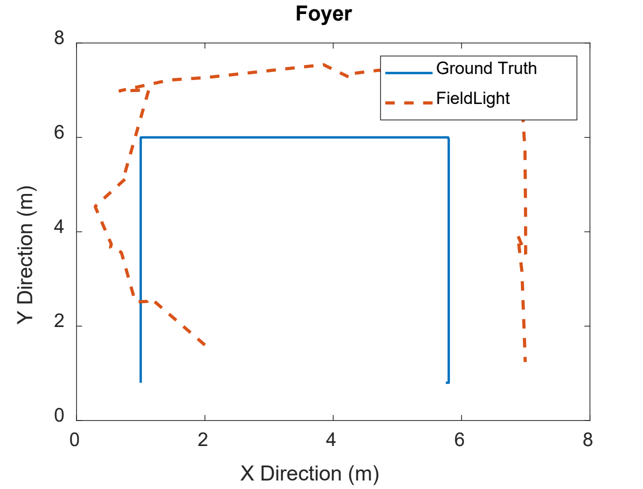

Fig. 12. Ground Truth path and FieldLight position estimates from a single trial in the Foyer environment

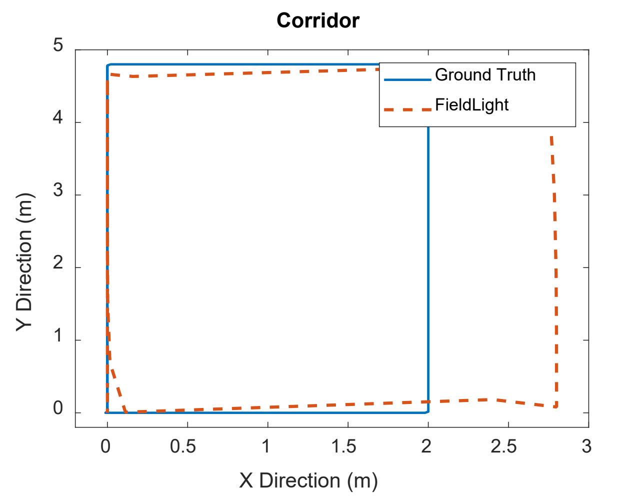

Fig. 13. Ground Truth path and FieldLight position estimates from a single trial in the Corridor

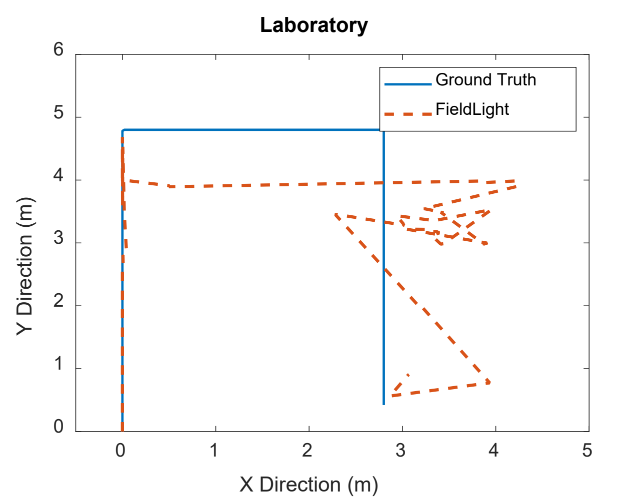

Fig. 14. Ground Truth path and FieldLight position estimates from a single trial in the Laboratory environment

However, in the foyer, the target walking through the middle of the room was over 3.5m away from the nearest PD. The impact of the traversing person on the RSS was extremely low at this distance creating dead spots where the node is not capable to

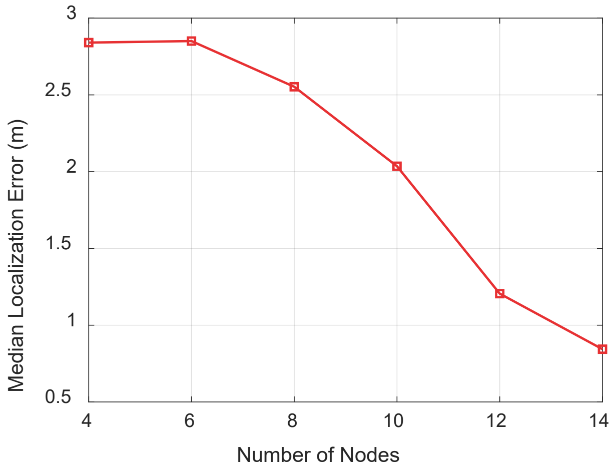

Fig. 15. Impact of number of light sensors on FieldLight's performance (shown as median localization error) in Laboratory environment.

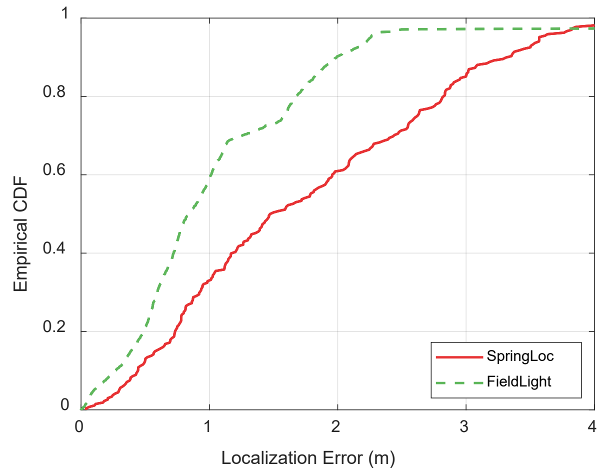

Fig. 16. FieldLight vs SpringLoc in the Laboratory environment

pick up the motion. This resulted in the erroneous output estimates.

The effect of reducing the number of receiving nodes employed for the localization is shown in Fig. 15. As expected, the localization accuracy decreases with fewer nodes.

To demonstrate how the FieldLight compares to the existing wireless-based approaches, that can be implemented using modern COTS equipment, it was benchmarked against SpringLoc [7]. SpringLoc has been proven to be one of the most accurate approaches among the DFL techniques that use the wireless RSSI metric. The laboratory environment (Fig. 7) was chosen for the comparison. SpringLoc uses a spring relaxation based DFL approach. It employs the Zigbee *received signal strength indicator* (RSSI) metric and creates virtual anchors within the environment, rather than employing the nodes themselves as anchors. The same number of nodes (14 nodes, each placed on the walls at a height of 1.4 m) were utilized for both the approaches. FieldLight used the PD-based sensors whereas SpringLoc utilized Texas Instrument CC2530 Zigbee radios.

The visible light based FieldLight surpassed the localization accuracy of the wireless SpringLoc approach as shown in Fig. 16 and Table V, when compared to the ground truth path. However, at the 98^{th}-100^{th} bands, SpringLoc approach displayed higher accuracy. This was because the wireless signals can operate in non-line of sight scenario, whereas the visible light-based nodes rely on the line of sight light paths. This means that in some cases FieldLight could suffer from a few large localization errors. For example, consider the entrance to the work area shown in the top right corner of Fig. 2(c). The ambient light level in this region is lower as there are significant furniture items obstructing the light propagation. When traversing this region, a roaming entity had a negligible impact on the nearby PDs, which contributed to several large localization errors in small areas, creating dead spots. The impact of this is shown in the top right corner of Fig. 14, as the target was temporarily lost as it passed in front of the occluding office furniture.

VI. Conclusion and Future Works

Existing VLP approaches require either a tagged subject, extensive infrastructure modifications, or significant offline training effort. FieldLight removes these limitations, while still providing at least a 1.2m median localization accuracy within multiple indoor environments. The research confirms that practical device-free VLP systems are plausible. However, further work is to be done to expand FieldLight to enable multiple targets tracking. FieldLights potential fields approach is not computationally complex, and the current factor limiting the maximum target speed is the 10Hz sample rate. If the system is required to track faster targets, either the sampling rate can be increased, at the cost of energy efficiency, or the stepsize constant can be increased, at the cost of low speed accuracy. Furthermore, FieldLight assumes there is a linear relationship between the portion of a nodes FOV that is affected by a target, and the total level of attenuation perceived. If more precise models are developed to accurately model this relationship, the overall localization accuracy could be improved. FieldLight was calibrated while the target wore a black t-shirt. While the system remains functional for multiple apparel colors, the performance would degrade. This could be addressed by utilizing multiple training models, for multiple colored apparels. Finally, FieldLight's performance degrades because of the dead spots caused by the subject traversing outside the sensing region of nearby nodes. Earlier work has reported that roof mounted nodes can measure the change in

TABLE IV
FieldLight Localization Performance

Environment	Standard Deviation (m)	Minimum Error (m)	Median Error (m)	95^{th} Percentile Error (m)	Maximum Error (m)
Foyer	1.40	0.04	1.20	1.65	8.83
Corridor	0.43	0.02	0.68	1.77	2.38
Laboratory	0.91	0.01	0.84	2.25	5.41

TABLE V
FieldLight vs SpringLoc Performance

Algorithm	Standard Deviation (m)	Minimum Error (m)	Median Error (m)	95^{th} Percentile Error (m)	Maximum Error (m)
FieldLight	0.91	0.01	0.84	2.25	5.41
SpringLoc	1.09	0.04	1.47	3.57	4.86

ground reflection to detect targets [27]. This suggests that careful node placement along both the roof and walls can potentially be used to ensure adequate coverage and optimize overall localization accuracy. Another option could involve fusing the FieldLight with a wireless DFL system to help remove the dead spots, as supported by the 98th-100th bands of SpringLoc, though more comparative tests are required to quantify the benefit a fused system could bring. Furthermore, the RSSI metric used by SpringLoc is a coarse metric when compared to Wi-Fi CSI. If CSI ever became readily accessible in COTS equipment, a fused system with CSI and visible light may bring further benefits. Finally, FieldLight uses potential fields as it is a computationally efficient method of providing localization, when compared to competing particle filters. However, potential fields approaches could potentially converge at incorrect local minimum, if the deployment area was large. It would be interesting to try detect these cases, and employ a backup algorithm (such as a particle filter) to ensure correct convergence.

REFERENCES

[1] A. Schieweck *et al.*, "Smart homes and the control of indoor air quality," *Renewable and Sustainable Energy Reviews,* vol. 94, pp. 705-718, 2018/10/01/ 2018, doi: 10.1016/j.rser.2018.05.057.

[2] H. Huang, G. Gartner, J. M. Krisp, M. Raubal, and N. Van de Weghe, "Location based services: ongoing evolution and research agenda," *Journal of Location Based Services,* vol. 12, no. 2, pp. 63-93, 2018/04/03 2018, doi: 10.1080/17489725.2018.1508763.

[3] H. Yigitler, R. Jantti, O. Kaltiokallio, and N. Patwari, "Detector Based Radio Tomographic Imaging," *IEEE Transactions on Mobile Computing,* vol. 17, no. 1, pp. 58-71, 2018, doi: 10.1109/tmc.2017.2699634.

[4] O. Kaltiokallio, R. Jantti, and N. Patwari, "ARTI: An Adaptive Radio Tomographic Imaging System," *IEEE Transactions on Vehicular Technology,* vol. 66, no. 8, pp. 7302-7316, 2017, doi: 10.1109/tvt.2017.2664938.

[5] Q. Wang, H. Yigitler, R. Jantti, and X. Huang, "Localizing Multiple Objects Using Radio Tomographic Imaging Technology," *IEEE Transactions on Vehicular Technology,* vol. 65, no. 5, pp. 3641-3656, 2016, doi: 10.1109/tvt.2015.2432038.

[6] S. Xu, H. Liu, F. Gao, and Z. Wang, "Compressive Sensing Based Radio Tomographic Imaging with Spatial Diversity," *Sensors (Basel),* vol. 19, no. 3, p. 439, Jan 22 2019, doi: 10.3390/s19030439.

[7] D. Konings, F. Alam, F. Noble, and E. M. K. Lai, "SpringLoc: A Device-Free Localization Technique for Indoor Positioning and Tracking Using Adaptive RSSI Spring Relaxation," *Ieee Access,* vol. 7, pp. 56960-56973, 2019, doi: 10.1109/access.2019.2913910.

[8] J. Wang, X. Chen, D. Fang, C. Q. Wu, Z. Yang, and T. Xing, "Transferring Compressive-Sensing-Based Device-Free Localization Across Target Diversity," *Ieee T Ind Electron,* vol. 62, no. 4, pp. 2397-2409, 2015, doi: 10.1109/tie.2014.2360140.

[9] R. Zhou, X. Lu, P. Zhao, and J. Chen, "Device-Free Presence Detection and Localization With SVM and CSI Fingerprinting," *Ieee Sens J,* vol. 17, no. 23, pp. 7990-7999, 2017, doi: 10.1109/jsen.2017.2762428.

[10] X. Dang, Y. Huang, Z. Hao, and X. Si, "PCA-Kalman: device-free indoor human behavior detection with commodity Wi-Fi," *Eurasip J Wirel Comm,* vol. 2018, no. 1, p. 214, 2018.

[11] H. Zou, Y. Zhou, J. Yang, W. Gu, L. Xie, and C. Spanos, "FreeDetector: Device-Free Occupancy Detection with Commodity WiFi," in *2017 IEEE International Conference on Sensing, Communication and Networking (SECON Workshops)*, 12-12 June 2017 2017, pp. 1-5, doi: 10.1109/SECONW.2017.8011040.

[12] H. Zhang *et al.*, "Wireless non-invasive motion tracking of functional behavior," *Pervasive Mob Comput,* vol. 54, pp. 29-44, 2019/03/01/ 2019, doi: 10.1016/j.pmcj.2019.01.006.

[13] X. Wang, L. Gao, S. Mao, and S. Pandey, "CSI-based Fingerprinting for Indoor Localization: A Deep Learning Approach," *IEEE Transactions on Vehicular Technology,* vol. 66, no. 1, pp. 1-1, 2016, doi: 10.1109/tvt.2016.2545523.

[14] Z. Yang, Z. Zhou, and Y. Liu, "From RSSI to CSI," *ACM Computing Surveys,* vol. 46, no. 2, pp. 1-32, 2013, doi: 10.1145/2543581.2543592.

[15] Y. Xie, Z. Li, and M. Li, "Precise Power Delay Profiling with Commodity WiFi," in *Proceedings of the 21st Annual International Conference on Mobile Computing and Networking - MobiCom '15*, Paris, France, 2015, 2790124: ACM, pp. 53-64, doi: 10.1145/2789168.2790124.

[16] D. Halperin, W. Hu, A. Sheth, and D. Wetherall, "Tool release," *ACM SIGCOMM Computer Communication Review,* vol. 41, no. 1, pp. 53-53, 2011, doi: 10.1145/1925861.1925870.

[17] G. Sun, Y. Xie, D. Liao, H. Yu, and V. Chang, "User-defined privacy location-sharing system in mobile online social networks," *Journal of Network and Computer Applications,* vol. 86, pp. 34-45, 2017/05/15/ 2017.

[18] D. Yang, W. Sheng, and R. Zeng, "Indoor human localization using PIR sensors and accessibility map," in *2015 IEEE International Conference on Cyber Technology in Automation, Control, and Intelligent Systems (CYBER)*, 2015: IEEE, pp. 577-581.

[19] J. Kemper and H. Linde, "Challenges of passive infrared indoor localization," in *2008 5th Workshop on Positioning, Navigation and Communication*, 2008: IEEE, pp. 63-70.

[20] G. Mokhtari, "Non-wearable human identification sensors for smart home environment: a review," *Sensor Review,* vol. 38, no. 3, pp. 391-404, 2018, doi: 10.1108/SR-07-2017-0140.

[21] O. B. Tariq, M. T. Lazarescu, J. Iqbal, and L. Lavagno, "Performance of Machine Learning Classifiers for Indoor Person Localization With Capacitive Sensors," *Ieee Access,* vol. 5, pp. 12913-12926, 2017, doi: 10.1109/ACCESS.2017.2721538.

[22] X. Tang and S. Mandal, "Indoor Occupancy Awareness and Localization Using Passive Electric Field Sensing," *Ieee T Instrum Meas,* 2019.

[23] B. Fu, F. Kirchbuchner, J. von Wilmsdorff, T. Grosse-Puppendahl, A. Braun, and A. Kuijper, "Performing indoor localization with electric potential sensing," *Journal of Ambient Intelligence and Humanized Computing,* vol. 10, no. 2, pp. 731-746, 2019.

[24] T. Grosse-Puppendahl *et al.*, "Platypus: Indoor localization and identification through sensing of electric potential changes in human bodies," in *Proceedings of the 14th Annual International Conference on Mobile Systems, Applications, and Services*, 2016: ACM, pp. 17-30.

[25] T. Kivimäki, T. Vuorela, P. Peltola, and J. Vanhala, "A review on device-free passive indoor positioning methods," *International Journal of Smart Home,* vol. 8, no. 1, pp. 71-94, 2014.

[26] Q. Wang and M. Zuniga, *Passive Sensing and Communication Using Visible Light: Taxonomy, Challenges and Opportunities*. 2017.

[27] Y. Yang, J. Hao, J. Luo, and S. J. Pan, "CeilingSee: Device-free occupancy inference through lighting infrastructure based LED sensing," in *2017 IEEE International Conference on Pervasive Computing and Communications (PerCom)*, 13-17 March 2017 2017, pp. 247-256, doi: 10.1109/PERCOM.2017.7917871.

[28] M. Ibrahim, V. Nguyen, S. Rupavatharam, M. Jawahar, M. Gruteser, and R. Howard, "Visible light based activity sensing using ceiling photosensors," in *Proceedings of the 3rd Workshop on Visible Light Communication Systems*, 2016: ACM, pp. 43-48.

[29] E. D. Lascio, A. Varshney, T. Voigt, and C. Pérez-Penichet, "LocaLight: a battery-free passive localization system using visible light: poster abstract," presented at the Proceedings of the 15th International Conference on Information Processing in Sensor Networks, Vienna, Austria, 2016.

[30] S. Zhang, K. Liu, Y. Ma, X. Huang, X. Gong, and Y. Zhang, "An Accurate Geometrical Multi-Target Device-Free Localization Method Using Light Sensors," *Ieee Sens J,* vol. 18, no. 18, pp. 7619-7632, 2018, doi: 10.1109/jsen.2018.2862412.

[31] V. Nguyen, M. Ibrahim, S. Rupavatharam, M. Jawahar, M. Gruteser, and R. Howard, "Eyelight: Light-and-Shadow-Based Occupancy Estimation and Room Activity Recognition," in *IEEE INFOCOM 2018 - IEEE Conference on Computer Communications*, 16-19 April 2018 2018, pp. 351-359, doi: 10.1109/INFOCOM.2018.8485867.

[32] T. Li, Q. Liu, and X. Zhou, "Practical Human Sensing in the Light," presented at the Proceedings of the 14th Annual International

Conference on Mobile Systems, Applications, and Services - MobiSys '16, Singapore, Singapore, 2016.
[33] T. Li, C. An, Z. Tian, A. T. Campbell, and X. Zhou, "Human Sensing Using Visible Light Communication," presented at the Proceedings of the 21st Annual International Conference on Mobile Computing and Networking - MobiCom '15, Paris, France, 2015.
[34] S. Hu, Q. Gao, C. Gong, and Z. Xu, "Efficient Visible Light Sensing in Eigenspace," *IEEE Communications Letters,* vol. 22, no. 5, pp. 994-997, 2018, doi: 10.1109/lcomm.2018.2808498.
[35] N. Faulkner, F. Alam, M. Legg, and S. Demidenko, "Smart Wall: Passive Visible Light Positioning with Ambient Light Only," in *2019 IEEE International Instrumentation and Measurement Technology Conference (I2MTC 2019) Proceedings*, Auckland, NZ, May 20-23 2019, pp. 1740-1745
[36] Q. Zhang, C. H. Foh, B.-C. Seet, and A. C. M. Fong, "Location Estimation in Wireless Sensor Networks Using Spring-Relaxation Technique," *Sensors,* vol. 10, no. 5, pp. 5171-5192, 2010.
[37] W.-T. Yu, J.-W. Choi, Y. Kim, W.-H. Lee, and S.-C. Kim, "Self-organizing Localization with Adaptive Weights for Wireless Sensor Networks," *Ieee Sens J,* vol. 18, no. 20, pp. 1-1, 2018, doi: 10.1109/jsen.2018.2866053.
[38] F. Alam, N. Faulkner, M. Legg, and S. Demidenko, "Indoor Visible Light Positioning Using Spring-Relaxation Technique in Real-World Setting," *Ieee Access,* vol. 7, pp. 91347-91359, 2019, doi: 10.1109/access.2019.2927922.
[39] D. Konings, B. Parr, F. Alam, and E. M. K. Lai, "Falcon: Fused Application of Light Based Positioning Coupled With Onboard Network Localization," *Ieee Access,* vol. 6, pp. 36155-36167, 2018, doi: 10.1109/access.2018.2847314.
[40] J. Barraquand, B. Langlois, and J. C. Latombe, "Numerical potential field techniques for robot path planning," (in English), *Ieee T Syst Man Cyb,* vol. 22, no. 2, pp. 224-241, Mar-Apr 1992, doi: 10.1109/21.148426.
[41] G. Li, Y. Tamura, A. Yamashita, and H. Asama, "Effective improved artificial potential field-based regression search method for autonomous mobile robot path planning," *International Journal of Mechatronics and Automation,* vol. 3, no. 3, pp. 141-170, 2013.
[42] H. Adeli, M. Tabrizi, A. Mazloomian, E. Hajipour, and M. Jahed, "Path planning for mobile robots using iterative artificial potential field method," *International Journal of Computer Science Issues (IJCSI),* vol. 8, no. 4, p. 28, 2011.
[43] A. Bhattacharyya, "On a measure of divergence between two statistical populations defined by their probability distributions," *Bull. Calcutta math. Soc.,* vol. 35, pp. 99-109, 1943 1943.
[44] Y. Zhao, N. Patwari, J. M. Phillips, and S. Venkatasubramanian, "Radio tomographic imaging and tracking of stationary and moving people via kernel distance," in *Proceedings of the 12th international conference on Information processing in sensor networks - IPSN '13*, Philadelphia, Pennsylvania, USA, 2013, 2461410: ACM, pp. 229-240, doi: 10.1145/2461381.2461410.
[45] D. Konings, F. Alam, F. Noble, and E. M. K. Lai, "Improved Distance Metrics for Histogram based Device-free Localization," *Ieee Sens J,* pp. 1-1, 2019, doi: 10.1109/jsen.2019.2922772.

Daniel Konings (M'17) received his BE(Hons) from Massey University, Auckland, New Zealand in Computer Systems and Electronics Engineering in 2014, where he is currently pursuing his Ph.D. degree with the School Food and Advanced Technology (SF&AT). His research interests include indoor localization, digital signal processing, machine learning, IoT & wireless sensor networks. Daniel is a Student Member of the Institute of Electrical and Electronics Engineers (IEEE).

Nathaniel Faulkner received his BE(Hons) from Massey University, Auckland, New Zealand in Electronic & Computer Engineering in 2016. He is currently pursuing Ph.D. at the same institute. His research interests include visible light positioning and internet of things.

Fakhrul Alam (M'17-SM'19) received his BSc (Hons) in Electrical & Electronic Engineering from BUET, Bangladesh and MS and Ph.D. in Electrical Engineering from Virginia Tech, USA. He is currently a senior lecturer at the School Food and Advanced Technology (SF&AT), Massey University, New Zealand. His research interests include indoor localization, 5G & visible light communication, disaster management with 5G, IoT & wireless sensor networks. He is a senior member of the Institute of Electrical and Electronics Engineers (IEEE) and a member of the Institution of Engineering and Technology (IET).

Edmund M-K Lai (M'82-SM'95) received his BE(Hons) and PhD from The University of Western Australia, both in Electrical Engineering, in 1982 and 1991 respectively. He is currently a Professor of Information Engineering at Auckland University of Technology, New Zealand. He has previously held faculty positions at universities in Australia, Hong Kong, and Singapore. His research interests include digital signal processing, digital communications and networks, computational and swarm intelligence, and artificial neural networks. Prof. Lai is a fellow of the Institution of Engineering and Technology (IET) and a senior member of the Institute of Electrical and Electronics Engineers (IEEE).

Serge Demidenko (M'91-SM'94-F'04) is Professor and Dean of the School of Science and Technology, Sunway University, Malaysia. He is also associated with Department of Mechanical and Electrical Engineering, School of Food and Advanced Technology, Massey University, New Zealand. He graduated in Computer Engineering from the Belarusian State University of Informatics and Radio Electronics, and received Ph.D. from the Institute of Engineering Cybernetics of the Belarusian Academy of Sciences. His research interests include electronic design and test, signal processing, instrumentation and measurements. He is also Fellow of IET and UK Chartered Engineer.

Conclusion

This work has resulted in 2 peer reviewed conference papers and 5 Journal Articles (4 of which have already been published in Q1 journals). Though each individual chapter contained within this thesis clearly outlines the novelty of the work done and the original contributions, a summary of the novel research contributions is provided below:

- Investigated the impact of Wi-Fi and microwave interference on the RSSI values of a co-located ZigBee network
- Experimental results from multiple full-scale visible light/ZigBee Active/DFL IPS solutions in real-world settings.
- A novel active localization and tracking algorithm which fused ZigBee RSSI and Visible light RSS. This is the first reported experimental work that utilizes a fusion of wireless and visible light for indoor localization.
- The first reported experimental implementation of all 3 major RSSI-Based wireless DFL techniques, in multiple realistic environments, utilizing varying walking trajectories, and providing an apple-to-apple comparison of the techniques.
- A novel RSSI-based wireless DFL solution using histogram distance and adaptive spring relaxation which:
    - is robust to varying walking trajectories,
    - maintains its performance under low node densities,
    - requires minimal calibration and
    - has low computational overhead.

This is the first reported work that used the concept of spring relaxation in the context of wireless DFL.

- The first reported work that investigates the impact of the histogram distance metrics on the localization performance on wireless-based DFL systems and finds a better suited replacement of the commonly used distance metric.
- A novel visible light-based DFL solution that does not require luminaire modifications or extensive offline measurements. This is the first reported work that utilizes the concept of potential fields-based energy minimization for visible light-based DFL solution.

Over the course of this project, we have collected numerous datasets of both fine-grained fingerprint data, and live data. We intend to upload both RF RSSI and Visible Light RSS datasets to the UCI Machine Learning Repository. This will allow researchers to test new localization algorithms in real-world environments, and enable them to make fair comparisons between different IPS approaches. This will also assist in future machine learning efforts.

Future Direction

In both our wireless and visible light implementations, the multiple target problem is left for future work. Recent literature has shown that, if the total number of individuals present is known, RSSI-based approaches can use background subtraction techniques to localize multiple targets. Since both SpringLoc and FieldLight have low runtime complexity, a separate spring network could be defined for each moving target. To enable this, further work needs to be done to provide both an accurate target count, and a way of using successive cancelation techniques to separate the influence of each entity from the raw values.

Future work also needs to be done to quantify how the influence of each target affects the whole network, when multiple targets converge on a common location. The developed algorithms also assume that the coordinates of the luminaires/static nodes are known. Future work could involve improving the calibration procedure to allow for the sensors to perform self-localization, before localizing the roaming targets.

Furthermore, the algorithms do not utilize the target's assumed gait. Their localization accuracy could potentially be improved if trajectory and gait information was used to update the previous state estimate, before calculating the current estimate. To assist with this, work should be done to infer a targets height, since this has a direct correlation with a target's stride length. This could potentially be achieved through using multiple sensor networks at various heights, which has successfully been used for IPS-based fall detection in existing literature.

The proposed algorithms also assume that the subjects maintain a speed consistent with average human walking pace. Future work could involve expanding the algorithms to allow for higher mobility, which could allow the system to work for autonomous indoor vehicles.

Work could also be done to develop open source Wi-Fi drivers that expose the CSI metric, reintroducing the metric to modern COTS equipment, and providing an avenue for Smart Home vendor support.

Further works can also utilize classification and pattern recognition. If data could be collected from multiple Smart Home wireless DFL deployments, with known target ground truths, new RSS features and behaviours could be identified, beyond the assumed shadowing effect. This could help to identify behaviours such as targets opening doors or sitting on chairs, which could potentially be generalised as a known feature.

Further work also needs to be done on interference mitigation and metric integrity, when Wi-Fi RSSI is used over ZigBee RSSI.

FieldLight proved that VLP based DFL is plausible with minimal changes made to the existing infrastructure. Since it is costly to replace all existing lighting infrastructure with VLC enabled luminaires, future work would could include deploying FieldLight within regions containing traditional lighting, alongside another VLP approach deployed within VLC capable regions. This would help extend the overall VLP coverage and reduce blindspots. Another option is to fuse FieldLight with wireless DFL, in a similar fashion to Falcon's implementation. This would help remove FieldLight's blind spots, caused by it traversing too far from the nearest VLP node.

FieldLight currently models all known affected photodiodes as attractive potential fields. The approach could potentially be improved by using all known unaffected photodiodes as repulsive potential fields, which would provide another data stream for localization purposes.

FieldLight also assumes that there is a simple linear relationship between the shadowing that the target causes to a photodiodes RSS, and the separation distance between them. More work should be done to create an accurate model of a target's influence on a photodiode's RSS, given known separation distances, and stationary illumination sources. Future work could also investigate how different fabrics and colours influences the accuracy of localization, and then develop mitigation strategies to calibrate accordingly.

As VLC technology becomes prevalent in Smart Homes, VLC receivers will likely either be embedded into future end user devices e.g. laptops, or within the environment, with a secondary wireless uplink. Work should be done to ascertain how various embedded photodiode orientations affect the accuracy of a visible light based DFL implementation.

Furthermore, as machine learning approaches become readily available on low power embedded platforms such as the NVidia Jetson, work can be undertaken to provide pre-trained abstracted neural networks that are transferable to standard end users. This will help minimize any required end user calibration procedure, while still allowing them to customise the deployment for their specific Smart Home.

The developed algorithm approaches were largely based on either spring-relaxation, or adaptive potential fields. These algorithms are known to have low complexity; however, they have the potential to converge on incorrect local minima. Further work needs to be done within large open plan indoor spaces to ensure, the algorithms still correctly converge when there is a significant distance between the target and the nearest node. Following on from this, work needs to be done to assess the stability of these algorithms, and to measure the overall energy consumption that these techniques use.

Future work could also look into standardizing DFL testing, as current standards only explicitly mention *active* tracking solutions.

Appendix 1

This appendix contains content from the following article, republished with permission. In accordance with IEEE's republishing policy, any full text that has been included is the unmodified accepted article. This means that while the content is identical to the published article, there may be stylistic differences.

The Effects of Interference On The RSSI Values Of A ZigBee Based Indoor Localization System

Daniel Konings[1], Nathaniel Faulkner[1], Fakhrul Alam[1], Frazer Noble[1] and Edmund M-K Lai[2]

[1] School of Engineering and Advanced Technology
Massey University
Auckland, New Zealand
d.konings@massey.ac.nz

[2] Department of Information Technology and Software Engineering
Auckland University of Technology
Auckland, New Zealand

Abstract— **Indoor positioning systems (IPS) have gained a lot of traction within the research community in recent years. Received Signal Strength Indicator (RSSI) of wireless networks are the most commonly used metric for indoor localization. The objective of this paper is to see how Wi-Fi interferers of different data rates affect the packet RSSI values of TX-RX links in a ZigBee based indoor localization system. The factors we examine also include the rate of corrupted packets and the overall packet loss. We also explore whether a Microwave Oven, a common source of interference for the ISM Band in a dwelling, perturb RSSI values in a localization system.**

Keywords— RSSI; mobile robot; wi-fi interference; 802.15.4; ZigBee; indoor localization; packet loss; packet corruption; Microwave interference

I. Introduction

In recent years, research into localization has become very popular as the proliferation of Wireless Sensor Networks (WSNs) grows. This has seen an increase in the number of proposed applications within sensor and robotics fields. Low power off the shelf radios have been employed for localization based implementations for detecting animal presence [1], outdoor mobile robot localization [2], biobot localization [3] or indoor mobile robot localization [4-7]. When these localization solutions are implemented indoors, they are termed as Indoor Positioning Systems (IPS) [8]. Simultaneous Localization and Mapping (SLAM) algorithms are commonly used to solve the localization problem for a mobile robot. The problem with these approaches is that they usually require expensive sensors, and even low cost approaches require the robot to carry multiple sensors [9]. Wireless network based localization is attractive as by using a single off the shelf robot mounted radio, with an associated sensor network, the implementation cost is reduced as the number of robots increases. Wireless solutions also have the benefit of not requiring visible light, which makes them more appropriate than camera based SLAM for emergency situations where a robot may have to traverse through rubble or a pipe.

A common metric used to implement IPS using wireless sensors is the Received Signal Strength Indicator (RSSI) due to its ready availability in off the shelf 802.15.4 [10] and Wi-Fi [11] equipment. This paper focusses on ZigBee which is more suitable for long term, battery operated, robotic solutions as it offers mesh networking and better power consumption than Wi-Fi [12]. For 802.15.4 ZigBee radios, RSSI is implemented as an 8-bit register. The register value is often scaled/offset to give a measured value in dBm. There are two types of RSSI measurement. The first type of measurement is used to estimate the ambient power within the channel itself (also known as an ED Scan). The second type of measurement is used to estimate the Received Signal Strength (RSS) of a received packet [10]. When this paper refers to RSSI, we are referring to the second type of measurement as this is most commonly used for localization purposes.

This paper presents experimental results on the effects of Wi-Fi and microwave oven interference on the magnitude of RSSI values, packet loss and corrupted packets within an 802.15.4 TX-RX link. Since packet RSSI has become a popular metric to use for localization, especially IPS, it is important to know whether it remains accurate and therefore usable in the presence of common interference sources. The impact of interference on ZigBee packet loss and throughput is well understood and has been extensively investigated in literature [13-17]. However the impact on the accuracy of packet RSSI values has not been investigated very thoroughly. Most studies focus on the impact of interference on ED scan RSSI values. The handful of studies that investigates the impact on packet RSSI are limited to low Wi-Fi data rates [18] that is impractical in today's wireless networks or TX-RX separation that is more in line with body area networks (BAN) [14] and not robotics and other typical application.

II. Background

An IPS using RSSI can be implemented through either Device-free Passive (DFP) [19] or Active localization [20, 21]. DFP works by creating a dense network of "linked pairs" as

each radio surrounding the area of interest can transmit and receive wireless signals. DFP systems analyze which links are currently experiencing change due to the robot passing through them, and thus a moving robots location can be detected as the intersection of multiple affected links [22]. Active tracking utilizes the same information (RSSI), but instead uses it as a form of wireless ranging where the tracked robot is in contact with several other nodes at any given time to contribute to the localization.
RSSI based localization will often use either a variation of one of the following methods, or a combination of multiple techniques.

A. Range-free Algorithims

Range-free algorithms use the concept of relative signal strength loss to locate a target node. They are often based on the assumption that RSSI decreases with distance, but do not use absolute point-to-point distances or angles to estimate a location [23].

B. Path-Loss Algorithms

Path-Loss based localization (also known as Range-based localization) create and employ a statistical model to estimate the distance (range) between a beacon and robot based on the TX-RX link power between them. This approach is then used by multiple known beacon nodes to infer location coordinates, often via a lateration approach [24].

The problem is that all these systems rely on either the RSSI values themselves, or the fluctuations between RSSI values to be accurate. Research into the effect of Wi-Fi on 802.15.4 networks has shown that strong Wi-Fi interference will cause significant packet losses and will increase the received signal strength of the 802.15.4 channels noise floor [25]. Further research into BAN has shown that a Wi-Fi interferer will cause significant packet losses in a ZigBee network but have minimal effect on the ZigBee packet based RSSI values [14]. From a localization perspective, it is common place to have ZigBee TX-RX links with up to 10m separation. Therefore further work needs to be done to ascertain the usability of packet RSSI values in networks with greater TX-RX separation than the 1.5m of a BAN.

Common existing solutions to the interference problem of a ZigBee network are as follows: Use 802.15.4 channel 25 or 26 [16], introduce a channel hopping protocol that changes channel based on the presence of interference [25] or introduce a MAC layer transmission protocol to mitigate interference [14]. Using the upper 802.15.4 channels is not viable as they are not globally free of Wi-Fi interference due to the use of Wi-Fi channels 13-14 in Europe and Asia. Introducing a channel hopping protocol only works if there are 802.15.4 channels available that are not affected by Wi-Fi. As the demand for higher data rates become more common due to advancing technology and services such as 4k content streaming becoming commonplace, Wi-Fi saturation could become more frequent. The problem with MAC layer protocol variants is that they are proprietary and therefore will not likely be compatible with global standards such as ZigBee 3.0. This means that any current solution using them either is incompatible with communicating to other ZigBee devices, or would require a very bespoke implementation. Therefore we assume the worst-case situation, a localization system operating in the presence of a strong Wi-Fi interferer and investigate whether the integrity of the system is affected by heavy Wi-Fi interference, i.e. do the RSSI values of correctly received packets change? This is important as interference induced packet RSSI fluctuations could seriously impair the accuracy of a RSSI based localization system.

We also investigate the effect of Microwave interference on ZigBee TX-RX links. We chose these interference sources as both Wi-Fi and Microwaves are common in indoor environments.

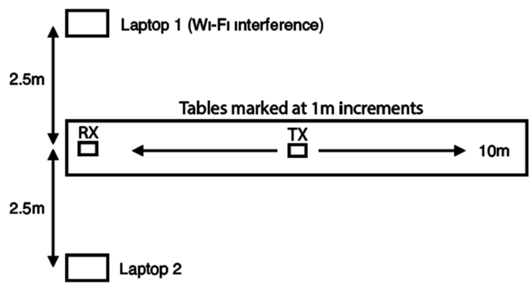

Fig. 1. Wi-Fi Interference Test Setup

III. Experimental Setup

We chose to use the TI CC2530 [26] which supports a fully compliant ZigBee stack and provides a good analog of a chip that may be used within Home Automation / Lighting Systems / Industrial Control or Health Care applications. The chip provides an affordable off-the-shelf system-on-chip that incorporates both a CC2530F256 RF transceiver and an enhanced 8051 MCU. We used a Rohde & Schwarz Spectrum Rider FPH [27] to analyze the spectrum of the test environment when either Wi-Fi or Microwave interference are present.

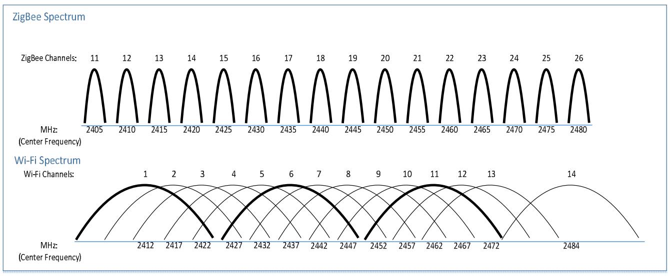

Fig. 2. ZigBee and Wi-Fi spectrum usage

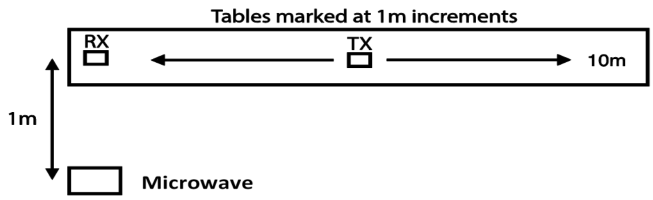

Fig. 3. Microwave interference Test Setup

Two experiments have been conducted to analyze the effect of Wi-Fi interference on 802.15.4. For the first experiment, we maintained a fixed CC2530 TX-RX separation of 5m while varying the Wi-Fi transmission rate from 0-20Mbps. For the second experiment, The RSSI was measured at 1m intervals as the CC2530 RX-TX separation increased from 1m - 10m, in the presence of a constant 10Mbps/20Mbps Wi-Fi interferer. In both experiments the duration of each result was defined by the 802.15.4 receiver having received 5000 packets (correct or corrupted). Both experiments were set up as per Fig. 1 with the laptops, acting as the Wi-Fi interference source, perpendicular to the CC2530 TX-RX pair. All Devices were sitting on tables 0.71m above the ground. The Laptops and CC2530 RX remained completely stationary between both experiments. When the CC2530 TX node was moved, antenna orientation was kept constant to ensure it would not affect the results. The experiments were performed with no humans or moving objects present to minimize any potential impact from varying multipath propagation. Wi-Fi (802.11n) interference was generated by sending constant traffic from Laptop 1 to Laptop 2 using the program iPerf3 [28]. Both experiments were performed inside an empty classroom in the evening at Massey University. Wi-Fi channel 6 was selected for the experiments as it was completely empty of other nearby Wi-Fi channel 6 access points during the time of testing. ZigBee (802.15.4) channel 18 was chosen as it is completely encompassed by Wi-Fi channel 6, as can be seen in Fig. 2, and therefore helps represent a worst case interference example.

We also did an experiment using a 1200w microwave as the interference source. The microwave was placed 1m away from the CC2530 RX node, perpendicular to the CC2530 TX-RX LOS path as seen in Fig. 3. The CC2530 TX-RX pair was operated on channels 11, 18 and 26 to observe whether RSSI was affected differently in different parts of the spectrum. In each trial a bowl of cold water was put into the microwave and it was set on High. This was done to verify whether a commonly present interferer within the 2.4 GHz band, but with a different profile to Wi-Fi would have the same effect on RSSI values as a Wi-Fi interferer.

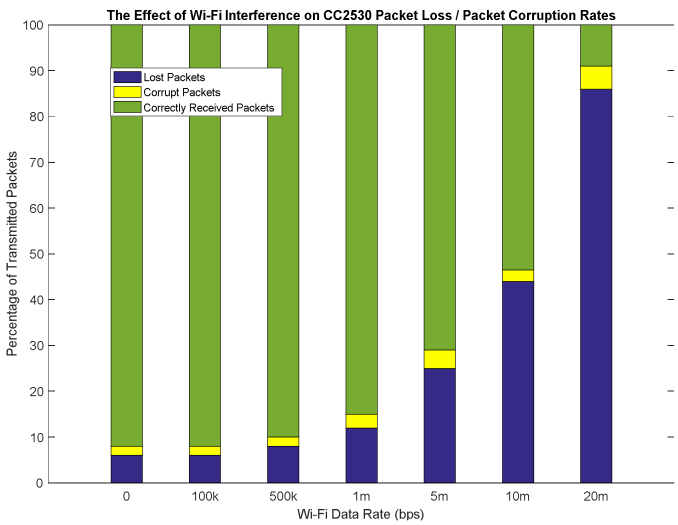

Fig. 4. The effect of Wi-Fi interference on a ZigBee 5m TX-RX links packet loss and corruption

IV. Results

A. Experiment 1

There are several interesting findings from experiment 1 that can be observed in Table 1 and Fig. 4. Firstly, as can be seen in Table 1, the RSSI of correctly received packets is unaffected by Wi-Fi interference, regardless of the Wi-Fi's data rate. Fig. 4 shows that packet loss increases significantly in the presence of a Wi-Fi interferer.

TABLE I.

	The Effect of Wi-Fi Interference on ZigBee RSSI values						
	Wi-Fi Data Rate (bps)						
RSSI (dBm)	No Interference	100k	500k	1m	5m	10m	20m
Correct Packets	-60	-58	-60	-60	-60	-59	-60

B. Experiment 2

Table 2 shows that RSSI values do not change due to the presence of a Wi-Fi interferer, even as the ZigBee TX-RX separation increases.

TABLE II.

	The Effect of Wi-Fi Interference on ZigBee RSSI values									
	ZigBee TX-RX Separation (m)									
RSSI (dBm)	1	2	3	4	5	6	7	8	9	10
No Interference	-33	-38	-47	-50	-60	-63	-74	-65	-64	-67
Wi-Fi 20Mbps	-34	-37	-47	-48	-60	-62	-74	-63	-64	-68

Fig. 5 shows that the packet loss associated with an interference source increases significantly for any TX-RX link that is longer than 2m.

The results also show that a Wi-Fi interferer has a more significant impact on lost packets than CC2530 TX-RX link separation for distances up to 10m. Experiments 1 and 2 show that the percentage of corrupt packets remains relatively stable and does not show a strong correlation to either Wi-Fi separation or CC2530 TX-RX separation for the distances tested.

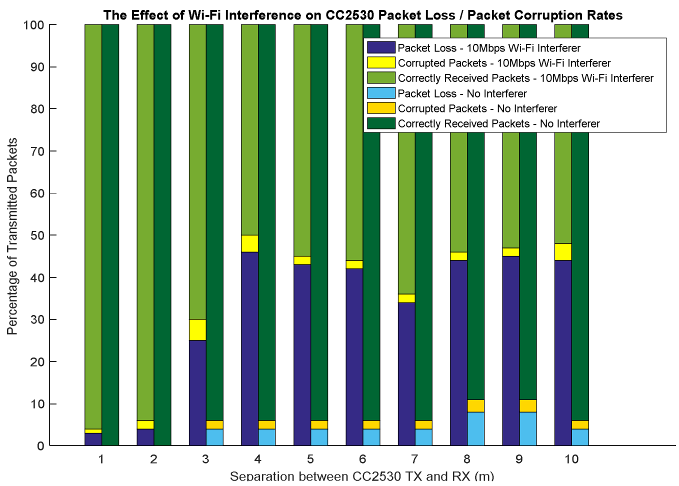

Fig. 5. The effect of a 10Mbps Wi-Fi Interferer on ZigBee packet loss and corruption

TABLE III.

RSSI (dBm)	The Effect of Microwave Oven Interference on ZigBee RSSI values		
	ZigBee Channel		
	11	18	26
No Interference	-55	-62	-63
Microwave Oven Interference	-55	-61	-63

C. *Experiment 3*

Experiment 3 with a Microwave Oven also showed that there was no influence of interference on the RSSI values of correctly received packets as seen in Table 3.

We also noticed that there was no increase in the number of corrupt packets or the number of lost packets. This is interesting as both the Wi-Fi source (Fig. 6(b)) and the Microwave source (Fig. 6(c)) had noticeable effects on the channel, when compared to the static environment (Fig. 6(a)), as measured from the ZigBee RX node. This is also contrary to results reported by [17] that suggest placing radios at least 2m away from microwaves to ensure reliable communication. We believe that this is caused by different microwaves having different radiation patterns, which in turn affect co-channel signals differently.

There is a significant relationship present between the Wi-Fi data rate and the number of lost packets as seen in Fig. 4, with an increase in Wi-Fi data rate resulting in an increase in lost packets. As the Wi-Fi data rate increases, so does the probability of a collision as there is more data travelling through the shared 2.4 GHz ISM band. When collisions do occur, the ZigBee receiver is often unable to decode the appropriate packet, thus turning a Wi-Fi – ZigBee collision into a ZigBee packet loss.

V. DISCUSSION

The experiments undertaken have clearly shown the effect a Wi-Fi interferer has on ZigBee communication. The findings can be concluded as follows:

1) Interference (both from Wi-Fi and Microwave Ovens) has no measurable impact on the RSSI values of correctly received packets within a ZigBee TX-RX link.

2) Wi-Fi interference causes a significant increase in lost ZigBee packets as its datarate increases.

3) An increasing Wi-Fi datarate has a stronger effect on ZigBee packet loss than increased ZigBee TX-RX link separation in an indoor network.

Since interference has no effect on the RSSI of correctly received packets, this suggests that the data integrity of a ZigBee RSSI based localization system would not be affected. This is important as it means the localization accuracy should not be affected due to the presence of a strong interferer. However if an algorithm that employs some form of time averaging [29], is implemented using ZigBee devices, latency could be made worse in the presence of interference due to the increased packet loss. This could occur for both Active Tracking solutions (such as tracking an autonomous/mobile robot) and DFP solutions. This means that and IPS containing mobile robots with low mobility should be largely unaffected but an IPS that requires high mobility and accuracy will need to take interference into account.

The results showed that a Wi-Fi interferer has a stronger effect on the systems packet loss than ZigBee node separation. With relation to a localization system this means that while the location of beacon nodes within the localization region is important, their separation distance will have less of an effect on tracking performance than an external interference source will.

VI. CONCLUSION

Through testing we have shown that interference from common sources like Wi-Fi and Microwave Ovens will not influence the RSSI values of correctly received links in a coexisting ZigBee network. We have also shown that a Wi-Fi interferer will greatly increase the rate of packet loss with a ZigBee network. Future work includes analyzing what level of Wi-Fi interference will noticeable affect the latency of common RSSI localization systems. Following this, we wish to investigate whether the RSSI of corrupt packets can be a secondary source of RSSI values when strong interferers are present.

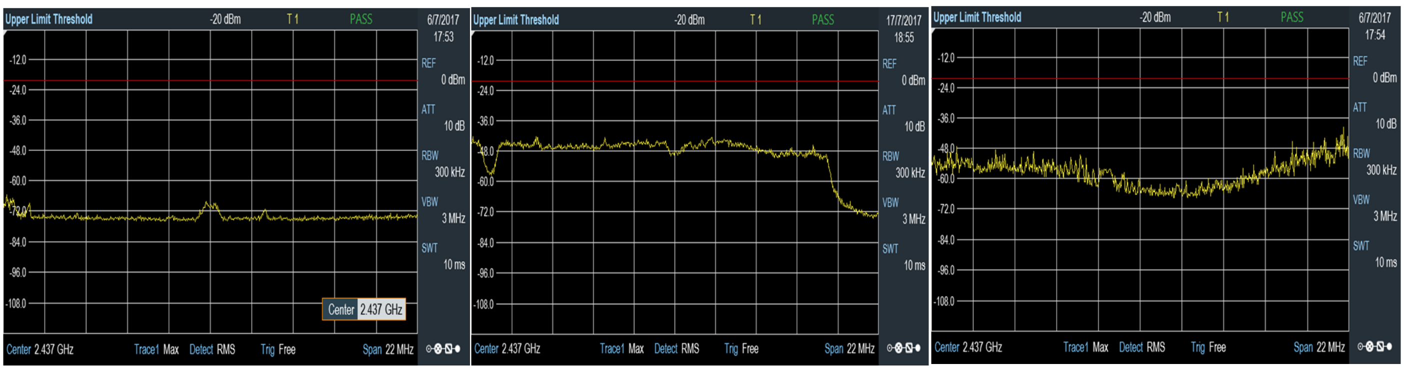

(a) (b) (c)

Fig. 6. Spectrum Images of Wi-Fi Channel 6. (a) No introduced interference. (b) Introduced Wi-Fi interference. (c) Introduced Microwave Oven interference

REFERENCES

[1] E. S. Nadimi, H. T. Søgaard, T. Bak, and F. W. Oudshoorn, "ZigBee-based wireless sensor networks for monitoring animal presence and pasture time in a strip of new grass," *Computers and Electronics in Agriculture,* vol. 61, pp. 79-87, 2008/05/01/ 2008.

[2] J. Graefenstein and M. E. Bouzouraa, "Robust method for outdoor localization of a mobile robot using received signal strength in low power wireless networks," in *2008 IEEE International Conference on Robotics and Automation*, 2008, pp. 33-38.

[3] H. Xiong, T. Latif, E. Lobaton, A. Bozkurt, and M. L. Sichitiu, "Characterization of RSS variability for biobot localization using 802.15.4 Radios," in *2016 IEEE Topical Conference on Wireless Sensors and Sensor Networks (WiSNet)*, 2016, pp. 1-3.

[4] L. Chia-How, Y. Su-Hen, C. Hong-Tze, and S. Kai-Tai, "Mobile robot intruder detection based on a Zigbee sensor network," in *2008 IEEE International Conference on Systems, Man and Cybernetics*, 2008, pp. 2786-2791.

[5] A. N. Raghavan, H. Ananthapadmanaban, M. S. Sivamurugan, and B. Ravindran, "Accurate mobile robot localization in indoor environments using bluetooth," in *2010 IEEE International Conference on Robotics and Automation*, 2010, pp. 4391-4396.

[6] M. B. Kilani, A. J. Raymond, F. Gagnon, G. Gagnon, and P. Lavoie, "RSSI-based indoor tracking using the extended Kalman filter and circularly polarized antennas," in *2014 11th Workshop on Positioning, Navigation and Communication (WPNC)*, 2014, pp. 1-6.

[7] A. Warda, B. Petković, and H. Toepfer, Scanning method for indoor localization using the RSSI approach vol. 6, 2017.

[8] [8] K. Curran, E. Furey, T. Lunney, J. Santos, D. Woods, and A. McCaughey, "An evaluation of indoor location determination technologies," *Journal of Location Based Services,* vol. 5, pp. 61-78, 2011/06/01 2011.

[9] L. Buonocore, S. R. B. d. Santos, A. A. Neto, and C. L. Nascimento, "FastSLAM filter implementation for indoor autonomous robot," in *2016 IEEE Intelligent Vehicles Symposium (IV)*, 2016, pp. 484-489.

[10] "IEEE Standard for Low-Rate Wireless Networks," *IEEE Std 802.15.4-2015 (Revision of IEEE Std 802.15.4-2011),* pp. 1-709, 2016.

[11] "IEEE Standard for Information technology--Telecommunications and information exchange between systems - Local and metropolitan area networks--Specific requirements - Part 11: Wireless LAN Medium Access Control (MAC) and Physical Layer (PHY) Specifications Amendment 2: Sub 1 GHz License Exempt Operation," *IEEE Std 802.11ah-2016 (Amendment to IEEE Std 802.11-2016, as amended by IEEE Std 802.11ai-2016),* pp. 1-594, 2017.

[12] P. Kinney, "Zigbee technology: Wireless control that simply works," in *Communications design conference*, 2003, pp. 1-7.

[13] L. Angrisani, M. Bertocco, G. Gamba, and A. Sona, "Effects of RSSI impairments on IEEE 802.15.4 wireless devices performance susceptibility to interference," in *2008 International Symposium on Electromagnetic Compatibility - EMC Europe*, 2008, pp. 1-6.

[14] J.-H. Hauer, V. Handziski, and A. Wolisz, "Experimental study of the impact of WLAN interference on IEEE 802.15. 4 body area networks," in *European Conference on Wireless Sensor Networks*, 2009, pp. 17-32.

[15] J. Huang, G. Xing, G. Zhou, and R. Zhou, "Beyond co-existence: Exploiting WiFi white space for Zigbee performance assurance," in *Network Protocols (ICNP), 2010 18th IEEE International Conference on*, 2010, pp. 305-314.

[16] P. Yi, A. Iwayemi, and C. Zhou, "Developing ZigBee Deployment Guideline Under WiFi Interference for Smart Grid Applications," *IEEE Transactions on Smart Grid,* vol. 2, pp. 110-120, 2011.

[17] W. Q. Guo, W. M. Healy, and M. C. Zhou, "Impacts of 2.4-GHz ISM Band Interference on IEEE 802.15.4 Wireless Sensor Network Reliability in Buildings," *Ieee Transactions on Instrumentation and Measurement,* vol. 61, pp. 2533-2544, Sep 2012.

[18] S.-Y. Lau, T.-H. Lin, T.-Y. Huang, I.-H. Ng, and P. Huang, "A measurement study of zigbee-based indoor localization systems under RF interference," presented at the Proceedings of the 4th ACM international workshop on Experimental evaluation and characterization, Beijing, China, 2009.

[19] N. Pirzada, M. Y. Nayan, F. Subhan, M. F. Hassan, and M. A. Khan, "Device-free Localization Technique for Indoor Detection and Tracking of Human Body: A Survey," *2nd International Conference on Innovation, Management and Technology Research,* vol. 129, pp. 422-429, 5/15/15 May 2014 2014.

[20] T. Alhmiedat, G. Samara, and A. O. A. Salem, "An indoor fingerprinting localization approach for ZigBee wireless sensor networks," *arXiv preprint arXiv:1308.1809,* 2013.

[21] [21] O. Hernandez, V. Jain, S. Chakravarty, and P. Bhargava, "Position location monitoring using ieee® 802.15. 4/zigbee® technology," *Beyond Bits, issue IV,* pp. 67-69, 2009.

[22] J. Wilson and N. Patwari, "Radio Tomographic Imaging with Wireless Networks," *Ieee Transactions on Mobile Computing,* vol. 9, pp. 621-632, May 2010.

[23] T. He, C. Huang, B. M. Blum, J. A. Stankovic, and T. Abdelzaher, "Range-free localization schemes for large scale sensor networks," presented at the Proceedings of the 9th annual international conference on Mobile computing and networking, San Diego, CA, USA, 2003.

[24] B. Dil, S. Dulman, and P. Havinga, "Range-based localization in mobile sensor networks," *Wireless Sensor Networks,* pp. 164-179, 2006.

[25] [25] R. M. E and A. Terzis, "Minimising the effect of WiFi interference in 802.15.4 wireless sensor networks," *International Journal of Sensor Networks,* vol. 3, p. 43, 2008.

[26] T. I. Inc. (Mar. 15). CC2530 - Second Generation System-on-Chip Solution for 2.4 GHz IEEE 802.15.4 / RF4CE / ZigBee. Available: http://www.ti.com/product/CC2530

[27] "R&S®Spectrum Rider FPH Handheld Spectrum Analyzer Specifications," ed: Rohde & Schwarz.

[28] *iPerf3*. Available: https://iperf.fr/

[29] M. Seifeldin, A. Saeed, A. E. Kosba, A. El-Keyi, and M. Youssef, "Nuzzer: A Large-Scale Device-Free Passive Localization System for Wireless Environments," *IEEE Transactions on Mobile Computing,* vol. 12, pp. 1321-1334, 2013.

Appendix 2

This appendix contains content from the following article, republished with permission. In accordance with IEEE's republishing policy, any full text that has been included is the unmodified accepted article. This means that while the content is identical to the published article, there may be stylistic differences.

doi: 10.1109/M2VIP.2017.8211505

HVLP: Hybrid Visible Light Positioning of a Mobile Robot

Daniel Konings[1], Baden Parr[1], Caleb Waddell[1], Fakhrul Alam[1], Khalid Mahmood Arif[1] and Edmund M-K Lai[2]

[1] School of Engineering and Advanced Technology
Massey University
Auckland, New Zealand
d.konings@massey.ac.nz

[2] Department of Information Technology and Software Engineering
Auckland University of Technology
Auckland, New Zealand

***Abstract*— In recent years energy efficient LEDs have become a commonplace lighting solution. It is possible to create an indoor positioning system (IPS) from existing lighting infrastructure by making minor modifications to the luminaire drivers. In this paper we develop and implement an IPS by augmenting the luminaires with collocated Zigbee radios. The Hybrid Visible Light Positioning (HVLP) system utilizes a two-stage process where it first localizes which room a mobile robot resides in, followed by estimating the robot's position within the room itself. Experimental results conducted in two adjacent rooms with dimensions 4.8 x 5.7 x 2.5, 4.8 x 3.3 x 2.5 show that the HVLP system attains a median error of 5.8 cm, which is a significant improvement on existing approaches.**

Keywords*— *Visible Light Positioning; RSSI; mobile robot; 802.15.4; Zigbee; indoor localization

I. INTRODUCTION

Localization techniques that utilize existing lighting infrastructure have become a hot topic of current research as they offer reduced cost and implementation complexity. Visible Light Communication (VLC) [1] is an emerging technology that intends to utilize LED luminaires for simultaneous illumination and communication. This can be extended further by developing Visible Light Positioning (VLP) that offer localization services. Existing VLP techniques typically make use of ceiling mounted consumer-grade LED luminaires, and an active device that uses photo-diodes to infer its position relative to the luminaires.

The smart automation industry manufactures network enabled lighting for both commercial and residential applications. This means that smart lights provide the opportunity to localize an entity by estimating the power of the incoming wireless and optical signals. In common wireless technologies like Zigbee and Wi-Fi, this estimate is readily available as the Received Signal Strength Indicator (RSSI). Wireless localization, while not as accurate as VLP, has the advantage of working in non line of sight (NLOS) scenario.

Indoor Positioning Systems (IPS) for mobile robots commonly rely on odometry or map-based techniques, due to unavailability of the absolute localization methods like GPS. There have been numerous research efforts to develop an absolute IPS by utilizing projected patterns on ceiling or walls, landmarks [2], radios [3], or lasers [4]. However, these methods suffer from various shortcomings. For example projected patterns only work on flat surfaces. Landmarks are not effective in crowded or dynamic environments. VLP looks to address this by having a low implementation cost, while also having high sensor density due to the utilization of luminaires within an existing built environment. This allows for the system to work within various indoor environments, including stairwells and crowded dwellings, which previously posed as issue for IPS implementations.

II. BACKGROUND

A number of approaches have been taken for VLP. Tanaka et al proposed a method for localizing an image sensor by detecting ceiling mounted coloured LEDs, followed by utilizing an accelerometer to determine system orientation [5]. The proposed method achieved an accuracy of 5cm which was sufficient to control a robot. However the coloured LEDs require intrusive environment modification and the requirement of a camera increases costs and limits the system's suitability for many applications.

Bai et al used TDOA with VLP to determine the position of vehicles approaching a traffic light intersection by using separate VLP sensors mounted in each of the vehicles headlights. Numerically they proved the feasibility of such an approach, however no physical testing was carried out and the simulation lacked a model for environmental noise [6]. Another popular approach is to use intensity modulated direct detection (IM/DD) with a single photo-diode. Lights are ceiling mounted in known locations and their intensity is modulated in

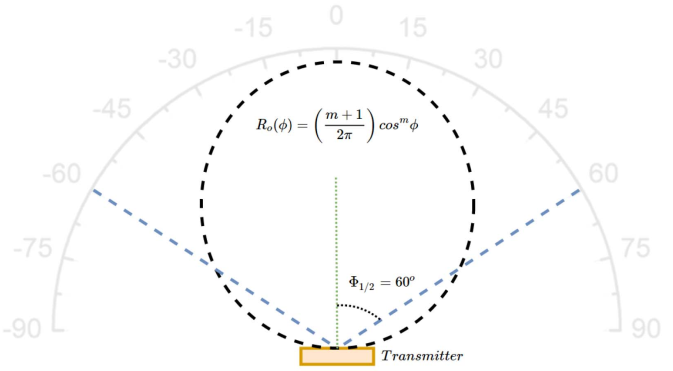

Fig. 1. Lambertian Radiance

a way that individual LEDs can be directly detected by the receiver's photo-diode [7].

Existing VLP room-scale approaches either do not meet the required accuracy [8-10], have a roof height that is unrealistic for existing built environments [11], or suffer a significant decrease in accuracy when moving outside the small (<1m^2) target area [12]. For robotics applications it is important to maintain a low localization error to allow for various tasks like docking maneuvers.

Localization services can also be provided for indoor positioning systems by the RSSI. RSSI is commonly utilized in localization systems due to its off-the-shelf availability in 802.15.4 [13] and Wi-Fi [14] equipment. This paper focusses on Zigbee as it offers mesh networking, does not introduce interference to existing Wi-Fi infrastructure and is commonplace within standard home automation lighting such as the Philips Hue bulbs [15].

III. Localization Approach

The proposed localization follows a two stage process. Stage 1 utilizes the Zigbee radios to locate which room the robot currently resides within. Stage 2 receives the room estimate from Stage 1 and utilizes the VLP system to provide an estimate of the robots position within the room.

A. Stage 1

During stage 1, the robot receives the Zigbee RSSI streams and estimates the median over a 3 second period for each stream. The median values are then added together for each room to attain a 'room score'. The room with the highest 'room score' is the room within which the robot is currently located. This is an extremely simplistic localization approach but benefits from requiring no calibration. Four streams per room may seem excessive to identify a room. However as discussed previously, Zigbee enabled smart lights are becoming readily available in a smart home. The benefit of utilizing 4 streams per room was that multipath induced RSSI variations (within a single stream) would not significantly affect the overall 'room score'. Our experience suggests that this approach requires at least 3 ceiling mounted Zigbee radios to function correctly, if no multipath mitigation is performed.

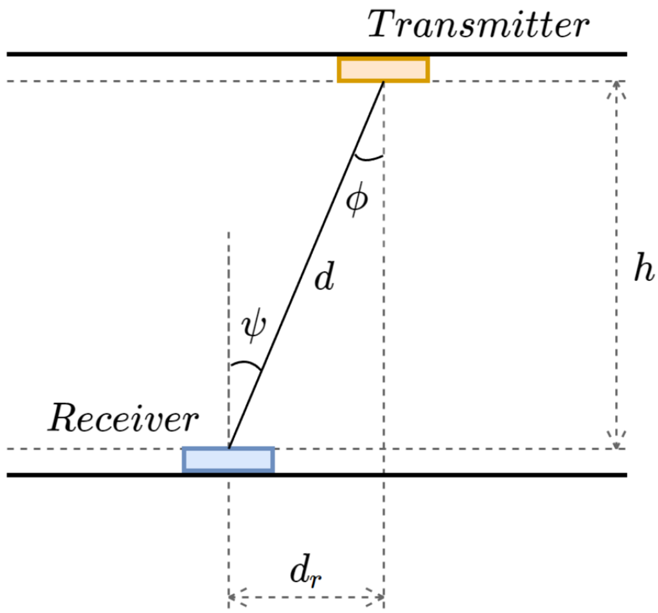

Fig. 2. Side view of VLP system

B. Stage 2

Once the room has been identified, the VLP takes over and estimates the position within that room. The distance between the line-of-sight (LOS) optical path is calculated using the RSS. Fig. 1 shows that LED transmitters in a VLP system can be described as a first order Lambertian emitter [16].

Equation 1 represents the power at the VLP receiver, which is equivalent to [10, eq. (5)].

$$P_r = \frac{P_t}{d^2}\left(\frac{m+1}{2\pi}\right) cos^m(\emptyset) A cos(\varphi) \qquad (1)$$

Where:

- P_t is the transmitted power
- d is distance between the transmitter / receiver
- m is the Lambertian order
- $\emptyset$ is the irradiation angle
- A is the area of the VLP detector
- φ is the incidence angle

By assuming the LEDs are a lambertian light source, the angle of divergence, i.e $\emptyset_{1/2} = 60^{\circ}$. This means that (1) can be simplified to:

$$P_r = \frac{P_t}{d^2}\left(\frac{m+1}{2\pi}\right) cos(\emptyset) A cos(\varphi) \qquad (2)$$

Since we are tracking an indoor autonomous robot with the VLP sensor mounted on the top plate, we have made the following assumptions:

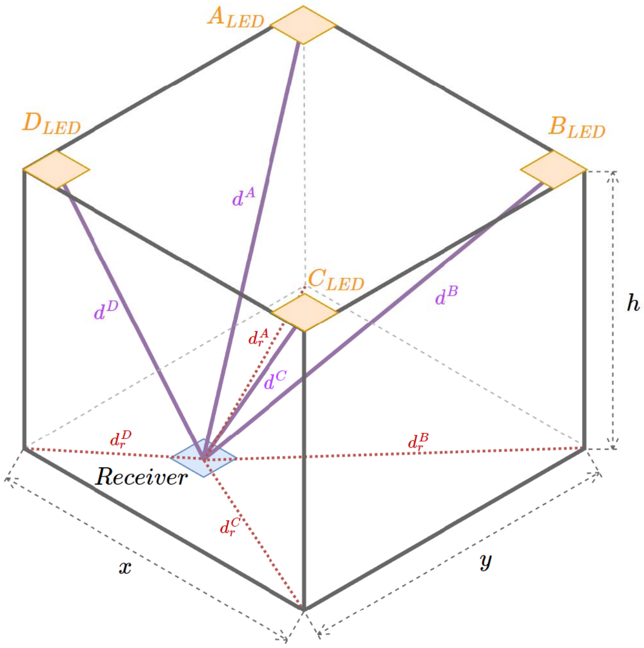

Fig. 3. VLP Triangulation

1) The distance between the robots VLP sensor and the roof (h) remains constant
2) The VLP receiver sensor remains parallel to the ceiling VLP transmitters , thus: $cos(\emptyset) = cos(\varphi) = \frac{h}{d}$

These assumptions allow (2) to be simplified to:

$$P_r = P_t G \frac{h^2}{d^4} \quad (3)$$

Where G is a constant gain of $A\left(\frac{m+1}{2\pi}\right)$.

We have followed the process of [17] and attain:

$$d = \sqrt[4]{\frac{P_t G h^2}{P_r}} \quad (4)$$

By using Pythagoras theorem, we can determine the radial distance is:

$$dr = \sqrt{d^2 - h^2} \quad (5)$$

$$dr = \sqrt{\sqrt{\frac{P_t G h^2}{P_r}} - h^2} \quad (6)$$

Utilizing triangulation with the radial distances from at least 3 VLP transmitters allows for the localization of the mobile robot as shown in Fig. 3.

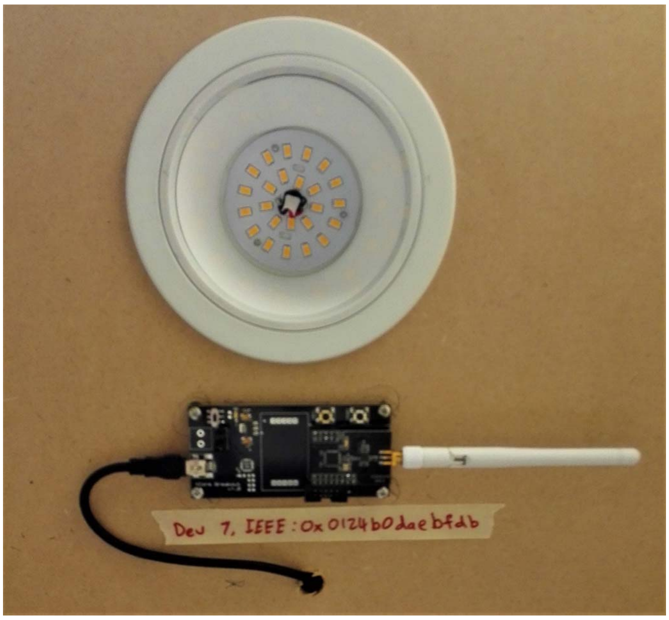

Fig. 4. Allume luminaire and Texas Instruments CC2530 board

IV. EXPERIMENTAL SETUP

We aimed to establish a lighting solution that is comparable to existing commercial offerings such as the Phillips Hue bulbs [15]. We coupled a standard ceiling mounted LED luminaire (Allume 3000K – PLU 73278) with a Zigbee radio, shown in Fig. 4, as an analog of a network enabled smart bulb.

The core of the Zigbee radio nodes is a TI CC2530 [18], with an RFX2401 PA/LNA front end as shown in Fig. 5. These chips are running a custom application built on TI's Z-Stack Home Automation 1.2.2a network stack. This firmware is therefore fully compliant with Zigbee Alliance standards [19], and ensures that this experiment is representative of commercial products running on similar network stacks. The RF network in this experimental setup consisted of 10 such Zigbee nodes, connected in a mesh network topology. The physical setup consists of a network coordinator connected to a PC via a COM port, an active router onboard the mobile robot, and 8 static routers collocated with the luminaires. Nodes transmit at +19 dBm, and operate at channel 0x26, which is free from in-band 802.11 interference.

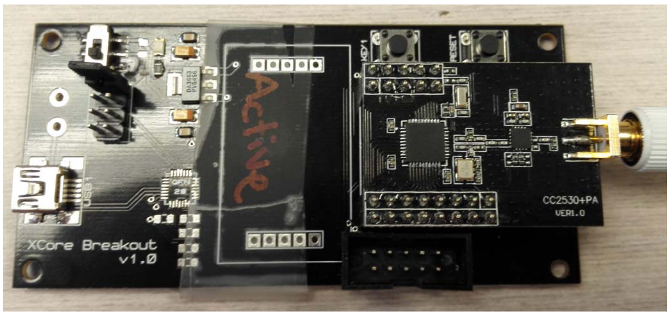

Fig. 5. Close-up of custom Texas Instruments CC2530 breakout board

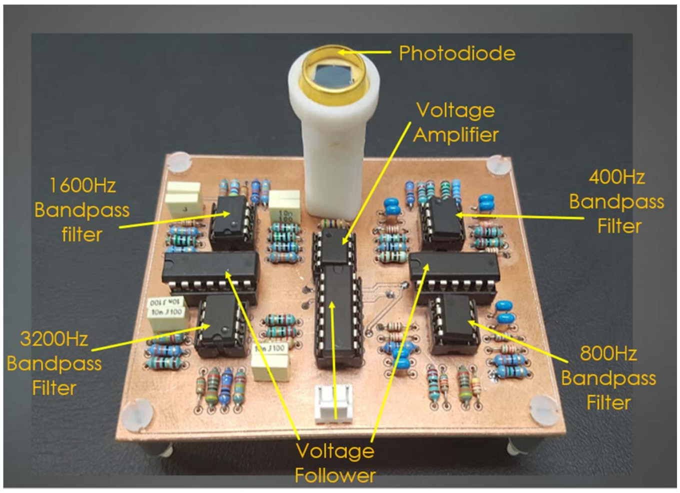

Fig. 6. Custom VLP receiver board

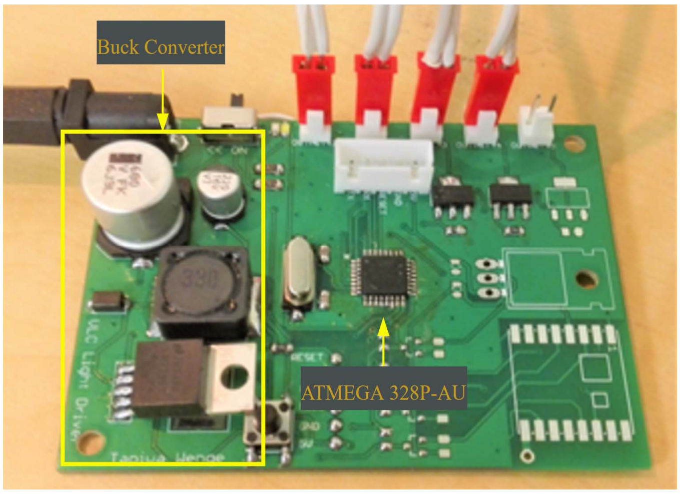

Fig. 7. VLP Driver Board

The network performs the following sequence to retrieve RSSI data from the network. First, the coordinator sends a multi-hop unicast to the active node. On receiving this packet, the active node sends a single-hop broadcast to all static routers within range. The packet's RSSI is recorded, and returned to the coordinator in the payload of a final multi-hop packet. The coordinator then sends this data, including the packet's source address, to the PC for processing, where the address is compared against a look up table. Algorithms to determine the coarse room-level location of the active node are then run in real time. All static routers transmit simultaneously, and rely on Clear Channel Assessment (CCA) and Carrier Sense Multiple Access\Collision Avoidance (CSMA/CA) to reliably transmit data.

The proposed VLP system requires multiple clusters of VLP transmitters with each cluster serving a particular region of a building. The implemented VLP system consists of two separate clusters of VLP transmitters. Each cluster serves a room and consists of 4 VLP transmitters operating on separate frequencies (400Hz, 800Hz, 1600Hz, and 3200Hz), and utilizing an on/off keying (OOK) modulation scheme [12]. The frequency assignment is based on the fact that square waves produce odd harmonics of the fundamental frequency. OOK was chosen for its simplicity which enables low cost modulator circuitry as well as a simplified VLP receiver, as shown in Fig.

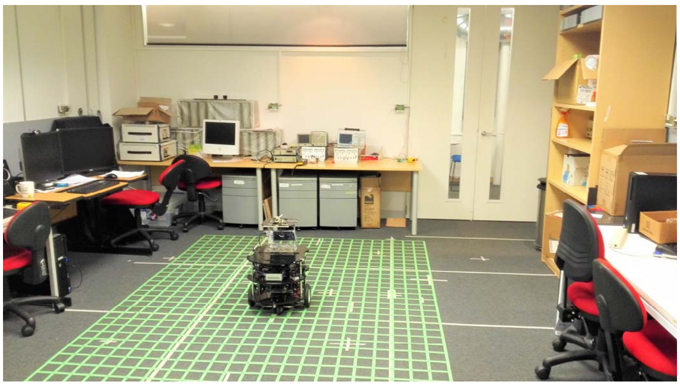

Fig. 8. Room 1 with HVLP autonomous robot

6. Fig. 7 shows the custom driver board we fabricated for the VLP transmitters.

The test environment consists of two adjacent rooms as shown in Fig. 8 and Fig. 9, with both rooms having a ceiling height of 2.5m. Each room contains 4 ceiling mounted luminaires coupled with collocated CC2530 radios. The HVLP receiver mounted on top of the mobile robot contains a CC2530 Zigbee radio and a custom VLP receiver board consisting of a photo-diode and associated bandpass filters for demultiplexing. The ceiling mounted CC2530 antennas were kept in parallel with the mobile robots CC2530 antenna to minimize RSSI variations caused by orientation changes.

V. Experimental Results

We randomly selected 30 test locations in Room 1, and 10 test locations in the smaller Room 2. It should be noted that we did not pick any test locations that were under desks as shown in Fig. 9. Fig. 10 shows the localization results for test locations within Room 1. Stage 1 of the localization process correctly estimated the robots current room with 100% accuracy.

The system performed accurately with lower than 6 cm median error in localization estimation, as reported in Table 1 below.

TABLE I.

Rooms	**HVLP Error (m)**			
	Mean	***Median***	***RMSE***	***Max***
Room 1	0.059	0.058	0.065	0.108
Room 2	0.069	0.058	0.083	0.151

It is interesting to note that the accuracy of the VLP system decreases as the tracked robot comes directly under one of the luminaires. This occurs because the received power at a

Appendices

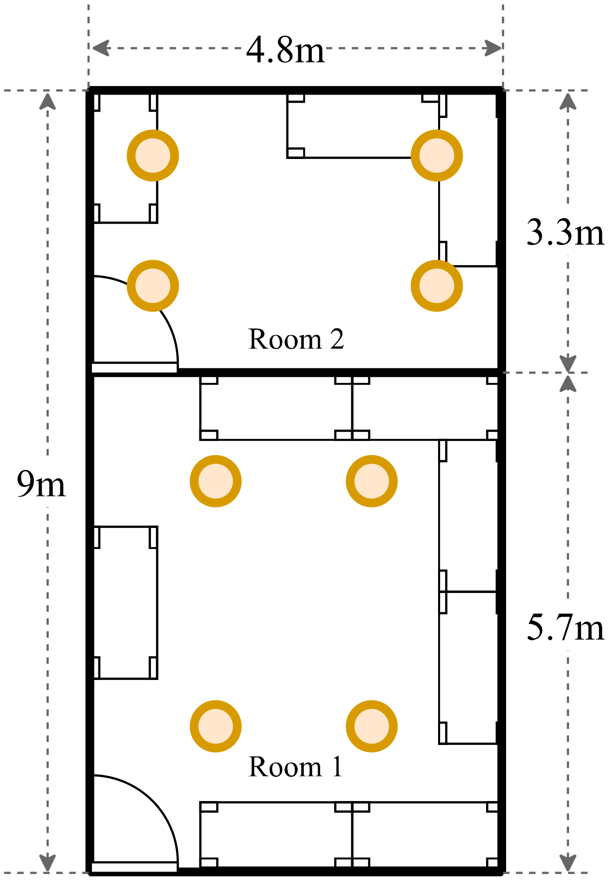

Fig. 9. Room 1 and Room 2 Layout

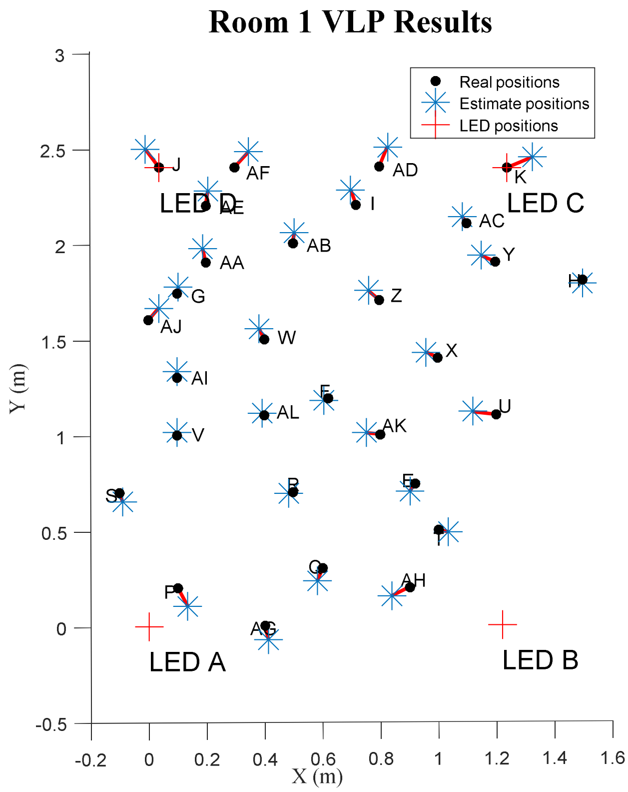

Fig. 10. Room 1 VLP Results

particular radial distance can be approximated by a cosine falloff. This means that when the radial distance is very small, the change in received power between distances is also very small. This results in a reduction in the Signal to Noise Ratio (SNR), leading to decreased accuracy.

VI. Conclusion

In this paper we presented the design and implementation of HVLP, an augmented wireless/visible light IPS system. Through testing we have shown that our HVLP system can accurately localize a robot within a typical office environment with a median error of 5.8cm. To the best of our knowledge this is the first reported work to attain sub 10cm accuracy in a room-scale IPS based on Visible Light without utilizing expensive sensors or actively reducing ambient light levels. Our work confirms the potential of visible light for high accuracy indoor localization, and demonstrates how some of its limitations can be overcome by augmenting it with Zigbee.

The developed method does not leverage wireless localization to eliminate potential blind spots of the VLP system. Future work should investigate how a fusion of wireless and visible light information using an extended Kalman filter can increase the accuracy and coverage. The OOK modulation based multiplexing scheme is not very efficient as it reduces the light from each luminaire by half. It also generates a lot of harmonics which puts a constraint on the number of lights that can be used in a cluster whilst still demultiplexing each signal. Future research should look into developing more efficient and scalable multiplexing schemes. Future work can also include whether applying a Fast Fourier Transform (FFT), rather than band-pass filters for demultiplexing can make the system more scalable and flexible. Further work needs to be done on increasing the accuracy of the system when the detector is directly under lights.

References

[1] T. Komine and M. Nakagawa, "Fundamental analysis for visible-light communication system using LED lights," IEEE Transactions on Consumer Electronics, vol. 50, pp. 100-107, 2004.

[2] M. Betke and L. Gurvits, "Mobile robot localization using landmarks," IEEE transactions on robotics and automation, vol. 13, pp. 251-263, 1997.

[3] J. Jung, S.-M. Lee, and H. Myung, "Indoor mobile robot localization and mapping based on ambient magnetic fields and aiding radio sources," IEEE Transactions on Instrumentation and Measurement, vol. 64, pp. 1922-1934, 2015.

[4] J. Kim and W. Chung, "Localization of a Mobile Robot Using a Laser Range Finder in a Glass-Walled Environment," IEEE Transactions on Industrial Electronics, vol. 63, pp. 3616-3627, 2016.

[5] T. Tanaka and S. Haruyama, "New Position Detection Method Using Image Sensor and Visible Light LEDs," presented at the Proceedings of the 2009 Second International Conference on Machine Vision, 2009.

[6] B. Bai, G. Chen, Z. Xu, and Y. Fan, "Visible Light Positioning Based on LED Traffic Light and Photodiode," in 2011 IEEE Vehicular Technology Conference (VTC Fall), 2011, pp. 1-5.

[7] H. Elgala, R. Mesleh, and H. Haas, "Indoor broadcasting via white LEDs and OFDM," IEEE Transactions on Consumer Electronics, vol. 55, pp. 1127-1134, 2009.

[8] K. Moriya, M. Fujimoto, Y. Arakawa, and K. Yasumoto, "Indoor localization based on distance-illuminance model and active control of lighting devices," in 2016 International Conference on Indoor Positioning and Indoor Navigation (IPIN), 2016, pp. 1-6.

[9] K. Qiu, F. Zhang, and M. Liu, "Visible Light Communication-based indoor localization using Gaussian Process," in 2015 IEEE/RSJ International Conference on Intelligent Robots and Systems (IROS), 2015, pp. 3125-3130.

[10] L. Li, P. Hu, C. Peng, G. Shen, and F. Zhao, "Epsilon: A Visible Light Based Positioning System," in NSDI, 2014, pp. 331-343.

[11] H. S. Kim, D. R. Kim, S. H. Yang, Y. H. Son, and S. K. Han, "An Indoor Visible Light Communication Positioning System Using a RF Carrier Allocation Technique," Journal of Lightwave Technology, vol. 31, pp. 134-144, 2013.

[12] Y.-S. Kuo, P. Pannuto, K.-J. Hsiao, and P. Dutta, "Luxapose: indoor positioning with mobile phones and visible light," presented at the Proceedings of the 20th annual international conference on Mobile computing and networking, Maui, Hawaii, USA, 2014.

[13] "IEEE Standard for Low-Rate Wireless Networks," IEEE Std 802.15.4-2015 (Revision of IEEE Std 802.15.4-2011), pp. 1-709, 2016.

[14] "IEEE Standard for Information technology--Telecommunications and information exchange between systems - Local and metropolitan area networks--Specific requirements - Part 11: Wireless LAN Medium Access Control (MAC) and Physical Layer (PHY) Specifications Amendment 2: Sub 1 GHz License Exempt Operation," IEEE Std 802.11ah-2016 (Amendment to IEEE Std 802.11-2016, as amended by IEEE Std 802.11ai-2016), pp. 1-594, 2017.

[15] Philips Hue white extension bulb A19. Available: http://www2.meethue.com/en-gb/productdetail/philips-hue-white-extension-bulb-a19

[16] J. M. Kahn and J. R. Barry, "Wireless infrared communications," Proceedings of the IEEE, vol. 85, pp. 265-298, 1997.

[17] H. Sharifi, A. Kumar, F. Alam, and K. M. Arif, "Indoor localization of mobile robot with visible light communication," in 2016 12th IEEE/ASME International Conference on Mechatronic and Embedded Systems and Applications (MESA), 2016, pp. 1-6.

[18] CC2530 - Second Generation System-on-Chip Solution for 2.4 GHz IEEE 802.15.4 / RF4CE / ZigBee. Available: http://www.ti.com/product/CC2530

[19] Zigbee Home Automation. Available: http://www.zigbee.org/zigbee-for-developers/applicationstandards/zigbeehomeautomation/

MASSEY UNIVERSITY
GRADUATE RESEARCH SCHOOL

STATEMENT OF CONTRIBUTION
DOCTORATE WITH PUBLICATIONS/MANUSCRIPTS

We, the candidate and the candidate's Primary Supervisor, certify that all co-authors have consented to their work being included in the thesis and they have accepted the candidate's contribution as indicated below in the *Statement of Originality*.

Name of candidate:	Daniel Konings
Name/title of Primary Supervisor:	Dr Fakhrul Alam
Name of Research Output and full reference:	
D. Konings, B. Parr, F. Alam, and E. M.-K. Lai, "Falcon: Fused Application of Light based positioning Coupled with Onboard Network localization," IEEE Access, vol. 6, pp. 36155- 36167, 2018.	
In which Chapter is the Manuscript /Published work:	Chapter 1
Please indicate:	
• The percentage of the manuscript/Published Work that was contributed by the candidate:	80
and	
• Describe the contribution that the candidate has made to the Manuscript/Published Work:	
The candidate led the development of the wireless hardware and performed the experiments with assistance from the second author. The candidate produced the first draft of the article based on suggestions from the co-author supervisors	
For manuscripts intended for publication please indicate target journal:	
Candidate's Signature:	Daniel Konings Digitally signed by Daniel Konings Date: 2019.07.19 10:34:39 +12'00'
Date:	18/07/2019
Primary Supervisor's Signature:	Fakhrul Alam Digitally signed by Fakhrul Alam Date: 2019.07.19 13:37:43 +12'00'
Date:	18/07/2019

(This form should appear at the end of each thesis chapter/section/appendix submitted as a manuscript/ publication or collected as an appendix at the end of the thesis)

MASSEY UNIVERSITY
GRADUATE RESEARCH SCHOOL

STATEMENT OF CONTRIBUTION
DOCTORATE WITH PUBLICATIONS/MANUSCRIPTS

We, the candidate and the candidate's Primary Supervisor, certify that all co-authors have consented to their work being included in the thesis and they have accepted the candidate's contribution as indicated below in the *Statement of Originality*.

Name of candidate:	Daniel Konings
Name/title of Primary Supervisor:	Dr Fakhrul Alam
Name of Research Output and full reference:	
D. Konings, F. Alam, F. Noble and E. M.-K. Lai, "Device-free Localization Systems Utilizing Wireless RSSI: A Comparative Practical Investigation," IEEE Sensors Journal, vol. 19, no. 7, pp. 2747- 2757, April 2019.	
In which Chapter is the Manuscript /Published work:	Chapter 2
Please indicate:	
• The percentage of the manuscript/Published Work that was contributed by the candidate:	80
and	
• Describe the contribution that the candidate has made to the Manuscript/Published Work:	
The candidate led the development of the wireless hardware and performed the experiments. The candidate produced the first draft of the article based on suggestions from the co-author supervisors regarding the narrative and results that	
For manuscripts intended for publication please indicate target journal:	
Candidate's Signature:	Daniel Konings Digitally signed by Daniel Konings Date: 2019.07.19 10:34:54 +12'00'
Date:	18/07/2019
Primary Supervisor's Signature:	Fakhrul Alam Digitally signed by Fakhrul Alam Date: 2019.07.19 13:38:03 +12'00'
Date:	18/07/2019

(This form should appear at the end of each thesis chapter/section/appendix submitted as a manuscript/ publication or collected as an appendix at the end of the thesis)

MASSEY UNIVERSITY
GRADUATE RESEARCH SCHOOL

STATEMENT OF CONTRIBUTION
DOCTORATE WITH PUBLICATIONS/MANUSCRIPTS

We, the candidate and the candidate's Primary Supervisor, certify that all co-authors have consented to their work being included in the thesis and they have accepted the candidate's contribution as indicated below in the *Statement of Originality*.

Name of candidate:	Daniel Konings
Name/title of Primary Supervisor:	Dr Fakhrul Alam
Name of Research Output and full reference:	
D. Konings, F. Alam, F. Noble and E. M.-K. Lai, "SpringLoc: A Device-free Localization Technique for Indoor Positioning and Tracking using Adaptive RSSI Spring Relaxation," IEEE Access, vol. 7, pp. 56960- 56973, 2019.	
In which Chapter is the Manuscript /Published work:	Chapter 3
Please indicate:	
• The percentage of the manuscript/Published Work that was contributed by the candidate:	80
and	
• Describe the contribution that the candidate has made to the Manuscript/Published Work:	
The candidate led the development of the wireless hardware and performed the experiments. The candidate produced the first draft of the article based on suggestions from the co-author supervisors regarding the narrative and results that	
For manuscripts intended for publication please indicate target journal:	
Candidate's Signature:	Daniel Konings Digitally signed by Daniel Konings Date: 2019.07.19 10:35:01 +12'00'
Date:	18/07/2019
Primary Supervisor's Signature:	Fakhrul Alam Digitally signed by Fakhrul Alam Date: 2019.07.19 13:38:13 +12'00'
Date:	18/07/2019

(This form should appear at the end of each thesis chapter/section/appendix submitted as a manuscript/ publication or collected as an appendix at the end of the thesis)

MASSEY UNIVERSITY
GRADUATE RESEARCH SCHOOL

STATEMENT OF CONTRIBUTION
DOCTORATE WITH PUBLICATIONS/MANUSCRIPTS

We, the candidate and the candidate's Primary Supervisor, certify that all co-authors have consented to their work being included in the thesis and they have accepted the candidate's contribution as indicated below in the *Statement of Originality*.

Name of candidate:	Daniel Konings
Name/title of Primary Supervisor:	Dr Fakhrul Alam
Name of Research Output and full reference:	
D. Konings, F. Alam, F. Noble and E. M.-K. Lai, "Improved Distance Metrics for Histogram based Device-free Localization," IEEE Sensors Journal, June 2019, 10.1109/JSEN.2019.2922772.	
In which Chapter is the Manuscript /Published work:	Chapter 4
Please indicate:	
• The percentage of the manuscript/Published Work that was contributed by the candidate:	80
and	
• Describe the contribution that the candidate has made to the Manuscript/Published Work:	
The candidate led the development of the wireless hardware and performed the experiments. The candidate produced the first draft of the article based on suggestions from the co-author supervisors regarding the narrative and results that	
For manuscripts intended for publication please indicate target journal:	
Candidate's Signature:	Daniel Konings Digitally signed by Daniel Konings Date: 2019.07.19 16:08:51 +12'00'
Date:	18/07/2019
Primary Supervisor's Signature:	Fakhrul Alam Digitally signed by Fakhrul Alam Date: 2019.07.19 13:38:30 +12'00'
Date:	18/07/2019

(This form should appear at the end of each thesis chapter/section/appendix submitted as a manuscript/ publication or collected as an appendix at the end of the thesis)

MASSEY UNIVERSITY
GRADUATE RESEARCH SCHOOL

STATEMENT OF CONTRIBUTION
DOCTORATE WITH PUBLICATIONS/MANUSCRIPTS

We, the candidate and the candidate's Primary Supervisor, certify that all co-authors have consented to their work being included in the thesis and they have accepted the candidate's contribution as indicated below in the *Statement of Originality*.

Name of candidate:	Daniel Konings
Name/title of Primary Supervisor:	Dr Fakhrul Alam
Name of Research Output and full reference:	
D. Konings, N. Faulkner, F. Alam, E. M.-K. Lai, and S.Demidenko, "FieldLight: Device-free Localization using Passive Visible Light Positioning and Artificial Potential Fields," IEEE Sensors Journal	
In which Chapter is the Manuscript /Published work:	Chapter 5
Please indicate:	
• The percentage of the manuscript/Published Work that was contributed by the candidate:	80
and	
• Describe the contribution that the candidate has made to the Manuscript/Published Work:	
The candidate performed the experiments with assistance from the second author. He produced the first draft of the article based on suggestions from the co-author supervisors regarding the narrative and results that was presented.	
For manuscripts intended for publication please indicate target journal:	
Candidate's Signature:	Daniel Konings Digitally signed by Daniel Konings Date: 2019.07.19 10:35:09 +12'00'
Date:	18/07/2019
Primary Supervisor's Signature:	Fakhrul Alam Digitally signed by Fakhrul Alam Date: 2019.07.19 13:38:40 +12'00'
Date:	18/07/2019

(This form should appear at the end of each thesis chapter/section/appendix submitted as a manuscript/ publication or collected as an appendix at the end of the thesis)

MASSEY UNIVERSITY
GRADUATE RESEARCH SCHOOL

STATEMENT OF CONTRIBUTION
DOCTORATE WITH PUBLICATIONS/MANUSCRIPTS

We, the candidate and the candidate's Primary Supervisor, certify that all co-authors have consented to their work being included in the thesis and they have accepted the candidate's contribution as indicated below in the *Statement of Originality*.

Name of candidate:	Daniel Konings
Name/title of Primary Supervisor:	Dr Fakhrul Alam
Name of Research Output and full reference:	
D. Konings, N. Faulkner, F. Alam, F. Noble, and E. M.-K. Lai, "The effects of interference on the RSSI values of a ZigBee based indoor localization system," in Mechatronics and Machine Vision in Practice (M2VIP), 24th International Conference on, 201	
In which Chapter is the Manuscript /Published work:	Appendix 1
Please indicate:	
• The percentage of the manuscript/Published Work that was contributed by the candidate:	80
and	
• Describe the contribution that the candidate has made to the Manuscript/Published Work:	
The candidate performed the experiments with assistance from the second author. He produced the first draft of the article based on suggestions from the co-author supervisors regarding the narrative and results that was presented.	
For manuscripts intended for publication please indicate target journal:	
Candidate's Signature:	Daniel Konings Digitally signed by Daniel Konings Date: 2019.07.19 10:35:31 +12'00'
Date:	18/07/2019
Primary Supervisor's Signature:	Fakhrul Alam Digitally signed by Fakhrul Alam Date: 2019.07.19 13:38:52 +12'00'
Date:	18/07/2019

(This form should appear at the end of each thesis chapter/section/appendix submitted as a manuscript/ publication or collected as an appendix at the end of the thesis)

MASSEY UNIVERSITY
GRADUATE RESEARCH SCHOOL

STATEMENT OF CONTRIBUTION
DOCTORATE WITH PUBLICATIONS/MANUSCRIPTS

We, the candidate and the candidate's Primary Supervisor, certify that all co-authors have consented to their work being included in the thesis and they have accepted the candidate's contribution as indicated below in the *Statement of Originality*.

Name of candidate:	Daniel Konings
Name/title of Primary Supervisor:	Dr Fakhrul Alam
Name of Research Output and full reference:	
D. Konings, B. Parr, C. Waddell, F. Alam, K. M. Arif, and E. M.-K. Lai, "HVLP: Hybrid visible light positioning of a mobile robot," in Mechatronics and Machine Vision in Practice (M2VIP), 2017 24th International Conference on, 2017, pp. 1-6: IEEE	
In which Chapter is the Manuscript /Published work:	Appendix 2
Please indicate:	
• The percentage of the manuscript/Published Work that was contributed by the candidate:	80
and	
• Describe the contribution that the candidate has made to the Manuscript/Published Work:	
The candidate performed the experiments with assistance from the second and third author. He produced the first draft of the article based on suggestions from the co-author supervisors regarding the narrative and results that was presented.	
For manuscripts intended for publication please indicate target journal:	
Candidate's Signature:	Daniel Konings Digitally signed by Daniel Konings Date: 2019.07.19 10:35:40 +12'00'
Date:	18/07/2019
Primary Supervisor's Signature:	Fakhrul Alam Digitally signed by Fakhrul Alam Date: 2019.07.19 13:39:05 +12'00'
Date:	18/07/2019

(This form should appear at the end of each thesis chapter/section/appendix submitted as a manuscript/ publication or collected as an appendix at the end of the thesis)